Properties of Visual Field Maps in Health and Disease

André D Gouws

PhD

Psychology

University of York

December, 2015

Abstract

The visual world that surrounds us is represented in and processed by multiple topographically organised maps in the human brain. The organising principle underlying these *retinotopic* maps is also apparent across other sensory modalities and appears highly conserved across species. Moreover, the template for these visual maps is laid down during development, without the need for visual experience. This thesis binds and summarises seven publications describing work to characterise the functional properties of visual maps in the human brain. Initially, we describe TMS and fMRI measurements designed to probe the functional specificity of two spatially distinct but spatially adjacent maps, LO-1 and LO-2. Concurrently I developed software (visualisation tools) for precise dissection of these areas and to more broadly facilitate the visualisation of neuroimaging data. Our experiment revealed a double dissociation in the functional specificity of these areas, with preferential processing of orientation and shape information by LO-1 and LO-2, respectively. We then used fMRI to examine the effect of spatial attention on the responses measured from visual field maps. We showed that attention modulated visual responses by both enhancing attended locations and suppressing unattended locations; these effects were evident in the maps of early visual cortex and subcortical structures including the lateral geniculate and pulvinar nuclei. Finally, we examined the properties of visual field maps in patients with retinal lesions. Although maps can be abnormally organised with certain congenital visual deficits, we asked whether *normally* developed maps were able to reorganise when input to them is lost later in life, specifically due to central retinal lesions. Our measurements showed no evidence of reorganisation in the maps of patients with macular degeneration: the extent of activity measured in these maps was both highly predictable based on individual retinal lesions and could be reliably simulated in normally sighted individuals.

Contents

List of figures

List of tables

pg.

Acknowledgements

I'll start with an apology. As it has taken me a *little* longer than envisaged to reach this point in my career I will inevitably forget the contributions, support and guidance of many individuals. Sorry if you don't get a mention here.

I would like to thank all my YNiC colleagues, past and present, for giving me the space to do some research and keeping YNiC a dynamic and fun place to work, often through testing times. I am particularly grateful to Paul Elliott & Mark Hymers who continue to repair everything that I break.

Many colleagues and collaborators have offered support and guidance over the years. I am particularly grateful to Tim Andrews, Alex Wade, Declan McKeefry and Dan Baker, all of whom struck the correct balance between encouragement and reality checks when I came up with my next wacky scheme or opinion.

I have also been fortunate to go through my apprenticeship alongside some fantastic fellow students - the future greats of the scientific world. Thanks to Ed Silson, Sam Strong, Alex Levine and *Morland Lab* for keeping the energy levels up and me on my toes.

Gary Green, the *Yes Man*, employed me on a whim many years ago. I have cursed him many times over the years for saying *yes* to so many people, but his unerring optimism and passion for science and the *next big thing* remains an inspiration to me. Thanks Gary.

No one has taken more interest in or had more influence on my career than Tony Morland. Despite his frustration at my apparent inability to stay focussed on a single project, turn up for meetings or just sit down and write, all he ever demanded was "progress". I am truly sorry that a bottle of Scotch has so often had to substitute for the lack of penmanship that leaves me unable to express my gratitude. Cheers.

Thank you to my kind examiners, Adrian Williams, Denis Schluppeck and Alex Wade.

And to Mom, Dad & KD: I told you we'd get there in the end. Sorry for the wait and thank you for the unwavering support and encouragement.

Author's declaration

I, André Gouws, declare that this thesis is a presentation of original work and I am the sole author. This work has not previously been presented for an award at this, or any other, University. All sources are acknowledged as References.

The author's contributions to the bound multi-author publications are summarised below, grouped by chapter and relevant bound paper number.

Papers bound in Chapter 1:

Paper 1. DataViewer3D: An Open-Source, Cross-Platform Multi-Modal Neuroimaging Data Visualization Tool. Gouws A, Woods W, Millman R, Morland A, Green G. (2009). Frontiers in Neuroinformatics 3:9.

A.D.G. wrote the software package and the manuscript.

Papers bound in Chapter 2:

Paper 2. The Non-Invasive Dissection Of The Human Visual Cortex: Using FMRI and TMS To Study The Organisation Of Vision In The Brain. McKeefry DJ, Gouws. A, Burton MP & Morland AB (2009). Neuroscientist 15: 489-506.

ADG acquired 12 hrs of structural and fMRI data on 4 subjects across two sessions each. ADG analyzed the neuroimaging data: processing of anatomical data including manual brain segmentation; processing of correlation analyses and subsequent definition of visual map boundaries; implemented the visual area position variability analyses. ADG prepared figures for analysis and publication, and made significant contributions to all drafts of the manuscript.

Paper 3. Specialized and independent processing of orientation and shape in visual field maps LO-1 and LO-2. Edward H Silson, Declan J McKeefry, Jessica Rodgers, Andre D Gouws, Mark Hymers & Antony B Morland (2013) Nature Neuroscience 16: 267-269.

ADG acquired 12 hrs of structural and fMRI data on 12 subjects. ADG co-analyzed the neuroimaging data: processing of anatomical data including manual brain segmentation; processing of correlation analyses and subsequent definition of visual map boundaries; implemented spatial analyses to calculate the ROI centres of mass for TMS targeting. ADG jointly designed and programmed the stimuli for the TMS experiments and aided in TMS data collection; co-implemented TMS variability (target error) analyses. ADG jointly prepared figures and made significant contributions to all drafts of the manuscript.

Papers bound in Chapter 3:

Paper 4. On the Role of Suppression in Spatial Attention: Evidence from negative BOLD in human subcortical and cortical structures. André D Gouws, Ivan Alvarez, David Watson, Maiko Uesaki, Jessica Rodgers and Antony B Morland (2014). J Neurosci. 34(31):10347-10360

A.D.G. and A.B.M. jointly designed the experiments. A.D.G. wrote the stimulus code. A.D.G. acquired ~ 100 hours of imaging data (Experiment 1 = 40hrs : 10 subjects, 1hr session per condition (3), 1hr structural and retinotopy; Experiment 2 = 56 hrs; 8 subjects, 45 min session per condition (8); 1 hr structural and retinotopy). A.D.G. analyzed the neuroimaging data: processing of anatomical data including manual brain segmentation; defined regions of interest based on anatomical and retinotopic scans; wrote an analysis toolbox to extract blink and pupil information from eye video data. A.D.G. prepared the first draft of the manuscript, which was then edited jointly with A.B.M.

Papers bound in Chapter 4:

Paper 5. The Organization of the Visual Cortex in Patients with Scotomata Resulting from Lesions of the Central Retina. Baseler, Heidi; Gouws, Andre; Morland, Antony (2009). Neuro-Ophthalmology Volume 33, Issue 3 June 2009, pages 149-157.

&

Paper 6. Large-scale remapping of visual cortex is absent in adult humans with macular degeneration. Baseler, H.A., Gouws, A., Haak, K.V., Racey, C., Crossland, M.D., Tufail, A., Rubin, G.S., Cornelissen, F.W. and Morland, A.B. (2011). Nature Neuroscience 14(5) pp 649-655.

A.D.G. acquired all the patient (n=22; 16 completed all sessions) and control(n=24) data presented in these manuscripts; A.D.G. was responsible for maintaining patient relationships and contact enabling coordination of multiple scanning sessions across two sites (Royal Holloway and York). A.D.G. made significant contributions to all types of data analyses; processing of anatomical data including manual brain segmentation. ADG jointly prepared figures and made significant contributions to all drafts of the manuscript.

Paper 7. Objective Visual Assessment of Anti-Angiogenic Treatment for Wet AMD. Baseler, Heidi, A., Gouws, A., Crossland, Michael D., Leung, Carmen, Tufnail, Adnan, Rubin, Gary, S. and Morland, Antony, B. (2011). Optometry and Vision Science.

(Ongoing project) A.D.G. acquired all the patient data; A.D.G. was responsible for maintaining patient relationships and contact enabling coordination of longitudinal scanning sessions. A.D.G. made significant contributions to data analyses; processing of anatomical data including manual brain segmentation. ADG jointly prepared figures and made significant contributions to all drafts of the manuscript.

Integrative Chapters:

Properties of Visual Field Maps in Health and Disease

"They were maps that lived, maps that one could study, frown over, and add to; maps, in short, that really meant something."

— Gerald Durrell, My Family and Other Animals

Introduction

The mapping of spatially adjacent locations in the world around by spatially organized representations in the brain appears to be a highly preserved feature underlying much of neural architecture. Gerald Durrell's cartographic adventure involved spending time in his geography lessons filling in maps of the world with often weird and wonderful details. Drawing cartoons of significant landmarks, animals and plants in relevant geographical locations helped him remember and understand those maps better. Our adventure characterizing maps in the human brain has its parallels. All maps are only representations of the world around us. In terms of spatial extent, maps are usually scaled representations of that real world. Once such a scaled representation of the real world is established, further copies of that map can be created and each copy can display a specific metric for every location on the map. Depending on what we aim to learn, we study these maps at different resolutions to make either more general or more spatially specific observations. We can study a location on a map to determine how extensively and how robustly it is connected to other locations on the map. We can infer, and sometimes measure, how the change in one represented metric on a map might have 'downstream' effects on other metrics represented on a copy of that map. And when our maps become compromised and no longer offer a complete or good representation of the current state of the world, we may have to interpolate and base our behaviour on experience of what those maps looked like before, or even what such a map should look like.

This thesis describes research characterizing maps in the human visual system. This research included the development and use of novel tools to interrogate the structural and functional properties of visual field maps in normally sighted individuals, culminating in the assessment of visual field map properties in patients with visual deficits.

What is a visual field map?

Rays of light are reflected by objects in the visual world, subsequently travelling through the lens of the eye. A *transformation* of the visual world occurs at the lens: the image of the world is flipped, i.e. rays from the upper left visual field fall on the lower right retina of either eye, rays from the lower right visual field on the upper left retina, etc. The spatial configuration of the optic nerve projection from the retina to the lateral geniculate nucleus (LGN) is arranged such that neurons arising from spatially adjacent locations in the retina project to spatially adjacent positions in the LGN, preserving the retinal visual hemi-field map. The same spatial configuration is preserved in the subsequent

projection from the LGN to primary visual cortex, V1. Neighbouring V1 is a secondary map, V2, and beyond that there are additional visual maps.

Figure 1 provides a schematic of the transformation of a visual scene to the cortex. The key features are: (1) the preservation of spatial adjacency (or mapping) from the scene to the brain's representations of that scene; (2) the transformation of the visual field to an inverted image from the left visual field to the right hemisphere (and vice versa); (3) that multiple hemi- and quarter-field maps of the scene emerge at the cortical level; (4) that a disproportionately large amount of cortex appears to be dedicated to the central visual field relative to the peripheral visual field.

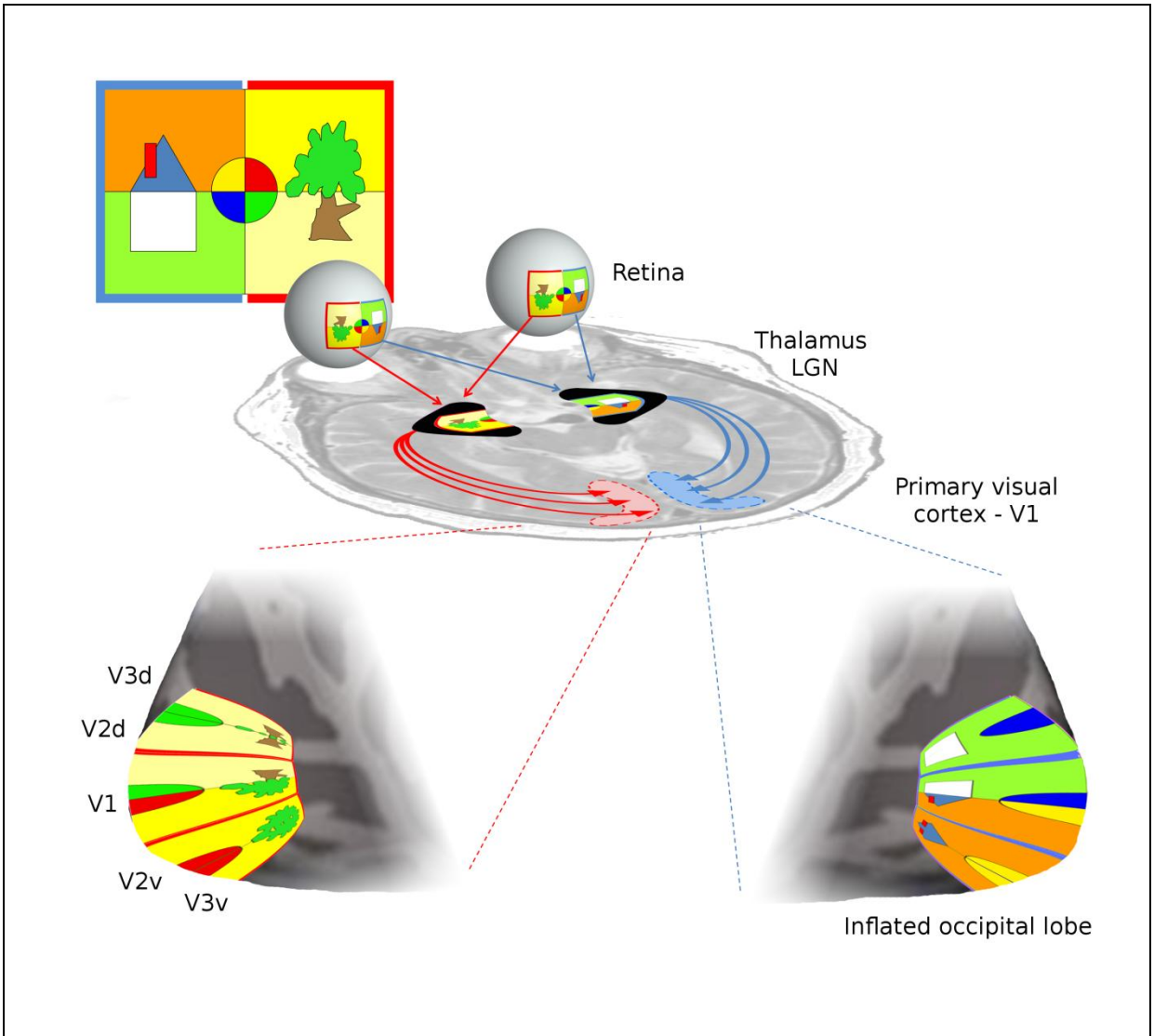

Figure 1. Transformations of the visual scene through the retina, to the LGN and on to primary visual cortex.

A brief history of visual field mapping

Although the camera obscura had been in use since the time of Aristotle, and lenses for nearly 300 years, it took until the 17th century for astronomer Johannes Kepler to understand and accurately describe the way that an inverted image could be produced through a lens. What made Kepler's works (Paralipomenes, 1604 and Dioptrica, 1611), truly revolutionary was his concept of a spatially organized replica or "image" ("pictura" or painting) of a scene that could be reproduced when rays of light reflected by objects in that scene were regrouped, or *focused*, by a lens onto a surface producing a *map*. The first evidence that these maps were preserved beyond the retina in the mammalian cortex began to emerge nearly 250 years later. While Munk (1881; focal ablations in dogs), Henschen (1893; patients with focal lesions) and Inouye (1909; war victims with focal injuries) all made significant contributions, it was the work of Holmes and Lister (Lister & Holmes, 1916; Holmes, 1918) on World War I casualties that started to reveal the complete spatial arrangement of primary visual cortex we are familiar with today. Holmes & Lister confirmed that the upper retina (lower visual field) is represented in the dorsal calcarine while the lower retina has a ventral calcarine representation; they also showed (as Inouye had suggested) that macular representations lay more posterior in the calcarine sulcus than representations of the peripheral visual field.

The ability to characterize maps *in vivo* in human subjects became reality some 70 years later with the advent of molecular and metabolic imaging techniques. Fox et al (1986) used positron emission tomography (PET) in alert human subjects to confirm the anterior/posterior calcarine representations of central/peripheral visual field representations, respectively. Horton and Hoyt (1991) used another technique, magnetic resonance imaging (MRI), to study the anomalies in brain structure of lesion patients, relating these lesions to the patients' observed visual deficits and revealing a "macular bias" or "cortical magnification" (e.g. Brewer et al., 2002; Qiu et al., 2006) previously reported in other species. Beyond being able to provide high resolution structural information, Ogawa and colleagues (Ogawa & Lee, 1990; Ogawa et al., 1990a; Ogawa et al., 1990b) revealed that MRI signal amplitude (or *response*) is sensitive to local blood oxygenation levels in the sampled tissue: the blood oxygen level dependent (BOLD) response. Measured over time, the inference was that local blood oxygenation changes would indicate changes in local metabolic demands, acting as a marker of varying brain activity. By alternating periods of sensory stimulation with periods of non-stimulation (*on-off* designs), several groups showed that the BOLD response was indeed modulated as a function of sensory stimulation, both in visual cortex (Kwong et al., 1992; Ogawa et al., 1992) and motor cortex (Bandettini et al., 1992). These results marked the birth of *functional* magnetic resonance imaging, fMRI, as we know it today.

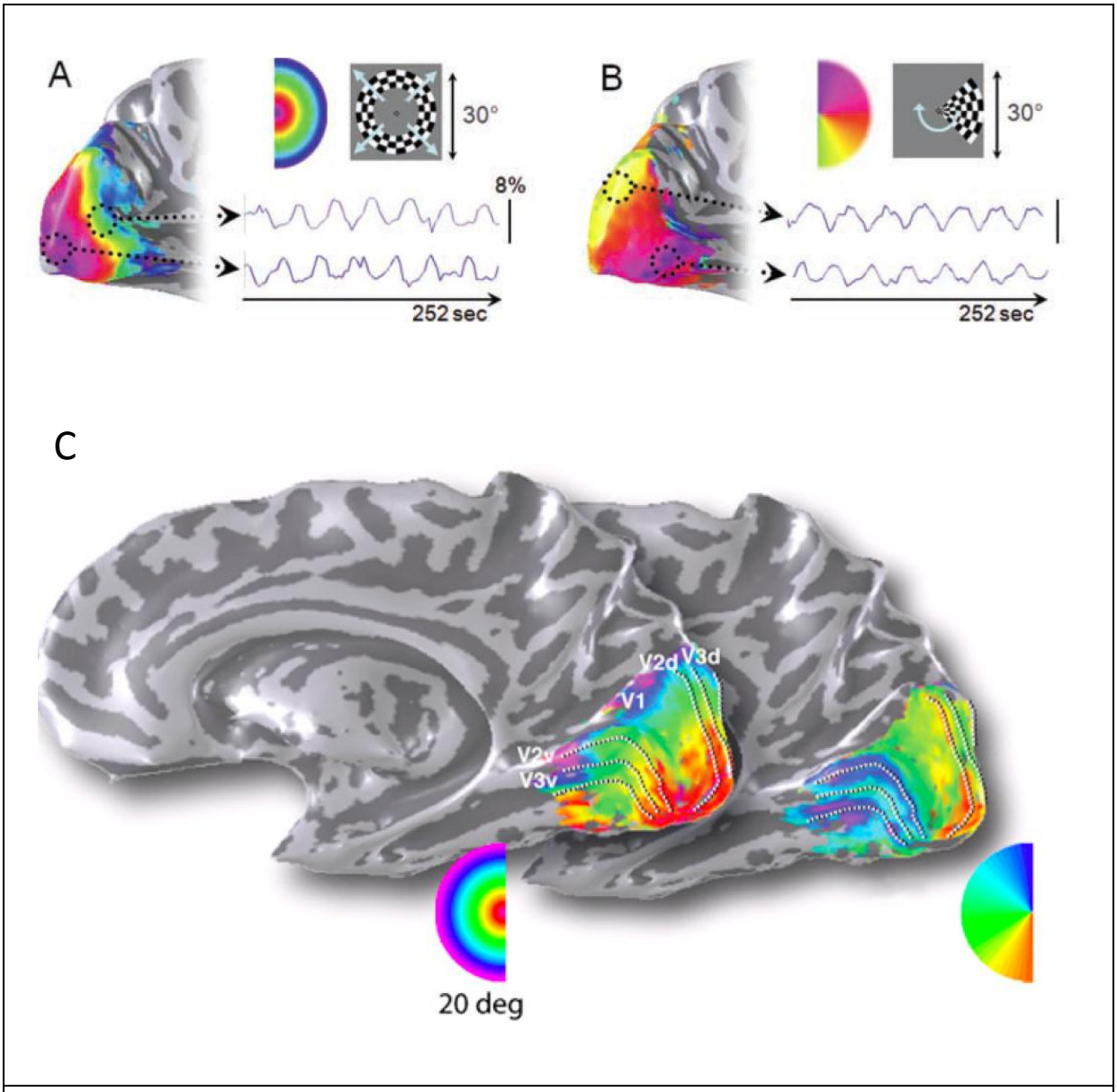

Figure 2. Phase-encoded retinotopic mapping. (A) Expanding ring and (B) rotating wedge contrast patterns elicit waves of cortical activity across visual areas in the occipital cortex. This activity is shown in false color on surface reconstructions of the occipital lobe. Each color represents a particular phase of the hemodynamic response waveform, which corresponds to the stimulation of a particular region in the visual field. The phase differences between two different regions are shown in the inset BOLD time series data for eccentricity (A) and polar angle (B) data. (C) Inflated representation of the right hemisphere showing eccentricity data (left) and polar angle data; also indicated are the boundaries of visual areas which can be inferred from the phase reversals in the color maps on the polar angle data. A&B adapted from McKeefry et al., 2009, C adapted from Wandell, 2007.

Other research groups were designing a set of stimuli optimized to highlight retinotopic representations in cortex. Instead of contrasting left vs. right visual field, or centre vs. periphery in on / off type block designs, these groups postulated that progressively moving a stimulus through spatially adjacent positions in the visual field should in turn activate spatially adjacent regions of cortex representing those stimulated sections of the visual field. While a continuous measurement is made from the brain, therefore, the peaks in the responses of two brain regions representing spatially adjacent locations in the visual field should be shifted in time relative to one another as a consequence of the stimulus moving through those regions at different times in the stimulus cycle. Crucially, these groups realized that two different stimulus types would be particularly useful: first, to represent increasing eccentricity from the centre to the periphery, a gradually expanding annulus stimulus could be used; second, a wedge-type stimulus rotating clockwise or anticlockwise about the centre of the display could be used to map polar angle. Results from three laboratories were subsequently published, proving that this technique was highly successful in allowing the reconstruction of retinotopic maps in human visual cortex (Engel et al., 1993, 1994; DeYoe et al., 1994; Engel et al., 1997; Sereno et al., 1995). This approach has become standard technique in neuroimaging, and is commonly referred to as "phase-encoded retinotopy" with analysis of the "traveling-wave of activation" across adjacent visual field representations. A graphical summary of the technique is presented in Figure 2.

In summary, by the late 1990s converging evidence gathered in lesion, electrophysiological, in vivo surgical electrocorticography and functional imaging studies, in a number of species, provided indisputable evidence that multiple maps of the visual field are present in the brain (for a review of more historical, non-imaging mapping see Glickstein & Whitteridge, 1987; for a review of more recent advances see Wandell et al., 2007). This raises a question: why do *multiple* maps exist?

Functional specialization and maps

In 1861, Paul Broca reported on two patients that presented with a profound and specific behavioural deficit: both patients had lost the ability to speak coherently despite being able to understand speech and, more broadly, normal cognitive functions. Intriguingly, Broca's post-mortem dissection revealed that these two patients had highly comparable, focal left frontal lobe lesions. Broca inferred that this region of left-frontal brain was *functionally specialized* for the production, but not detection or understanding of language.

Functional specialization has subsequently been revealed to be fundamental organizing principle across all lobes of the brain and across species (e.g. Zeki, 1990). This 'modularized processing' has

been most extensively characterized in the visual brain, where the aforementioned mapping experiments had already confirmed the presence of multiple representations of the visual world. Although the list is growing, currently there are thought to be as many as 20 visual areas (maps) in the human brain (Wandell, 2009). Functionally specific activity measured within individual maps reflects stimulus group or feature preference of the neurons forming that map and appears highly conserved across higher primates, as confirmed with a number of techniques (e.g. Zeki, 1990; Malach et al., 1995; Kanwisher et al., 1997). Homology of visual areas can be demonstrated both by function and structure: the macaque middle temporal area (V5/MT) for example has been shown to show very similar response characteristic to visual area 5 (V5/MT+) in humans, both being highly specialized to the processing of different types of motion while showing distinctly higher myelination than other corresponding homologous retinotopic maps (e.g. V2, V3 and V4/hV4; see Glasser & Van Essen, 2011). More recent developments based on, but extending phase-encoded retinotopy techniques allow estimates of metrics like receptive field size of the neural subpopulations within a given map (e.g. Dumoulin & Wandell, 2008). Again, these receptive field size estimates derived from fMRI data proved to be highly consistent with measurements made in a variety of species with a number of techniques.

Visual maps can be detected even before the cortex, in the superior colliculus, lateral geniculate nucleus and pulvinar nucleus of multiple species (e.g. Chen et al., 1999; Katyal et al., 2010; Li et al, 2013). Beyond the visual domain, maps are a feature of the sensory human brain in general. Features in the world that are topographically organized can be mapped in the brain, as shown by somatosensory and motor cortices where adjacent body parts are represented by adjacent cortical regions (e.g. Servos et al., 1998). Spatial maps of the auditory spatial surround remain elusive in humans although evidence exists in other species (e.g. Knudsen, 1982), while maps along the continuum of pitch (frequency) have been detected (Pantev et al., 1997; Wessinger et al., 1997; Barton et al., 2011; Jiang et al., 2014). Indeed, other behaviourally relevant features that can be organized along a continuum appear to be mapped by the brain too, for example numerosity in the parietal cortex (Harvey et al., 2013).

We now turn our attention to the specific research questions relating to visual field maps that I have tried to address in the articles bound in this thesis.

The aims of this thesis: What were we aiming to learn about maps?

My research interests lie in interrogating different maps to untangle the roles that those brain regions play in the processing of visual features. The papers bound in this thesis addressed the following questions:

1. Where are maps? – Individual differences in location elucidated with fMRI
2. Do maps in lateral occipital cortex exhibit functional specificity? – investigated using TMS
3. Are signals in maps modulated by attention?
4. Do maps change as a result of disease of the retina?

My approach to addressing these questions, with relevant publications, is broken down as follows in the main body of this thesis:

Chapter 1: Developing visualization software

Before embarking on my interrogation of visual maps, I needed to develop software tools to bring the data formats and localization procedures for the different techniques into a common framework. In *DataViewer3D: An Open-Source, Cross-Platform Multi-Modal Neuroimaging Data Visualization Tool,* I described the development of a software package to bring together data from different imaging modalities, operating platforms and software packages, introducing some novel and useful techniques for interrogating data that were not available at the time. While this software was developed with my research goals in mind, it also serves as a general purpose piece of neuroimaging visualization software, which is now in its 4th version and is freely available to the research community.

Chapter 2: Probing visual field maps with TMS

In this section of the thesis I described how we quantified individual differences in map location, and subsequently probed visual map function with TMS. In *The Non-Invasive Dissection Of The Human Visual Cortex: Using FMRI and TMS To Study The Organisation Of Vision In The Brain,* the software tools I developed gave novel insights into the variability in visual map location in individuals. Having highlighted the importance of using fMRI-guided TMS rather than more traditionally used 'fiducial-reference-frame' guided TMS, we used these techniques to locate spatially distinct (but adjacent) visual field maps and used TMS to dissociate the functional properties of these maps at a spatial scale not previously thought possible with TMS. These results are described in *Specialized and independent processing of orientation and shape in visual field maps LO-1 and LO-2*.

Chapter 3: Assessing the effect of attention on maps

In parallel with probing the specialization of higher visual areas, we were also interested in finding out where in the visual system attention modulates responses. We were particularly interested in the interaction between responses at attended locations in the visual field and suppression of responses at unattended locations. In *On the Role of Suppression in Spatial Attention: Evidence from negative BOLD in human subcortical and cortical structures*, we examined cortical and subcortical maps and the dependence of the responses there on spatial attention. In this work we also revealed the importance of accounting for systematic blinking, which can contaminate fMRI measures of visual responses.

Chapter 4: Visual field maps in retinal disease.

As maps appear to be such a highly preserved feature of cortical organization, we also questioned what happens to these maps when input to them, caused by retinal disease, is removed. This chapter summarizes the results published in a series of 3 manuscripts that sought changes in maps in a relatively large cohort of patients with retinal disease. In *The Organization of the Visual Cortex in Patients with Scotomata Resulting from Lesions of the Central Retina* we summarized preliminary findings and later in *Large-scale remapping of visual cortex is absent in adult humans with macular degeneration* published a full account of the study. We subsequently went on to study longitudinal changes in maps in AMD patients receiving treatments aimed at restoring retinal function. A case study from this ongoing investigation was reported in *Objective Visual Assessment of Anti-Angiogenic Treatment for Wet AMD*.

Exploring maps in health and disease: How do my publications form a coherent body of work?

The software I developed, described in Chapter 1, allows visual maps to be localized. This allowed me to demonstrate relatively large individual differences in visual area location with respect to scalp landmarks in the first part of Chapter 2. Consequently, when probing the functional specialization of visual maps with TMS, careful localization of maps in each individual was essential. This was particularly important when TMS was applied to small neighbouring visual areas, as in the second paper of Chapter 2 which demonstrated dissociable functional properties in the visual field maps of LO-1 and LO-2. In Chapter 3, we examined the effect of attention on visual field maps and showed that maps can elicit varying levels of response, both activation and suppression, that vary as a function of task and the spatial extent of the locus of attention. Furthermore, In Chapter 4, we considered what happens to the responses in these highly conserved, developmentally established maps when input to

them is removed later in life as a result of retinal lesions. I showed that there is very little evidence that the responses in the parts of maps that no longer receive input change after retinal lesion, challenging the notion that visual maps can ‘reorganize’ in the absence of visual input. The work as a whole therefore probes the individual differences in map locations, the difference between the processing undertaken in neighbouring maps, how an early attention dependent suppression can be observed in early maps of the visual system and finally how maps appear robust to change in adulthood when input is removed. The research is therefore highly related and forms a coherent body of work.

Chapter 1: Developing visualization software

Bound thesis paper 1. *DataViewer3D: An Open-Source, Cross-Platform Multi-Modal Neuroimaging Data Visualization Tool*. Gouws A, Woods W, Millman R, Morland A, Green G. (2009). Frontiers in Neuroinformatics 3:9.

A.D.G. wrote the software package and the manuscript.

Advances in neuroimaging technology have lead to a boom in human neuroscience over the past 25 years. The ability to non-invasively study the human brain with increasingly sophisticated and affordable equipment means that neuroscientists often also take a more *multimodal* approach to studying the brain.

Depending on the question being asked, there are clear advantages and disadvantages to certain techniques over others. The high temporal precision of EEG / MEG help to inform us about the evolution of cortical processing across a network of brain regions, but only give us a very coarse estimate of the spatial arrangement of the nodes within that network. Conversely, PET, fMRI and fNIRS (functional near-infrared spectroscopy) allow us to locate the physical location of the sources of brain activity with much higher spatial precision, but are unable to provide accurate information about the temporal evolution of cortical activity. Structural MRI techniques including diffusion weighted imaging can be used to inform us about the structural integrity and the likely routes of information transmission between nodes in the brain network. And yet none of the aforementioned techniques can really tell us anything about the causality of the relationships between the signals we have measured. For this we need to study patients with focal lesions or turn to techniques like TMS that allow us to disrupt activity focally at certain nodes in the brain network. These disruptions allow us to see what the impact on signals elsewhere in the network is, and to measure any correlated changes in behaviour and perception. Collaboration across different imaging acquisition techniques therefore gives the neuroimaging community the opportunity to compare and contrast results from different modalities and analysis approaches, and the potential to provide converging evidence to support the answers to their research questions.

Beyond the political and financial challenges facing laboratories taking a multimodal approach to neuroimaging, at least one other significant hurdle was evident to me in early days of my research. This hurdle is a result of the complex and diverse range of neuroimaging acquisition and analysis packages available to researchers. Often data acquisition packages are vendor specific and may result in vendor specific data output formats. Subsequent data analysis packages may also be vendor or site specific. Furthermore, data visualization formats and packages that represent the final step in the

processing stream may also be vendor or site specific. As acquisition and analysis packages are often customized solutions developed by a specific site to address their own specific requirements, the sharing of data and the reproducibility of results across sites can be challenging. Even within site, researchers may have to compare the visual output of two or more different packages side-by-side, sometimes comparing two-dimensional outputs from one package with 3-dimensional outputs from another. The lack of a like-for-like comparison of results in a common coordinate space increases the potential for misinterpretation of results.

With this in mind, I began development of one of the first software packages that attempted to bridge a gap: a software package that allows researchers to bring together the results from a number of different analysis packages and visualize the results in a common coordinate space and display two-dimensional, three-dimensional or even 4 dimensional data. The software package, Dataviewer3D (DV3D) was built with the following core design principles in mind:

- A visualization tool for the output of existing analysis packages – not an analysis tool per se
- Modular, transparent, scalable (and thus accessible) open-source framework that is platform independent
- Support (modularly expandable) for different data types and formats
- Support for 2D, 3D and 4D data
- A common coordinate space for multi-modal data types
- Co-registration with published atlases
- Export routines for sharing and publication
- A reproducible workflow to support provenance (e.g. generation of saved scripts to reproduce images used in publications)

Further detail and examples of how each goal was achieved at the time of the first release package (2008) are available in the manuscript.

In the following pages of this thesis, I provide a panel of images highlighting the capabilities of DV3D. In addition to the core design principles of DV3D, I also attempted to address the lack of certain features not available in already existing software packages. In Figures 4-6 in the following pages, the image panels demonstrate these features for reference, as we will refer back to some of these features in later publications bound in this thesis. They include:

- Figure 3. The ability to extract surface representations (especially cortical surface) very quickly without having to perform large amount of pre-processing;

- Figure 4. The provision of a technique to better illustrate the spatial extent of 3D volumetric statistical maps (i.e. 3D blobs of activation on a 3D brain);

- Figure 5. The ability to interactively re-slice (reformat) 3D volumetric data in real time in any plane.

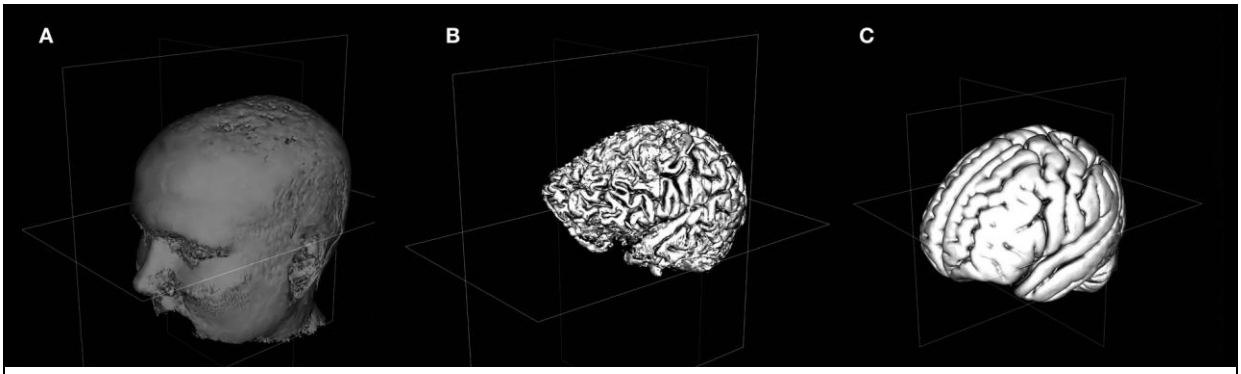

Figure 3. Extracting surfaces from volumetric data. Isosurface techniques, the ability to extract a surface based on 'joining the dots' of manifold at a single scalar value in a volumetric dataset, can be used to extract the scalp (A) or cortex (B) in high resolution structural MRI data in matter of seconds. (C) The equivalent cortical surface extraction for the MNI brain. Adapted from Gouws et al., 2009.

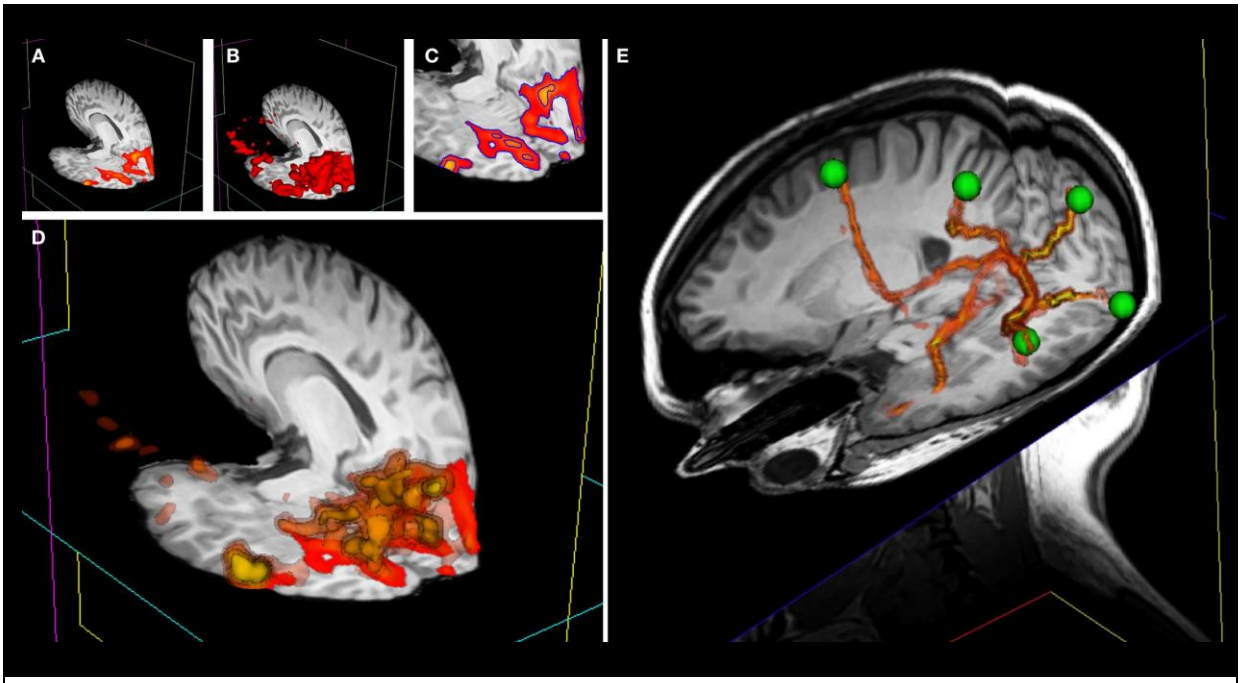

Figure 4. A novel technique for rendering 3D volumetric statistical maps. (A) Standard technique for displaying statistical data on 2D planes. (B) As in Figure 4, isosurface techniques are used to extract a single surface at a particular scalar value in the volumetric data resulting in a 3D representation of the statistically significant volume at a given threshold. (C) A 2D depiction highlighting how isosurface techniques are capable of 'outlining' multiple scalar values simultaneously, iso-lines shown here in blue. (D) Multiple isosurfaces can be extracted and rendered simultaneously, with disticnt color mapping of all boundaries between the lowest and highest extracted boundary; here the lowest values are rendered with higher transparency so that underlying, higher-threshold surfaces can be seen simultaneously. (E) The technique described in (D) is useful for probabilistic MRI tract visualization: output from FSL's Probtrack toolbox is rendered using the 3D overlay technique as yellow-to-red isosurfaces. The green spheres indicate the seed and target points. Adapted from Gouws et al., 2009.

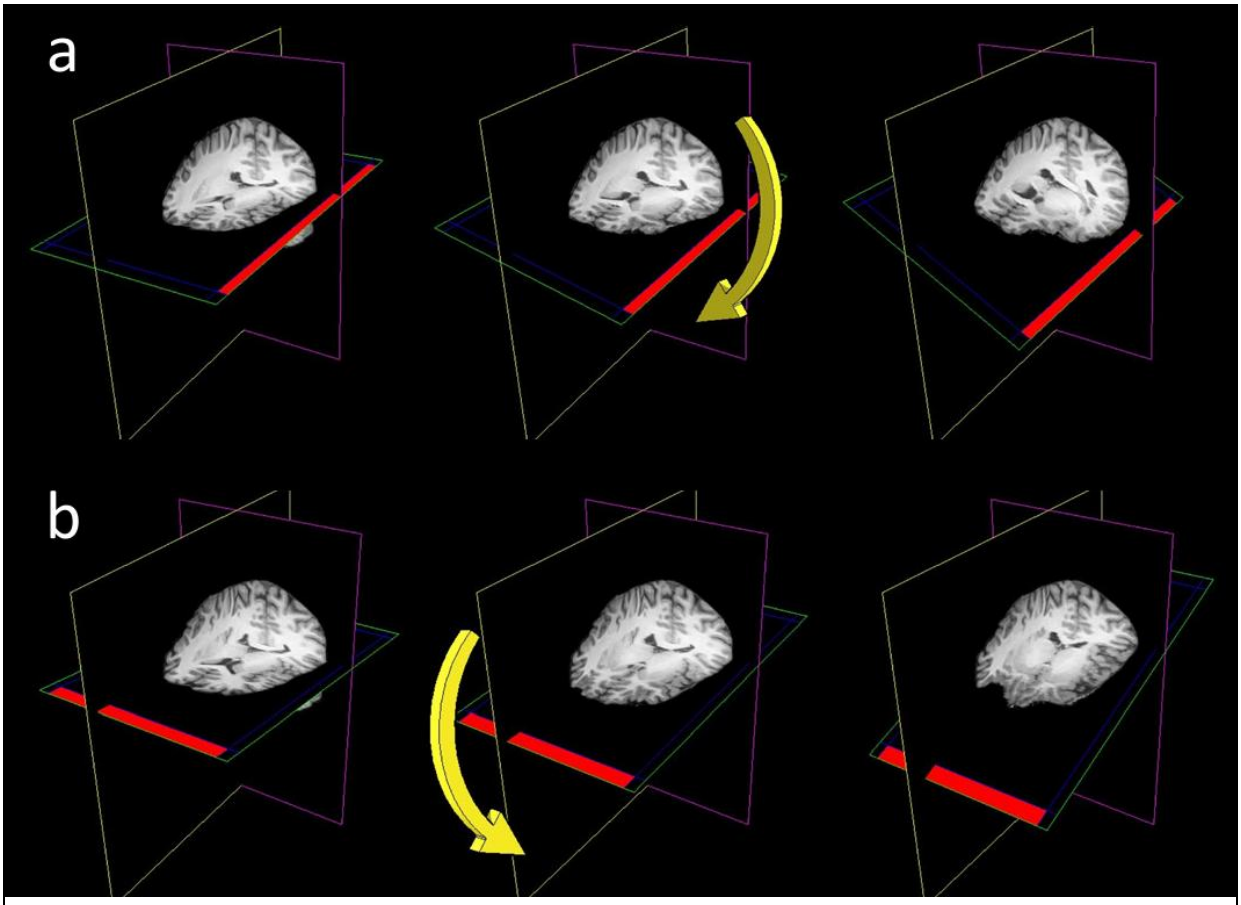

Figure 5. The use of plane widgets to show 3D volume data. Real-time reformatting of data (re-slicing in any direction) is possible by tilting planes around their origin. (a) Axial plane is rotated around the y-axis by clicking the edge (show in red) and moving the mouse. (b) Axial plane is rotated around the x-axis by clicking on another edge (shown in red). Adapted from Gouws et al., 2009.

Software feature	FSLView	MRICron	3D Slicer	DV3D
NEUROIMAGING DATA SUPPORT				
Optimised for neuroimaging	✓	✓	–	✓
Structural MRI	✓	✓	✓	✓
Functional MRI	✓	✓	✓	✓
DTI – probabilistic	✓	–	–	✓
DTI – tractography	–	–	Calculated online	Loaded from memory
DTI – 2d vectors	✓	–	–	✓
DTI – 3d vectors	–	–	✓	✓
MEG/EEG contour plots (2D and/or 3D)	–	–	–	✓
MEG/EEG 3d time-series on surface	–	Single instant	–	Full dynamic
MEG/EEG dipoles	–	–	–	✓
MEG/EEG butterfly plots	–	–	–	✓
DATA EXPLORATION				
2D statistical map overlay	✓	✓	✓	✓
3D statistical map overlay	✓	–	–	✓
Interactive surface extraction	–	–	Complex watershed	Simple isosurfaces
Real-time atlas cross-referencing	If data in MNI space	–	–	4 × 4 Transform required
COMPLEX VISUALIZATION FUNCTIONS				
Real-time reformatting	–	–	Single plane	Multiple planes
Interactive data intersection	–	–	–	✓
Interactive time-series interrogation	2d fMRI only	–	–	2D and 3D fMRI, EEG and MEG
Batch processing from command line	✓	–	–	✓
EXPORT				
Static images	–	✓	✓	✓
Movies	–	–	✓	✓
Real-time streaming	–	–	–	✓
TECHNICAL				
Main code base language	C,C++,Tcl/Tk	Pascal	C++,Tcl/Tk	Python
Platform independent code base	–	–	–	✓
Access to parallel processing	–	–	–	✓

Table 1. Feature summary and comparison of imaging data visualization packages.

In summary, we achieved the majority of the design objectives we set for ourselves when first designing DV3D. The key features and functionality achieved with DV3D, relative to similar programs available at the time (2008) are summarized in Table 1. Since 2008, development on the package has continued and a new version of the program is in the pipeline to address the software and platform changes that have occurred over the past 7 years. In the context of this thesis, the 3D isosurface rendering and interactive reformatting (re-slicing) techniques in particular would prove invaluable tools for assessing maps in our subsequent studies.

Chapter 2: Probing visual field maps with TMS

Bound thesis paper 2. ***The Non-Invasive Dissection Of The Human Visual Cortex: Using FMRI and TMS To Study The Organisation Of Vision In The Brain*****. McKeefry DJ, Gouws. A, Burton MP & Morland AB (2009). Neuroscientist 15: 489-506**.

ADG acquired 12 hrs of structural and fMRI data on 4 subjects across two sessions each. ADG analyzed the neuroimaging data: processing of anatomical data including manual brain segmentation; processing of correlation analyses and subsequent definition of visual map boundaries; implemented the visual area position variability analyses. ADG prepared figures for analysis and publication, and made significant contributions to all drafts of the manuscript.

Bound thesis paper 3. ***Specialized and independent processing of orientation and shape in visual field maps LO-1 and LO-2.*** **Edward H Silson, Declan J McKeefry, Jessica Rodgers, Andre D Gouws, Mark Hymers & Antony B Morland (2013) Nature Neuroscience 16: 267-269.**

ADG acquired 12 hrs of structural and fMRI data on 12 subjects. ADG co-analyzed the neuroimaging data: processing of anatomical data including manual brain segmentation; processing of correlation analyses and subsequent definition of visual map boundaries; implemented spatial analyses to calculate the ROI centres of mass for TMS targeting. ADG jointly designed and programmed the stimuli for the TMS experiments and aided in TMS data collection; co-implemented TMS variability (target error) analyses. ADG jointly prepared figures and made significant contributions to all drafts of the manuscript.

fMRI excels at spatially localizing activity correlated to a stimulus. It also offers the ability to characterize the relative activity in the localized region to different stimulus manipulations. However, the method alone cannot tell us whether the functional activity observed is *necessary* for a particular percept or behaviour. To establish a causal link between the activity in a region and behaviour, we can use TMS. The effect of TMS is often referred to as a 'transient virtual lesion' and has been extensively used to probe regional brain function (e.g. Pascual-Leone et al., 2000; Cowey & Walsh, 2000; Haung et al., 2005; Cowey, 2005). TMS is thus well suited to probing the function of individual visual maps to establish causal brain-behaviour relationships.

We used TMS to probe the functional specificity of two higher visual areas located in the lateral occipital cortex: LO-1 and LO-2. Broadly speaking, these areas are thought to have a role in the processing of objects and shape (e.g. Larson & Heeger, 2006; Larson et al., 2006). As the retinotopically organized maps of LO-1 and LO-2 lie immediately adjacent to one another, it is

particularly important that we have maximum possible confidence that we are targeting each map *selectively* in each individual subject. One common approach to defining TMS target sites has been the use of *fiducial references*, where anatomical landmarks (like the inion) on the surface of the scalp are used as reference points. From here, the coil is displaced a pre-defined distance across the surface of the scalp to a target position, typically defined by previous literature. This approach takes no account of the individual subject's anatomy other than the starting reference point, and is likely to induce errors in our attempted selective stimulation of either LO-1 or LO-2 with TMS. An alternative approach is to localize maps in individual subject anatomies for use as as targets, i.e. to use fMRI-guided TMS. But how much error *could* fiducial-guided TMS really induce?

Variability in visual areas is a challenge for TMS

The variability in size and location of visual areas across human subjects is well documented (e.g. Watson et al., 1993; Andrews et al., 1997, McKeefry & Zeki, 1997; Dougherty et al. 2003; Kammer et al. 2005a, 2005b). In the first paper bound in this chapter, *The Non-Invasive Dissection Of The Human Visual Cortex: Using FMRI and TMS To Study The Organisation Of Vision In The Brain*, we aimed to empirically re-demonstrate just how variable the position of higher visual areas can be, and highlight the implications this variation would have in the context of studies not using fMRI-guided TMS.

Phase-encoded retinotopic mapping was conducted in MRI for four subjects over multiple acquisition sessions. Visual area location can be viewed in the individual subject's brain by virtual dissection of the MRI data. Using the DV3D package we generated images of the locations of the visual areas in all four subjects. One such "cut-away" image of the individual anatomy was included in the manuscript, and demonstrates a clear qualitative difference in the position of V3a relative to variable scalp anatomy and local cortical folding patterns (Figure 6).

The "cut-away" technique used in Figure 6 allows no judgment of the map size or position relative to other maps, even within an individual, as the spatial representation of the map is two dimensional (the 'slice' we see). We used DV3D's 3D surface extraction techniques (Chapter 1) to extract a cortical surface for the individual subject and a surface representation of each visual map in the subject's dorsal stream (V1, V2d, V3d and V3a). By making the cortical surface transparent and overlaying color-coded 3D blobs representing the different visual areas, it is possible to visualize the relative map sizes and locations in the individual subject's brain. Furthermore we transformed each subject's anatomy into a canonical anatomical space (MNI) brain to allow a cross-subject quantitative assessment (normalized for within-subject brain size/shape) of the variation in visual area.

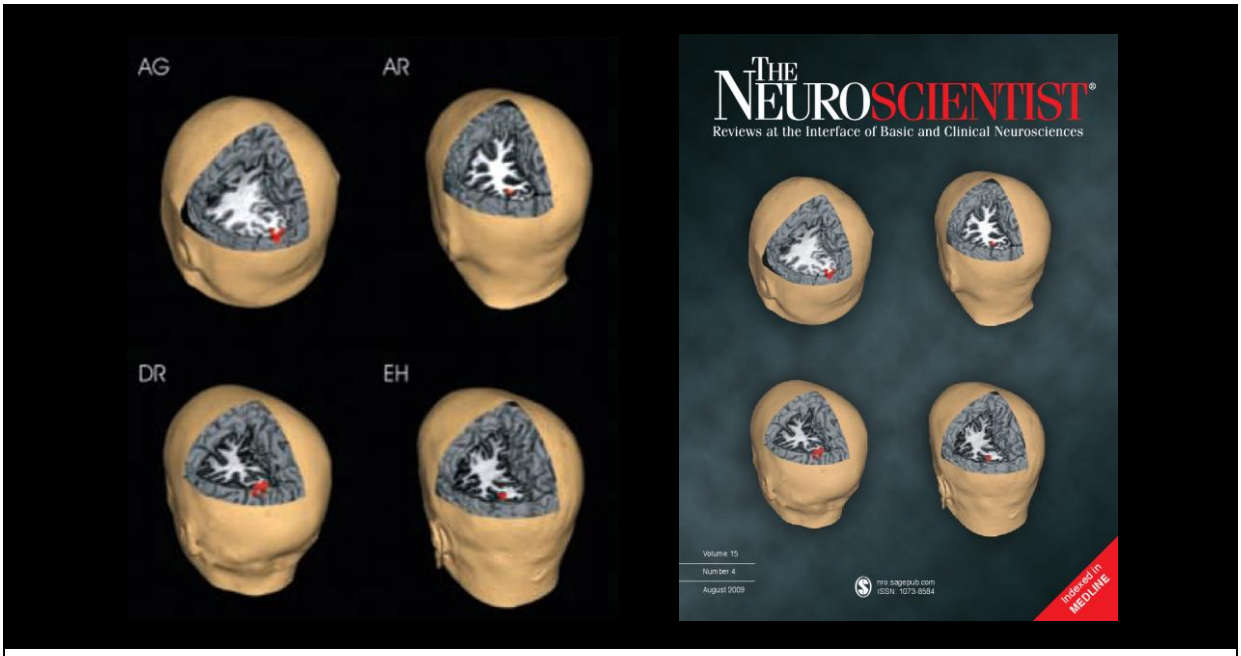

Figure 6. Position of V3a (red) is highly variable across individuals. Adapted from McKeefry et al., 2009.

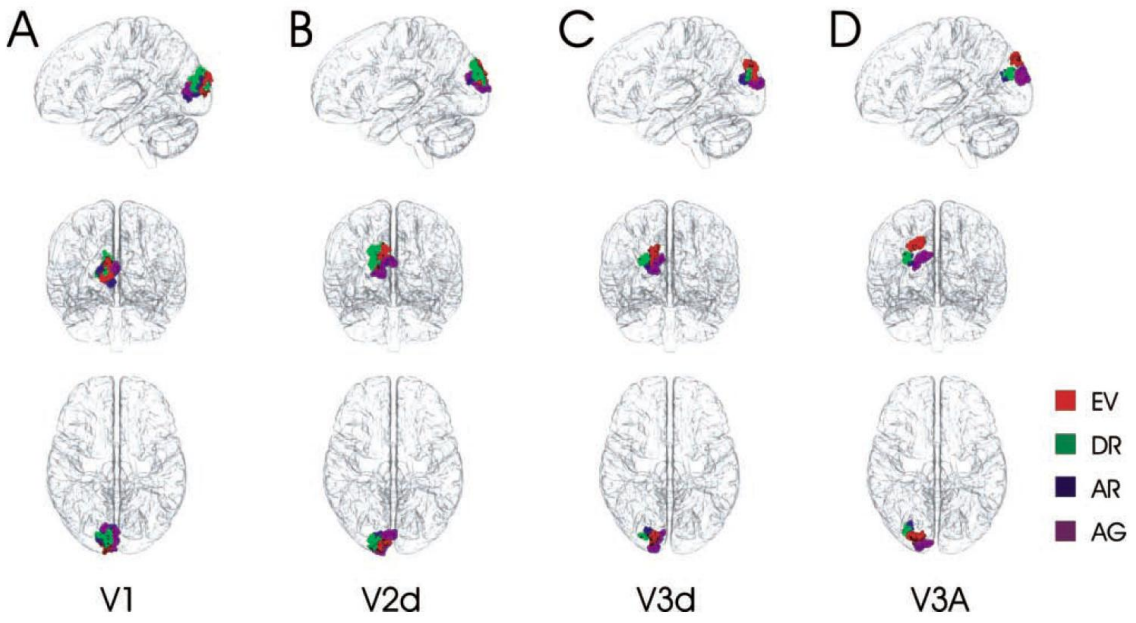

Figure 7. Variation in dorsal visual areas across subjects in MNI space. Each column (A-D) shows the spatial volume occupied by a particular visual area in four subjects, color-coded by subject. Adapted from McKeefry et al., 2009.

In Figure 7a we rendered the cortical surface of the standard brain and overlaid 3D visual area blobs representing the spatial extent of each subjects 'normalized' left hemisphere V1, colour-coded by subject. There are clear qualitative differences in both the position and size of V1, as expected based on previous work (Andrews et al., 1997). As we move further up the visual area hierarchy, through V2d, V3d and V3a (Figure 7b,c,d respectively), this individual variation in map location appears progressively more marked. Having successfully demonstrated qualitative differences in the position of visual areas across individuals (both in the individual anatomy and 'standard' space), we wanted to provide a more quantitative estimate of the effect that this variability could have on fiducial-guided TMS. DV3D was used to extract individual subjects' scalp surfaces and inion position for use as a reference point. We calculated the centre of mass of left V3a in the same coordinate space and the coordinate on the scalp mesh that had the shortest Euclidian distance from this target, the optimum position of the TMS coil for stimulation of V3a. Coordinates were first transformed into a canonical anatomical space (MNI). Figure 8 shows the variation in the position of this optimum coil placement position for the four subjects. Assessing the variation in the four coil positions revealed a mean Euclidian displacement difference of 19.8mm (from the mean of the four locations), with a range of 10.7 – 26.9mm.

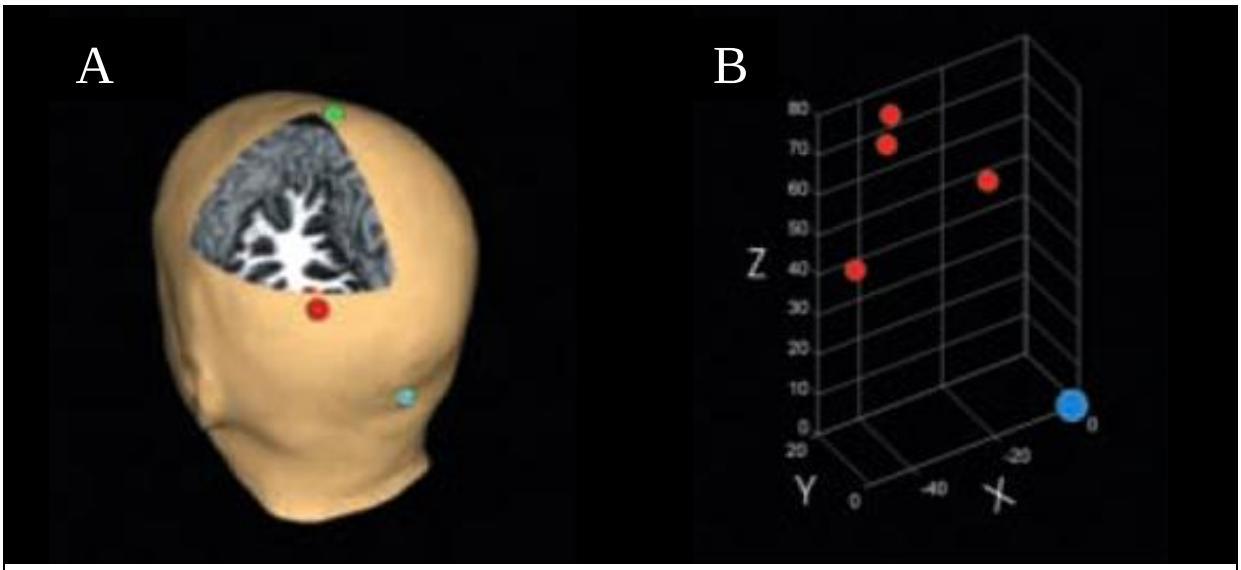

Figure 8. Optimum coil position for V3a stimulation by TMS is highly variable across subjects. **A**: the anatomy of a single subject, with the inion reference marked in cyan and optimum coil position for V3a stimulation in red. **B**: Red markers represent the optimum coil position in real world mm coordinates relative to the inion of four subjects, showing considerable variation (blue marker at the inion, X,Y,Z=0,0,0). Adapted from McKeefry et al., 2009.

Anatomical landmarks and standardized coordinates are thus insufficient for TMS to successfully dissect the functional properties of spatially distinct but adjacent visual field maps. Our subsequent TMS experiments on LO-1 and LO-2 thus used fMRI to generate target TMS sites. After all, the position of LO-1, lying immediately adjacent to V3a, would vary similarly to, if not more than, the position of V3a across individuals. The spatial separation between LO-1 and LO-2 is small meaning that the use of anatomical landmarks would likely result in non-specific disruption of these maps.

Using fMRI-guided TMS to dissociate function in adjacent visual maps: LO-1 and LO-2

A relatively large, object-selective (Malach et al, 1995) region of cortex commonly named the LOC (lateral occipital complex) extends from the dorsal aspect of the lateral occipital cortex into posterior aspect of the fusiform gyrus. At least two retinotopically organized neighbouring visual field maps, labeled LO-1 and LO-2, can be detected in or near this region (Larson & Heeger, 2006; Larson et al., 2006). Larson & Heeger (2006) used fMRI to show that LO-1 exhibits greater selectivity for the processing of orientation information, while LO-2 appears to show increased activity with increasing object complexity. LO-2 was therefore thought to perform more complex computations than LO-1, reflecting the processing of "shape".

We carried out measurements using fMRI-guided TMS to probe the function of LO-1 and LO-2 to establish a causal role in perception of orientation and shape. Based on Larson & Heeger's findings, we hypothesized: (a) that subjects would see a decrease in their ability to perform orientation discrimination judgments of a luminance grating relative to a reference grating when TMS was applied to LO-1 but not when applied to LO-2, a control site or with no TMS; (b) that subjects would see a decrease in their ability to correctly judge whether the shape of a radial frequency (RF) pattern was "smoother" or "pointier" than a reference RF pattern with TMS to LO-2 but not with TMS to LO-1, a control site or with no TMS.

In each subject we acquired retinotopic mapping data to define ROIs and determined 75% correct thresholds for a shape and orientation discrimination task. The sequence and timing of stimulus presentation was the same in both tasks, and also in the subsequent TMS test conditions. Under TMS conditions, a train of pulses was delivered concurrently with the presentation of the test stimulus (Figure 9a).

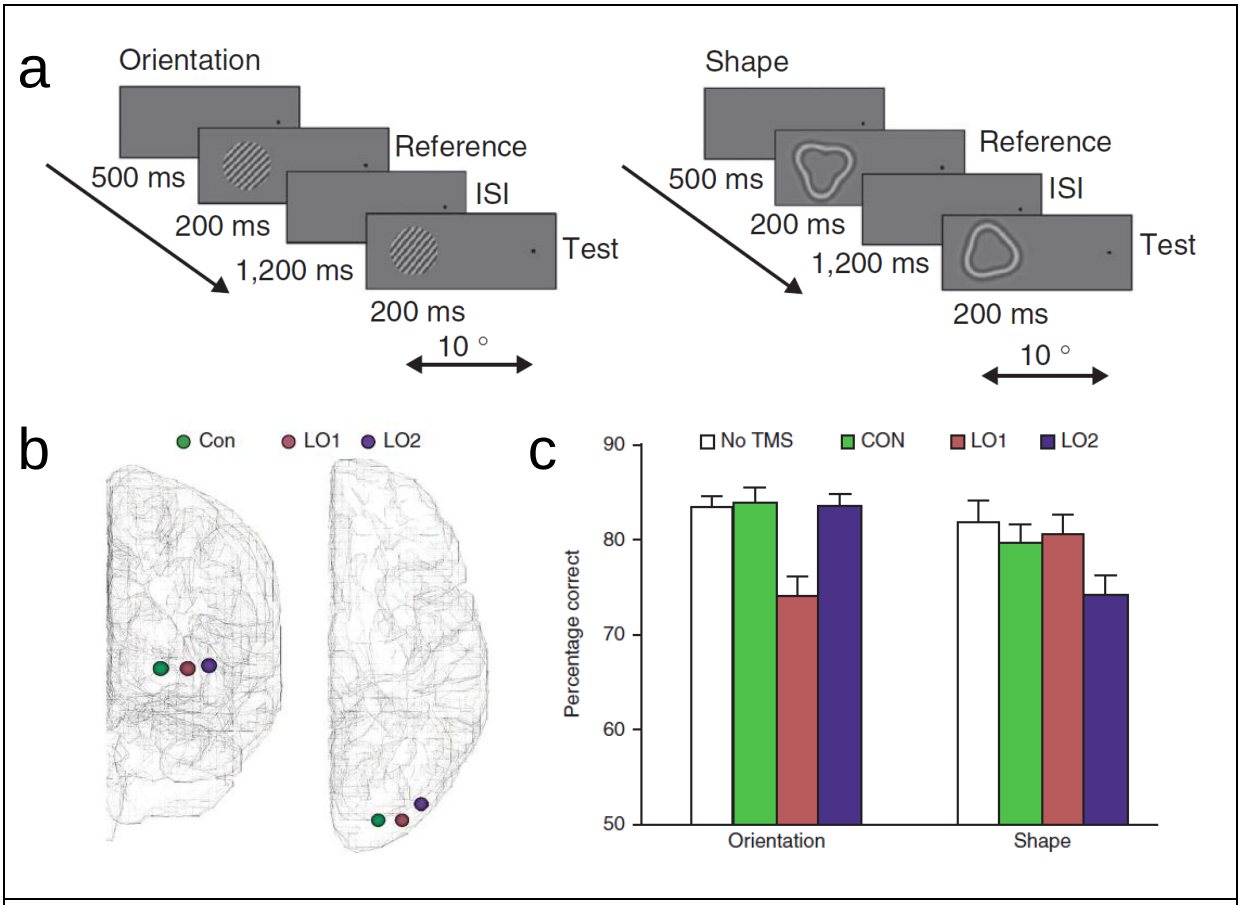

Figure 9. (a) Stimulus configuration and timings in the orientation task (left) and shape task (right). (b) Using DV3D to demonstrate the location and proximity of the centers of mass of the target regions, Control (Con) region, LO-1 and LO-2 in an exemplar subject. (c) Group mean % correct scores (n=12) under the three different TMS target site and a No TMS condition. Error bars are standard errors of the mean. Adapted from Silson et al., 2013.

The group mean % correct scores for the two tasks, under the 4 TMS conditions are shown in Figure 9c. As hypothesized, the data suggest that a decrement in performance in the shape task is only evident when TMS is applied to LO-2, and not when LO-1 or the control site are stimulated, or no TMS is applied. Conversely, a decrement in orientation discrimination is only evident when TMS is applied to LO-1 and not under any of the other conditions. Statistical analyses support these observations: a two-way ANOVA testing main factors of TMS site and task revealed a significant interaction between site and task, with no main effect of task but a main effect of TMS site. No pairwise target site comparisons proved significant. Post-hoc one-way ANOVAs grouped by task revealed a significant main effect of TMS site for both the shape and orientation tasks. In both cases, the significant effect of site was carried entirely by the hypothesized region of interest, LO-1 in the orientation task and LO-2 in the shape task.

It is possible that a more elegant stimulus manipulation could have been used in this study. The orientation discrimination task was performed on grating stimuli rather than the radial frequency patterns used in the shape discrimination task. While it may be possible to titrate the stimulus parameters of the radial frequency patterns to allow for these stimuli to be used for both tasks, our original pilot measurements attempting to do this proved more challenging than expected. We thus opted to test orientation discrimination with the more commonly used grating stimuli. Future work could address this issue.

The results of this study suggest that LO-1 and LO-2 perform preferred, specialized computations of different stimulus features *independently* of one another, as revealed by the double dissociation. Thus the computations performed in the "lateral occipital complex" may mimic the more general processing configuration present in other visual processing pathways where independent, parallel processing of different stimulus features has been identified (e.g. face processing in the ventral stream; Kanwisher et al., 1997). Furthermore, we demonstrated that TMS, when used within the correct spatial framework, can dissociate function in brain maps, even when those maps lie immediately adjacent to each other in the cortex.

Chapter 3: Assessing the effect of attention on visual field maps.

Bound thesis paper 4. ***On the Role of Suppression in Spatial Attention: Evidence from negative BOLD in human subcortical and cortical structures.*** **André D Gouws, Ivan Alvarez, David Watson, Maiko Uesaki, Jessica Rodgers and Antony B Morland (2014). J Neurosci. 34(31):10347-10360**

A.D.G. and A.B.M. jointly designed the experiments. A.D.G. wrote the stimulus code. A.D.G. acquired ~ 100 hours of imaging data (Experiment 1 = 40hrs : 10 subjects, 1hr session per condition (3), 1hr structural and retinotopy; Experiment 2 = 56 hrs; 8 subjects, 45 min session per condition (8); 1 hr structural and retinotopy). A.D.G. analyzed the neuroimaging data: processing of anatomical data including manual brain segmentation; defined regions of interest based on anatomical and retinotopic scans; wrote an analysis toolbox to extract blink and pupil information from eye video data. A.D.G. prepared the first draft of the manuscript, which was then edited jointly with A.B.M.

When attention is directed towards a behaviourally relevant stimulus, perception of that stimulus is enhanced while perception of unattended stimuli is impoverished (Posner, 1980; Duncan, 2006). While improved perception may result from enhanced neural activity at attended locations, suppressed neural activity at unattended locations could also contribute. As these opposite modulations in neural activity should occur in representations of different visual spatial locations they should be measurable in visual field maps with fMRI. Much of the literature that has examined attention-related changes in visual BOLD responses in humans (e.g. Gandhi et al., 1999; Martínez et al.,1999; Somers et al., 1999; O'Connor et al., 2002) has failed to take suppression into account, despite autoradiography experiments providing evidence of attention-related suppression in V1 and LGN in macaque (Vanduffel et al., 2000). Additionally, a potential signature of neural suppression is often routinely observed in fMRI experiments: when one area of cortex with a topographic representation of the world undergoes selective stimulation, resulting in an increase in BOLD response, the neighbouring regions of cortex that are concurrently non-stimulated often show a *decrease* in the BOLD response, or a *negative BOLD response* in the absence of stimulation.

It has been argued that negative BOLD responses simply reflect the reallocation of blood from non-stimulated cortex to adjacent stimulated cortex ("blood-stealing"). The work of Smith and colleagues (2004) however showed that a stimulus lateralized to a single visual hemifield not only produced activity in the contralateral V1, but also produced negative BOLD in V1 ipsilateral to the lateralized

stimulus. The arterial blood supply to left and right V1 are largely independent, suggesting that blood-stealing alone cannot account for the presence of negative BOLD responses. With respect to our main interest - visual field mapping - negative BOLD responses are interesting in that they may represent the action of a genuine, spatially organized mechanism that acts to *suppress* neural activity. This working hypothesis makes another prediction: the negative BOLD responses in these regions may be dependent on other factors like the attentional load dedicated to locations where relevant stimuli appear. An earlier study (Smith et al., 2000) had already showed that cortical negative BOLD signals were task (attention) dependent. Another study (O'Connor et al., 2002) demonstrated that attention modulates ("enhances") positive BOLD responses to attended locations at the level of the LGN. Is it thus also possible to find signature of suppression of unattended locations in LGN maps and, if so, to characterize the relationship between these subcortical signals of suppression with those measured in cortical maps?

Our experiment was thus designed to address the following questions: First, we asked whether or not we could detect negative BOLD in subcortical structures; Second, if detected either cortically and/or subcortically, are these negative BOLD responses dependent on attention to the stimulus; Third, does the amount of suppression at unattended locations in early visual areas present as a scaled inversion of the enhancement of responses at attended locations?

We used a stimulus (large, high contrast drifting grating) lateralized to a single visual field that would drive a positive response in the contralateral hemisphere and (hopefully) negative BOLD in the ipsilateral hemisphere (Smith et al., 2004). Functional imaging of subcortical structures is particularly challenging due to a number of factors, the most obvious of which is size. The LGN not only varies in size across subjects, but is small (typically 100-150 mm^3; Andrews et al., 1997) compared to the cortical structures we image, giving only a few voxels (circa 20-30) to measure from. This lateralized stimulus was chosen to give us maximum chance of detecting negative BOLD in the LGN ipsilateral to the stimulus as such suppression would be spatially distinct from the responses in the contralateral LGN. We could manipulate subjects' spatial attention in 3 ways: (1) no attention: view the scene passively; (2) lateralized attention: attend to the drifting grating; (3) sustained central attention: count configurational changes at fixation ignoring the rest of the scene.

In 10 subjects, we first performed phase-encoded retinotopic mapping in MRI, and acquired standard (whole head T1-weighted) and less standard (proton density) images. Early cortical visual areas (V1-V3) were reliably identified using the retinotopy data. V5 can be reliably identified from landmarks in high resolution anatomy (Dumoulin et al., 2000) and the LGN from the tissue contrast in proton density-weighted images (Fujita et al., 2001), both process benefitting from the real-time re-slicing

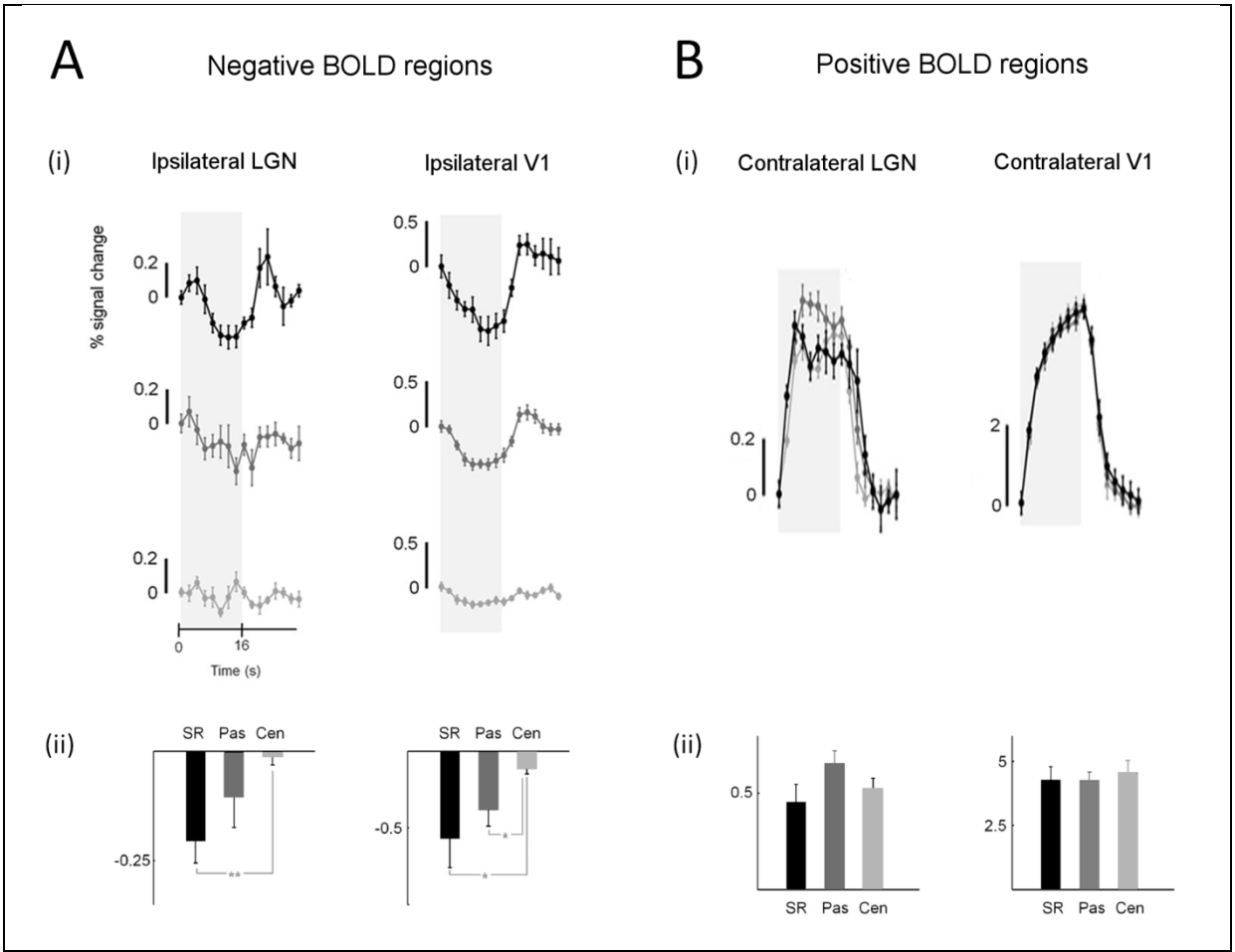

Figure 10. Modulation of negative (A) and positive (B) BOLD responses as a function of task in the LGN and V1. Upper part of each panel (i) shows the group- mean single-cycle time series for the region of interest; these are separated by task for negative BOLD conditions, but overlaid for positive BOLD conditions. Significant variability is evident in negative BOLD responses of LGN and V1, as highlighted by the ANOVA results in the lower row (A.ii); no significant differences are evident or emerge statistically in the positive BOLD responses as a function of task (B ii). Adapted from Gouws et al., 2014.

capabilities of DV3D. We performed 3 functional scanning sessions per subject, one for each attentional task described above, averaging over multiple scans per session. The results from this experiment are summarized in Figure 10. These results show that negative BOLD responses can be detected in the ipsilateral LGN, and thus negative BOLD is not a purely cortical phenomenon. This negative BOLD response is also present in ipsilateral V1, and both cortical and subcortical response amplitudes reduce as a function of task, being lower under passive viewing conditions and all but abolished under central task conditions. While these negative BOLD results alone were compelling, we felt slightly concerned about a feature in our positive BOLD responses: strikingly, and contrary to previous literature (e.g. Gandhi et al., 1999; O'Connor et al., 2002) measuring attentional effects in

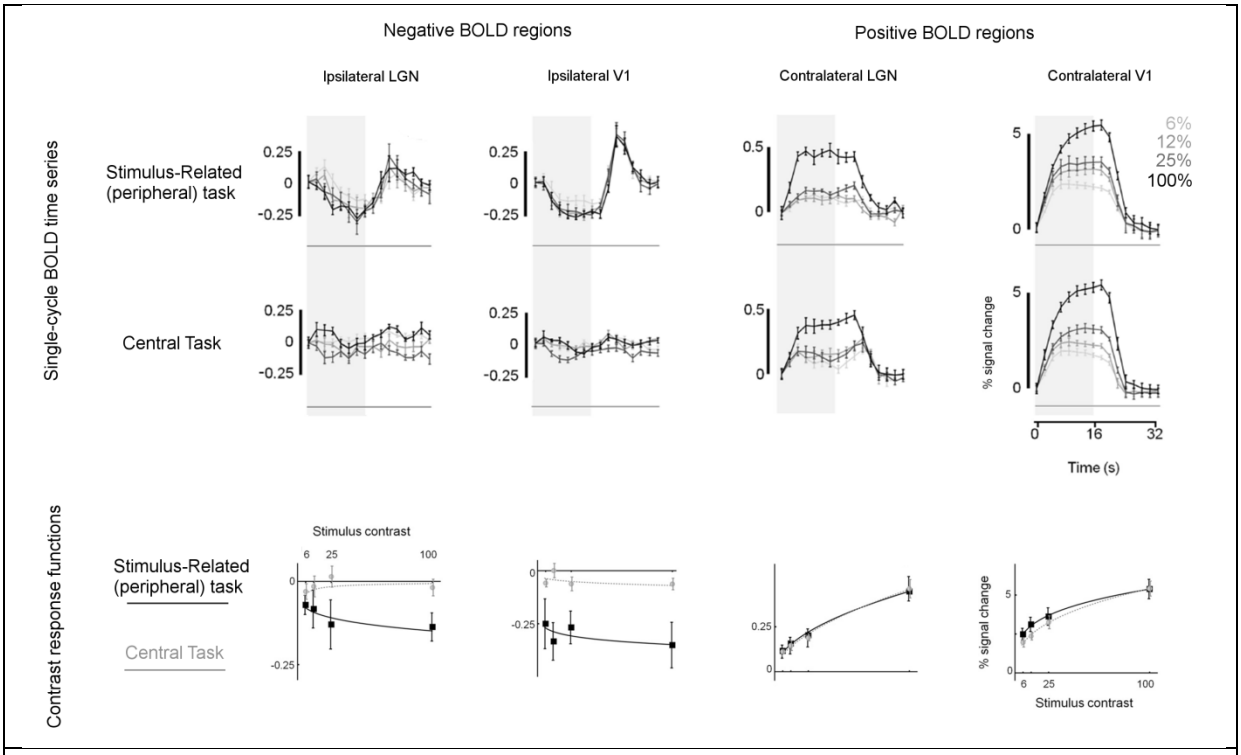

Figure 11. Modulation of negative and positive BOLD responses as a function of task *and* stimulus luminance contrast in V1 and LGN. Adapted from Gouws et al., 2014.

early visual areas, we found no evidence of an enhancement (i.e. increased positive BOLD) of attended locations in V1 or the LGN as a function of task. Many of the previous studies that reported enhanced responses in early visual representations of attended locations tested responses to stimuli at low-intermediate luminance contrasts, while our stimuli were at 100% contrast. This means that the positive BOLD responses we measured in contralateral V1 and LGN may have been sufficiently saturated by our stimulus such that an additional effect of attentional modulation could not be measured.

To address this difference, we tested a range of luminance contrast levels. As the first experiment showed the largest effect for lateralized, stimulus-related attention vs. central attention, we omitted the 'passive viewing' condition from further measurements. In 8 subjects we again acquired / used existing phase-encoded retinotopy data and anatomies, defining regions of interest as in the first experiment. In a further 8 scan sessions, subjects underwent the full combination of measurements, completing 4 scans in each session for a given combination of task (stimulus-related or central) and luminance contrast (4 levels: 6%, 12%, 25% and 100%). The 100% luminance contrast condition was chosen to allow us to plot the full contrast response curve but has the added benefit of allowing us to reproduce the initial finding. The results from this experiment are summarized in Figure 11.

Thus we were able to reliably record cortical and subcortical negative BOLD signals at high stimulus contrast with a peripheral task, reproducing our initial experimental findings. Negative BOLD responses are highly task dependent but appear largely contrast invariant. Positive BOLD responses on the other hand show the converse relationship with our stimulus factors: they appear highly contrast dependent, but largely task invariant in early visual areas. The effect of task on positive BOLD is not significant in the contralateral LGN but reaches significance in V1 with model fitting as previously used (e.g. Buracas & Boynton, 2007). The effect in V1 is however very subtle, and not measurable at maximum stimulus contrast, nor nearly as marked as the effects across all contrast levels seen in higher visual areas like V5 (data provided in bound manuscript).

Although we set out to perform region of interest rather than whole head analyses, a second observation from the data lead us to do just that. It was apparent that the contrast response function fit to the negative BOLD data in the ipsilateral LGN is not an exact linear replica of that seen in the contrast response function fit to the ipsilateral V1 negative BOLD data. This difference in ipsilateral V1 and LGN negative BOLD signals suggests that feedback from V1 to the LGN alone could not account for the negative BOLD signal in the LGN. To explore other potential contributors to the LGN signal, we took a whole-head fMRI analysis approach, bringing the group data into a standard space (MNI using FSL). This analysis revealed that the negative BOLD detected in the ipsilateral thalamus extends beyond what could be considered the LGN, into the adjacent (ipsilateral) medio-dorsal pulvinar nucleus. Strikingly, no negative BOLD was seen in the pulvinar contralateral to the stimulus; here, rather, we found positive BOLD responses that extended beyond the LGN into the dorsolateral pulvinar. The task and contrast dependence in contra- and ipsilateral pulvinar mimic but are not identical to the results found in their adjacent geniculate counterparts. These signals suggest that the pulvinar nucleus, with its extensive array of input/output connections to multiple visual areas, is an integral part of the cortico-thalamic attention loop and may act by mediating the top-down influences of feedback to the LGN.

Although the dataset acquired for these experiments was large, we could potentially have made additional measurements to further inform our interpretations. In particular, it would have been interesting to characterize the negative BOLD responses at very low (1-3%) or even zero percent luminance contrast as the contrast response function measured here (with positive BOLD) is known to be highly non-linear.

The results and conclusions drawn from this manuscript clearly demonstrated a number of important considerations that need to be made when making fMRI measurements from visual field maps. Such measurements are susceptible to a wide spectrum of influences, from relatively low-level features like stimulus- or task-related changes in luminance (e.g. those on the retina induced by variable blinking)

to one of the most-high level, top-down influences: attention. Crucially, the degree to which these low- or high-level factors exert their effects also varies depending *where* in the visual hierarchy and thus on *which maps* they are acting.

Chapter 4: Visual field maps in retinal disease.

Bound thesis paper 5. ***The Organization of the Visual Cortex in Patients with Scotomata Resulting from Lesions of the Central Retina.*** **Baseler, Heidi; Gouws, Andre; Morland, Antony (2009). Neuro-Ophthalmology Volume 33, Issue 3 June 2009, pages 149-157.**

Bound thesis paper 6. ***Large-scale remapping of visual cortex is absent in adult humans with macular degeneration.*** **Baseler, H.A., Gouws, A., Haak, K.V., Racey, C., Crossland, M.D., Tufail, A., Rubin, G.S., Cornelissen, F.W. and Morland, A.B. (2011). Nature Neuroscience 14(5) pp 649-655.**

A.D.G. acquired all the patient (n=22; 16 completed all sessions) and control data (n=24) presented in these manuscripts; A.D.G. was responsible for maintaining patient relationships and contact enabling coordination of multiple scanning sessions across two sites at Royal Holloway and York. A.D.G. made significant contributions to all types of data analyses; processing of anatomical data including manual brain segmentation. ADG jointly prepared figures and made significant contributions to all drafts of the manuscript.

Bound thesis paper 7. ***Objective Visual Assessment of Anti-Angiogenic Treatment for Wet AMD.*** **Baseler, Heidi, A., Gouws, A., Crossland, Michael D., Leung, Carmen, Tufnail, Adnan, Rubin, Gary, S. and Morland, Antony, B. (2011). Optometry and Vision Science.**

(Ongoing project) A.D.G. acquired all the patient data; A.D.G. was responsible for maintaining patient relationships and contact enabling coordination of longitudinal scanning sessions. A.D.G. made significant contributions to data analyses; processing of anatomical data including manual brain segmentation. ADG jointly prepared figures and made significant contributions to all drafts of the manuscript.

Visual field maps initially arise during development as the result of self organizing processes driven by molecular markers (e.g. McLaughlin & O'Leary, 2005). In short, there is evidence that a highly preserved molecular control mechanism has evolved across species to lay out topographic representations of the world around us without us even having experience of that world. If this fundamental architecture is laid out during development, is it possible that these maps can be changed

after birth, or even later in life? In this section, I will summarize our efforts to examine whether visual maps have the ability to change later in life when input to them is removed due to retinal disease. Clear and widely accepted evidence for abnormal organization of visual maps has emerged from animal lesion models (e.g. Kaas et al., 1990; Heinen & Skavenski, 1991) and in humans with *congenital* visual deficits including albinism (Hoffman et al., 2003) and rod achromotopsia (Baseler et al., 2002). The cone cells in the retina of a rod achromat are abnormal resulting in a loss of central (foveal) vision. Baseler et al. (2002) showed that the primary visual cortex at the occipital pole, which would normally map the fovea, showed responses to intact peri-foveal visual stimulation. The region of cortex onto which the retinal lesion projects, the lesion projection zone (LPZ), had 'remapped' to represent the periphery.

Evidence for reorganization of visual maps in subjects with retinal lesions acquired later in life is less clear cut, with different interpretations of data measured from the acquired LPZ sparking some controversy. The major controversy likely arises from methodological differences. Using a relatively 'low-level' stimulus – a checkerboard stimulus and no task - Sunness et al. (2004) showed no evidence activity in the LPZ with full-field stimulation. Subsequent studies reporting evidence of 'reorganization of visual processing' (e.g. Baker et al., 2005) typically used more 'high-level' stimuli – performing a one-back task with faces presented in the periphery produced islands of activity in the LPZ of their 2 patients. Another laboratory used data from 4 patients to show that full-field, low-level (checkerboard) stimuli with no task produced no activation in the LPZ, but higher-level stimuli (faces) presented peripherally with task did (Masuda et al., 2008). They suggest that the activity detected in the LPZ under stimulus-related task conditions represents feedback from higher visual areas with larger receptive fields to the LPZ of V1.

We carried out a study that used relatively simple stimuli optimized to characterize *visual maps* in a relatively large number of patients. Using standard retinotopic mapping stimuli we tested a relatively large group of patients with acquired retinal lesions due to macular degeneration (MD), seeking evidence of map reorganization similar to that reported in rod achromats. In addition to qualitatively assessing visual maps for patterns of activation, we compared the group mean patient data with age matched controls and with data from normal subjects with simulated retinal lesions. Furthermore, we went on to examine whether tracking the activity in primary visual cortex longitudinally provides a good index of visual function in patients being treated for MD.

Examining retinotopy in acquired central visual lesions

In the *The Organization of the Visual Cortex in Patients with Scotomata Resulting from Lesions of the Central Retina* we reported preliminary findings of the full study performed on 16 patients with established bilateral central retinal lesions - *Large-scale remapping of visual cortex is absent in adult humans with macular degeneration*. Eight patients had Stardgardt's disease, a juvenile form of MD that typically presents in teenage years (mean age 30 when studied). The remaining 8 patients were elderly (mean age 76 when studied) and had acquired MD later in life.

All participants, including 12 age-matched controls, monocularly viewed standard retinotopic mapping stimuli while maintaining fixation. The main outcome measure was signal coherence, estimates of which were extracted for 3 regions of interest (ROIs) for each subject and then averaged to produce a group mean: (a) OP, an ROI at the occipital pole, representative of the central visual field (the LPZ in patients); (b) CS, an ROI more anterior in the calcarine sulcus (intact in all subjects); (c) CR, a control region in non-visual, frontal cortex. The results of this analysis are summarised in Figure 12. In elderly patients, a two-way ANOVA with main factors of ROI and visuals status (MD or control) reveal significant main effects for both factors as well as a significant interaction. Post-hoc pairwise comparisons revealed significant differences between patients and controls in OP, but not CS or CR. In the younger patient group, the same pattern of results as those observed in the elderly MD group emerged. Therefore, independent of the age of acquisition of retinal lesions, these data provide no evidence for 'large-scale remapping' of visual cortex.

To mimic the effects of a central visual field lesion, an additional assessment was made in 12 control subjects (mean age 27). We acquired expanding ring retinotopic data in these subjects under two conditions. In the first, subjects passively viewed the entire, standard stimulus. In the second, a central disc of 7.5° radius was used to mask the centre of the expanding ring stimulus. The second condition mimics a central visual field lesion as no *central-stimulus-related* stimulation should reach the occipital pole. The typical pattern of cortical activity for these two conditions is shown in an exemplar subject in Figure 12c. A clear 'hole' appears in the coherence map at the occipital pole with the masked stimulus. A two way ANOVA compared the signals from the OP and CS ROIs in this lesion control group with the signals observed in the younger MD group and the non-lesion controls originally acquired. The results are summarized in the lower panel of Figure 12c. We found a significant main effect of ROI and visual status (MD, control or lesion control) as well as a significant interaction between the two factors. Post-hoc pairwise comparison revealed significant differences between lesion controls and controls in OP, as well as the previously reported difference between

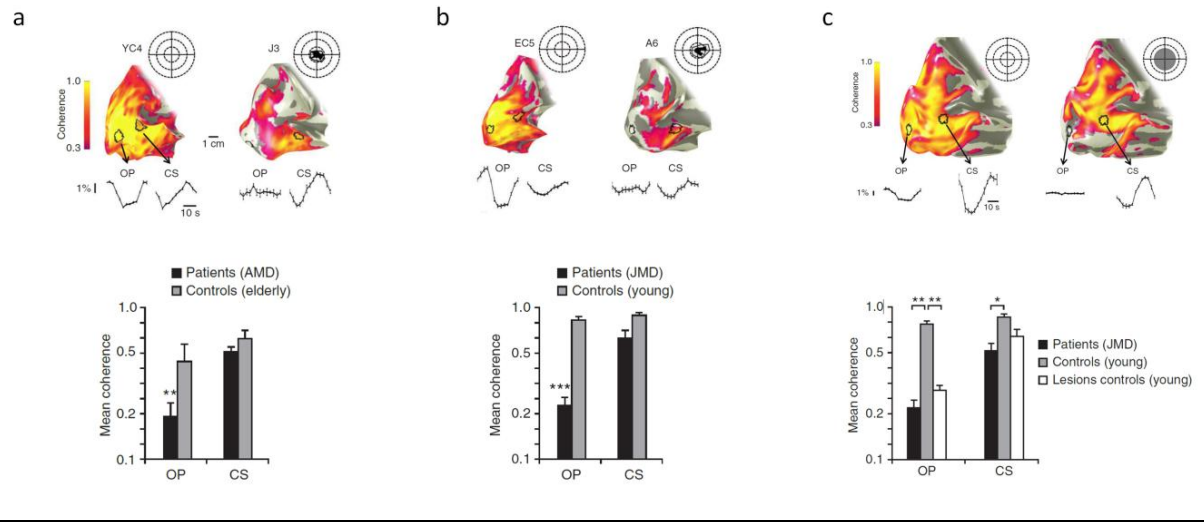

Figure 12. Coherence in intact visual representations and in the LPZ. The upper row of all panels (a-c) depicts inflated representations of subjects' occipital lobes with coherence values at each position in a false red-yellow colour map; an exemplar control subject on the left and an exemplar patient to the right; insets show extent of the visual field lesion; below these the single-cycle mean BOLD response is also shown. (a) Elderly MD patients and controls: patients show little coherent activity in OP relative to controls; lower panel shows the results of a two way ANOVA confirming a significant difference in OP but not CS. (b) Juvenile MD patients and controls; as in (a), patients have significantly lower mean coherence in OP but not CS relative to controls. (c) Simulated lesion results: upper panel depicts the coherence map in the same subject for the control and simulated lesion condition, showing a 'hole' at the OP; the lower panel shows the results of a two way ANOVA comparison between controls, lesion controls (simulated) and patient data. *p>0.05; **p>0.01; ***p>0.001. Adapted from Baseler et al., 2011.

young MD patients and controls at the OP. Again, these results provide no support for the suggestion that central retinal lesions, real or simulated, result in remapping within the lesion projection zone. For the ROI analyses we performed to show evidence of reorganization, such reorganization would need to be "large-scale" (or indeed almost complete) as suggested by Baker and colleagues (2005). To look for evidence of more subtle reorganization, we quantitatively assessed how much activity we would *expect* for a clearly defined lesion (simulated or real) and compared this with the activity *actually recorded* in lesion controls and patients. The ratio or measured activity to predicted activity was compared across participant groups and revealed no significant effect of group (AMD, JMD or simulated lesion controls). Furthermore, any individual group's measured to predicted activity ratio was not significantly different to unity, showing that the area of active primary visual cortex could be accurately predicted on the basis of normal, non-reorganized retinotopic maps in all groups. Even the ratio data were collapsed across the AMD and JMD patient groups (into a single MD group) for comparison with their age matched control groups, no significant difference emerged. This additional analysis provides strong, quantitative evidence that the extent of early visual cortical activity in both patient and normal or simulated-lesion control groups can be predicted on the basis of normal retinotopic maps.

Our experiments therefore provide no evidence of the large scale remapping within the LPZ reported by some previous studies. It is important to realize however that this lack of reorganization may prove to be beneficial to patients. Some of the potentially most effective treatments in restoring vision are targeted at restoring retinal function (e.g. retinal prosthetics, stem-cell therapy and antiangiogenics). If normal retinal vision could be restored, any changes in previously normal mapping between the retina and cortical visual areas would first *need to be reversed* for normal visual perception to return. While it is known that long-term deprivation of input to visual cortex is associated with cortical atrophy (e.g. Boucard, 2009), treatments like those using antiangiogenics are usually delivered to suitable patients within weeks of diagnosis. It is not clear whether the populations of neurons in the LPZ have degraded sufficiently over this relatively short period to render them irrecoverable, or whether they can regain normal function if and when normal retinal input is restored. For this reason, we started a study to assess cortical responses longitudinally in patients receiving anitangiogenic treatments with Lucentis (ranibizumab). This remains an ongoing study at the time of this thesis, but I will summarize here the content of an initial case report that we published in *Objective Visual Assessment of Anti-Angiogenic Treatment for Wet AMD*.

The main objective of this study was to determine whether we could find evidence of increased cortical function in the LPZ that corresponds to a recovery of retinal input to that region. This is not only of scientific value in assessing the reorganization of visual maps, but has important implications for clinical practice. By using fMRI to estimate brain function related to the treatment, we are able to provide clinicians with additional information in the form of a more objective measure of visual function that is independent of fixation.

This case study describes the fMRI protocol, measurements and results for a patient with bilateral neovascular AMD, and the relationship of the fMRI data with clinical measures (including visual acuity, microperimetry, and reading ability). The patient was scanned 24 hours before their first intravitreal injection with Lucentis, and then periodically before their 3 subsequent treatments resulting in four data points. Patients viewed full-field contrast reversing stimulus alternating with periods of uniform gray background. As with previously reported data (Figure 12), we can assess the coherence maps for evidence of activity in the LPZ.

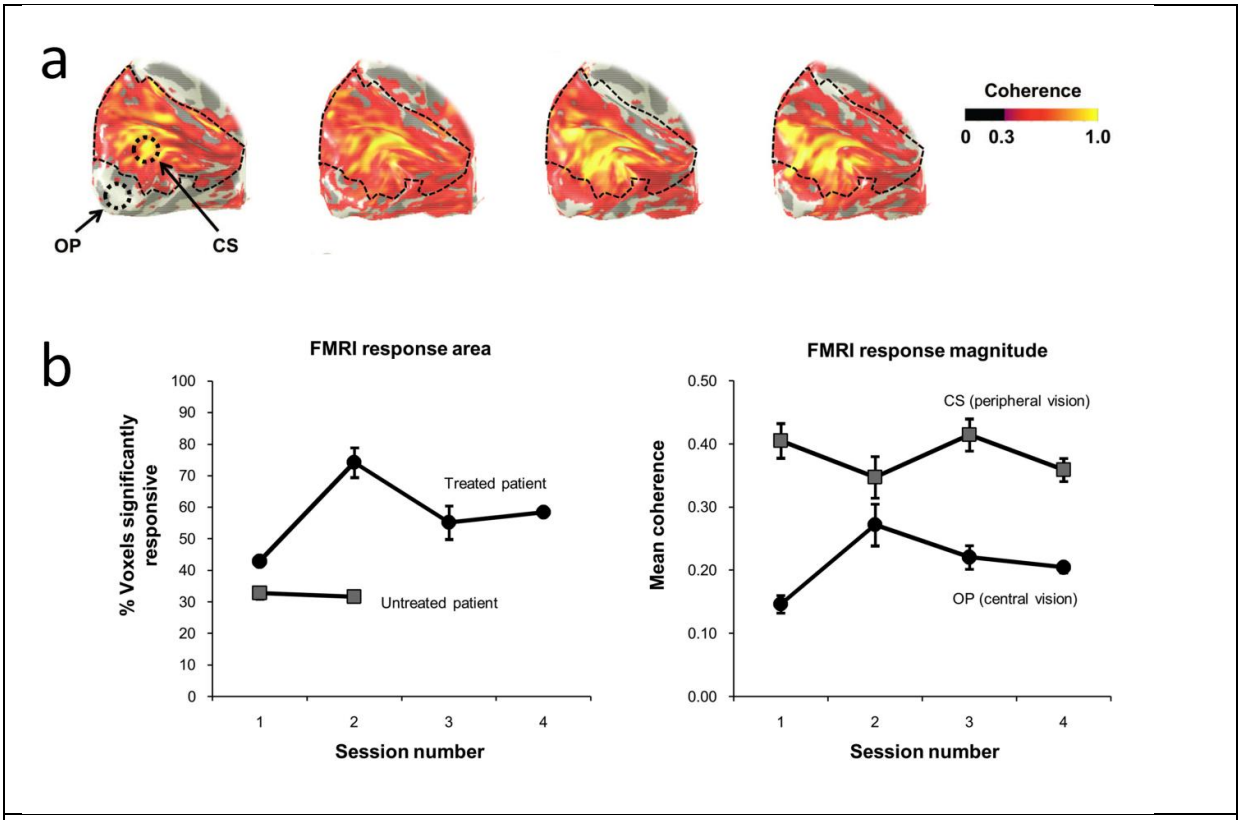

Figure 13. Tracking changes in treatment-related activity in the LPZ. (a) Topographic changes in activity in the LPZ and intact visual field representations signified by changes in coherence over four consecutive treatments in the patient for session number 1 (pre-first treatment) to 4, from left to right. (b) Within the LPZ (OP region), both the number of voxels responding to the stimulus and the amplitude of the response increase after the first treatment, and appear to subsequently stabilise. Adapted from Baseler et al., 2011.

In Figure 13a we qualitatively assess changes in the topographic distribution of voxels responding to the stimulus over sessions. There is a clear increase in coherence at the OP from session 1 to 2, and this appears to be maintained in subsequent sessions. More quantitative assessments of the signals (summarised in Figure 13b) revealed a significant increase in cortical activity in the LPZ from session 1 to 2. While subsequent treatments did not yield any further increase, the initial increase was maintained. Crucially, while the clinical measures all showed a general improvement with treatment, the improvement estimates were not consistent across different techniques over multiple sessions.

In this study we showed that increased cortical function in the LPZ corresponding to recovery of retinal input to that region can be measured and quantified using fMRI. Although these studies were specifically designed to test responses *in maps* using stimuli *optimized for maps*, one shortcoming and potential "missed opportunity" in our study was the absence of "higher level" stimuli. It would have been ideal to present to our large patient group, as others have done in small patient groups (e.g. Baker et al.,2005; Masuda et al., 2008), stimulus sets including faces under different task conditions to shed light on inconsistent findings in the literature. Notwithstanding, we have shown here that when used in the clinical environment, fMRI could provide an objective, non-invasive measure of the function of visual field maps that is independent on the patient's fixation ability, mobility, response capabilities, or cognitive status which may make clinical behavioural measures less reliable.

Future directions

The work bound here has investigated multiple properties of visual field maps. Characterising the functional specialisation of maps, exemplified by the double dissociation we described in LO-1 and LO-2, will continue to be a priority for future research. Our approach was to use relatively low-level stimulus features to begin to test the unique processing properties of these maps. Quantification of selectivity in these maps for other relatively low-level features (e.g. local curvature, contour discontinuity) as well as higher-order stimulus parameter (e.g. global form, texture) should help to further inform on the exact nature of the processing within these maps. We also showed that factors beyond the stimulus characteristics, like spatial attention, can affect the responses measured in visual maps. We showed the importance of considering both enhancement of attended locations and suppression of unattended locations. In these experiments, no stimulus ever occupied the unattended locations. Thus future work should examine the interaction of the suppression with a physical stimulus at the unattended location. The responses of a subcortical network correlated with the enhancement and suppression we measured cortically also warrants further investigation: what is the relationship between these nodes, and how do the subcortical responses relate more broadly to the responses observed in higher visual areas and non-visual, attention-related areas (e.g. parietal cortex) with which they have extensive reciprocal connections? And, alongside the characterisation of the specialisation of visual field maps in normally-sighted subjects, we will continue to assess changes in the visual field maps of patient groups. First, we will continue work to establish whether our ability to use the activity in visual field maps as an indicator of visual recovery generalises across the macular degeneration patient group. Given the opportunity, we will also characterise maps in patient groups where abnormal organisation may be detected, either due to developmental abnormalities (e.g. albinism) or lesions (retinal or cortical) acquired early or later in life.

References

Andrews TJ, Halpern SD, Purves D (1997) Correlated size variations in human visual cortex, lateral geniculate nucleus, and optic tract. J Neurosci 17: 2859--2868.

Baker CI, Peli E, Knouf N, Kanwisher NG (2005) Reorganization of visual processing in macular degeneration. J Neurosci 25: 614--618.

Barton B, Venezia JH, Saberi K, Hickok G, & Brewer AA (2012). Orthogonal acoustic dimensions define auditory field maps in human cortex. PNAS, 109(50), 20738–20743.

Bandettini PA, Wong EC, Hinks RS, Tikofsky RS, Hyde JS (1992) Time course EPI of human brain function during task activation. Magn Reson Med 25: 390--397.

Baseler HA, Brewer AA, Sharpe LT, Morland AB, Jagle H, Wandell BA (2002) Reorganization of human cortical maps caused by inherited photoreceptor abnormalities. Nat Neurosci 5: 364--370.

Boucard CC, Hernowo AT, Maguire RP, Jansonius NM, Roerdink JBTM, Hooymans JMM, Cornelissen FW (2009) Changes in cortical grey matter density associated with long-standing retinal visual field defects. Brain 132: 1898--1906.

Brewer AA, Press WA, Logothetis NK, Wandell BA (2002) Visual areas in macaque cortex measured using functional magnetic resonance imaging. J Neurosci 22: 10416--10426.

Buracas GT, Boynton GM (2007) The effect of spatial attention on contrast response functions in human visual cortex. J Neurosci 27: 93--97.

Chen W, Zhu X-H, Thulborn KR, & Ugurbil K (1999). Retinotopic mapping of lateral geniculate nucleus in humans using functional magnetic resonance imaging. PNAS, 96(5), 2430–2434.

Cowey A (2005) The Ferrier Lecture 2004 what can transcranial magnetic stimulation tell us about how the brain works? Philos Trans R Soc Lond B Biol Sci 360: 1185--1205.

Cowey A, Walsh V (2000) Magnetically induced phosphenes in sighted, blind and blindsighted observers. Neuroreport 11: 3269--3273.

DeYoe EA, Bandettini P, Neitz J, Miller D, Winans P (1994) Functional magnetic resonance imaging (FMRI) of the human brain. Journal of Neuroscience Methods 54: 171-187.

Dilks DD, Baker CI, Peli E, Kanwisher N (2009) Reorganization of visual processing in macular degeneration is not specific to the "preferred retinal locus". J Neurosci 29: 2768--2773.

Dougherty RF, Koch VM, Brewer AA, Fischer B, Modersitzki J, Wandell BA (2003) Visual field representations and locations of visual areas V1/2/3 in human visual cortex. J Vis 3: 586--598.

Dumoulin SO, Bittar RG, Kabani NJ, Baker CL, Goualher GL, Pike GB, Evans AC (2000) A new anatomical landmark for reliable identification of human area V5/MT: a quantitative analysis of sulcal patterning. Cereb Cortex 10: 454--463.

Dumoulin SO, Wandell BA (2008) Population receptive field estimates in human visual cortex. Neuroimage 39: 647--660.

Duncan J (2006) EPS Mid-Career Award 2004: brain mechanisms of attention. Q J Exp Psychol 59:2--27.

Engel SA, Glover GH, Wandell BA (1997) Retinotopic organization in human visual cortex and the spatial precision of functional MRI. Cereb Cortex 7: 181--192.

Engel SA, Rumelhart DE, Wandell BA, Lee AT, Glover GH, Chichilnisky EJ, Shadlen MN (1994) fMRI of human visual cortex. Nature 369: 525.

Engel SA, Rumelhart DE, Wandell BA, Lee AT, Glover GH, Chichilnisky EJ, Shadlen MN t (1993) Functional MRI measurements of human striate cortex 19: 335.

Fox PT, Mintun MA, Raichle ME, Miezin FM, Allman JM, Van Essen DC (1986) Mapping human visual cortex with positron emission tomography. Nature 323: 806--809.

Fujita N, Tanaka H, Takanashi M, Hirabuki N, Abe K, Yoshimura H, Nakamura H (2001) Lateral geniculate nucleus: anatomic and functional identification by use of MR imaging. AJNR Am J Neuroradiol 22: 1719--1726.

Gandhi SP, Heeger DJ, Boynton GM (1999) Spatial attention affects brain activity in human primary visual cortex. Proc Natl Acad Sci U S A 96: 3314--3319.

Glasser MF, & Van Essen DC (2011). Mapping Human Cortical Areas in vivo Based on Myelin Content as Revealed by T1- and T2-weighted MRI. J Neurosci 31(32), 11597–11616.

Glickstein M, Whitteridge D (1987). Tatsuji Inouye and the mapping of the visual field on the human cerebral cortex. Trends Neurosci. 10:350–353.

Harvey BM, Klein BP, Petridou N, Dumoulin SO (2013) Topographic representation of numerosity in the human parietal cortex. Science 341: 1123--1126.

Heinen SJ, Skavenski AA (1991) Recovery of visual responses in foveal V1 neurons following bilateral foveal lesions in adult monkey. Exp Brain Res 83: 670--674.

Henschen S (1893) On the Visual Path and Centre Brain 16: 170-180.

Hoffmann MB, Tolhurst DJ, Moore AT, Morland AB (2003) Organization of the visual cortex in human albinism. J Neurosci 23: 8921--8930.

Holmes G (1918) Disturbances of Visual Orientation. Br J Ophthalmol 2: 506--516.

Horton JC, Hoyt WF (1991) The representation of the visual field in human striate cortex. A revision of the classic Holmes map. Arch Ophthalmol 109: 816--824.

Huang Y-Z, Edwards MJ, Rounis E, Bhatia KP, Rothwell JC (2005) Theta burst stimulation of the human motor cortex. Neuron 45: 201--206.

Inouye T (1909) Die Sehstroungen bei Schussverietzungen der kortikalen Sehsphare.

Jiang F, Stecker GC, & Fine I (2014). Auditory motion processing after early blindness. Journal of Vision, 14(13), 4.

Kaas JH (1997) Topographic maps are fundamental to sensory processing. Brain Res Bull 44: 107--112.

Kaas JH, Krubitzer LA, Chino YM, Langston AL, Polley EH, Blair N (1990) Reorganization of retinotopic cortical maps in adult mammals after lesions of the retina. Science 248: 229--231.

Kammer T, Puls K, Erb M, Grodd W (2005) Transcranial magnetic stimulation in the visual system. II. Characterization of induced phosphenes and scotomas. Exp Brain Res 160: 129--140.

Kammer T, Puls K, Strasburger H, Hill NJ, Wichmann FA (2005) Transcranial magnetic stimulation in the visual system. I. The psychophysics of visual suppression. Exp Brain Res 160: 118--128.

Kanwisher N, McDermott J, Chun MM (1997) The fusiform face area: a module in human extrastriate cortex specialized for face perception. J Neurosci 17: 4302--4311.

Katyal S, Zughni S, Greene C, Ress D (2010). Topography of covert visual attention in human superior colliculus. J Neurophysiol. 104(6):3074-83.

Knudsen E (1982). Auditory and visual maps of space in the optic tectum of the owl. J Neurosci 2(9): 1177-1194.

Kwong KK, Belliveau JW, Chesler DA, Goldberg IE, Weisskoff RM, Poncelet BP, Kennedy DN, Hoppel BE, Cohen MS, Turner R (1992) Dynamic magnetic resonance imaging of human brain activity during primary sensory stimulation. Proc Natl Acad Sci U S A 89: 5675--5679.

Larsson J, Heeger DJ (2006) Two retinotopic visual areas in human lateral occipital cortex. J Neurosci 26: 13128--13142.

Larsson J, Landy MS, Heeger DJ (2006) Orientation-selective adaptation to first- and second-order patterns in human visual cortex. J Neurophysiol 95: 862--881.

Li K, Patel J, Purushothaman G, Marion RT, Casagrande VA (2013). Retinotopic maps in the pulvinar of bush baby (Otolemur garnettii). The Journal of comparative neurology 521(15):10

Lister WT, Holmes G (1916) Disturbances of Vision from Cerebral Lesions, with Special Reference to the Cortical Representation of the Macula. Proc R Soc Med 9: 57--96.

Liu T, Cheung S-H, Schuchard R, Glielmi C, Hu X, He S, Legge GE (2010) Incomplete cortical reorganization in macular degeneration Invest. Ophthalmol. Vis. Sci. : iovs.09-4926.

Malach R, Reppas JB, Benson RR, Kwong KK, Jiang H, Kennedy WA, Ledden PJ, Brady TJ, Rosen BR, Tootell RB (1995) Object-related activity revealed by functional magnetic resonance imaging in human occipital cortex. Proc Natl Acad Sci U S A 92: 8135--8139.

Marshall LH, Magoun HW (1998) Discoveries In The Human Brain. Neuroscience Prehistory, Brain Structure, And Function .

Martínez A, Anllo-Vento L, Sereno MI, Frank LR, Buxton RB, Dubowitz DJ, Wong EC, Hinrichs H, Heinze HJ, Hillyard SA (1999) Involvement of striate and extrastriate visual cortical areas in spatial attention. Nat Neurosci 2:364--369.

Masuda Y, Dumoulin SO, Nakadomari S, Wandell BA (2008) V1 projection zone signals in human macular degeneration depend on task, not stimulus. Cereb Cortex 18: 2483--2493.

McKeefry DJ, Gouws A, Burton MP, Morland AB (2009) The noninvasive dissection of the human visual cortex: using FMRI and TMS to study the organization of the visual brain. Neuroscientist 15: 489--506.

McKeefry DJ, Zeki S (1997) The position and topography of the human colour centre as revealed by functional magnetic resonance imaging. Brain 120 (Pt 12): 2229--2242.

McLaughlin T, O'Leary DDM (2005) Molecular gradients and development of retinotopic maps. Annu Rev Neurosci 28: 327--355.

O'Connor DH, Fukui MM, Pinsk MA, Kastner S (2002) Attention modulates responses in the human lateral geniculate nucleus. Nat Neurosci 5: 1203--1209.

Ogawa S, Lee TM (1990) Magnetic resonance imaging of blood vessels at high fields: in vivo and in vitro measurements and image simulation. Magn Reson Med 16: 9--18.

Ogawa S, Lee TM, Kay AR, Tank DW (1990) Brain magnetic resonance imaging with contrast dependent on blood oxygenation. Proc Natl Acad Sci U S A 87: 9868--9872.

Ogawa S, Lee TM, Nayak AS, Glynn P (1990) Oxygenation-sensitive contrast in magnetic resonance image of rodent brain at high magnetic fields. Magn Reson Med 14: 68--78.

Ogawa S, Tank DW, Menon R, Ellermann JM, Kim SG, Merkle H, Ugurbil K (1992) Intrinsic signal changes accompanying sensory stimulation: functional brain mapping with magnetic resonance imaging. Proc Natl Acad Sci U S A 89: 5951--5955.

Pantev C, Roberts LE, Elbert T, Ross B, Wienbruch C (1996) Tonotopic organization of the sources of human auditory steady-state responses. Hear Res 101: 62--74.

Pascual-Leone A, Walsh V, Rothwell J (2000) Transcranial magnetic stimulation in cognitive neuroscience--virtual lesion, chronometry, and functional connectivity. Curr Opin Neurobiol 10: 232--237.

Posner MI (1980) Orienting of attention. Q J Exp Psychol 32:3--25.

Qiu A, Rosenau BJ, Greenberg AS, Hurdal MK, Barta P, Yantis S, Miller MI (2006) Estimating linear cortical magnification in human primary visual cortex via dynamic programming. Neuroimage 31: 125--138.

Sereno MI, Dale AM, Reppas JB, Kwong KK, Belliveau JW, Brady TJ, Rosen BR, Tootell RB (1995) Borders of multiple visual areas in humans revealed by functional magnetic resonance imaging. Science 268: 889--893.

Servos P, Zacks J, Rumelhart DE, Glover GH (1998) Somatotopy of the human arm using fMRI. Neuroreport 9: 605--609.

Shmuel A, Augath M, Oeltermann A, Logothetis NK (2006) Negative functional MRI response correlates with decreases in neuronal activity in monkey visual area V1. Nat Neurosci 9: 569--577.

Shmuel A, Yacoub E, Pfeuffer J, de Moortele PFV, Adriany G, Hu X, Ugurbil K (2002) Sustained negative BOLD, blood flow and oxygen consumption response and its coupling to the positive response in the human brain. Neuron 36: 1195--1210.

Smith AT, Singh KD, Greenlee MW (2000) Attentional suppression of activity in the human visual cortex. Neuroreport 11(2):271--7.

Smith AT, Williams AL, Singh KD (2004) Negative BOLD in the visual cortex: evidence against blood stealing. Hum Brain Mapp 21: 213--220.

Somers DC, Dale AM, Seiffert AE, Tootell RB (1999) Functional MRI reveals spatially specific attentional modulation in human primary visual cortex. Proc Natl Acad Sci U S A 96:1663--1668.

Sunness JS, Liu T, Yantis S (2004) Retinotopic mapping of the visual cortex using functional magnetic resonance imaging in a patient with central scotomas from atrophic macular degeneration. Ophthalmology 111: 1595--1598.

Vanduffel W, Tootell RB, Orban GA (2000) Attention-dependent suppression of metabolic activity in the early stages of the macaque visual system. Cereb Cortex 10:109--126.

Wandell BA, Dumoulin SO, Brewer AA (2007) Visual field maps in human cortex. Neuron 56: 366--383.

Watson JD, Myers R, Frackowiak RS, Hajnal JV, Woods RP, Mazziotta JC, Shipp S, Zeki S (1993) Area V5 of the human brain: evidence from a combined study using positron emission tomography and magnetic resonance imaging. Cereb Cortex 3: 79--94.

Wessinger CM, Buonocore MH, Kussmaul CL, Mangun GR (1997) Tonotopy in human auditory cortex examined with functional magnetic resonance imaging. Hum Brain Mapp 5: 18--25.

Zeki S (1990) Parallelism and functional specialization in human visual cortex. Cold Spring Harb Symp Quant Biol 55: 651--661.

frontiers in
NEUROINFORMATICS

ORIGINAL RESEARCH ARTICLE
published: 27 March 2009
doi: 10.3389/neuro.11.009.2009

DataViewer3D: an open-source, cross-platform multi-modal neuroimaging data visualization tool

André Gouws*, Will Woods, Rebecca Millman, Antony Morland and Gary Green

Department of Psychology, York NeuroImaging Centre, University of York, UK

Edited by:
Rolf Kötter, Radboud University Nijmegen, The Netherlands

Reviewed by:
Stephen C. Strother, Baycrest, Canada; University of Toronto, Canada
David Kennedy, Harvard Medical School, USA

****Correspondence:***
André Gouws, York NeuroImaging Centre, University of York, York Science Park, York YO10 5DG, UK.
e-mail: andre.gouws@ynic.york.ac.uk

Integration and display of results from multiple neuroimaging modalities [e.g. magnetic resonance imaging (MRI), magnetoencephalography, EEG] relies on display of a diverse range of data within a common, defined coordinate frame. DataViewer3D (DV3D) is a multi-modal imaging data visualization tool offering a cross-platform, open-source solution to simultaneous data overlay visualization requirements of imaging studies. While DV3D is primarily a visualization tool, the package allows an analysis approach where results from one imaging modality can guide comparative analysis of another modality in a single coordinate space. DV3D is built on Python, a dynamic object-oriented programming language with support for integration of modular toolkits, and development of cross-platform software for neuroimaging. DV3D harnesses the power of the Visualization Toolkit (VTK) for two-dimensional (2D) and 3D rendering, calling VTK's low level C++ functions from Python. Users interact with data via an intuitive interface that uses Python to bind wxWidgets, which in turn calls the user's operating system dialogs and graphical user interface tools. DV3D currently supports NIfTI-1, ANALYZE™ and DICOM formats for MRI data display (including statistical data overlay). Formats for other data types are supported. The modularity of DV3D and ease of use of Python allows rapid integration of additional format support and user development. DV3D has been tested on Mac OSX, RedHat Linux and Microsoft Windows XP. DV3D is offered for free download with an extensive set of tutorial resources and example data.

Keywords: visualization software, multi-modal neuroimaging, Python, VTK, fMRI, MEG, DTI, DV3D

INTRODUCTION

This paper describes DataViewer3D (DV3D), a software package built with Python[1] and designed and optimized to address many of the issues encountered when visualizing multi-modal neuroimaging data.

The combination of analyses from multiple imaging modalities is an important and growing trend in neuroimaging (e.g. McDonald, 2008; Stufflebeam and Rosen, 2007). Researchers are conscious of the limitations of individual imaging techniques and their associated analysis methods (e.g. Coltheart, 2006). With sites having access to more than one data acquisition technology, the neuroimaging community has the opportunity to compare and contrast results from different modalities and analysis approaches. Multi-modal techniques are used to exploit differences in results obtained from different techniques (e.g. Liu et al., 2006) and potentially provide converging evidence concerning researchers' hypotheses.

A variety of neuroimaging analysis packages are available to researchers, facilitating analysis of data from a complex and diverse range of data acquisition techniques. The Neuroimaging Informatics Tools and Resources Clearinghouse[2] list many of these tools. Commercial analysis software packages include ANALYZE™[3] and BrainVoyager[4]. Widely used open-source analysis toolboxes for MATLAB[5] are exemplified by Statistical Parametric Mapping (Frackowiak et al., 1997), Fieldtrip[6], EEGLAB (Delorme and Makeig, 2004), mrVista (Teo et al., 1997; Wandell et al., 2000) and NUTMEG[7]. Stand-alone, cross-platform analysis packages include FSL[8] and FreeSurfer[9]. In addition to analysis packages, a number of stand-alone visualization packages have been developed, some to complement particular analysis packages (e.g. FSL's FSLView[10]) and others independently of analysis packages (MRICron[11]; 3D Slicer[12]).

Both analysis and stand-alone visualization packages are often customized solutions developed by a site to address their specific requirements. Many software packages are later extended to provide analysis frameworks for a more diverse range of hardware platforms, data types and analysis methods. Sharing and distribution of platform independent software with unified data formats allows the neuroimaging community increased access to analysis

[1]http://www.python.org/
[2]http://www.nitrc.org/
[3]http://www.analyzedirect.com/Analyze/
[4]http://www.brainvoyager.com/
[5]http://www.mathworks.com/products/matlab/
[6]http://www.ru.nl/fcdonders/fieldtrip/
[7]http://nutmeg.berkeley.edu/
[8]http://www.fmrib.ox.ac.uk/fsl/
[9]http://surfer.nmr.mgh.harvard.edu/
[10]http://www.fmrib.ox.ac.uk/fslview
[11]http://www.sph.sc.edu/comd/rorden/mricron/
[12]http://slicer.org/

methods. Researchers may have to compare the visual outputs of two or more different packages side by side, often comparing two-dimensional (2D) outputs from one to 3D outputs of another. The lack of a like-for-like comparison of results in a uniform coordinate space can increase the potential for misinterpretation of results. Reproducibility of results and consistency in analysis, interpretation, and display of results may be compromised when comparing results from different analyses and visualization software (e.g. Mackenzie-Graham et al., 2008).

DV3D does not attempt to compete with existing analyses packages in terms of analysis routines but rather acts as a support tool for neuroimaging analysis packages. DV3D allows users to integrate results from a number of different analysis packages, in a variety of formats and in an open-source, platform independent implementation. DV3D is designed to offer 2D and 3D visualization support for results from a number of neuroimaging acquisition modes and analysis techniques including magnetic resonance imaging (MRI), magnetoencephalography (MEG), positron emission tomography, computed axial tomography and diffuse optical imaging. DV3D has a highly modular, transparent design and is optimized for integration of additional display routines and file format support. DV3D provides export routines for high-resolution images, movies and objects created by the program for data sharing.

FSLView, 3D Slicer and MRICron are three of the most widely used stand-alone packages for visualizing neuroimaging data, and thus DV3D's functionality will be most closely compared and contrasted to them. None of these packages (and no other single stand-alone package to the best of our knowledge) offer support for all of the multiple analysis outputs of the aforementioned imaging technologies. DV3D is designed to fill this gap.

DV3D is built on Python, a cross-platform interpreted programming language. In DV3D, Python is used to wrap familiar, system-native Graphical User Interface (GUI) functionality using wxWidgets[13] and powerful graphics rendering using the Visualization Toolkit[14] (VTK). DV3D's code base is completely platform independent allowing code to run on any system with Python, VTK and wxWidgets installed. This minimizes code translation time and system-dependent error handling, increasing the efficiency of software development and new process integration.

First we outline the design objectives for DV3D. Following this we will discuss the value of using an open-source, platform independent framework for developing such a package, focusing on Python as the programming language to facilitate cross-platform software development. We will then outline the current functionality of the release package of DV3D and how it achieves our design objectives. We will conclude by comparing DV3D's functionality to similar existing tools, highlighting how DV3D currently provides more comprehensive functionality in a single package, as well as an accessible framework for future development by the neuroimaging community.

SOFTWARE DESIGN AND FRAMEWORK: DESIGN OBJECTIVES

While the exact requirements of every neuroimaging research environment are different, we note that many researchers regularly use a number of core functions when either exploring their data visually or reporting results to their peers. The key requirements that we have tried to address in the development of DV3D are discussed below. They are:

- Dealing with different data types
- A common space for data
- Co-registration with atlases
- Export routines for sharing and publication
- An efficient working environment.
- A flexible, scalable and accessible open-source framework

DEALING WITH DIFFERENT DATA TYPES

Considering the number of different data sources in neuroimaging, many different ways to display the results of neuroimaging data have been adopted.

Due to the nature of their individual underlying analysis methods, many existing software packages are optimized for displaying results in their own preferred way. **Figure 1** summarizes some of these conventions using FSL, SPM, DTI-Studio[15], FreeSurfer, mrVista and EEGLab as examples. Most packages are, understandably, optimized for the display of imaging results from a limited number of technologies, protocols, analysis methods and file formats. DV3D provides a platform in which the user can display a wider range of data in a number of different formats, be they 2D or 3D.

When considering the data types that a multi-modal neuroimaging visualization tool may be required to handle, there are at least four levels of abstraction we need to consider. An example of the complexity of the data structures that require consideration for neuroimaging data processing streams is shown in **Figure 2**. Analyzing and presenting data from MRI protocol subtypes alone requires a support for a broad range of data formats. A software package capable of supporting multi-modal data thus needs to consider: (a) the technology being used to acquire the different data types, (b) the acquisition settings (or protocol) being used to acquire the data, (c) the analysis techniques used to analyze the acquired data, and (d) the format in which the data and results are stored.

The first key objective of DV3D is to ensure flexibility in design that will enable users to integrate neuroimaging data whether it comes from different technologies, from different acquisition protocols, from different analysis approaches and independently of which data format they are saved in.

A COMMON SPACE FOR DATA

In order to sensibly overlay data for visualization of multi-modal analyses, we need to display the data in a common reference frame. An MEG data set, for example, will typically have a coordinate space defining the sensor positions, the participant's head shape and head position relative to the sensors. To overlay this data onto, for example, a surface extracted from an MRI scan, we need to align the coordinate space of the MRI scanner to that of the MEG scanner. Many analysis packages already have algorithms and processes for computing these alignments. Affine 3D transformation matrices are used to describe linear transformations as in FLIRT

[13]http://www.wxwidgets.org/

[14]http://www.vtk.org/

[15]https://www.mristudio.org/

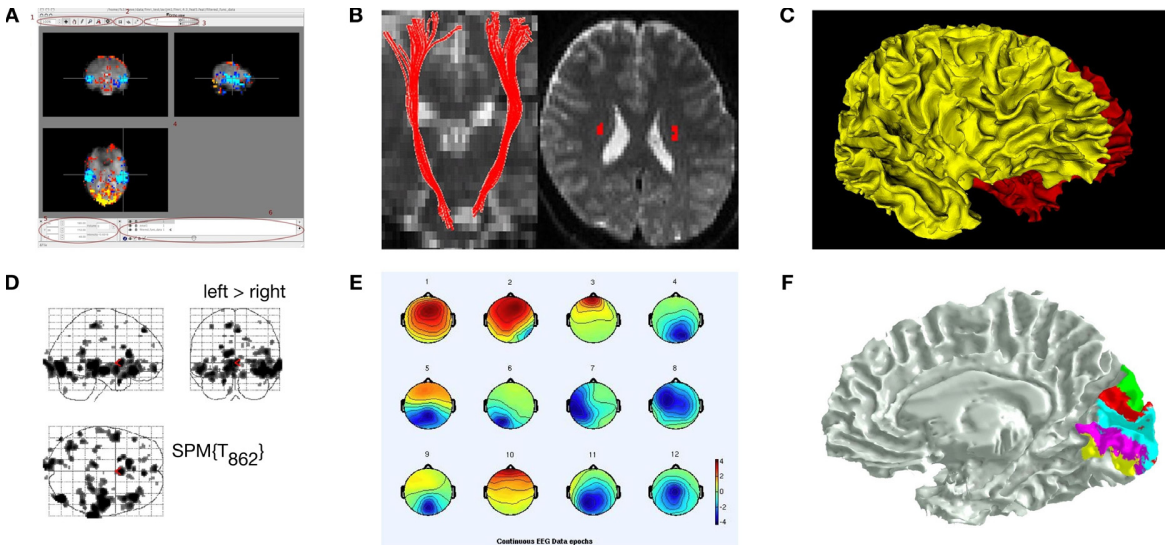

FIGURE 1 | Some common display conventions for neuroimaging data. Examples of some of the methods commonly used to display neuroimaging data. **(A)** FSL's FSLView is used in this example to show the overlay of fMRI data onto three orthogonal planes generated for a 3D MRI volume. **(B)** DTIStudio can display DTI-fiber paths as streamlines mapped onto orthogonal planes generated from 3D MRI Volumes. **(C)** FreeSurfer can be used to display surfaces extracted from MRI data. In this example the grey matter to white matter boundary is displayed in 3D, with separate surfaces for the left (red) and right (yellow) hemispheres of the brain. **(D)** SPM can be used to output 2D projections of regions of statistical significance to a 'glass brain' view. **(E)** EEGLab can be used to show iso-contour patterns of changing electrical fields over the scalp in 2D. **(F)** mrVista can be used to map scalar values (here different visual areas are represented by different colors) to a cortical surface.

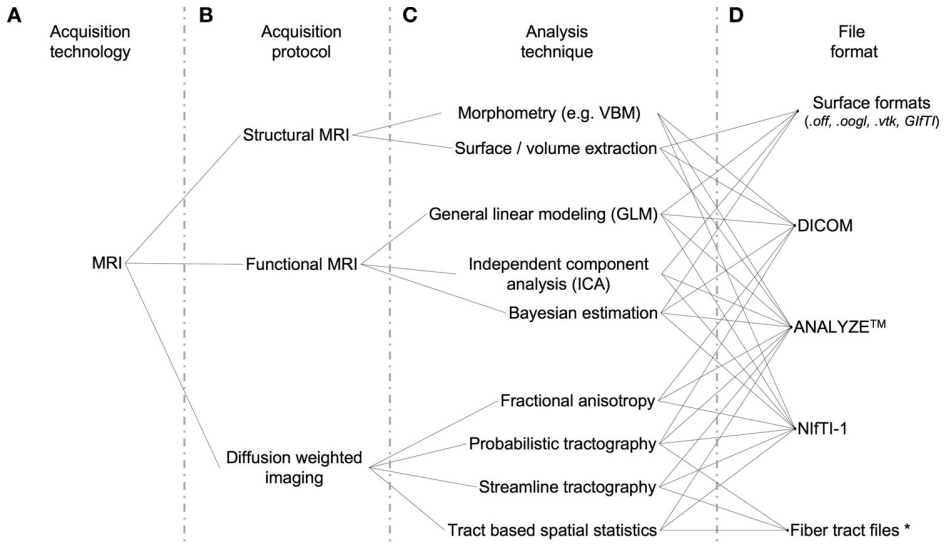

FIGURE 2 | Data handling complexity in MRI analysis streams. A schematic representation of the some of the levels of abstraction considered when preparing software capable of handling multi-modal neuroimaging data. **(A)** The technology type used: Here we use MRI as an example. **(B)** Some MRI acquisition protocols or sub-types: a researcher using a combination of protocols may, for example, be looking for changes in blood oxygenation using functional MRI, localizing the regions of activation to specific brain regions using structural MRI, and then looking for anatomical connections between these regions using Diffusion weighted MRI. They may then wish to overlay the results from each modality to explore spatial relationships. **(C)** Examples of the types of different analysis algorithms and routines for any given protocol. **(D)** Examples of data formats: although researchers may use the same technology, the same protocol, and even the same analysis technique/algorithm, they may save their results in different file formats not immediately accessible to software utilized at other sites. **In the case of Fiber tract files, few standard file formats have been developed specifically for DTI data, and even fewer for saving the results of fiber tracking algorithm output. The.nrrd file format* (http://www.na-mic.org/Wiki/index.php/NAMIC_Wiki:DTI:Nrrd_format) *is used by 3D Slicer to load DTI values and parameters into memory. Fibers are subsequently calculated and can be saved to a vtk file format, unspecific for DTI fibers but useful for import and conversion by any VTK based programs, including DV3D.*

(Jenkinson et al., 2002). Non-linear coregistration routines, as used in SPM (Ashburner et al., 1999) and FNIRT[16], provide nonlinear, one-to-one coordinate mapping between data sets.

Data overlay in some existing packages is also limited by the resolution of the inputs. In FSL's current FSLView, for example, MRI data with a voxel resolution of $2 \times 2 \times 2$ mm^3 cannot be overlaid onto a data set with a $1 \times 1 \times 1$ mm^3 resolution, even if the data sets are defined in the same coordinate space.

The second key objective of DV3D is to enable users to align different data sets into a common reference space. As DV3D is not an analytical tool, we will refrain from calculating alignments on the fly. The alternative is to facilitate alignment by providing tools to load previously calculated transformations from other software packages. Additionally, once data sets are aligned, the resolution of the data sets should already have been interpreted and processed accordingly to allow sensible overlay and corresponding scaling.

CO-REGISTRATION WITH ATLASES

Neuroimaging analysis results often describe spatial distributions of significant activity in the brain. These *maps* are typically overlaid in 2D onto an individual or group brain data, as in **Figure 1A**, so that this spatial distribution can be seen.

In addition to viewing data in an individual or across a group, it is common practice in many neuroimaging data modalities to compare these spatial distributions to equivalent positions, and thus brain structures, in some reference brain space. These reference brains, or atlases, include the MNI brain (Mazziotta et al., 2001), the Talairach brain (Talairach and Tournoux, 1988), the Harvard-Oxford cortical and sub-cortical structural atlases[17] and the ICBM-DTI-81 white-matter labels atlas (Wakana et al., 2004). At the time of this submission, the current version of FSLView cross-references and reports information for the equivalent structures in all of the above atlases if the data set loaded has been transformed into the MNI coordinate space. An alternative for users not using FSLView would be to transform their data into the MNI coordinate space and then use the online MNI-Talairach daemon[18] to manually check every point of interest – a more time-consuming process.

Incorporation of functionality to allow cross-referencing with other standardized brain volume data is thus the third key objective of DV3D. The ability to do this in real-time, without any additional software dependencies is also preferable.

EXPORT ROUTINES FOR SHARING AND PUBLICATION

The production of informative, high-resolution images for communication of results in publications, presentations and educational material is a fundamental requirement in neuroimaging. Many neuroimaging data analysis packages have export routines to capture screen contents to static reports, individual frames to high-resolution images and even short movies of rotating 3D objects or time-series data. Researchers using a specific analysis package can also share data sets with each other. By providing another user with a data set and a set of instructions, the secondary user can reproduce the same analysis or visualization result.

As a fourth objective, DV3D should facilitate the export of data from the visualization screen to a number of formats with options for control of resolution. Movie export options should allow users more freedom in terms of temporal and spatial interaction with data visible on the screen. DV3D should also provide a functionality for users to share results, even without having to provide raw data sets from which the results have been produced.

AN EFFICIENT WORKING ENVIRONMENT

Analysis of neuroimaging data can be a very labor-intensive process. Visualization and interpretation of obtained results adds significantly to this workload. Any functionality that saves the user a significant amount of time and effort is valuable. Many approaches can be taken to increase the efficiency of processing pipelines in software. Perhaps the most obvious is to ensure that, at the design stage, the processing pipeline for a software package is optimized for the hardware and software framework it is built on.

Current computing gives researchers access to multiple processors that can handle computations independently or in parallel. Many computing facilities extend this model to computing clusters with multiple nodes across which processes can be distributed or parallelized. Access to parallel processing is already a feature of a few of the existing neuroimaging software packages. FSL's Bayesian Estimation of Diffusion Parameters Obtained using Sampling Techniques (BEDPOST) toolbox[19], for example, can be easily configured to run over Sun Grid Engine[20], or even simply distributed across any additional local processors.

While parallel processing in the context of BEDPOST is utilized to reduce the amount of processing time required to generate results, the principle can be applied to computationally expensive visualization routines when viewing results. Loading surfaces with millions of vertices and rendering them is an example; a user wanting to load multiple surfaces into memory may still have to wait in the order of minutes for them to load and render. While computers have increasingly large amounts of memory, allocation and management of memory is still a problem that any software designer needs to take into account. This is especially poignant when handling neuroimaging data where data sets can be very large. It is common for MEG data sets acquired at high sampling rates to exceed 1 GB in size. Memory allocation errors are often terminal, causing a computer program to crash if allocation fails. This can be both frustrating and inefficient.

Many of the analysis routines applied to neuroimaging data are repetitive; analysis of data from each individual in a group is an example. Automation of processing streams for similar data sets is an increasing feature in neuroimaging data analysis. Users often use scripts to pass list of arguments and settings into a program that can be accessed via a command line. This can help to reduce the overheads associated with repetitive GUI interaction. In this way, a researcher can apply the same processing, thresholding, and result export routines for each individual in a large group with a single file and a single button press, even if they then do have to wait several hours for the process to complete. This principle can be a useful feature for the visualization of results. A user may want

[16]http://www.fmrib.ox.ac.uk/fsl/fnirt/

[17]http://www.cma.mgh.harvard.edu/

[18]http://www.talairach.org/applet/

[19]http://www.fmrib.ox.ac.uk/fsl/fdt/fdt_bedpostx.html

[20]http://gridengine.sunsource.net/

to, for example, provide an instruction list to a program to load a particular surface, overlay a statistical result file, threshold to a specified value, export a high-resolution image from a top-down view and save a movie. The user would then have a template to process different statistical results, different thresholds, or simply different participants without having to manually run each individual through a GUI.

Some software packages help to increase user productivity by saving metadata files that describe the current status of the workspace the user is working in. The MATLAB toolbox, mrVista, is a good example. In this package users have a session file for each individual. Many settings, file paths, and associated analysis outputs are automatically loaded for the user the next time they load a previously processed participant's data. Evidently, a metadata file describing the processes applied to a data set, its overlays, and dependent thresholds is potentially time-saving when dealing with the visualization of neuroimaging data sets. Furthermore, such a file could easily be shared with another researcher to ensure a consistent result when viewing the same input data.

Saving of processing metadata and automated processing scripts both provide a reference which describes the processes and routines used to produce a set of results. The use of scripts to drive analysis and visualization routines decreases the chances of inconsistencies due to user error. Provenance, the description of the history of a set of data, is important with the recent increases in cross-site collaboration and data sharing (e.g. Mackenzie-Graham et al., 2008). The LONI Inspector[21], an application for examining medical image files, is an example of a tool developed for the comparison of the metadata stored with and between different file types. Metadata is particularly informative when files are converted from one format to another. Assumptions about default orientations, for example, can cause left-right flipping of the data during the conversion process and can cause errors in subsequent visualization and interpretation.

Access to parallel processing, command line scripting, session or workspace metadata and efficient memory management are all ways in which a neuroimaging visualization tool can increase user productivity. As such, the fifth objective in the development of DV3D is to utilize a software and hardware framework that encompasses as many of these features as possible.

A FLEXIBLE, SCALABLE AND ACCESSIBLE OPEN-SOURCE FRAMEWORK

An open-source software package with a self-supporting user community can be a viable solution for scientific software development. With a community contributing to code development and maintenance, costs can be minimized. Other factors need to be considered when developing useful, sustainable open-source software packages.

Transparency is a factor that concerns many researchers, although this is more often related to the implementation of analysis algorithms. While there is very little analysis *per se* in stand-alone visualization packages, researchers should have access to processing routines that generate the visual output (e.g. the color lookup tables applied to thresholded statistical overlay data and interpolation routines applied to loaded data).

[21]http://www.loni.ucla.edu/Software/

Accessibility of the code base can be an issue that restricts interested users from understanding and developing programs. At least three factors can be considered to affect the accessibility of software:

- *Educational resources* are crucial to aid users in learning how to use a package. Documentation and tutorial routines are often lacking in software packages restricting the range of potential users.
- *Platform independence* is an increasingly common feature in neuroimaging software packages. Software that runs on any hardware platform is not only more accessible to any individual site, but aids collaboration across different sites with potentially different hardware infrastructures.
- *Coding language.* Some coding languages are more complex and / or less intuitive than others. While it is impossible to provide a coding language that every programmer would like, it may be sensible to settle for a compromise between a language that is simple to read and use, and one that is very powerful and efficient.

Extendibility and flexibility of software is a measure of how easily the software can be expanded to incorporate additional processing routines. Since the authors have not set out to predict every possible permutation of input-to-output requirement of potential users, it is crucial that the software framework is designed to facilitate incorporation of additional routines with minimal effort. A modular software framework not only facilitates such independent development, but allows for incorporation of appropriate tools and routines often developed for completely different purposes. We could, for example, choose to incorporate an implementation of an algorithm for decimating surfaces, borrowing the code from an external mathematics toolbox. Once imported into the package as an independent module one could simply pass a brain surface to this module as a set of vertices and run the module to down-sample the number of vertices for increased rendering speed.

DV3D has been designed with an open-source, user community developed model in mind. As such it is imperative that the package is built on a software framework that is accessible to a wide variety of users on a wide range of hardware platforms, extendible by non-specialist developers, intuitive to use, and well documented.

METHODS: IMPLEMENTING A Python FRAMEWORK

Having outlined the key objectives for a new multi-modal neuroimaging data visualization tool, we can now consider the implementation of the project. The software package can be considered to consist of three main components:

1. The visualization engine: this is the lowest level of the program, i.e., the functions that actually do the rendering of the images to the screen.
2. A user interaction interface: this is the component of the program that allows users to control the rendering routines of the visualization engine in an interactive and intuitive manner.
3. A master control program: the component of the program that binds or wraps the functionality of the underlying components and allows them to run on the operating system.

We will discuss each of these components in turn, highlighting the requirements and implemented solution for each.

THE VISUALIZATION ENGINE: VTK

The Visualization ToolKit (VTK) is a widely used, free, open-source software package for data visualization and image processing, with support for 2D and 3D graphics rendering. With an active and vast international development community, VTK is a model for open-source software development.

VTK has an extensive set of implemented visualization algorithms. Routines for processing scalar, vector, tensor, texture, and volumetric methods exist. VTK offers a large variety of complex algorithms as part of the standard toolkit, many of which are directly useful for visualizing neuroimaging data. Contouring, surface decimation and triangulation, re-sampling, cutting, and interception detection are just a few examples. Many of these algorithms are directly integrated into widgets allowing users to interactively interrogate combinations of 2D and 3D data in real time. VTK is licensed under the BSD license. VTK is reported to have been installed and tested on nearly every Unix-based platform, Windows PC, and Mac OSX Jaguar or later. VTK is an efficient and fast toolkit consisting of an extensive C++ class library, access to which is available via several interpreted interface layers including Tcl/Tk, Java, and Python.

USER INTERFACE: WXWIDGETS

Learning to use a new software package can be challenging. In a program with a number of complicated functions, the provision of a highly interactive GUI and familiar workspace environment should benefit the user. wxWidgets is a free, open-source toolkit that provides developers with an API (application programming interface) for writing GUI applications on multiple platforms. wxWidgets is licensed under the *wxWindows license*, essentially the L-GPL (Library General Public License), with an exception stating that derived works in binary form may be distributed on the user's own terms. By using each platform's own native controls rather than emulating them, wxWidgets applications look and feel familiar to the operating system's, and should thus be immediately more familiar to the user. The list of widgets and features offered is extensive and the code base is very mature. wxWidgets can be called via interface layers for a variety of languages including C++, Python, and Perl.

Either C++ code or Python could be used to produce a program with a GUI in wxWidgets containing a VTK window for rendering. The relative ease of use of Python over C++, combined with the large array of readily accessible functionality offered by Python, makes this the preferred choice for our application.

THE MASTER ENVIRONMENT: Python

Python is a dynamic, object-oriented programming language that is reported to run successfully on Linux, Windows, FreeBSD, Macintosh, Solaris, and other operating systems. Since Python is an interpreted language, it internally converts and translates source code into the native language of the computer and then runs it. Once Python has been installed on a system, users do not have to compile a Python program or worry about library linkage and loading. Python programs are portable: copying the source code from one operating system onto another (which has Python installed) will allow the software to run.

The Python-specific *Python license* is compatible with GPL licensing. Python is distributed with extensive standard libraries. The list of functions implemented in Python is extensive. Additional modules for Python include a number of mathematical, numerical methods and plotting toolboxes that are useful for manipulating numerical lists and arrays, before passing data into VTK for rendering. Some Python modules support parallel processing and threading often with as few as three lines of additional code (an example is provided in **Figure 10**). Modules allowing access to system command calls and environmental variables are abundant, allowing the user to spawn and even control external processes and applications from within the Python environment application. Python supports integration with other languages and tools (including wxWidgets and VTK), which are often loaded by nothing more than using the *import* command.

Python and individually distributed toolboxes can be built from source and installed independently. At the time of this submission an increasing number of developers are producing binary installers for entire Python distributions with many core modules including VTK. Using the academic download of the Enthought Python Distribution[22], users on Windows, Mac OSX, or RedHat Linux have access to a 'one click installation' of the Python framework required to run DV3D.

In short Python was chosen over C++ for the development of DV3D because of its relative ease of use, the vast array of additional functionality available, and because it allows access to the core underlying components (wxWidgets and VTK) in a single programming language.

DEPENDENCIES AND INSTALLATION

Dependencies

For the reasons we have already discussed in detail above, DV3D is designed to be as platform independent as possible.

DV3D has few software or hardware dependencies and requires only the following to run:

- Python 2.4.1 or later
- wxPython 2.6 or later
- VTK 5.0.3 or later
- The Numpy module for the appropriate version of Python installed
- A Windows, Mac OSX, or Linux platform.

Installation

We have already outlined that Enthought provide a binary installer for Microsoft Windows, Mac OSX, and RedHat Linux. Use of these installers provides a comprehensive build of the core components and additional modules required to run DV3D. Use of the Enthought installers is currently free for academic use. Users with platforms not supported by these installers can often find binary installers for the individual components on operating specific support sites. All modules can be built from source on platforms by users wanting additional installation options and control.

[22]http://www.enthought.com/products/epd.php

DATA IMPORT

Supported formats

DV3D currently supports the following formats:

- DICOM. Digital Imaging and Communications in Medicine is a standard for handling, storing, printing, and transmitting information in medical imaging[23]. Many MRI scanners now export their data directly to this format. The DICOM format provides private header fields that can be utilized to store additional scan information. Unfortunately many sites now use these fields in a non-uniform manner (according to the DICOM standard). Different DICOM readers do not always correctly interpret metadata describing data acquisition and storage protocols in the file. DV3D addresses inconsistencies in DICOM headers by adjusting the DICOM reading routines provided by Python to specific scan protocols and scanner types.
- ANALYZE™ (*.hdr* and.*img*) is an image processing program developed by The Biomedical Imaging Resource at the Mayo Foundation. This program uses the ANALYZE™ format (www.mayo.edu/bir/PDF/ANALYZE75.pdf) which is currently widely used in neuroimaging. Many programs (including FSL, SPM, AFNI, Cox, 1996, FreeSurfer and MRICron) are able to read and write the format. The files typically store voxel-based volumes in two files: the binary data itself is stored with a filename extension.*img*; another file acts as a header (*.hdr*) describing information about the data such as voxel size, slice numbers and data origin. As with DICOM, some software packages use the ANALYZE™ format header in different ways. Some software packages interpret ANALYZE™ volumes differently due to differences in header writing conventions across sites. DV3D addresses inconsistencies in ANALYZE™ headers by adjusting the reading routines to detect which program was used to produce the file (where possible).
- NIfTI-1 (*.nii* or.*nii.gz*) is an adaptation of the ANALYZE™ 7.5 file format[24]. NIfTI-1 uses unassigned spaces in the ANALYZE 7.5 header to add several new features. Since it is possible to compress data stored in NIfTI-1 files the *nii.gz* file format is often utilized. DV3D supports the.*nii* or.*nii.gz file formats.*
- GIfTI (*.gii*). Support for the unified XML-based GIfTI file format[25] is provided.
- VTK polydata files(*.vtk*). VTK provides routines for exporting objects in memory to its own native polygon data files. Additional routines allow these objects to be read into VTK applications at a later date. This offers an incredibly useful tool for users wanting to save objects created in a VTK session for sharing or later access without the need for regeneration. DV3D offers visualization routines for.*vtk* files in binary or ascii format.
- OFF (*.off*). The Object File Format is described by the Geomview package[26]. It is used to represent collections of planar polygons with possibly shared vertices. This is a useful format used to describe surfaces by programs including SurfRelax (Larsson, 2001). DV3D offers visualization routines for.*off* files in binary or ascii format.
- FREESURFER surfaces (*lh.* and rh.* are examples*). Surfaces generated by typical default processing in FreeSurfer include left and right hemisphere cortices representing the white matter and grey matter surfaces, with anatomically correct and inflated versions. DV3D offers support for these standard surfaces and additional surfaces generated by post-processing routines (an extracted scalp for example). DV3D is also capable of handling additional scalar descriptors for these files, including curvature values. DV3D offers visualization routines for FreeSurfer files in binary or ascii format.
- 4-D Neuroimaging (4DNI) MEG data (*.m4d*). Creation of a.*m4d* file using the *pdf2set* program allows direct reading of 4DNI MEG data. DV3D currently supports the 4DNI output format, but could easily be extended to support other MEG and EEG time-series formats.

Although many of the formats discussed above have a standard description, i.e., a set of instructions for file creation designed to maintain conformity across sites, not all packages use these formats to read and write files in the standardized way. There will always be corner-cases where the readers used to import data into DV3D may fail. Fortunately, the previously discussed power of Python allows developers to easily amend existing readers or write new ones to handle these inconsistencies. Users are actively invited to submit failing data sets with descriptions of acquisition parameters and header formats so that current readers can be amended or new readers developed.

Supported software packages

Since DV3D currently supports all the data formats outlined above, it should, in theory, support at least some of the formats from a wide range of existing neuroimaging analysis packages. Any package capable of writing these formats could be used. This is not so simple in practice, as we have alluded to in the Section 'Supported Formats' of this paper. There are complications when different sites and packages adopt varying standards for data export to specific formats. We look forward to collaborating with sites with additional data sets in order to resolve as many of these disparities as possible.

Program processing pipeline

On startup, the user can choose to launch DV3D in one of two modes.

- *MRI-overlay mode*. This mode is traditionally used where a 'base' MRI volume is initially loaded. Other objects aligned to the coordinate space of this volume can then be loaded and overlaid onto the base volume. The 'base' MRI volume thus defines the coordinate space into which additional objects are loaded.
- *Non-overlay mode*. The user can choose to not load a base volume. In this case the program will launch with an empty renderer and pre-created 2D or 3D objects can be loaded by the user.

A graphical representation outlining DV3D's processing pipeline is shown in **Figure 3**.

[23]http://medical.nema.org/

[24]http://nif.ti.nimh.nih.gov

[25]http://www.nitrc.org/projects/gifti/

[26]http://www.geomview.org/docs/html/OFF.html#OFF

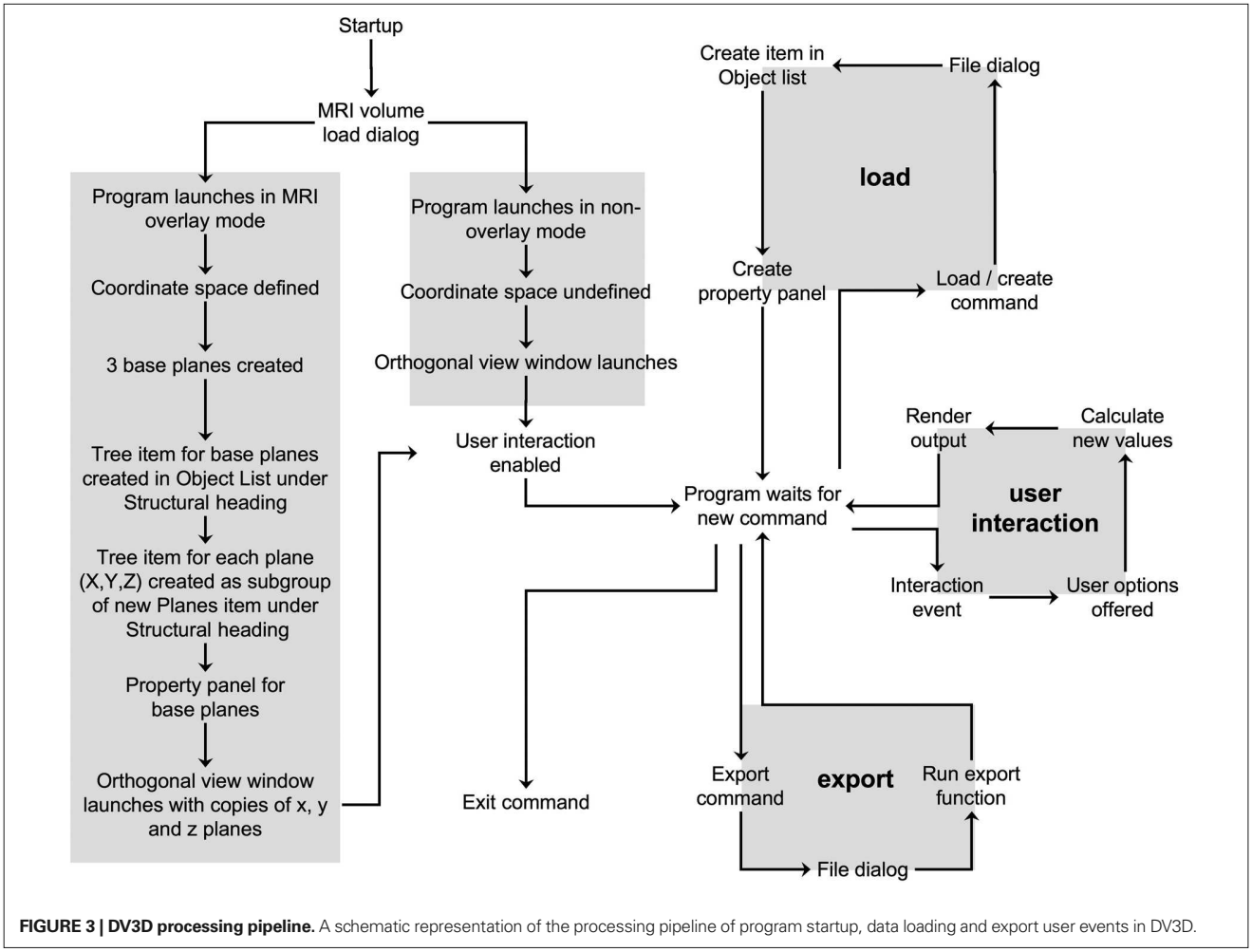

FIGURE 3 | DV3D processing pipeline. A schematic representation of the processing pipeline of program startup, data loading and export user events in DV3D.

RESULTS

DV3D is accompanied by user documentation, example data sets and tutorial videos. Links to this information are provided in the Supplementary Material section of this paper. The fine detail describing interaction with the application is described in these documents and tutorials. Here instead we will discuss the broad concepts and functions of the program, and how they satisfy our design objectives.

DESIGN OBJECTIVE: A COMMON SPACE FOR MULTIPLE DATA TYPES

DV3D's workspace

DV3D provides a single, common workspace for viewing neuroimaging data, simultaneously in 2D and 3D. The main workspace environment of DV3D consists of two windows:

Main application window (**Figure 4**). This window is divided into quadrants:

- *VTK window*. The bottom-right quadrant holds the *wxVTKRenderWindowInteractor*, the VTK class that allows a functional VTK session to be embedded in a *wxPython* program. We will refer to this as the *VTK window*. When data objects are loaded into or created by DV3D they are added to this window. The *VTK window* is the core tool allowing us to provide a common space for simultaneous multi-modal data overlay.
- *Button Panel.* The top-right quadrant is constructed from a *wxNotebook* object that we will refer to as the *Button Panel*. It consists of a number of pages which each contain a panel of buttons and widgets which allow the user to interact with the *VTK window*. A tab labeled with the title of the panel denotes each page. Each page is brought to the front by clicking on its tab. Pages group functions of similar types together for ease of navigation. The *Button Panel* can be extended to have many more pages, allowing for a multitude of additional functions to be added to DV3D at a later date without excessively cluttering an individual button page. Potential developers will also be interested to note that each page here is derived from a separate class allowing easy parallel development and integration.
- *Object List*. The bottom-left panel holds a *wxTreeCtrl* that we will refer to as the *Object List*. It displays its items in a tree like structure similar to many operating systems' file browsing dialogs. An item may be either collapsed (meaning that its children are not visible) or expanded (meaning that its children are shown). Whenever a new object is loaded into the program

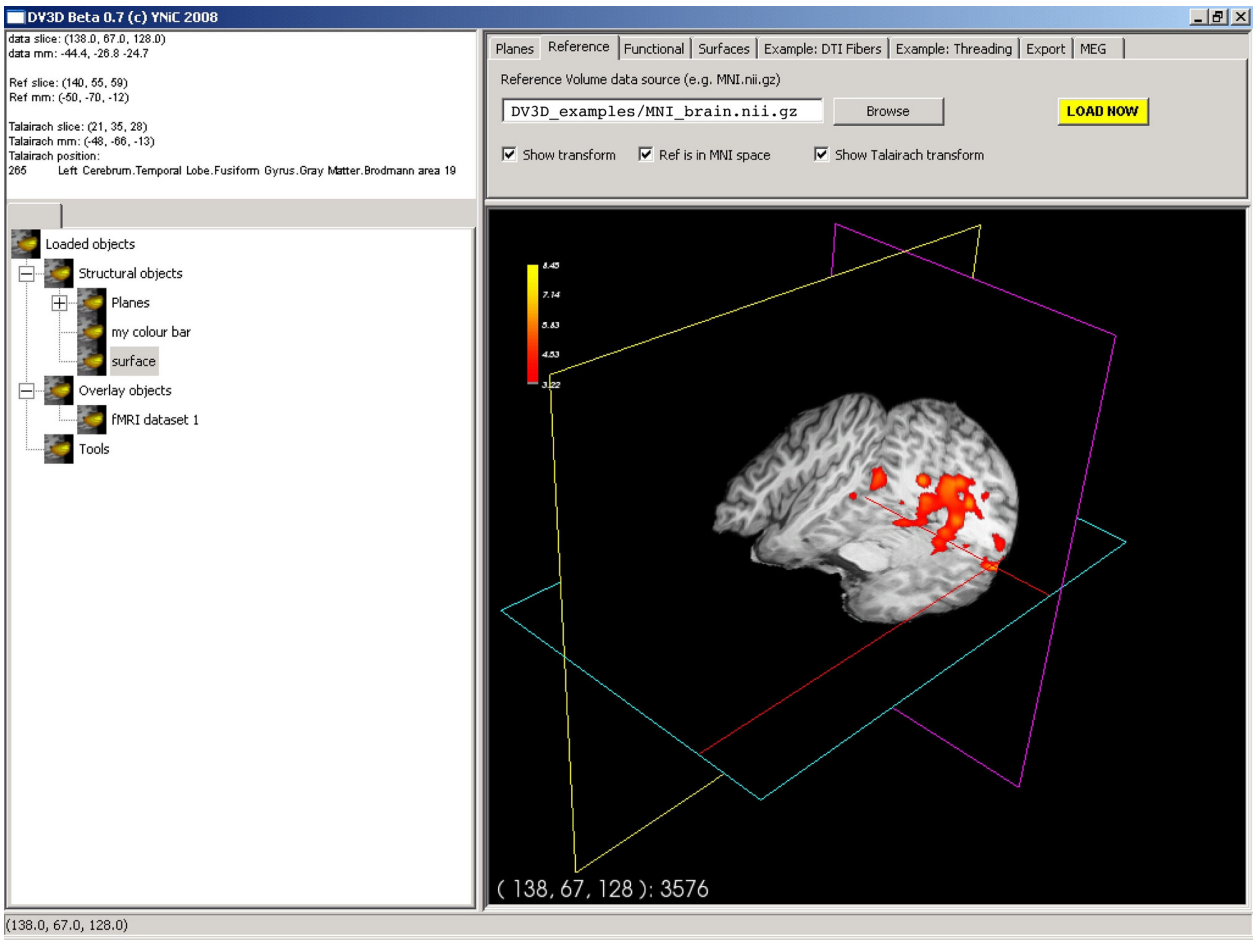

FIGURE 4 | DV3D's main application window. The main window for data interaction in DV3D. The bottom-right quadrant holds the *VTK window* where all 3D rendering takes place. The top-right holds the *Button Panel,* which consists of multiple sub-pages allowing a large array of user interaction functions. The top-left quadrant holds the *Message dialog* which displays the current coordinates of the interaction cross hair in the VTK window. The bottom-left quadrant holds the *Objects List*: a list of all objects loaded in the the *VTK window*. Panels can be resized by clicking and dragging the vertical and horizontal dividers between each panel. Views in the *VTK window* are neurological by convention.

or generated by one of DV3D's routines, a tree item is added to this list. In addition to this, a property panel is created for each new object. This panel has a number of different buttons and tools used to manipulate the display properties of the objects in the *VTK window*. Since a unique item identifier identifies each item in the tree, it can be linked to the object in the *VTK window*. This allows us to manipulate some of the properties of the object in the *VTK window* associated with a specific item in the *Object List* simply by clicking on the object in the list. Each item has its own (optional) icon and a label. Users can simply rename the item in the tree to a more meaningful string without losing the interaction with the associated object in the *VTK window*. The *Object List* offers an intuitive and efficient tool for managing the content of the *VTK window*.

- *Message Dialog*. The top-left quadrant, which we will refer to as the *Message Dialog*, holds a *wxTextCtrl*. This object is effectively a text box that is updated with information for the user as the program is used. Interaction coordinates from the *VTK window* (bottom right quadrant) are displayed in the *Message Dialog* if a base MRI volume is loaded.
- *Sizers*. A vertical and horizontal sizer bar define the boundaries of the quadrants. Clicking and dragging these sizers allows the user to alter the relative sizes of the quadrants of the *Main application window*.

The *Main application window*'s *VTK window* allows us to display multi-modal data, whilst the *Button Panel, Object List* and object associated *Property Panels* allow us to manipulate the properties of the displayed objects.

In addition to the 3D viewing capabilities of the *VTK window,* DV3D provides traditional 2D orthogonal views of the 3D window via the *Orthogonal view window.* This window consists of three orthogonal projections of the VTK window's content. The options panel in this window allows the user to set the refresh frequency of the viewports, increasing program performance. Plane orientation and placement of the viewpoints is also fully customizable.

Viewing conventions

It is important to make the default visualization conventions of DV3D clear at this stage.

Radiological vs. neurological. Data viewed in the 3D *VTK window* of the *Main application window* is rendered according the neurological convention as described by FSL[27]. Data viewed in the 2D *Orthogonal view window* also conforms to the neurological convention, but can be switched to the radiological convention.

Perspective vs. parallel projection. To make 3D visualization more natural, the *VTK window* utilizes a perspective projection algorithm during rendering to infer depth in the scene. Since the planes in the *Orthogonal view window* are effectively 2D we refrain from using this algorithm (since it carries some processing overhead) and revert to parallel projection.

Aligning different data sets

Transformations. DV3D allows the user to add different data sets of different types into the same coordinate space (the *VTK window*). Data is loaded into a millimeter coordinate frame defined by the data set's header description (e.g. the sform or qform matrices held in the header of NIfTI-1 files). By using header transformation matrices, DV3D can automatically align data. Alternatively, the user can provide additional affine transformations (4×4 matrices) to apply previously calculated alignment parameters (typical examples include affine transformations provided by FSL's FLIRT when coregistering an individual MRI to the MNI brain). This principle applies to any volumes or surfaces loaded. DV3D does not currently calculate new transformations, but rather handles those pre-calculated in external analysis packages.

Resolution and scaling. Unlike many other visualization packages (e.g. FSLView), DV3D does not require MRI data to be at the same resolution. DV3D uses a millimeter coordinate space. All data loaded into the *VTK window* are scaled according to the header information (e.g. the *pixdim* values in ANALYZE™ and NIfTI headers describe the voxel dimensions).

DESIGN OBJECTIVE: DEALING WITH DIFFERENT DATA TYPES

Viewing volume data in 2D and 3D

The vtkImagePlaneWidget is the core tool utilized by DV3D to display and interact with volumetric MRI data and associated overlay volumes. This widget works by creating a plane that can be interactively placed in an image volume. Readers may ask why a 2D tool is incorporated in a 3D data viewer. VTK allows the user to manipulate this plane in real time, using the third dimension to tilt, rotate, or translate the plane in virtually any orientation. Thus a 2D plane becomes a diverse data exploration tool. **Figure 5A** shows a set of planes created for an MRI data set. The functionality of the vtkImagePlaneWidget is described in detail in the tutorial examples and documentation. In short, it offers the following functionality:

- *Coordinate lookup.* DV3D captures the slice number data displayed by the vtkImagePlaneWidget and uses it to calculate the equivalent millimeter coordinates in the underlying data set. The slice number and calculated millimeter coordinates are then displayed in the *Message Dialog* of the *Main application window*. **Figure 5B** shows the lookup cross-hair activated in the plane.
- *Interactive volume re-slicing.* The core functionality of the widget relies on the vtkImageReslice class that takes the image volume data as an input, re-slices (or 'reformats') it as required and then passes the output to the texture mapping pipeline. This tool allows real time slicing through volumetric data at virtually any angle. **Figures 5C–E** show this functionality in action.
- *Brightness and contrast*. In addition to rotation and translation of the planes, it is also possible to change the windowing and level of the data. This effectively adjusts the brightness and contrast of the data displayed in the window. Slider style controls are provided to control the absolute values of the window width and level for more precise user control. The default behavior allowing the mouse to control window width and level can be re-enabled in *User Preferences*.

Using multiple vtkImagePlaneWidgets, DV3D allows simultaneous overlaying of statistical data in 2D. Once a base volume has been loaded and its planes have been created, additional volumes can be loaded and overlaid onto this volume. The overlay load routine is accessed via the *Functional* tab on the *Button Panel.* Overlay volumes currently have to be transformed into the coordinate space of the base volume but do not need to be at the same resolution. For every overlay volume loaded, an additional set of planes is created; one for each axis in the *VTK window* and one for each axis in the *Orthogonal view window*. The overlay data is initially assigned a yellow (for its minimum value) to red (for its maximum) color lookup table before it is rendered. As with the base image planes, two additional objects are created: an *Object List* label and a *Property Panel.* Sliders control the window width and window level of the overlay layer only, i.e. the effective scalar range for the data that are visible in the overlay layer. This acts as a real time 2D and 3D statistical thresholding tool. The color map currently in use can also be altered using the color map selection dialog.

Viewing 3D surfaces

DV3D provides methods for loading and generating surfaces for display in the *VTK window*. Surfaces are created in memory as *vtkPolyData* objects, which have a number of native properties that the program is able to manipulate to increase user interactivity. Examples include access to the global transparency and color properties of the object. These properties can then be altered using the property panel automatically created for any surface loaded or generated.

Loading surfaces. Surface load routines are accessed via the Surfaces tab on the *Button Panel*. Clicking the Load button opens a file dialog offering the import of a number of different file formats. Surface inputs currently supported by DV3D include:

- FreeSurfer output surfaces (including inflated surfaces).
- SurfRelax output surfaces in the Geomview binary.off file format.

[27]http://www.fmrib.ox.ac.uk/fslfaq/#general_radiologicaldef

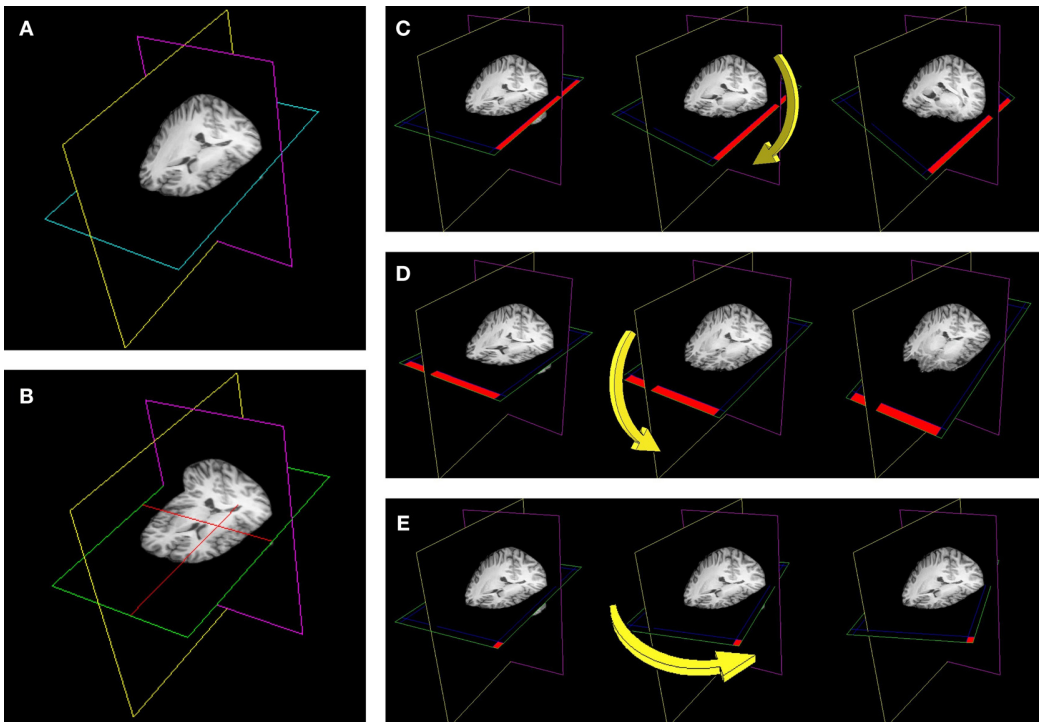

FIGURE 5 | The use of plane widgets to show 3D volume data. (A) A set of three orthogonal planes, each intersecting a single 3D MRI volume. **(B)** Left clicking on any one plane with a mouse will make a cross-hair visible (in red) allowing data from a specific coordinate in the data set to be displayed. Real-time reformatting of data (re-slicing it in any plane direction) is possible by tilting the planes around their current origin. **(C)** The axial plane is rotated around the *y*-axis by clicking on the edge of the plane (show in red) and moving the mouse. **(D)** The axial plane is rotated around the *x*-axis by clicking on another plane edge (shown in red). **(E)** The axial plane is rotated around the *z*-axis by clicking in the corner of the plane (shown in red).

- mrVista.mrm outputs.
- vtkPolyDataWriter output files (.vtk).
- Any surface exported to the GIfTI format.

Once the surface load dialog completes the object is loaded and automatically added to the *VTK window* and the *Orthogonal view window*. The automatically generated property panel will also be displayed.

Generating surfaces. VTK provides techniques for dynamically generating surfaces from volume data in memory. DV3D uses the *vtkContourFilter* to calculate and extract surfaces from underlying MRI data volumes. The *vtkContourFilter* interrogates the volume data set, finding points in the volume where the scalar value corresponds to a value stipulated by the user. It then scans through the data volume, connecting points of the same value and creating isocontour lines (in 2D) or isosurfaces (in 3D). Since the stipulated search value may occur several times in the data volume, multiple isolines or isocontours can be returned by the algorithm. An additional option offered by the algorithm is to retain only the largest connected surface, i.e., the surface with the largest number of vertices.

It may be interesting to generate surfaces from underlying data for a number of reasons. In **Figure 6** we show an example of a rough estimate of a scalp (**Figure 6A**) and rough cortical surface (**Figure 6B**) representative of the white-matter/gray-matter boundary, extracted from the same individual's data. Isosurfaces extraction is highly sensitive to homogeneity inconsistencies in the MRI image volume and produces better results with intensity normalized volumes. In **Figure 6C** we show the same routine applied to the skull-stripped $1 \times 1 \times 1$ mm^3 MNI brain distributed with FSL 4.0. It should be evident that this result is less noisy than that shown in **Figure 6B**, a result of the intensity normalization of the MNI brain. Surface generation for cortical surfaces using DV3D is meant to aid quick data exploration and is not nearly as informative or accurate as the algorithms utilized by programs like FreeSurfer, FSL's FAST[28] or SurfRelax. The speed with which an individual can extract a rough representation of this surface is however very useful. DV3D can give a user a quick insight into the cortical shape in just 30 s, where other packages take between 15 min and several hours to run.

Activation color mapping. In addition to offering access to the global transparency and color properties of the object, *vtkPolyData* objects allow access to the properties of individual vertices that define the shape of the surface. Each vertex can have a scalar value associated with it. VTK allows the user to create a color lookup table covering the range of all scalar values associated with the vertices of a surface. The color presented at each vertex on the surface can

[28]http://www.fmrib.ox.ac.uk/fsl/fast4/

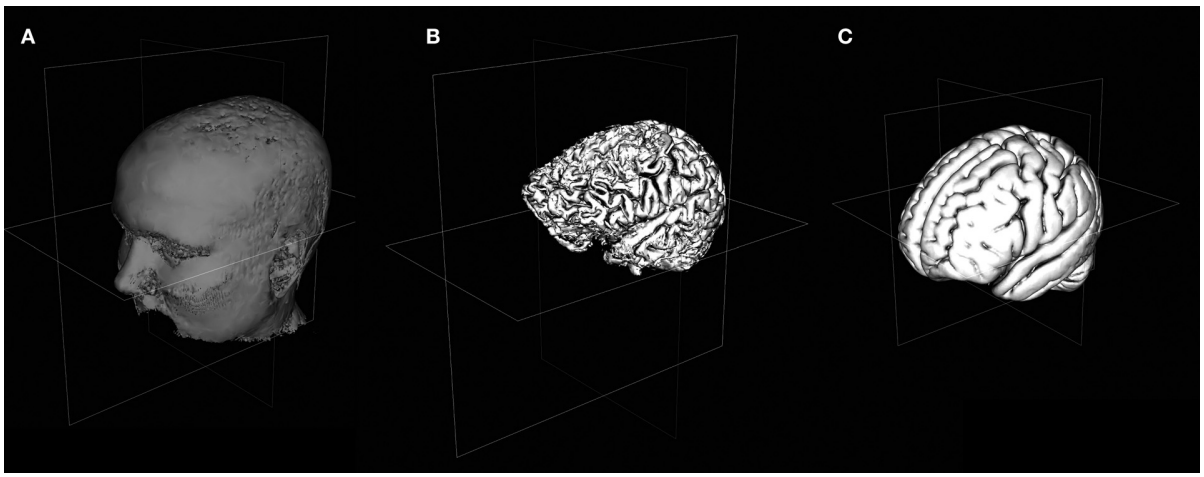

FIGURE 6 | Viewing 3D Surfaces in DV3D. (A) Example of a rough estimate of a scalp using the surface extraction technique. **(B)** Example of a rough estimate of a cortex using the same technique. Here the data set has been skull stripped first using FSL's Brain Extraction Tool. **(C)** A rough cortical extraction of the 1 × 1 × 1 mm^3 MNI brain distributed with FSL 4.0.

then be directly mapped through this lookup table to the scalar value at that point. This offers an easy way to map patterns of activation to a surface.

Viewing time-series data

Interactive time-series data visualization is another data exploration technique supported by DV3D. The ability to follow real time changes in signal amplitude at specified locations in data sets relies on VTK's aforementioned ability to map scalar data to individual vertices of loaded surfaces. DV3D extends the ability of VTK to map scalar data by allowing users to pass new values into surface objects' scalar arrays. By allowing users to update the scalar values mapped to surfaces with data from any time point in a time-series, DV3D allows dynamic viewing of time-series data in 2D and 3D by stepping through successive time points. DV3D also supports extraction of sensor time-series data for MEG and EEG data (e.g. Butterfly plots).

Numpy[29] is a mathematical methods module for Python that allows, amongst many other mathematical functions, the use and manipulation of arrays and matrix mathematics in Python. Python's automatic memory management, coupled with the power of Numpy matrix manipulations means that DV3D has access to efficient temporary data storage of large data arrays. VTK also offers techniques for data arrays to be passed directly into VTKArray classes, further increasing processing efficiency.

Two time-series objects are shown in **Figure 7**. A 3D contour plot and a minimum norm solution (techniques used for visualizing and analyzing MEG and EEG data) for two MEG data sets are shown in **Figures 7A,B**, respectively. The user first provides a coordinate file that describes the surface that is to be added to the *VTK window*. This file provides the coordinates for the vertices and edges of the surface to be generated. The user then provides a time-data file that holds an array of scalar values. This file holds multiple values for each vertex, arranged chronologically to represent the time-series at each location or vertex in the coordinate file. Independently of the exact file formats, DV3D generates a surface from the coordinate file, and then loads the time-data file into memory, constructing a Numpy array to hold the time-series data. As the user interacts with the object, stepping to subsequent or previous time points, DV3D simply steps to the appropriate point in the array and extracts the relevant values. These values are then converted to a VTKArray and passed directly to the scalar value representation of the object. Although this process may seem rather complex, it is an extremely efficient technique for managing large data arrays without restricting rendering speed when visualizing time-series data.

Advanced interaction techniques

We have shown the way in which DV3D can load surfaces or generate them from underlying data, or re-slice volume data in real time using image planes. We will now briefly describe three of the more advanced features demonstrated in the user documentation and tutorials to show the data exploration potential of DV3D.

3D overlay data. This visualization technique relies on the previously described method for extracting isosurfaces from MRI volumes using the vtkContourFilter. We previously described extracting a rough representation of the cortex by passing a base sMRI volume to the vtkContourFilter. Following the same principle, we can pass an overlay volume to the vtkContourFilter in the place of the structural volume. This volume could, for example, be a statistical z-score map of the activation resulting from a contrast analysis of fMRI data. This is illustrated with a visual motion fMRI data set in **Figure 8**. The 2D overlay data is shown in **Figure 8A**.

Isocontouring with depth-dependent transparency mapping is a technique that can be applied to a variety of neuroimaging data types or result files. **Figure 8E** shows how this technique can be applied to probabilistic DTI visualization (e.g. FSL's Probtrack[30]

[29]http://numpy.scipy.org/

[30]http://www.fmrib.ox.ac.uk/fsl/fdt/fdt_probtrackx.html

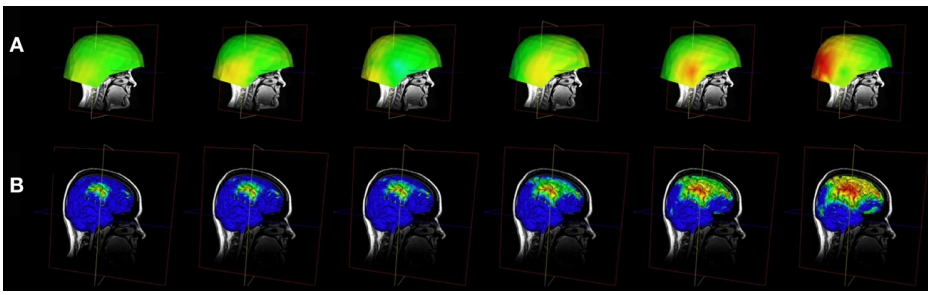

FIGURE 7 | Viewing time-series data in DV3D. (A) Evolution of an MEG field displayed via 3D-contour plot. **(B)** Evolution of a minimum norm projection via surface scalar lookup table. In both instances frames can be automatically generated by cycling data and exported for movie creation.

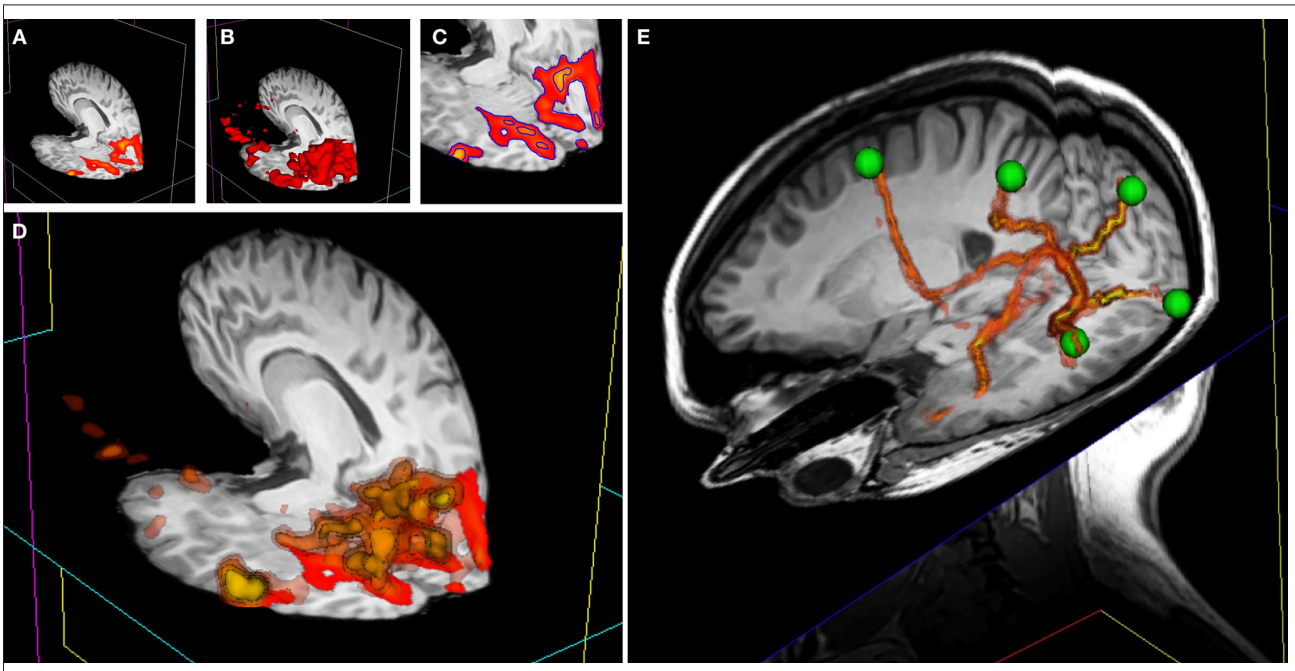

FIGURE 8 | 3D overlay data using isosurface transparency. (A) 2D overlay data from an fMRI experiment overlaid onto a structural MRI volume. **(B)** The vtkContourFilter can be applied to create an isosurface through the data at a specific threshold value, say z = 2.3. The returned 3D surfaces will encompass all areas in the data set that have a z-score of z = 2.3 or above. We could repeat the process, asking the vtkContourFilter to return smaller surfaces as we increase the threshold. **(C)** A 2D representation (using isocontours shown in blue) of 2 separate isovalues used to extract surfaces. **(D)** If we simultaneously render five sets of surfaces, at z-scores of z = 2.3, 3.3, 4.3, 5.3, and 6.3, for example, the only set of surfaces visible would be that at z = 2.3, since all other surfaces are inside this surface. We can manipulate the transparency and color of the vtkPolyData class to make the distribution of activation visible and overcome this problem. By making the outermost surface (at the lowest threshold value) 80% transparent, the second outermost 60% transparent, the third 40% transparent, the fourth 20% transparent, and the highest threshold surface completely opaque, we make all surfaces simultaneously visible. To emphasize this effect, we can also apply a color gradient (yellow to red) across the surface threshold range. Interacting with this mode of visualization in 3D gives an instantaneous percept of the entire distribution of the activation in 3D. **(E)** This image shows a number of tracts output from FSL's Probtrack toolbox rendered using the 3D overlay technique. The tracts are seen as yellow to red isosurfaces. The green spheres indicate the positions of seed and target points as defined in Probtrack.

output) to give a clear representation of the entire extent of probable connectivity between regions. In addition to being a tool for producing interesting 3D images of the connectivity probability distribution of the DTI data set, this technique has another potential benefit for DTI. Standard DTI fiber tracking techniques tend to represent 3D results at streamlines or stream-tubes in 3D space. With this technique, the colors mapped to each surface have actual probabilistic value and can be mapped along the length of the tract or network path with a visible color bar.

Surface interrogation of overlay volume data. The vtkContourFilter interrogates data volumes, finding specific scalar values and then extracting the 3D coordinates with corresponding scalar values, constructing isolines or isosurfaces by effectively 'connecting the

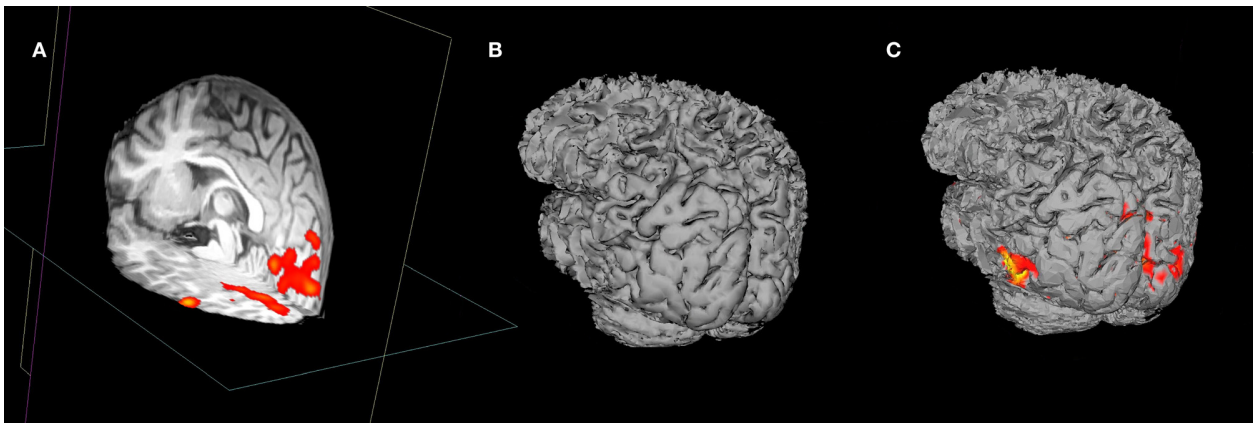

FIGURE 9 | A demonstration of surface interrogation of overlay volume data. (A) Structural MRI space with fMRI data overlay. **(B)** Rough cortical extraction from underlying structural MRI data. **(C)** Rough cortex with overlay intersection data rendered onto the surface at the user defined thresholds.

dots'. VTK also offers techniques to do the reverse: having a surface in the same coordinate space as a data volume, we can find where each vertex of the surface intercepts with the data volume and extract the volume's scalar value at this point. We have already shown (in **Figure 7**) that when a scalar values are provided for each vertex of a surface, we can use a color lookup table to overlay a color map of the distribution of the scalar value amplitudes across the surface.

Figure 9 demonstrates the usefulness of this technique. An overlay volume can be loaded into sMRI space (**Figure 9A**). The user can then create or load a surface (**Figure 9B**) into the same space. From the property panel of this surface the user can choose to map statistical data to the surface (at the current threshold and color map defined by the overlay plane's property set). This gives the user a very quick way to visualize activation distributions in 3D (**Figure 9C**).

DESIGN OBJECTIVE: COREGISTRATION TO ATLASES

Automatic atlas lookup

DV3D provides methods for real-time cross referencing with brain atlases. Atlas lookups are currently only possible on MRI-overlay mode. Once the user has loaded a base MRI volume, they can load a second volume into memory. On the *Reference* tab of the *Button Panel*, the user can select a file to load as the reference volume to compare to the base volume. Once the user selects a volume, they are prompted to supply a transformation matrix describing the mapping of the base volume (e.g. an individual's brain) to the reference volume (e.g. the MNI brain). DV3D is currently optimized for use with FSL output data, allowing referencing with the MNI and Talairach brains. If a user supplies the MNI brain as a reference, the user can select to automatically lookup the equivalent Talairach coordinates and brain label. DV3D uses the MTT-pooled transform for the MNI brain to the Talairach brain (Lancaster et al., 2007). Coordinates and slice numbers of the current and reference data set are displayed in the *Message Dialog* of the *Main application window*. The Talairach label, slice number and coordinate is displayed in the *Message dialog* if the supplied reference volume is the MNI brain and the user has checked the *Ref is MNI* and *Show Talairach Transform* check boxes on the *Button Panel*. Interaction with a base MRI volume, with cross referencing to the MNI and Talairach atlas is demonstrated in **Figure 4**.

DESIGN OBJECTIVE: EXPORT ROUTINES FOR SHARING AND PUBLICATION

Surfaces

Any surface currently displayed in DV3D's VTK window can be written out to a file for sharing or reloading at a later time. Export routines for surfaces can be called by selecting the required surface's label in the *Object List*, clicking on the list item with the right mouse button and selecting the *Export surface* option. This will launch the operating system's native '*Save file as*' dialog. The file can then simply be saved and re-loaded where required.

Images

DV3D offers a number of different options for saving out images, capturing the content of the *VTK window* and the *Orthogonal view window* as required. The user has full control over the resolution of the image output and is given the option of multiple output formats (including JPEG, TIFF, BMP and PNG). Controls enable the user to export the current view to single image, or export a sequence of views as separate frames (e.g. 360° rotation of the viewport to multiple, sequential images).

Movies

DV3D offers options for saving and creating movies from of the *VTK window*. The user has full control over the resolution of the image output since the frames of the movie are simply captured at the dimensions of the *VTK window* as it is displayed on the computer monitor. On the *Export tab* of the *Button Panel* the user can select:

- *Export 360°* directly to.AVI movie. VTK provides a vtkAVIWriter class that is capable of writing renderer contents directly to AVI format video files. Currently this export routine does the same as the *Export 360° to multiple images* routine, rotating the camera through 360° around the object over 180 frames

and creating the output as a movie. Depending on the build options used at VTK installation time or the installer that the user has chosen to use, the vtkAVIWriter class is not always automatically compiled. The Enthought Python distribution, for example, builds this class on Windows by default, but not on OSX. Users wanting access to this functionality should consider manual installation of the VTK modules, or see the more advanced functionality of the streaming routine described in *Start interactive streaming*.

- *Start interactive streaming*. This is the most advanced interaction capture technique currently available with DV3D. It has the capability to capture user interactions in real time, periodically capturing frames from the *VTK window* as the user changes objects in it. Clicking the start interactive streaming button launches the operating system's '*Choose folder dialog*', allowing the user to specify a folder for the output to be saved in. With this routine, frames are saved to memory as they are captured rather than being written out immediately. The user will notice very little jittering during interaction due to the decreased processing load. The individual frames are then written out when the Stop stream button in pressed. Individual frames can then be combined into a move format by external software programs such as Apple's QuickTime Pro.

Examples of all export routines are provided at the software website references in the Supplementary Material section of this paper.

DESIGN OBJECTIVE: AN EFFICIENT WORKING ENVIRONMENT

A number of features of DV3D are designed to aid users to optimize the working environment of the package.

User preferences

A user preferences file can be accessed via the Preferences panel. This allows users access to environmental variables including:

- Automatic property panel display: users can choose whether the property panels generated for each loaded object are automatically displayed or not.
- Orthogonal window orientations: these settings allow the user finer control over the layout of the orientations of the Orthogonal view window panels.
- Automatically render orthogonal window: this setting toggles whether the program default is to automatically render the Orthogonal window when the VTK window changes, or whether the user calls this manually.

Parallel processing

Python offers access to parallel processing via a number of different modules. While there is little need for this at present, we have included a sample of how Python can manage separate threads with this release as a demonstration of how easy it is to implement, and how much potential there is for speeding up user interaction. The demonstration can be run from the *Threading* tab on the *Button Panel*. This function runs the load routine for a surface file with over one million vertices. The routine is run in the background while the user continues to interact with the program. Loading the same surface without threading requires the user to wait between 20 and 45 s for the process to complete. An example of the simplicity of the code required to access this functionality is shown in **Figure 10**.

Workspace saving

At any point during use of DV3D, users can choose to save the current status of the workspace to a file. This file holds metadata that an be loaded at the start of a later session to load the current working environment, with many of the current settings in use by the user, including all loaded objects and color / transparency settings. This file hard-codes the paths of input files and will fail if files are moved between sessions.

Surface decimation

Upon loading surfaces into memory, DV3D can be set to run a decimation routine to down-sample the number of vertices of each surface by between 10 and 90%. This surface is not shown automatically (the high-resolution surface is visible by default), but the user can choose to toggle between the decimated and original surface during interaction to help increase the speed of rendering.

Command line access for scripting

In addition to handling workspace files, DV3D offers the ability to handle explicit arguments passed to the program on the command line. This allows users access to advanced scripting options for automation of processing streams.

A

```
def OnButtonClick(self, event):
        my_file = ChooseFile(self, '*.off)
        Load_surface_file(my_file, parent_frame)
        print 'file loaded ... continue'
```

B

```
import threading
class RunFunctionInThread( threading.Thread):
        def run(self):
                my_file = ChooseFile(self, '*.off')
                Load_surface_file(my_file, parent_frame)

self.my_thread = RunFunctionInThread()

def OnButtonClick(self, event):
        self.my_thread.start()
        print 'file loading in background ... continue'
```

FIGURE 10 | A demonstration of code simplicity in Python: enabling threading. (A) This code example demonstrates how a function may be linked to a button press in a standard Python script using the thread running the main program. On the button click, the program asks the user to choose a file to load. The program then passes the file to the subroutine (Load_surface_file) and runs the subroutine. While the subroutine is running the user has to wait for the object to be loaded and returned to the main program before continuing. **(B)** This second code example shows that we can produce the same result using Python's threading module. First the threading module is imported. The functionality of code example in **(A)** is then added as a function (RunFunctionInThread). The button click in this instance calls a thread (my_thread.start) and runs the load routine will run in the background allowing the user to continue working while it is prepared. Note that threading only requires a few extra lines of simple code.

DESIGN OBJECTIVE: A FLEXIBLE, SCALABLE AND ACCESSIBLE OPEN-SOURCE FRAMEWORK

Our implementation of a flexible, scalable and accessible open-source framework is described largely in the Section 'Methods: Implementing a Python Framework' of this paper. We show that the combination of Python, wxWidgets and VTK gives us the ability to produce a code base that is freely distributable and platform independent. This implementation has all the functionality required to process a number of different file types and formats, is highly modularized for ease of understanding and promotes future user development due to the relative simplicity of Python as a programming language (for an example, see **Figure 10**).

DISCUSSION

The 'Results' Section of this paper shows that DV3D satisfies each of the key design objectives identified as important for a multi-modal neuroimaging data visualization package. In summary, DV3D allows users to view data from many different imaging modalities and analysis streams in a single coordinate space. Data can be cross-referenced with standard spaces in real-time, from 2D or 3D objects. DV3D supports the display of a large number of input data formats, and allows the user to export data in a number of different formats. The user workspace can be customized to allow optimum productivity and allows access for both casual and power users (command line scripting and parallelization). DV3D's platform independence (due to Python) makes it flexible, and the modularity and simplicity of the code base makes it both accessible and scalable.

Readers may ask about the novelty of DV3D. While we (to the best of our knowledge) are unaware of any other software package that utilizes isocontouring with depth-dependent transparency mapping to display 3D statistical overlays (see Advanced Interaction Techniques), we do not claim that any other techniques utilized by DV3D are novel. **Table 1** summarizes the features of DV3D,

Table 1 | Feature summary and comparison of imaging data visualization packages. This table summarizes some of DV3D's key features and compares DV3D's functionality with three commonly used imaging data visualization tools, FSLView, MriCron and 3D Slicer. Features are accurate as at the time of initial development of DV3D.

Software feature	FSLView	MRICron	3D Slicer	DV3D
NEUROIMAGING DATA SUPPORT				
Optimised for neuroimaging	✓	✓	–	✓
Structural MRI	✓	✓	✓	✓
Functional MRI	✓	✓	✓	✓
DTI – probabilistic	✓	–	–	✓
DTI – tractography	–	–	Calculated online	Loaded from memory
DTI – 2d vectors	✓	–	–	✓
DTI – 3d vectors	–	–	✓	✓
MEG/EEG contour plots (2D and/or 3D)	–	–	–	✓
MEG/EEG 3d time-series on surface	–	Single instant	–	Full dynamic
MEG/EEG dipoles	–	–	–	✓
MEG/EEG butterfly plots	–	–	–	✓
DATA EXPLORATION				
2D statistical map overlay	✓	✓	✓	✓
3D statistical map overlay	✓	–	–	✓
Interactive surface extraction	–	–	Complex watershed	Simple isosurfaces
Real-time atlas cross-referencing	If data in MNI space	–	–	4 × 4 Transform required
COMPLEX VISUALIZATION FUNCTIONS				
Real-time reformatting	–	–	Single plane	Multiple planes
Interactive data intersection	–	–	–	✓
Interactive time-series interrogation	2d fMRI only	–	–	2D and 3D fMRI, EEG and MEG
Batch processing from command line	✓	–	–	✓
EXPORT				
Static images	–	✓	✓	✓
Movies	–	–	✓	✓
Real-time streaming	–	–	–	✓
TECHNICAL				
Main code base language	C,C++,Tcl/Tk	Pascal	C++,Tcl/Tk	Python
Platform independent code base	–	–	–	✓
Access to parallel processing	–	–	–	✓

comparing the resulting functionality achieved by DV3D with similar packages already available. We show that, while DV3D is not an entirely comprehensive solution for visualizing neuroimaging data, it does represent a utility that can offer a single solution to users of a variety of neuroimaging analysis packages. Being optimized for neuroimaging data, this single package offers more options to researchers interested in multi-modal neuroimaging data analysis than any alternative stand-alone visualization package.

While visualization packages are primarily used to display the results output by analysis packages, many visualization tools have developed to include techniques to physically manipulate loaded results files with complex analytical algorithms. 3D Slicer, for example, utilizes complex segmentation algorithms to allow tissue segmentation from any MRI volume acquired at any part of the body. This allows 3D Slicer to be regarded as a tool that is suited to generalized medical imaging analysis and visualization rather than being neuroscience specific. When handling neuroimaging data, 3D Slicer is also more analytically driven than MRICron or DV3D. 3D Slicer does not load fiber-tracking results from external analysis packages. Rather it analyzes diffusion-weighted MRI data to calculate fiber tracts[31]. This move away from being a pure visualization tool, specific for neuroimaging data, does mean that 3D Slicer has more demanding development and maintenance overhead and can take longer to become familiar with, compared to MRICron or DV3D.

DV3D was designed to be a tool optimized for the visualization of neuroimaging data and not an analysis tool *per se*. Although many algorithms and calculations underlie the functionality of DV3D, they are primarily image processing functions allowing VTK to display results of analyses conducted in other software packages. If DV3D were solely a data visualization tool, it would simply take user input and display it in its raw format. We have shown however that DV3D offers routines for manipulating loaded data to add value to the visualization environment: DV3D can average raw MEG time series data by epoch and display this average as a contour plot; DV3D can manipulate volume grid data and extract and interpolate 3D surfaces from this data to display isosurfaces and isovolumes; DV3D offers the ability to decimate large surface data sets to increase rendering speed. DV3D has thus already began to evolve from a pure visualization tool to a tool that allows users to interact with their data. DV3D does not, however, lose focus of its optimization for neuroimaging data processing.

Since DV3D has the potential to be more than a visualization tool, we have considered extending its functionality. Including more functions in DV3D will allow a more extensive range of tools for users to interrogate data. The modularity of the framework and platform independence of the code base allows access for rapid development and extension to include additional file format support and processing routine extension. Many functions have already been requested by interested parties and are under current consideration for inclusion in subsequent releases. Python offers modules for handling pipes on operating systems, allowing the potential for system calls and data exchange between system processes. We are currently exploring the capability to include calls to DV3D to/from a number of packages. Other examples of user requests currently under development include the ability to align volumes and/or surfaces manually or with automated error-minimization routines, and functions to measure distances, areas, and volume size between/on displayed objects. Future development of DV3D will focus on support for additional formats, increased automation of processing streams, extended local settings customization, and more extensive data sharing options. We will also consider including the GIfTI format as a surface export option due to the significant increases in performance reported when handling these files relative to the.*vtk* format (Harwell et al., 2008).

Python has a large and diverse international user base, and promotes the development of increasingly accessible and comprehensive solutions for current computing and analysis requirements. The use of Python as the base for DV3D allows a cross-platform, transparent, and extendible code base for user development. By using Python to wrap existing toolkits, including tools for visualization, rendering, parallelization and GUI generation, DV3D development has required minimal new code to be written to solve complex computations. In addition to the functionality DV3D currently offers, DV3D can also be easily expanded to meet users' changing needs because of its modular, open-source design. DV3D's framework is intentionally modularized to provide concise working examples, illustrating the power of VTK and how easily this power can be harnessed by Python. While the authors are keen to extend the package, provision of an open-source package is intended to stimulate and facilitate further development of the software by the user community. Example code illustrating the extension of the functionality of the package is provided for users interested in contributing code or developing the package for their own purposes. DV3D's code base currently consists of circa 12,000 lines of Python code. 3D Slicer has over 550,000 lines of C++ code, although this includes a large amount of additional analytical functionality that DV3D does not have. We suggest that the simplicity of Python relative to C++, and the vastly smaller code base, make DV3D more accessible in terms of community extension and development prospects.

DV3D's primary function is to allow easy, interactive display of multi-modal neuroimaging data. DV3D has been successfully implemented on many platforms and is currently used by local users from a variety of disciplines. DV3D is provided as a free, open-source package built on Python's platform independent model. DV3D can thus be used and, more importantly, developed by the wider neuroimaging community.

ACKNOWLEDGMENTS

The authors would like to acknowledge the developers of Python, VTK and wxWidgets for their ongoing support of open-source software provision. The reviewers are to be thanked for their insightful comments, some of which have already resulted in additional functionality being incorporated into the package.

SUPPLEMENTARY MATERIAL

DOWNLOADING THE SOFTWARE, EXAMPLES AND EDUCATIONAL RESOURCES

DV3D, examples output and input files and interactive user tutorials can be freely downloaded from http://www.ynic.york.ac.uk/software/dv3d.

[31]http://www.slicer.org/slicerWiki/index.php/Slicer3:DTMRI

REFERENCES

Ashburner, J., Andersson, J., and Friston, K. J. (1999). High-dimensional nonlinear image registration using symmetric priors. *NeuroImage* 9, 619–628.

Coltheart, M. (2006). What has functional neuroimaging told us about the mind (so far)? *Cortex* 42, 323–331.

Cox, R. W. (1996). AFNI: software for analysis and visualization of functional magnetic resonance neuroimages. *Comput. Biomed. Res.* 29, 162–173.

Delorme, A., and Makeig, A. (2004). EEGLAB: an open-source toolbox for analysis of single-trial EEG dynamics. *J. Neurosci. Methods* 134, 9–21.

Frackowiak, R. S. J., Friston, K. J., Frith, C. D., Dolan, R. J., and Mazziotta, J. C. (1997). Human Brain Function. San Diego, Academic Press.

Harwell, J., Bremen, H., Coulon, O., Dierker, D., Reynolds, R. C., Silva, C., Teich, K., Van Essen, D. C., Warfield, S. K., and Saad, Z. S. (2008). GIfTI: Geometry Data Format for Exchange of Surface-Based Brain Mapping Data. *OHBM – Poster Presentation*

Jenkinson, M., Bannister, P. R., Brady, J. M., and Smith, S. M. (2002). Improved optimisation for the robust and accurate linear registration and motion correction of brain images. *NeuroImage* 17, 825–841.

Lancaster, J. L., Tordesillas-Gutiérrez, D., Martinez, M., Salinas, F., Evans, A., Zilles, K., Mazziotta, J., and Fox, P. T. (2007). Bias between MNI and Talairach coordinates analyzed using the ICBM-152 brain template. *Hum. Brain Mapp.* 28, 1194–1205.

Larsson, J. (2001). Imaging Vision: Functional Mapping of Intermediate Visual Processes in Man. Ph.D. thesis, Karolinska Institute, Stockholm.

Liu, Z., Kecman, F., and Bin, H. (2006). Effects of fMRI–EEG mismatches in cortical current density estimation integrating fMRI and EEG: A simulation study. *Clin. Neurophysiol.* 117, 1610–1622.

Mackenzie-Graham, A. J., Van Horn, J. D., Woods, R. P., Crawford, K. L., and Toga, A. W. (2008). Provenance in neuroimaging. *NeuroImage* 42, 178–195.

Mazziotta, J., Toga, A., Evans, A., Fox, P., Lancaster, J., Zilles, K., Simpson, G., Woods, R., Paus, T., Pike, B. et al. (2001). A four-dimensional atlas of the human brain. *J. Am. Med. Inform. Assoc.* 8, 401–430.

McDonald, C. R. (2008). The use of neuroimaging to study behavior in patients with epilepsy. *Epilepsy Behav.* 12, 600–611.

Stufflebeam, S. M., and Rosen, B. R. (2007). Mapping cognitive function. *Neuroimaging Clin. N. Am.* 17, 469–484.

Talairach, J., and Tournoux, P. (1988). Coplanar Stereotaxic Atlas of the Human Brain: 3-Dimensional Proportional System – An Approach to Cerebral Imaging. New York, Thieme Medical Publishers.

Teo, P. C., Sapiro, G., and Wandell, B. A. (1997). Creating connected representations of cortical gray matter for functional MRI visualization. *IEEE Trans. Med. Imaging* 16, 852–863.

Wakana, S., Jiang, H., Nagae-Poetscher, M., van Zijl, P. C. M., and Mori, S. (2004). A fiber-tract based atlas of Human white matter anatomy. *Radiology* 230, 77–87.

Wandell, B. A., Chial S., and Backus, B. (2000). Visualization and measurement of the cortical surface. *J. Cogn. Neurosci.* 12, 739–752.

Conflict of Interest Statement: The authors declare that the research was conducted in the absence of any commercial or financial relationships that could be construed as a potential conflict of interest.

Received: 12 September 2008; paper pending published: 25 October 2008; accepted: 05 March 2009; published online: 27 March 2009.

*Citation: Gouws A, Woods W, Millman R, Morland A and Green G (2009) DataViewer3D: an open-source, cross-platform multi-modal neuroimaging data visualization tool. Front. Neuroinform. (2009) **3**:9. doi: 10.3389/neuro.11.009.2009*

Review

The Noninvasive Dissection of the Human Visual Cortex: Using fMRI and TMS to Study the Organization of the Visual Brain

The Neuroscientist
Volume 15 Number 5
October 2009 489-506

10.1177/1073858409334424
http://nro.sagepub.com

Declan J. McKeefry, Andre Gouws, Mark P. Burton, and Antony B. Morland

The development of brain imaging techniques, such as fMRI, has given modern neuroscientists unparalleled access to the inner workings of the living human brain. Visual processing in particular has proven to be particularly amenable to study with fMRI. Studies using this technique have revealed the existence of multiple representations of visual space with differing functional roles across many cortical locations. Yet, although fMRI provides an excellent means by which we can localize and map different areas across the visual brain, it is less well suited to providing information as to whether activation within a particular cortical region is directly related to perception or behavior. These kinds of causal links can be made, however, when fMRI is combined with transcranial magnetic stimulation (TMS). TMS is a noninvasive technique that can bring about localized, transient disruption of cortical function and can induce functional impairments in the performance of specific tasks. When guided by the detailed localizing and mapping capabilities of fMRI, TMS can be used as a means by which the functional roles of different visual areas can be investigated. This review highlights recent insights that the techniques of fMRI and TMS have given us with regard to the function and contributions of the many different visual areas to human visual perception.

Keywords: visual areas; fMRI; TMS; retinotopic mapping; cortical function

Our sense of vision, although based on information received from the external world, is essentially a construct of the brain that is dependent on the processing capabilities of many different visual areas. Previously, our knowledge of these areas relied heavily on data obtained from nonhuman primates. The visual cortex of the macaque monkey, in particular, has been mapped and explored in somewhat dizzying detail compared with that of the human brain. There is a wealth of data from the monkey that have variously identified visual areas on the basis of their (1) functional properties, (2) anatomical connectivity with other brain areas, (3) structural anatomy, and (4) possession of a regular representation of the visual field. These data have also been integral to the formulation of a number of key organizational principles relating to visual processing in the nonhuman primate brain. Additional to the fact that there are multiple visual areas (more than 30 have been identified in the macaque brain), another important characteristic is that these areas are connected to many other cortical areas and that this connectivity is reciprocal (Felleman and Van Essen 1991). Signals emanating from a particular visual area can therefore be transmitted simultaneously to multiple sites within the brain. As a result, visual or, indeed, any aspect of brain function may be thought of as being dependent on the operation of a number of parallel networks, each of which may be involved in the processing of particular kinds of sensory information or in the control of different aspects of behavior.

The study of the nonhuman primate brain has undoubtedly provided us with a robust framework within which we can examine the organization of visual processing. However, the study and understanding of our own visual system remain an important goal, not least because of the differences in size as well as the structural and functional complexity that exists between the human and macaque brain. To this end, the development of modern brain-imaging techniques, such as PET and fMRI, has provided neuroscientists with unparalleled access to the human brain in vivo. Prior to the advent of these neuroimaging tools, information regarding the organization of the human visual cortex was sparse in comparison to that obtained from the monkey brain. Data tended to be gleaned from individuals with pathological or traumatic damage to the brain. But these cases were limited in terms of what they could tell us about the organization of visual processing, not least because such damage tends not to respect the anatomical and physiological boundaries that exist between visual areas. Notwithstanding such

From the Bradford School of Optometry and Vision Science, University of Bradford, UK (DJM, MPB), Department of Psychology and York Neuroimaging Centre, University of York and Hull-York Medical School, UK (AG, ABM).

The support of the BBSRC to DJM and MPB is acknowledged (grant—BB/E00413X/1). AG and ABM are supported by the Medical Research Council, UK.

Address correspondence to: D. J. McKeefry, PhD, Division of Optometry, School of Life Sciences, University of Bradford, Bradford, BD7 1DP, W. Yorks, UK; e-mail: d.mckeefry@bradford.ac.uk.

shortcomings, human lesion studies taken as a whole made clear that the human visual cortex was retinotopic (Holmes 1918; Horton and Hoyt 1991) and that damage to different regions of the occipital lobe leads to deficits that are specific to the perception of different visual attributes or features (color—Meadows 1974a; Zeki 1990; faces—Meadows 1974b; motion—Zihl and others 1983). But it has been the explosion of neuroimaging data that, over the past two decades, has really helped us gain insights into the normally functioning human visual brain and revealed the extent to which it both adheres to and differs from the organizational principles that have been revealed by study of the macaque brain (Zeki and others 1991; Sereno and others 1995; Wandell and others 2007).

Yet, although brain-imaging techniques such as PET and fMRI have undoubtedly revealed much about visual processing in the human brain, they are not without their limitations. Just like many other tools available to the modern neuroscientist, they provide a restricted spatial and temporal window through which different aspects of brain function can be studied. For example, because of their low temporal resolution, brain-imaging techniques in isolation can only provide limited information relating to the timing of neural events in the brain. Therefore, in an attempt to compensate for these limitations, PET and fMRI are now being used in conjunction with other noninvasive techniques such as electroencephalography (EEG), magnetoencephalography (MEG), and transcranial magnetic stimulation (TMS) to study the human visual brain. The last of these, TMS, is particularly useful in that it can be used to transiently disrupt the function of underlying cortical areas, the effects of which can then be assessed using behavioral/psychophysical paradigms. Another problem with fMRI, which relies on a measure of blood oxygenation level-dependent (BOLD) contrast, is that resultant brain activations are correlative. Therefore, it is not possible to determine whether they provide a direct measure of the contribution of a particular brain area to a particular function. The use of TMS, which can directly disrupt and interfere with the normal function of an underlying region of the cerebral cortex, has the potential to allow us to make causal links between neural activity in specific regions of the brain and its contribution to specific functional tasks (Sack 2006). There are a number of ways in which brain imaging can be used in conjunction with TMS (see Paus 1999, 2005). The techniques can be used sequentially; for example, fMRI might be performed first to identify visual areas prior to being targeted by TMS (e.g., Sack and others 2006). This constitutes so-called fMRI-guided or neuronavigated TMS and essentially relies on the prior identification of visual areas on a functional or retinotopic basis. fMRI and TMS can also be combined in a concurrent fashion. In these kinds of experiments, the simultaneous use of both methods can be used to examine not only the changes in brain function at the actual site of TMS application but also those that are induced at more distant cortical sites (Bestmann and others 2008; Ruff and others 2006). Thus, concurrent fMRI and TMS has the potential to study interconnectivity between brain areas. In addition, imaging data might be acquired subsequent to TMS to measure long-term changes induced by TMS (Paus 1999).

This article reviews work that has employed fMRI and TMS in the noninvasive dissection of the functional anatomy of the human visual brain. In the first instance, it will examine how fMRI has been used to localize and map the many different visual areas that exist in the cortex. Second, it examines how this information has been used to guide the examination of the functional properties of these areas using TMS. As such, emphasis focuses on sequential fMRI-TMS studies, where fMRI data have been used to selectively target specifically identified visual areas for TMS—the so-called fMRI-guided or neuro-navigated TMS approach. However, we also examine recent insights into the organization of visual processing that have been provided by concurrent fMRI-TMS methods. These methods are proving to be particularly useful in studying the connectivity between visual areas and the modulatory effects that can exerted by "higher" brain areas on those associated with more low-level visual processing.

Integral to all of the approaches that use fMRI and TMS methodologies is the importance placed on TMS users having a precise knowledge of the underlying organization of visual areas in the cerebral cortex. Visual areas vary not only in terms of their position across individual brains but also in their positions relative to anatomical landmarks. These landmarks include both external features, such as those on the scalp surface (e.g., the inion), as well as internal sulcal and gyral features on the surface of the cortex itself. Faced with this degree of variability in terms of the localization of visual areas, we argue that the need for structural *and* functional MRI data from individual participants is paramount in TMS studies. This is so strong, conclusions can be made relating the contributions of different brain areas to visual perception.

Identification of Visual Areas in the Human Brain Using fMRI

Neuroimaging studies have revealed that approximately 20% of the human cerebral cortex has some visual function (Wandell and others 2007). A large proportion of this visually responsive cortex is found posteriorly in the brain, in the occipital lobes. However, visual areas do extend more anteriorly into the parietal and temporal cortices on the ventral, lateral, and dorsal

Box 1. Retinotopic Mapping with fMRI

Conventional retinotopic mapping performed with fMRI uses visual stimuli that move progressively through the visual field (see Figure 1). As stimuli move through the visual field, the activity on the surface of the cortex of a visual field map (visual area) also moves (Engel and others 1994). The time at which the activity is elicited in the visual cortex corresponds to the position in the visual field of the stimulus that causes the activity. Typically, visual stimuli are presented so they cycle through the visual field many times; in the examples we show here, seven cycles were presented. If the period (and duty cycle) of the stimulus cycle is selected appropriately, the cortical response elicited takes the form very similar to a sine wave because of the temporal properties of the hemodynamic response function. In the example given in Figure 1, the period of the stimulus was 36 seconds, and the sinusoidal nature of the cortical response is evident in the two time-series plots shown in each of the panels A and B. Given the sinusoidal nature of the response, a straightforward way to establish the time at which the response is elicited is to perform a fast Fourier transform (FFT) on the time series (of each voxel) from which the phase of the response can be derived for each cortical location. It is this phase measure that encodes the visual field location that elicits the response. Typically, two stimulus configurations are used to encode the two dimensions of eccentricity and polar angle. These stimuli therefore take the form of rings, for mapping eccentricity and wedges for polar angle mapping. The rings can either expand or contract, and some investigators use both, in separate experiments, as a means of discounting the hemodynamic delay of the BOLD response. The wedge stimuli rotate, and as with rings, opposite directions of motion of the stimuli can be used to correct for the systematic phase lag associated with the hemodynamics of BOLD. In panel A, a surface reconstruction of the occipital cortex is presented with the phase (corrected for lag) rendered onto it in false color. The false color code of phase relates to visual field eccentricity in the way shown in the semicircular color key. The stimulus presented to the participant in this experiment is depicted in the inset in panel A and comprises the checkerboard that underwent pattern reversal at 6 Hz.

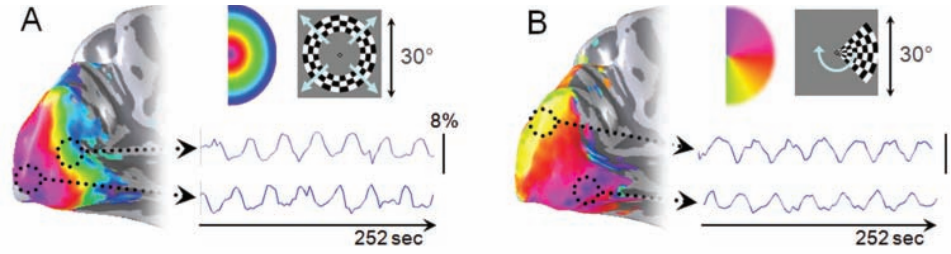

Figure 1. Phase-encoded retinotopic mapping. (A) Expanding ring and (B) rotating wedge contrast patterns elicit waves of cortical activity across visual areas in the occipital cortex. This activity is shown in false color on surface reconstructions of the occipital lobe. Each color represents a particular phase of the hemodynamic response waveform, which corresponds to the stimulation of a particular region in the visual field (see text for a full description).

The phase of the BOLD response shows a systematic and smooth progression from values indicating sensitivity to central visual field locations (purple) at the occipital pole to values indicating sensitivity to more eccentric visual field locations (blue) in the anterior occipital cortex. Time series of the BOLD response are shown for two cortical locations, as indicated by the broken circles and arrows. The time series show a clear cyclic form but are clearly occurring at different phases, corresponding to different visual field locations. In panel B, results from the complementary experiment are presented, and here the phase of the BOLD response indicates the polar angle of wedge that drives the cortical response (as the semicircular key indicates). The phase map of the BOLD response now forms colored bands that converge on the occipital pole. Representations of the horizontal (red), upper vertical (blue), and lower (green) are clearly visible with the vertical meridian representations demarcating the boundary of the primary visual cortex, V1.

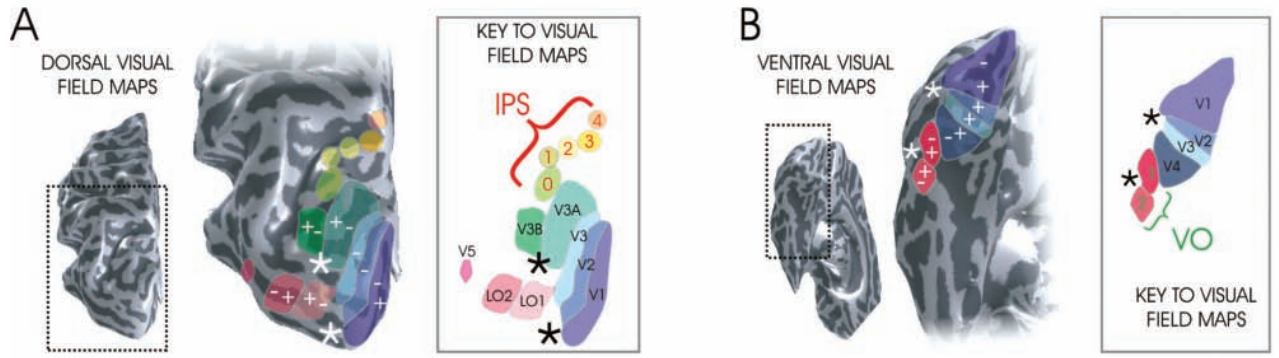

Figure 2. Visual areas in the occipital lobe of the human brain. (A) A schematic of dorsal and lateral visual field maps rendered on a partially inflated representation of the interface between gray and white matter. To the left is an image of the left hemisphere with a dotted line showing the region that is magnified in the middle panel. The middle panel shows where the visual field maps fall onto the gray-white matter interface, with stars indicating the locations of foveal representations. The upper and lower quadrant representations are denoted by + and – symbols, respectively. Visual maps without these symbols represent the visual hemifield, that is, both quadrants. To the right, a key is provided for the visual field maps shown in the middle panel. IPS refers to the intraparietal sulcus, where as many as five visual field maps have been reported. Maps with a V prefix are visual areas that are routinely mapped with retinotopic techniques. LO refers to lateral occipital cortex, where at least two visual field maps have been reported. V3B has been referred to as KO in the literature, and some dispute whether in fact it is a part of V3A and whether it has a hemifield or lower quadrant representation. (B) A schematic of ventral visual areas. Inset to the left is a view of the left hemisphere with the dotted line indicating the magnified region in the central panel. As in A, visual field maps are displayed on the interface between the gray and white matter. To the right, a key to the visual areas is provided. VO corresponds to ventral occipital cortex, where two visual field maps have been reported.

surfaces of the brain. Like the macaque brain, this large expanse of visually responsive cortex does not constitute a single homogeneous entity but instead comprises a patchwork of different visual areas, each with its own representation of the external visual world and/or functional role (see Figure 2). Retinotopic brain-mapping techniques have made enormous strides in clarifying how and where the visual field is mapped across the visual brain. Notwithstanding the different means by which we can define a visual area, the presence of multiple representations of the visual field in itself implies that our visual sense, like that of the monkey, is the result of activity across a broad network of interconnected brain areas.

Occipital Visual Areas

Brain-imaging studies have demonstrated that at least in the early stages, the organization of the human visual brain and that of the monkey is quite similar. There is a group of core visual areas (V1, V2, V3, V4, and V5) that is similar in terms of their retinotopic mapping and the functional roles they perform in the human and macaque brain (Sereno and others 1995).

V1

Area V1, or the primary visual (or striate) cortex, is the region of the brain that receives the majority of visual information arising from the retinogeniculate pathway. V1 is situated within the calcarine sulcus in the occipital lobe, and in each cerebral hemisphere, it contains a precise representation of the contralateral visual field (i.e., it is retinotopically organized). The superior visual field is mapped onto the lower surface of the calcarine sulcus, and the inferior visual field is mapped on the upper surface. The central or macular regions of the visual field are mapped toward the posterior occipital pole with more peripheral parts of the visual field being mapped anteriorly along the calcarine sulcus.

V2

Area V1 is surrounded by a second representation of the visual field, and this is known as area V2. In each cerebral hemisphere, V2 is split into dorsal and ventral regions, which respectively contain retinotopic maps of the inferior and superior quadrants of the contralateral visual field. V1 and V2 are joined at the representations of the vertical meridian. Results from brain-imaging studies have indicated that at least in the early stages, the organization of the human visual brain and that of the monkey is quite similar. It would appear that as far as V1 and V2 are concerned, there is very little difference across the species. V1 and V2 appear to be present in all species and perform similar roles of distribution and segregation of visual information.

V3

V3 forms the next representation of the visual field, and it surrounds V2 and has a similar dorsal/ventral split between the representations of the inferior and superior parts of the visual field (V3d and V3v). Earlier

work on the macaque monkey suggested that the dorsal and ventral maps of V3 actually constituted separate visual areas, termed V3 and VP (Burkhalter and others 1986). However, more recent imaging work indicates that, in the human brain at least, the ventral and dorsal maps are part of the same visual area (Wandell and others 2007). V2 and V3 abut at the representations of the horizontal meridian.

V3A and V3B

Area V3A is a visual region that lies dorsal to V3 in the occipitoparietal cortex and with it contains a full hemifield representation of the contralateral visual field, which differentiates it from dorsal and ventral V2 and V3, which map only a quadrant of the contralateral field (Tootell and others 1997). Smith and others (1998) identified another map area, V3B, lying more lateral to V3A along the transverse occipital sulcus. This area had previously been referred to as the kinetic occipital (KO) area in view of its activation by kinetic boundaries (Dupont and others 1994), but subsequent studies have demonstrated that this region of the brain is not uniquely selective for these kinds of stimuli (Zeki and others 2003). It also seems that V3B has a representation of the lower quadrant, and the existence of a "counterpart" visual map in the ventral cortex that would represent the upper quadrant is controversial (Brewer and others 2005; Zeki and others 2003).

V4

Cortical areas located on the ventral surface of the brain are involved in the processes that underpin object recognition and color perception. But the position of these visual areas on the ventral occipitotemporal cortex, just above the cerebellum, makes them difficult to access using TMS. Retinotopic mapping procedures have managed to reveal the presence of a number of visual areas in this region of the brain. One complete hemifield representation can be found anterior to ventral V3, on the fusiform gyrus, and is referred to as human V4 (McKeefry and Zeki 1997; Wade and others 2002).

V5/MT+

Probably one of the most intensively studied visual regions of the human brain is area V5/MT, which is found on the lateral surface of the brain occipitotemporal cortex (see Figure 2). It is highly responsive to visual motion and has been consistently activated in many neuroimaging studies (e.g., Zeki and others 1991; Watson and others 1993; Tootell and others 1995). The convention of late has been to refer to it as the V5/MT *complex*, or simply V5/MT+, to highlight the likelihood that there are a number of motion areas, each with a separate representation of the visual field in this region of the cortex (Huk and others 2002). This view is supported by the discovery of both contra- and ipsilateral visual hemifields maps in this region of the brain (Dukelow and others 2001). The presence of these subdivisions within the human motion responsive visual cortex is consistent with that found in the macaque brain, where homologous visual areas MT and MST have a similar retinotopic organization.

Dorsal Visual Areas beyond V3A

The posterior parietal cortex (PPC) in the human brain constitutes a transitional region in terms of processing, where brain areas take on a more multimodal role compared with the emphasis on visual function than is in evidence in the occipital cortex. The higher degree of complexity within the PPC in terms of its functional organization is consistent with the notion that it supports a variety of sensory and cognitive functions such as visuospatial judgments, visuomotor control, control of attention, working memory, and multimodal integration. This multifunctional role places the PPC right at the interface between vision and other aspects of cognitive function. Previously, neuroimaging experiments had only been able to identify visual areas within the PPC on a functional basis. Typically, these relied on the use of more complex cognitive tasks involving saccadic planning or attention, for example (Schluppeck and others 2005), compared to the more passive visual tasks used in retinotopic mapping. However, more recent brain-imaging studies have started to reveal that this region of the brain also contains regular representations of the visual field that can be mapped in a similar fashion to their occipital counterparts (Swisher and others 2007).

V6

On the medial surface of the brain in the posterior parietal occipital sulcus and anterior to areas V3A and V3, another representation of the contralateral hemifield has been described. This visual area has been termed area V6 and, like its homologue in the macaque brain, is activated by coherent motion of random dot stimuli, as well as possessing a similarly large representation of the peripheral visual field (Pitzalis and others 2006).

IPS0-4

Anterior to areas V3A and V3B in the PPC lie a number of visual areas that have been shown to possess regular topographic maps of the visual field (see Figure 2A). Up to five different representations of the visual field have been identified using retinotopic mapping procedures along the medial bank of the intraparietal sulcus (IPS): V7 (IPS0), IPS1, IPS2, IPS3, and IPS4 (Swisher and others 2007). It is as yet unclear how these recently

described retinotopically defined areas correspond to those that have been defined primarily on a functional basis in the monkey and human PPC. One of these functional areas is known as the anterior intraparietal cortex (AIP) and appears to be involved in grasping and the analysis of basic object properties, such as size and shape. Another area, the ventral intraparietal area (VIP), is a multimodal area in that it is responsive to moving stimuli that may be defined on a visual, tactile, or even auditory basis. More posteriorly in the intraparietal sulcus of the monkey brain lies a region known as the lateral intraparietal area (LIP), which is important for the planning and control of eye movements. Its homologue in the human brain is sometimes referred to as the parietal eye field (PEF), and it has been suggested that this area may be equivalent to IPS3 (Sereno and others 2001).

Lateral Visual Areas

Lateral Occipital Visual Areas

On the lateral surface of the brain bounded posteriorly by dorsal V3, superiorly by areas V3A and V3B, and anteriorly by V5/MT+ lies a region of the brain that was previously termed the lateral occipital complex (LOC) and showed selectivity for visual objects. Originally, it was considered as lacking in any regular retinotopic organization, but more recent work has demonstrated that there are in fact two representations of the contralateral hemifield, termed L01 and L02, which overlap with the posterior portion of the LOC and area V3B (Larsson and Heeger 2006; see Figure 2A). As well as containing separate hemifield representations, L01 and L02 are reported to have different functional properties. L01 exhibits orientation selectivity and is thought to be involved in the analysis of boundary information of shapes. L02, on the other hand, appears to be responsive to more complex aspects of shape perception (Larsson and Heeger 2006).

Ventral Areas beyond V4

V01, V02

Anterior to V4 lie a further two hemifield representations, V01 and V02, which have large foveal representations (Brewer and others 2005; Larsson and Heeger 2006; see Figure 2B). In keeping with the role played by the ventral cortex in the analysis of objects are functionally defined regions that are selectively responsive to different object categories. Anterior to V4, for example, are the fusiform face and the parahippocampal place areas. The former, as the name implies, is activated by face stimuli and the latter by images of places (Op de Beeck and others 2008).

Investigation of the Function of Visual Areas with TMS

Although fMRI has been useful in that it has provided a good deal of information concerning the anatomical localization of the different areas within the visual brain, the technique has a major limitation: it cannot definitively demonstrate that activity in a specific part of the brain is essential to particular aspect perception or cognition. The use of TMS, with its capability to induce localized disruption to cortical activity, offers the opportunity to make such causal links between brain activity and behavior. When combined with the precise information about the location of visual areas within the cerebral cortex that can be obtained with fMRI, TMS provides the potential to investigate the contribution of specific cortical areas to the performance of particular tasks in an accurately targeted fashion.

Despite the fact that the basic organizational pattern of visual areas may be consistent from person to person, it is well-known that the size and anatomical location of visual areas can vary widely across human subjects (Watson and others 1993; McKeefry and Zeki 1997; Dougherty and others 2003; Kammer and others 2005a, 2005b). Figure 3 provides an example of how the dorsal portions of visual areas V1, V2, V3, and V3A can vary in position across four different individuals. This variability can be problematical from the point of view of TMS studies, where placement of the coil on the surface of the scalp has often been performed with limited knowledge of the participant's underlying cortical organization. A number of TMS studies have used stimulation sites based on the external anatomy of the skull using sites such as the inion, for example, which is a bony protuberance found at the back of the head. Such systems do not allow for the potential for variability between participants. Stimulation sites based on standard brain atlases (e.g., Talairach and Tournoux 1988) face a similar problem in that these coordinate systems are based on averages across subjects, and the individual may depart from this ideal (Ryan and others 2006). Therefore, if techniques such as TMS are going to prove a useful means by which we can dissect the visual brain and cortical function, it is imperative that we have data relating to individual brains and a knowledge of how and where specific visual areas are mapped across the cortical surface. The variations in location are not ones that can be easily overcome by using anatomical landmarks on an individual's scalp or cortex. The essential step therefore is to provide a spatial framework within which visual areas are specified for each individual. This can be provided only by mapping visual areas in individuals with fMRI. Data presented in Figure 4 emphasize this point by showing interindividual variability of the location of one particular visual area, V3A, relative to the position of the inion. The

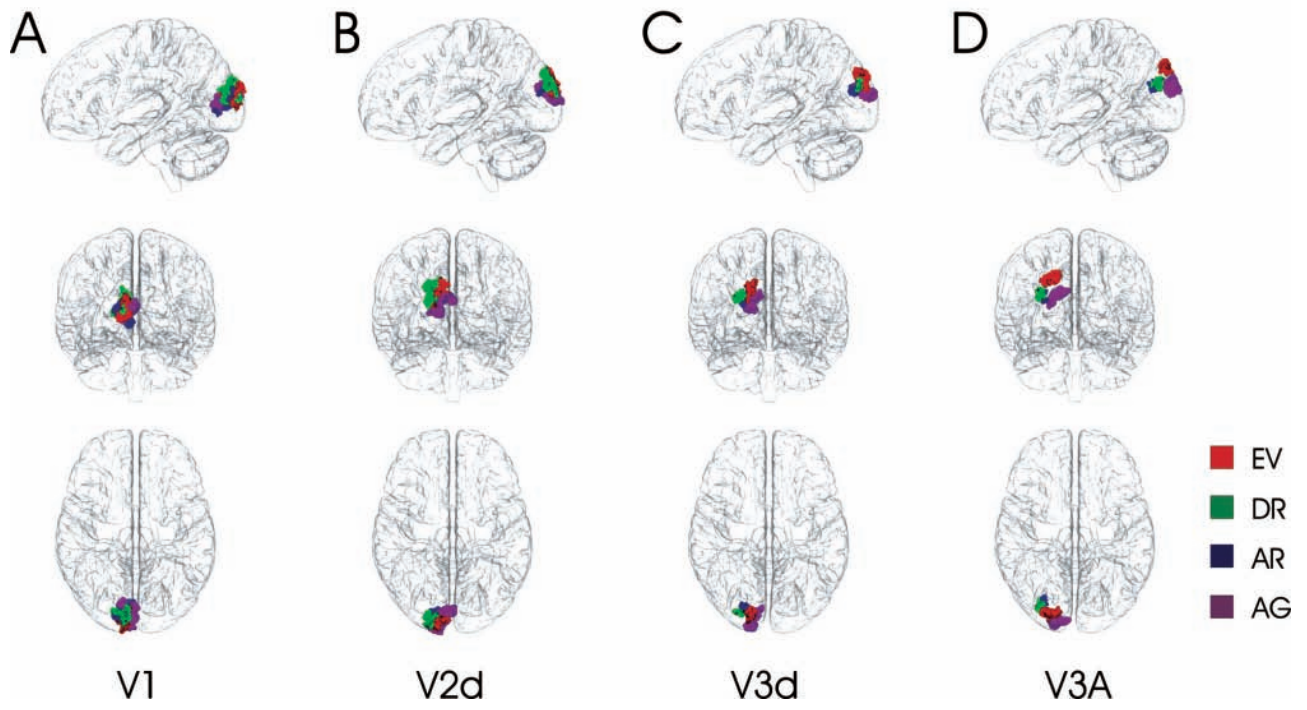

Figure 3. Variations in visual area locations in Montreal Neurological Institute space. Dorsal visual areas, identified on the basis of fMRI retinotopic mapping procedures (described in Box 1). Each area—V1, V2d, V3d, and V3A—has been plotted for four participants in panels A, B, C, and D, respectively. We illustrate here for clarity the dorsal representations of V2 and V3, which have ventral counterparts.

magnitude of this variation is large compared with the differences in the location of neighboring visual areas within an individual. This finding makes clear therefore that in the absence of mapping visual areas, it is likely that TMS would target different visual areas in different individuals, rendering experiments low powered at best and misleading at worst.

For TMS to succeed in dissecting the function of the visual cortex, it has to be targeted accurately in the context of the locations of an individual's visual areas. The use of both structural and functional MRI data can provide information relating to the variability in anatomy and function that exists between individual brains and can improve this accuracy. Coregistration of MRI data with the TMS coil position can be used to enable the targeted disruption of specifically identified regions of the visual cortex. Once this coregistration has taken place, movement of the coil with respect to the subject's head can be registered and visualized in real time. Figure 5 shows an example of how this can be performed in the selection of area V5/MT for investigation by TMS. The coil can then be navigated over specific visual areas with accuracy and its position maintained on a trial-by-trial basis during the performance of behavioral tasks.

TMS of Occipital Visual Areas

The application of TMS to the occipital visual areas in the human brain generates two kinds of effects: (1) it disrupts visual function by reducing sensitivity to visually presented stimuli, thereby generating field defects or scotomas. (2) It induces visible phosphenes, seen by observers as shaped gray or light flashes in specific regions of the visual field (Amassian and others 1989; Kastner and others 1998; Kammer and others 2005a, 2005b). These two effects are likely to be the functional consequences of inhibitory and excitatory influences on neural activity that are known to be exerted by TMS (Hallett 2007; Kammer and others 2005a). The reductions in sensitivity, or scotomas, are the result of inhibitory processes that reduce the firing rates of responsive neurones, but on the other hand, phosphenes are the result of the excitatory increases in background neural activity (see Box 2).

The experiments performed by Kammer and colleagues (2005a, 2005b) attempted to relate the effects of applying TMS to the occipital cortex with the underlying cortical organization of early visual areas, V1, V2, and V3. Their experiments used fMRI and TMS in a sequential fashion, using retinotopic mapping procedures to localize visual areas V1 to V3 in individual brains. This allowed them to correlate the position and extent of phosphenes and sensitivity losses with the application of TMS to specific visual areas. Kammer and others found that phosphenes and reductions in sensitivity were generated within coextensive regions of the cortex and could be induced by application of TMS to virtually all of the early visual areas, incorporating

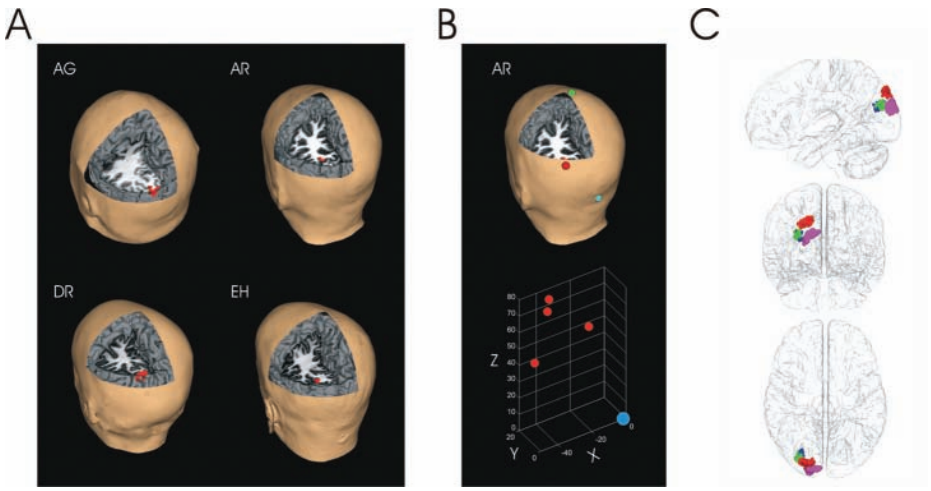

Figure 4. Variation in the position of V3A. (A) Visual area V3A localized on the basis of retinotopic mapping procedures in four participants. Activations are rendered, in red, on the surface of the cortex and in the gray matter of the cut-through slices. There is clear evidence of variability in the position of V3A. The scalp surface is also rendered so that the activity can be assessed in the context of the locus for transcranial magnetic stimulation (TMS) coil positioning. (B) In the upper panel, a reconstruction of one subject's (AR) brain is shown, viewed from the same location as in A. In this case, however, the scalp surface has been raised up in the axial plane so the TMS coil position on the scalp can be seen, the red marker. The green and cyan markers indicate fudicial points at Cz and the inion. These points, used together with the coordinates of the nasion, allow a frame of reference to be constructed, with the inion at the origin, the inion-nasion representing the *y*-axis, and the plane through the three fudicials representing the $x = 0$ plane. The lower panel shows the coil locations plotted in the frame of reference for the four participants shown in A. Clear variation in coil position is evident and shows that using scalp reference points is unlikely to provide an accurate localization of, in this case, V3A. (C) Shows the location of V3A in a standard (MNI) anatomical space. In this case, therefore, the data have been coregistered to one canonical anatomical space, but still considerable variation in the location of V3A is evident.

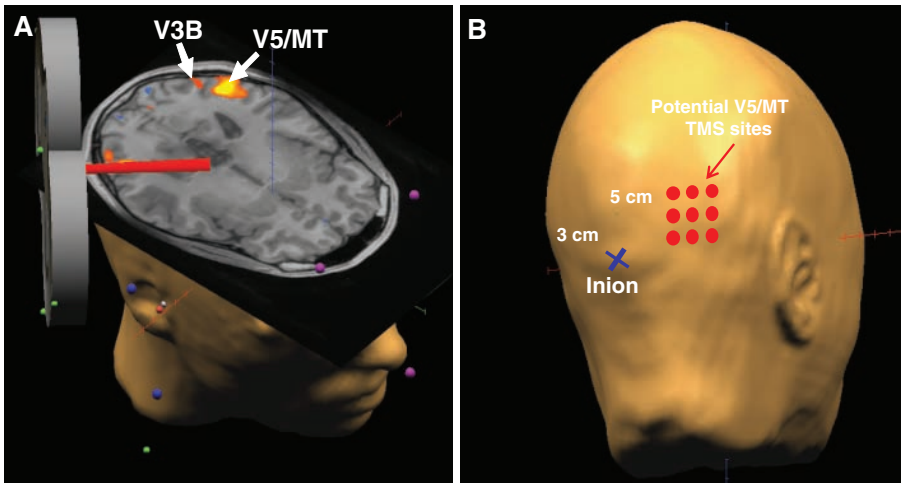

Figure 5. Identifying visual areas for transcranial magnetic stimulation (TMS). (A) A single frame of a real-time sequence showing how a TMS coil (shown in gray) and its beam of action (shown in red) can be coregistered with a single subject's structural and functional fMRI data. The pink dots show the positions of three ultrasound transmitters that are placed on the head. These are linked to three anatomical landmarks (only one of which can be seen in this view) shown by the white dots. The landmarks used in this case were the nasion and the two incisurae intertragicae. The points were then coregistered with the same predefined anatomical points on the head representation derived from the MRI data. Similarly, a local coordinate system was set up for the TMS coil by linking prespecified points (green dots) with the additional ultrasound transmitters (blue dots). The brain activations (shown in orange and yellow) represent visual areas that are responsive to visually presented moving stimuli and in the plane, shown in the right and left hemispheres, the position of V5/MT and a small portion of V3B located more posteriorly toward the occipital pole. In this experiment, TMS was targeted so as to disrupt the normal function of V5/MT in the subject's right hemisphere. (B) A representation of the external scalp of the same subject shown in A. An alternative method that has been used previously to localize area V5/MT makes use of the external anatomy of the skull and characterizes its position relative to the inion (blue cross). Modifications of this procedure have involved the use of hunting strategies where the TMS coil is systematically placed at a number of different scalp positions (red dots) to elicit the strongest functional deficit or perceived moving phosphenes. Compared with the precise detail that is available about the position of visual areas using the methodology shown in A, the approach here provides little information with regard to the underlying functional anatomy of the cortex, thus making it difficult to state with any certainty precisely which visual areas are likely to be stimulated.

Box 2: How Does TMS Work?

TMS works on the principle that a rapidly changing electrical current carried within a stimulation coil induces a magnetic field, the flux lines of which are oriented perpendicular to the plane of the coil. When the stimulation coil is placed on the human scalp, the induced magnetic field penetrates into the cerebral cortex, inducing external and internal electrical currents that interfere with normal neuronal activity and temporarily alter the function of underlying brain areas. However, the exact manner by which TMS brings about these alterations in function is still not entirely understood. Confusingly, the delivery of TMS has been found to both facilitate and suppress various aspects of cortical function. This is due to the fact that TMS of the cerebral cortex generates both excitatory and inhibitory effects on neural activity and that the relative predominance of either type of effect is highly dependent on the timing of delivery, the strength, and the temporal structure of the TMS pulse sequences (Hallett 2007). TMS can be delivered in a variety of different ways, the most basic being in the form of a single pulse. Repetitive trains of pulses can also be used in so-called repetitive TMS (rTMS). Under these conditions, when the temporal rate of stimulation is low (0.2–1 Hz), this tends to accentuate the inhibitory effects of TMS, whereas at faster rates of repetition (>5 Hz), the excitatory effects TMS come to the fore. The temporal structure of delivery has also been modified further in a technique known as "theta burst TMS." This involves the delivery of short bursts of TMS pulses that are of high frequency, typically between 50 and 100 Hz, and these bursts are delivered at a rate of approximately 5 per second (e.g., Huang and others 2005). The excitatory and inhibitory effects of the TMS can be manipulated either by the continuous or intermittent delivery of these theta bursts over time.

A direct neurophysiological demonstration of the excitatory and inhibitory effects of TMS has been demonstrated in the cat visual system by Allen and others (2007). They showed that the application of TMS to the visual cortex during the presentation of visual stimuli leads to a transient increase in the rate of discharge from neurons that otherwise would not be responsive to the visual stimulus (see Figure 6). Additional to this increase in background spontaneous activity, TMS also simultaneously inhibits the firing rate of neurons that are actually responsive to the visual stimulus. This inhibition is of a more sustained nature and can bring about suppression of visually evoked neural activity for up to 10 minutes following the delivery of TMS. These changes in neural activity were also shown to be coupled with changes in oxygenation and blood supply to the cortical tissue.

The findings of Allen and others (2007) are of particular relevance because behavioral investigations typically describe TMS as interfering with cognitive processes via the introduction of random neural events, which bring about a reduction in the strength of the relevant neural signal, relative to the irrelevant background neural noise. Such decreases in signal-to-noise ratios may result either via the suppression of neural signal relating to the target stimulus itself (Harris and others 2008) or via an increase in the background or spontaneous neural noise (Walsh and Cowey 2000; Silvanto and others 2007). The physiological data of Allen and co-workers from the cat visual cortex support the involvement of both these alternatives. The resultant effects of TMS are therefore dependent on the interplay between these facilitatory and suppressive effects on neural activity.

Yet another confounding factor is that the relative predominance of either facilitation or suppression is also dependent on the initial activation state of cortical neurons. In experiments where the activity of a particular population of neurons is diminished by a prolonged period of prior exposure to a stimulus (i.e., adaptation), TMS has been shown to actually enhance their responses when it is applied. At the same time, however, it would seem to suppress the activity of neurons that have been unaffected by the processes of adaptation (Silvanto and others 2007). Based on these results, TMS is deemed to act upon the least active neural population, facilitating the perceptual attributes encoded by these neurons.

(continued)

Box 2: (continued)

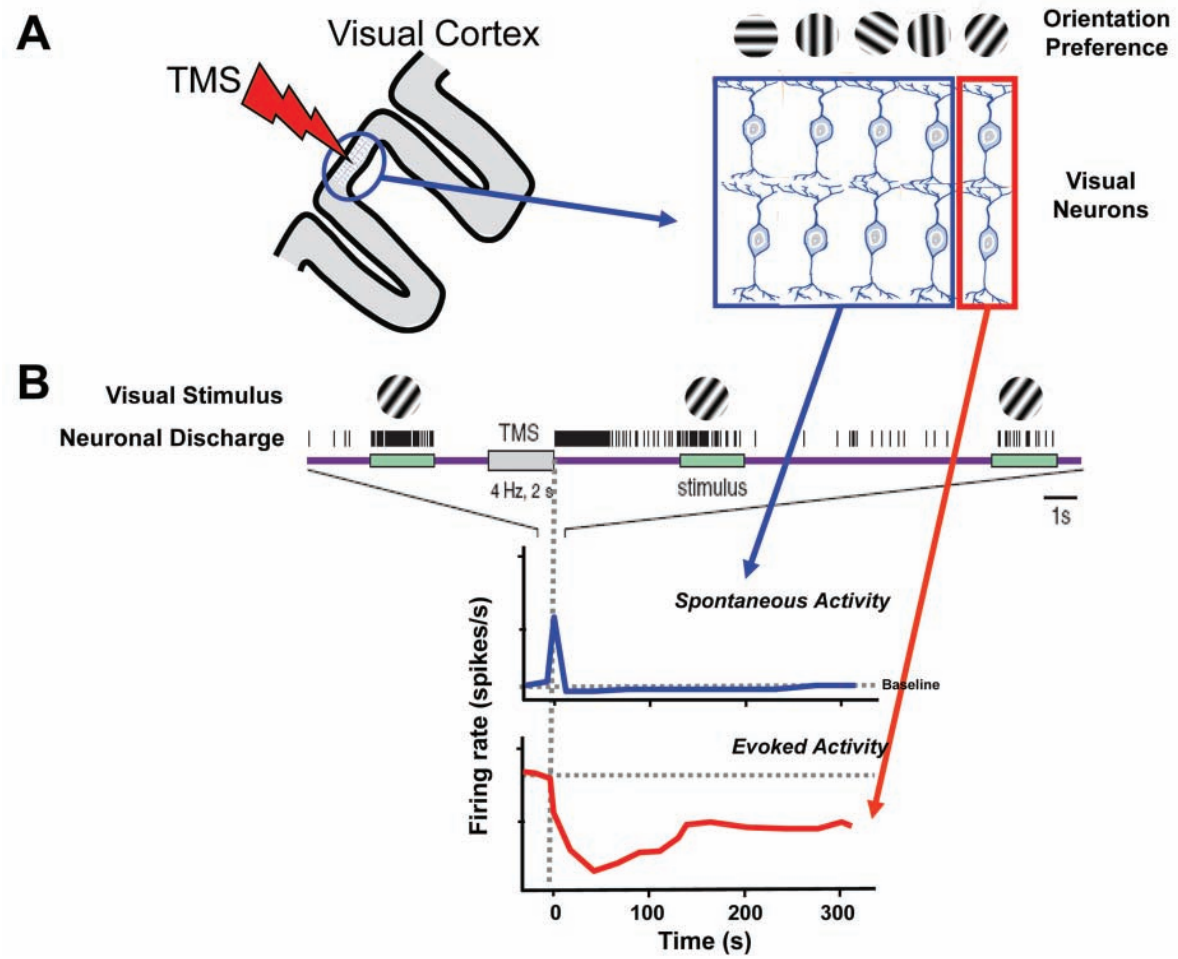

Figure 6. The neurophysiological basis of transcranial magnetic stimulation (TMS). (A) A schematic representation of the effects of TMS on neurons in the cat visual cortex. The application of TMS to the surface of the visual cortex will influence the activity of a large population of underlying visual neurons. These neurons will have a wide range of response properties, and in this figure, we have highlighted orientation selectivity. (B) If a visual stimulus is presented (in this case, a grating oriented at 45 degrees), only a small subpopulation of visual neurons with matching orientation selectivity will be responsive to this stimulus (highlighted in red). In the absence of TMS, these neurons will fire vigorously to this stimulus. However, when TMS is applied, there is a long-term suppression of this activity, which greatly reduces the firing rate of this subpopulation of neurons (red line on the lower graph). In contrast, there is a larger population of visual neurons that are not responsive to this particular stimulus, and they will fire minimally during its presentation. The effect of TMS on this group of neurons is very different, and following its delivery, there is a transient increase in the spontaneous activity of these normally minimally responsive neurons (blue line, upper graph). The suppression of the visually evoked responses, coupled with the increases in the background spontaneous activity, has the resultant effect of decreasing the signal-to-noise ratio. This figure is adapted from the work of Allen and others (2007).

striate as well as extra-striate regions (Kammer and others 2005b). The application of TMS to the occipital pole is most likely to generate phosphenes in the lower part of the visual field. This is due to the fact that dorsal visual areas (which map the inferior visual field), particularly in areas V2 and V3, are more likely to be affected by TMS than their ventral counterparts, which are located on the less accessible ventral surface of the brain. In fact, it has been argued that lower field peripheral phosphenes (>4 degrees of eccentricity) are mainly due to the effects of TMS in dorsal V2 and V3 rather than V1. In V1 itself, the upper and lower visual field representations lie much closer together, and as a result, the effects arising from TMS to this area can spread into the superior visual field (Kastner and others 1998).

In many instances, TMS-induced phosphenes had a sector-like shape, and their location in the visual field did not correspond exactly with the known retinotopy

of early visual areas. This led Kammer and colleagues to speculate that the application of TMS to the occipital cortex not only affects the visual cortical areas themselves but also affects the transmission of signals within the fiber tract pathways that interconnect the striate and extra-striate visual areas. These tracts include the optic radiations, which provide input from the subcortical visual pathways to V1, as well as the forward- and back-projecting fibers to and from V2 and V3. This reciprocal connectivity between the extra-striate visual areas and V1 has been shown to be particularly important in visual perception.

One of the great advantages offered by TMS is the precision with which the timing and delivery of single TMS pulses to the brain can be controlled. This has been of significant benefit in the study of the temporal organization of processing within the visual brain (Pascual-Leone and others 2000). By temporal organization in this instance, we mean the time windows during which neural activity in different visual areas makes a contribution to visual perception. In a seminal study, Pascual-Leone and Walsh (2001) demonstrated that back-projections from V5/MT to V1 are essential for the awareness of visual stimuli. Their experiments exploited the temporal properties of TMS, which they used to deliver precisely timed disruption to cortical function to areas V5/MT and V1, which were first localized on a structural basis using MRI scans. When TMS is applied to area V5/MT, observers are sometimes able to perceive moving phosphenes. However, Pascual-Leone and Walsh found that the ability of observers to report the presence of these phosphenes was severely impaired when the delivery of TMS to V5/MT was followed by the delivery of low-intensity TMS to V1 5 to 45 ms after stimulation of V5/MT. The basis of this result lies in the fact that the timing of the application of TMS to V1 coincides with the arrival of neural signals back from V5/MT, and it is the disruption of this information, derived from back-projections, that degrades the perception of moving signals. No such interference is measured when TMS is applied to V1 in advance of V5/MT. The importance of experiments such as this lies in the fact that it highlights the utility of TMS in the study of the connectivity (both feed-forward and feed-backward) between visual areas, something that we know from the monkey brain is a key organizational characteristic of visual processing. In this respect, TMS has an added advantage over fMRI in that it enables a temporal dissection of the interactions between visual areas.

TMS of Lateral Visual Areas

V5/MT and Visual Areas Responsive to Motion

The perception of motion by the human visual system has proven to be particularly amenable to study using TMS. Its application, primarily to area V5/MT, has been shown to degrade performance on a variety of tasks that depend on motion, including direction discrimination, perception of motion-defined form, visual search, and speed perception, to name but a few (Beckers and Zeki 1995; Anand and others 1998; Walsh and others 1998; Matthews and others 2001). There are, however, inconsistencies across studies with regard to the precise timing at which the delivery of TMS to V5/MT induces maximum disruption to the perception of motion. These may have, in part, arisen as a result of the inaccurate localization of area V5/MT. Sack and co-workers (2006) have argued that the spatial localization of cortical areas such as V5/MT, based on external anatomical landmarks, as was commonplace in earlier studies, is fraught with difficulties. Not least among these is the fact that V5/MT in humans can vary by as much as 2 to 3 cm across individual subjects (Watson and others 1993). Other methods of localizing V5/MT are also open to question. The use of moving phosphenes has been advocated as a means of determining when a TMS coil is positioned directly over V5/MT (Stewart and others 2001). However, human brain-imaging studies have demonstrated that, in addition to V5/MT, moving stimuli can generate activity across a broad network of different cortical regions incorporating areas V1, V2, V3d, V3v (or VP) V3A, or V3B (or KO area; Smith and others 1998). The last of these areas, V3B, is of particular relevance as is it is located very close to V5/MT, lying just posterior to it on the lateral surface of the brain (see Figure 5A). The possibility that moving phosphenes can be generated by motion-responsive areas such as V3B has not been ruled out (Fernandez and others 2002). In view of the potential limitations in accurately localizing V5/MT, Sack and others (2006) took the approach of identifying motion-responsive regions of the cortex using fMRI imaging techniques in which participants viewed moving stimuli. Using these data in conjunction with a frameless stereotactic localization system, they were able to accurately target TMS to area V5/MT in each participant. Using this so-called neuro-navigated TMS methodology, they were able to demonstrate a clear causal link between V5/MT activity and motion perception. They showed that the delivery of TMS to V5/MT during two temporal windows (the first 40–30 ms prior to stimulus onset and the second 130–150 ms after stimulus offset) disrupted the ability of observers to judge the direction of coherent motion in a random dot pattern.

As emphasized earlier, our sense of vision is the result of neural activity, not just within a single isolated visual area but instead is the result of activity distributed across a network of interconnected cortical areas. In the case of motion perception, although area V5/MT is the region that undoubtedly possesses the highest sensitivity to motion, other regions of the visual cortex are also responsive to such stimuli (see above). However, little is known about the contributions of these areas, and relatively few

studies have examined the effects of applying TMS to other cortical regions that are activated by motion (i.e., V1, V2, V3d, V3v, V3A, and V3B). This has largely been due to the difficulties in the accurate identification and localization of the different visual areas in individual brains. The combination of retinotopic fMRI brain-mapping procedures with TMS offers the possibility of gaining fresh insight into the contribution of other cortical regions in this network of visual areas responsive to motion. One area in this network, V3A, is worthy of investigation for two reasons: first, V3A has been shown to be second only to V5/MT in terms of its sensitivity to motion (Tootell and others 1997). Second, in the macaque brain, area V3 has been traditionally considered to be the more important region for motion processing, containing as it does a high proportion of neurons that are selective for motion and direction. In a combined TMS/fMRI study of motion processing in the human brain, McKeefry and others (2008) identified the constituent visual areas of the motion network on the basis of their retinotopy as well as their activation by moving stimuli (see Figure 7). These data allowed the accurate targeting with TMS of visual areas such as V3A and V5/MT, enabling their individual contributions to motion perception to be studied. McKeefry and colleagues employed a delayed speed discrimination task and showed that the application of rTMS to both V3A and V5/MT+ interferes with human speed perception, inducing both a perceived slowing of moving stimuli and elevations in speed discrimination thresholds. The fact that we can induce deficits in perception by applying rTMS to area V3A indicates that behaviorally relevant information about speed is encoded not only by activity in human area V5/MT+ but also by activity in area V3A. Other visual areas in the motion network were found not to be essential for the performance of this speed discrimination task. When TMS was applied to cortical areas V3B and V3, for example, there were no deficits in performance. Figure 7 demonstrates the cortical specificity of the effects of TMS in this experiment. When TMS is applied to V3A or V5/MT+, the effects on performance are demonstrated by the shifts to the right and the changes in slopes of the psychometric curves. These deficits are not observed when the site of application lies outside of these two regions, in areas V3 and V3B. Thus, although motion might generate activation across a number of visual areas within the brain, the relative contribution of these areas to the performance of specific tasks may differ considerably. TMS in conjunction with fMRI is only beginning to give us insights into the functional contributions made by visual areas that make up such cortical networks.

TMS of the Lateral Occipital Complex

Compared with V5/MT+, relatively few studies have deployed TMS in the investigation of the contribution of lateral occipital cortical areas to visual perception. Studies that have been carried out have, thus far, tended to confirm the involvement of lateral occipital areas in shape perception (Ellison and Cowey 2006, 2007). In these experiments, lateral occipital areas were identified on an anatomical basis. However, there is a paucity of studies that have identified lateral occipital visual areas in different individuals on a functional basis. This is important from the perspective that, similar to many other areas in the visual brain, there is a high degree of variability in the position of lateral occipital areas. In addition, there is now evidence to suggest that this region of the cortex can be subdivided into areas L01 and L02 (Larsson and Heeger 2006), which not only have separate visual field representations but may also have different functional roles that are ripe for investigation by TMS.

TMS of Posterior Parietal Visual Areas

The involvement of the PPC in a variety of different aspects of perception and cognition, including attention, visuomotor control, and the representation of space, has meant that the investigation of its function using TMS has been approached from different standpoints. As a result, there is a vast literature on this topic, and this review covers only a small proportion of this work that relates to the contribution of the PPC to visual perception. For more detailed reviews on the use of TMS in the study of other aspects of parietal function, the reader is directed to more comprehensive treatments of this literature (e.g., Rushworth and Taylor 2006).

Eye Movements

The PPC plays an important role in the planning and control of eye movements. Studies have shown that the application of TMS to this region of the brain can increase the latency of saccadic and vergence eye movements, as well as disrupt the accuracy of memory-guided saccades (Yang and Kapoula 2004; Oyachi and Ohtsuka 1995). One study in this field has a strong resonance with one of the central themes of this review in that it highlights the importance of accurate localization of cortical areas prior to TMS delivery. The study, performed by Ryan and others (2006), examined the variability of the functional effects on saccadic eye movements elicited by TMS when it was applied to the human PPC. Importantly, the placement of the TMS coil was determined on the basis of three different techniques: the coil position was positioned with respect to (1) external anatomical landmarks of the participants' skulls, (2) the structural anatomy of the IPS in each participant, and (3) averaged stereotaxic coordinates for the IPS. Ryan and co-workers found a mean difference in coil position of 2 to 3 cm based on these different localization methods, a distance that, in cortical terms,

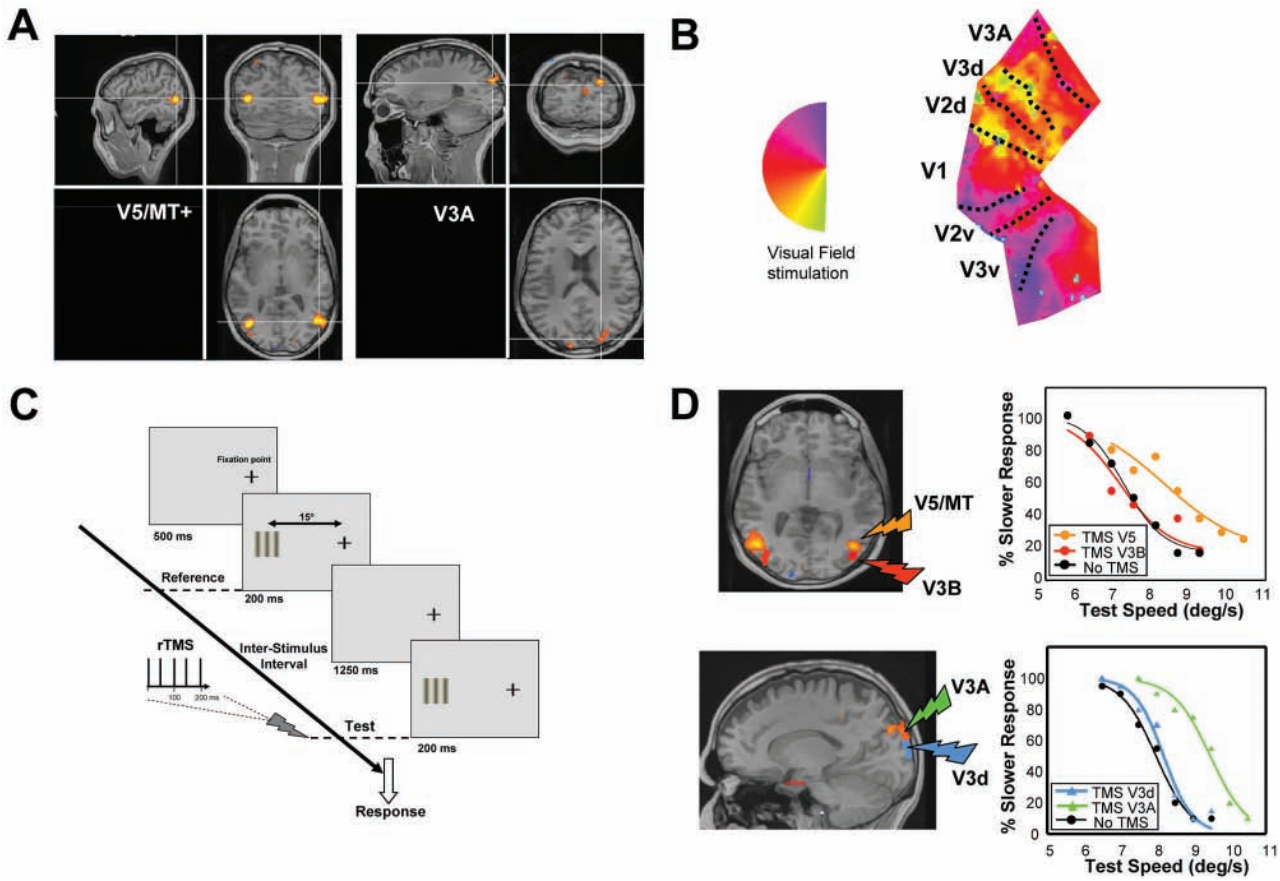

Figure 7. Studying the network of cortical areas responsive to motion. (A) The regions of the brain that are most significantly activated by the passive viewing of moving gratings, V5/MT+ and V3A, in a single subject. There is bilateral activation of the lateral occipitotemporal cortex in a location that is consistent with that of area V5/MT+. In addition, bilateral activation in a region of the superior occipitoparietal cortex can also be observed, which lies in close proximity to an area that has been previously identified as V3A. (B) Retinotopic identification of visual areas in the same subject. The blood oxygenation level-dependent (BOLD) response phase is depicted in false color on a flattened representation of the right hemisphere occipital gray matter. Broken lines indicate locations of visual area boundaries, which occur at reversals in the phase distributions. The inserted representation of the left hemifield allows a direct comparison between the BOLD phase and the region of the visual field stimulated. This mapping confirmed the identity of the visual areas activated by the functional paradigm shown in panel A. (C) The temporal sequence of stimulus presentation used in the delayed speed discrimination paradigm. The moving reference and test stimuli were presented 15 degrees to the left of the fixation point. The reference and test stimuli were separated in time by an interstimulus interval (ISI) of 1250 ms. In this experiment, the delivery of the repetitive transcranial magnetic stimulation (rTMS) pulses was coincident with the onset of the test stimulus but could be placed at any point along the timeline. (D) When TMS is targeted to disrupt the function of visual areas V5/MT and V3A, it can induce deficits in speed perception. However, in other visual areas such as V3 and V3B that are also responsive to motion, the application of TMS has little effect. The effects on performance of stimulation at these sites are shown in the psychometric curves on the right. When TMS is applied to V5/MT (upper plot, orange line/symbols) and V3A (lower plot, green line symbols), the psychometric curves are shifted to the right relative to the no-TMS condition (black line/symbols). This indicates that TMS induces a perceived slowing of the motion of the test stimulus. However, when the site of TMS is shifted to adjacent visual areas V3B (red line/symbols) and V3 (blue line/symbols), the curves are not significantly different from the no-TMS performance, indicating that disruption of these visual areas has had little or no effect on the ability of the individual to perform this particular speed-matching task. This figure is adapted from the results of McKeefry and others (2008).

could span across several visual areas. Moreover, it raises the more general question as to what constitutes a reliable technique to guide the placement of TMS coils on the scalp when attempting to target specific cortical areas. Ryan and others found that even stimulation of the same anatomical areas in different subjects did not always elicit the same functional deficits. This is indicative of a high degree of variability across individuals, in terms of the functional organization of saccadic control in the PPC. The results of this study clearly emphasize the need in TMS experiments for accurate identification of cortical areas, on a subject-by-subject basis, if we wish to make strong claims about the contributions of particular areas to behavior.

Visuospatial Processing

Brain-imaging studies have demonstrated that the PPC is activated in a wide variety of tasks that involve visuospatial judgments, such as the mental rotation of

objects or location matching. In an experiment that combined the use of TMS with fMRI in the investigation of parietal function, Sack and others (2002) first identified, on a functional basis with fMRI, regions of the PPC that were activated during the performance of a task that involved discriminating differences in angle between the hands on a clock face. These activated regions were then targeted using TMS to assess their contribution to the behavioral task. Only on the visuospatial judgment tasks, as opposed to other control tasks involving color judgments, did TMS disrupt performance. The results clearly demonstrate a causal link between neural activity in the PPC and the ability to perform visuospatial judgments.

Visuomotor Control

Yet another aspect of PPC functionality is in the integration of information from multiple sensory modalities to build a multimodal representation of the relationship between our bodies and the external environment. This kind of representation is essential in visuomotor control. Desmurget and others (1999) performed an experiment in which they measured the ability of human observers to look and point to visual stimuli that were presented in their peripheral visual fields. In some instances, the visual stimuli changed position, and the participants had to make an adjustment to the direction in which they were pointing. When TMS was applied to the anterior PPC in the left cerebral hemisphere, participants were still able to point to the initial visual stimuli. However, they were unable to make the necessary adjustments to their pointing direction when the stimuli changed position. This implies that the parietal cortex is concerned with making on-line adjustments to motor plans that are necessary in the performance of particular visual motor tasks. Another suggestion is that the PPC allows for the planning of different motor systems, such as eye or head movements, within a common reference space (Iacobani 2006).

Concurrent fMRI and TMS Experiments

Much of the foregoing discussion has concentrated on the insights that have been gained regarding the organization of visual processing in the human brain from the sequential use of fMRI and TMS methodologies. However, a rapidly developing field uses the simultaneous or concurrent use of these two methodologies in the study of relationships between brain and behavior. Importantly, the concurrent use of TMS and fMRI has the potential to extend our knowledge of brain function in that it allows the examination of interconnectivity between different and often spatially remote brain areas (Bestmann and others 2008). In the investigation of the functional connectivity between visual areas in the primate brain, neuroscientists have often tended to concentrate on studying the effects of disruption to retinal input or input from antecedent visual areas on the processing capacity of a particular visual area. However, as has been emphasized, not only is the operation of visual areas influenced by a feed-forward pattern of connectivity and flow of information, but that function can also be modulated via reciprocal connectivity with "higher" brain areas in a feed-backward or "top-down" manner (e.g., Desimone and Duncan 1995). Certain parietal and frontal regions of the brain (e.g., frontal eye field [FEF]) have been shown in the monkey brain to exert modulatory influence or top-down control on earlier occipital visual areas (Ekstrom and others 2008).

Concurrent fMRI-TMS has been particularly useful in the study of these top-down influences in the human brain. Following earlier experiments, which demonstrated that the application of TMS to the FEF could modulate the sensitivity and physiological responses of earlier occipital visual areas (Paus and others 1997; Silvanto and others 2006), Ruff and colleagues (2006) went on to show how TMS of the right FEF can induce changes in the fMRI signal in visual areas V1 to V4. An interesting property of these changes was that they were retinotopically specific, in that application of TMS to the FEF induced decreases in the fMRI signal in the central representations of the visual field but led to an increase in signal in the peripheral field representations (see Figure 8). Importantly, Ruff and colleagues found that these peripheral fMRI signal increases were mirrored by improvements in peripheral visual sensitivity. Using a psychophysical task, they measured increases in peripheral relative to central contrast sensitivity, revealing that these top-down modulatory effects have measurable functional consequences.

Concurrent fMRI-TMS can also be used to study cortical networks that are involved in specific cognitive processes. Sack and colleagues (2007), for example, have shown that the application of TMS to the right parietal cortex during the performance of a visuospatial task can induce changes in levels of fMRI activation not only in brain areas that are local and distal to the site of stimulation. The influence of TMS also can be measured across a range of frontoparietal cortical areas that are the same areas that are activated during the execution of visuospatial judgments. This result emphasizes the fact that deficits induced by the delivery of TMS are likely to be the result of disruptions across specific cortical networks rather than to single cortical sites. Results such as these emphasize the fact that although neuroscientists may wish to investigate the function of visual areas in isolation, their operation within perception and cognition takes place within the wider context of interconnectivity and influence from a network of different cortical areas.

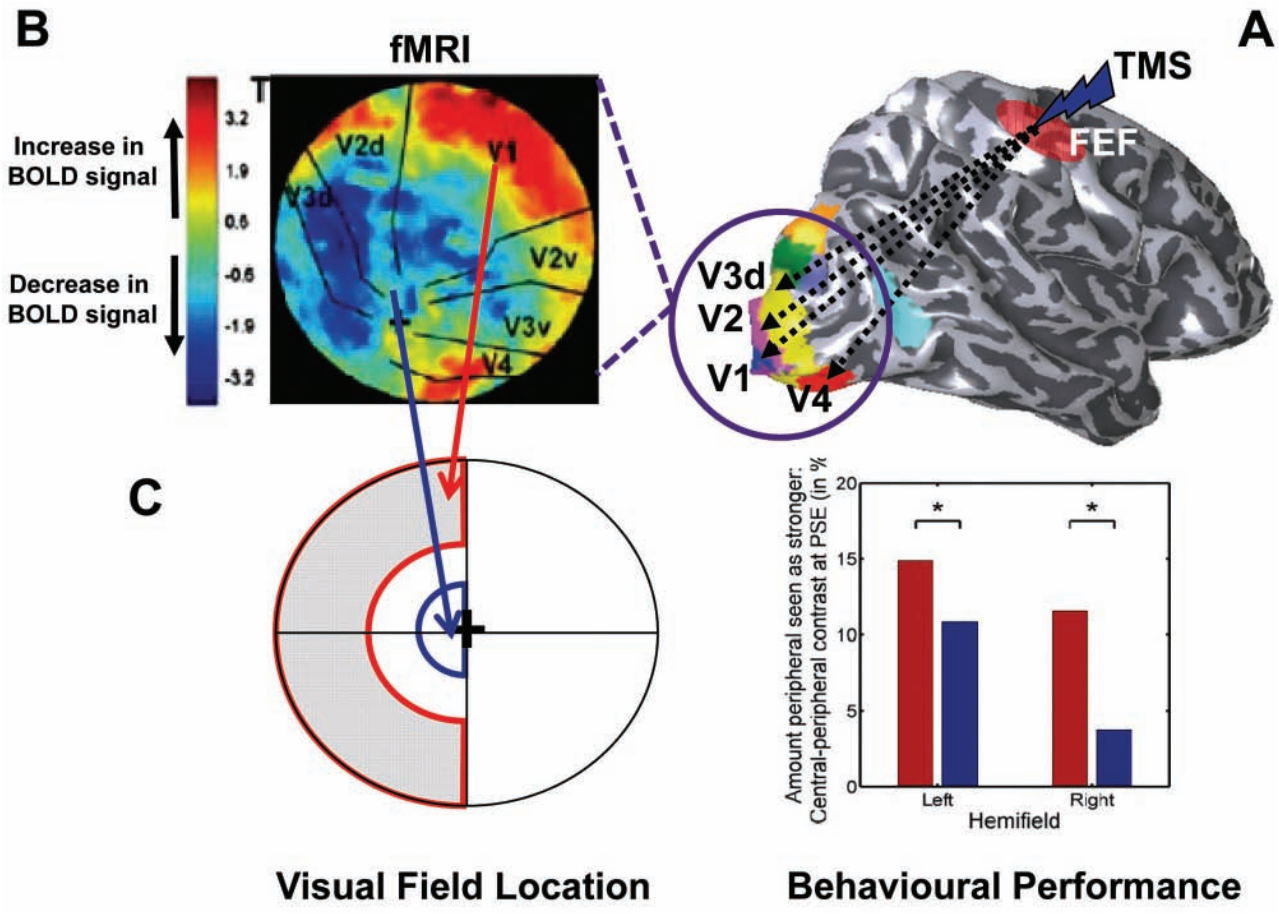

Figure 8. Schematic diagrams illustrating the main principles of a concurrent fMRI–transcranial magnetic stimulation (TMS) experiment. (A) In this experiment, TMS is applied to the frontal eye field (FEF) in the right hemisphere of the human brain. The modulatory effects of this application can be measured in the form of blood oxygenation level-dependent (BOLD) signal changes in spatially remote visual areas (V1, V2, V3, and V4) found in the occipital cortex, using fMRI. (B) A flattened representation of the occipital cortex showing the borders of retinotopically defined areas V1, V2, V3, and V4. The mapping also shows the changes induced in the BOLD signal following the application of TMS to the FEF. Applying TMS to the FEF elicits an increase in BOLD signal (shown by the warmer colors) in regions of the brain where the peripheral visual field is mapped. In contrast, those areas of the brain where the central field is mapped exhibit decreases in the BOLD (shown by the cooler colors). (C) The increases in brain activation in those areas that map the peripheral visual field lead to measurable improvements in behavioral performance. When visual stimuli of similar contrast are presented simultaneously in the peripheral and central regions of the visual field, the peripherally presented stimuli are perceived as being more visible, despite the fact that they are physically identical. This figure is based on results from Ruff and others (2007).

Conclusions

1. In this article, we have attempted to outline how fMRI and TMS can be used to complement each other in dissecting the functions of the visual cortex and other regions of the brain that contain visual maps. One of the key issues to reflect on is the need to accurately localize a visual area or visual field map within an individual. It is only with this information that appropriate inferences about the role of specific visual areas on our visual perception can be made. We have demonstrated in this review that it is becoming increasingly possible to accurately dissect, in individuals, the visual areas of the brain with fMRI and that this information is vital because of the individual differences that exist in visual area locations. We believe, therefore, that to truly harness the power of TMS, one must perform visual area mapping in individuals. This approach is a significant departure from the commonly employed fMRI group study, which would at best provide low-powered experiments.
2. Although TMS and fMRI can be shown to be complementary, it is also important to note limitations of TMS and the extent to which fMRI can guide us in using TMS optimally. TMS is best applied to superficial cortical structures because when it is applied to deeper structures, to some extent, it has to stimulate more superficial ones. This limitation has

hindered progress in learning how ventral visual areas are causally involved in visual perception with TMS experiments. However, fMRI is capable of highlighting which visual areas of the brain are amenable to TMS in individuals. In this context, we have identified L01 and L02 as superficial lateral occipital regions that are ripe for investigation with TMS.

3. As we have indicated in this review, the identification of visual areas with fMRI has advanced rapidly since retinotopic mapping procedures were first reported. There exists an extensive network of interconnected visual maps that cover occipital, temporal, and parietal lobes. It seems clear that we are now in the position to probe the function of the visual brain at a level of precision that allows us to answer questions that are specific to human visual perception, and to some extent, our dependence on animal models is diminishing. Future fMRI investigations, perhaps with the advantages of higher field strength scanners, will likely yield more visual maps in the human brain and allow them to be targeted with TMS.
4. Finally, although quite rarely employed, the use of TMS and fMRI together allows the influence of TMS in one area of the brain on another to be explored. This approach allows the connectivity of brain regions to be examined explicitly and again with hypotheses that are specific to human visual perception.
5. Overall, we have attempted to show how fMRI and TMS can be brought together to examine visual cortical function and its relationship to visual perception. It appears that, as with many other aspects of neuroscience, the visual system presents us with an ideal model to examine the relationship between brain and behavior, with the underlying organization of multiple visual maps yielding a series of hypotheses concerning the roles of different areas and their interconnectivity tenable with TMS.

References

Allen EA, Pasley BN, Duong T, Freeman RD. 2007. Transcranial magnetic stimulation elicits coupled neural and hemodynamic consequences. Science 317:1918–21.

Amassian VE, Cracco RQ, Maccabee PJ, Cracco JB, Rudell A, Eberle L. 1989. Suppression of visual perception by magnetic coil stimulation of human occipital cortex. Electroenceph Clin Neurophysiol 74:458–62.

Anand S, Olson JD, Hotson JR. 1998. Tracing the timing of human analysis of motion and chromatic signals from occipital to tempero-parieto-occipital cortex: a transcranial magnetic stimulation study. Vis Res 38:2619–27.

Beckers G, Zeki S. 1995. The consequences of inactivating areas V1 and V5 on visual motion perception. Brain 118:49–60.

Bestmann S, Ruff CC, Blankenburg F, Weiskopf N, Driver J, Rothwell JC. 2008. Mapping causal interregional influences with concurrent TMS-fMRI. Exp Brain Res 191:383–402.

Brewer AA, Liu J, Wade AR, Wandell BA. 2005. Visual field maps and stimulus selectivity in human ventral occipital cortex. Nat Neurosci 8:1102–9.

Burkhalter A, Felleman DJ, Newsome WT, Van Essen DC. 1986. Anatomical and physiological asymmetries related to visual areas V3 and VP in macaque extrastriate cortex. Vision Res 26: 63–80.

Desimone R, Duncan J. 1995. Neural mechanisms of selective visual attention. Ann Rev Neurosci 18:193–222.

Desmurget M, Epstein CM, Turner RS, Prablanc C, Alexander GE, Grafton ST. 1999. Role of the posterior parietal cortex in updating reaching movements to a visual target. Nat Neurosci 2:563–7.

Dougherty RF, Koch VM, Brewer AA, Fischer B, Modersitzki J, Wandell BA. 2003. Visual field representations and locations of visual areas V1/2/3 in human visual cortex. J Vis 3:586–98.

Dukelow SP, DeSouza JF, Culham JC, van den Berg AV, Menon RS, Vilis T. 2001. Distinguishing subregions of the human MT+ complex using visual fields and pursuit eye movements. J Neurophysiol 86:1991–2000.

Dupont P, Orban GA, De Bruyn B, Verbruggen A, Mortelmans L. 1994. Many areas in the human brain respond to visual motion. J Neurophysiol 72:1420–4.

Ekstrom LB, Roelfsema PR, Arsenault JT, Bonmassar G, Vanduffel W. 2008. Bottom-up dependent gating of frontal signals in early visual cortex. Science 321:414–7.

Ellison A, Cowey A. 2006. TMS can reveal contrasting functions of the dorsal and ventral visual processing streams. Exp Brain Res 175:618–25.

Ellison A, Cowey A. 2007. Time course of the involvement of the ventral and dorsal visual processing streams in a visuospatial task. Neuropsychologia 45:3335–9.

Engel SA, Rumelhart DE, Wandell BA, Lee AT, Glover GH, Chichilnisky EJ, and others. 1994. fMRI of human visual cortex. Nature 369:525.

Felleman DJ, Van Essen DC. 1991. Distributed hierarchical processing in the primater cerebral cortex. Cereb Cortex 1:1–47.

Fernandez E, Alfaro A, Tormos JM, Climent R, Martinez M, Vilanova H, and others. 2002. Mapping of the human visual cortex using image-guided transcranial magnetic stimulation. Brain Res Protoc 10:115–24.

Hallett M. 2007. Transcranial magnetic stimulation: a primer. Neuron 55:187–99.

Harris JA, Clifford CWG, Miniussi C. 2008. The functional effect of transcranial magnetic stimulation: signal suppression or neural noise generation? J Cog Neurosci 20:1–7.

Holmes G. 1918. Disturbances of vision by cerebral lesions. Br J Ophthalmol 2:353–84.

Horton JC, Hoyt WF. 1991. The representation of the visual field in human striate cortex: a revision of the classic Holmes map. Arch Ophthalmol 109:816–24.

Huang YZ, Edwards MJ, Rounis E, Bhatia KP, Rothwell JC. 2005. Theta burst stimulation of the human motor cortex. Neuron 45:201–6.

Huk AC, Dougherty RF, Heeger DJ. 2002. Retinotopy and functional subdivision of human areas MT and MST. J Neurosci 22:7195–205.

Iacobani M. 2006. Visuo-motor integration and control in the human posterior parietal cortex: evidence from TMS and fMRI. Neuropsychologia 44:2691–9.

Kammer T, Klaas P, Erb M, Grodd W. 2005b. Transcranial magnetic stimulation in the visual system: II. Characterization of induced phosphenes and scotomas. Exp Brain Res 160:129–40.

Kammer T, Klaas P, Strasburgr H, Hill NJ, Wichman FA. 2005a. Transcranial magnetic stimulation in the visual system: I. The psychophysics of visual suppression. Exp Brain Res 160:118–28.

Kastner S, Paul I, Ziemann U. 1998. Transient visual field defects induced by transcranial magnetic stimulation over the occipital lobe. Exp Brain Res 118:19–26.

Larsson J, Heeger DJ. 2006. Two retinotopic visual areas in human lateral occipital cortex. J Neurosci 26:13128–42.

Matthews L, Luber B, Qian N, Lisanby SH. 2001. Transcranial magnetic stimulation differentially affects speed and direction judgments. Exp Brain Res 140:397–406.

McKeefry DJ, Burton MP, Vakrou C, Barrett B, Morland A. 2008. Induced deficits in speed perception by transcranial magnetic stimulation of human cortical areas V5/MT+. J Neurosci 28:6848–57.

McKeefry DJ, Zeki S. 1997. The position and topography of the human colour centre as revealed by functional magnetic resonance imaging. Brain 120:2229–42.

Meadows JC. 1974a. Disturbed perception of colours associated with localized cerebral lesions. Brain 97:615–32.

Meadows JC. 1974b. The anatomical basis of prosopagnosia. J Neurol Neurosurg Neurophysiol 37:489–501.

Op de Beeck HP, Haushofer J, Kanwisher NJ. 2008. Interpreting fMRI data: maps, modules and dimensions. Nat Rev Neurosci 9:123–35.

Oyachi H, Ohtsuka K. 1995. Transcranial magnetic stimulation of the posterior parietal cortex degrades accuracy of memory-guided saccades in humans. Invest Ophthalmol Vis Sci 36:1441–9.

Pascual-Leone A, Walsh V. 2001. Fast backprojections from the motion to the primary visual area necessary for visual awareness. Science 292:510–2.

Pascual-Leone A, Walsh V, Rothwell J. 2000. Transcranial magnetic stimulation in cognitive neuroscience: virtual lesion, chronometry and functional connectivity. Curr Opin Neurobiol 10:232–7.

Paus T. 1999. Imaging the brain before, during, and after transcranial magnetic stimulation. Neuropsychologia 37:219–24.

Paus T. 2005 Inferring causality in brain images: a perturbation approach. Philos Trans R Soc Lond B Biol Sci 360:1109–14.

Paus T, Jech R, Thompson CJ, Comeau R, Peters T, Evans AC. 1997. Transcranial magnetic stimulation during positron emission tomography: a new method for studying connectivity of the human cerebral cortex. J Neurosci 17:3178–84.

Pitzalis S, Galletti C, Huang RS, Patria F, Committeri G, Galati G, and others. 2006. Wide-field retinotopy defines human cortical visual area V6. J Neurosci 26:7962–73.

Ruff CC, Blankenburg F, Bjoertomt O, Bestmann S, Freeman E, Haynes JD, and others. 2006. Concurrent TMS-fMRI and psychophysics reveal frontal influences on human retinotopic visual cortex. Curr Biol 16:1479–88.

Rushworth MFS, Taylor PCJ. 2006. TMS in the parietal cortex: updating representations for attention and action. Neuropsychologia 44:2700–16.

Ryan S, Bonilha L, Jackson SR. 2006. Individual variation in the location of the parietal eye fields: a TMS study. Exp Brain Res 173:389–94.

Sack AT. 2006. Transcranial magnetic stimulation, causal structure function mapping and networks of functional relevance. Curr Opin Neurobiol 16:593–9.

Sack AT, Kohler A, Bestmann S, Linden DE, Dechent P, Goebel R, and others. 2007. Imaging the brain activity changes underlying impaired visuospatial judgments: simultaneous FMRI, TMS, and behavioral studies. Cereb Cortex 17:2841–52.

Sack AT, Kohler A, Linden DEJ, Goebel R, Muckli L. 2006. The temporal characteristics of motion processing in hMT/V5+: combining fMRI and neuronavigated TMS. Neuroimage 29:1326–35.

Sack AT, Sperling JM, Prvulovic D, Formissano E, Goebel R, Di Salle F, and others. 2002. Tracking the mind's image in the brain II: transcranial magnetic stimulation reveals parietal asymmetry in visuospatial imagery. Neuron 35:195–204.

Schluppeck D, Glimcher P, Heeger DJ. 2005. Topographic organization for delayed saccades in human posterior parietal cortex. J Neurophysiol 94:1372–84.

Sereno MI, Dale AM, Reppas JB, Kwong KK, Belliveau JW, Brady TJ, and others. 1995. Borders of multiple human visual areas in humans revealed by functional MRI. Science 268:889–93.

Sereno MI, Pitzalis S, Martinez A. 2001. Mapping of contralateral space in retinotopic co-ordinates by a parietal cortical area in humans. Science 294:1350–4.

Silvanto J, Lavie N, Walsh V. 2006. Stimulation of the human frontal eye fields modulates sensitivity of the extra-striate visual cortex. J Neurophysiol 96:941–5.

Silvanto J, Muggleton NG, Cowey A, Walsh V. 2007. Neural adaptation reveals state-dependent effects of transcranial magnetic stimulation. Eur J Neurosci 25:1874–81.

Smith AT, Greenlee MW, Singh KD, Kraemer FM, Henning J. 1998. The processing of first- and second-order motion in human visual cortex assessed by functional magnetic resonance imaging (fMRI). J Neurosci 18:3816–30.

Stewart L, Walsh V, Rothwell J. 2001. Motor and phosphene thresholds: a TMS correlation study. Neuropsychologica 39:415–9.

Swisher JD, Halko MA, Merabet LB, McMains SA, Somers DC. 2007. Visual topography of human intraparietal sulcus. J Neurosci 27:5326–37.

Talairach J, Tournoux P. 1988. Co-Planar Stereotaxic Atlas of the Human Brain. New York: Thieme Medical Publishers.

Tootell RBH, Mendola JD, Hadjikhani NK, Ledden PJ, Liu AK, Reppas JB, and others. 1997. Functional analysis of V3A and related areas in human visual cortex. J Neurosci 17:7060–78.

Tootell RBH, Reppas JB, Kwong KK, Malach R, Born RT, Brady TJ, and others. 1995. Functional analysis of human MT and related visual cortical areas using magnetic resonance imaging. J Neurosci 15:3215–30.

Wade AR, Brewer AA, Rieger JW, Wandell BA. 2002. Functional measurements of human ventral occipital cortex: retinotopy and colour. Philos Trans R Soc B 357:963–73.

Wandell BA, Dumoulin SO, Brewer AA. 2007. Visual field maps in human cortex. Neuron 56:366–83.

Watson JD, Myers R, Frackowiak RS, Hajnal JV, Woods RP, Mazziotta JC, and others. 1993. Area V5 of the human brain: evidence from a combined study using positron emission tomography and magnetic resonance imaging. Cereb Cortex 3:79–94.

Walsh V, Ellison A, Battelli L, Cowey A. 1998. Task-specific impairments and enhancements induced by magnetic stimulation of human visual area V5. Proc Roy Soc B 265:537–43.

Walsh V, Cowey A. 2000. Transcranial magnetic stimulation and cognitive neuroscience. Nat Rev Neurosci 1:73–9.

Yang Q, Kapoula Z. 2004. TMS over the left posterior parietal cortex prolongs latency of contralateral saccades and convergence. Invest Ophthalmol Vis Sci 45:2231–9.

Zeki S. 1990. A century of cerebral achromatopsia. Brain 113:1721–77.

Zeki S, Watson JDG, Lueck CJ, Friston KJ, Kennard C, Frackowiak RSJ. 1991. A direct demonstration of functional specialization in human visual cortex. J Neurosci 11:641–9.

Zeki SM, Perry RJ, Bartels A. 2003. The processing of kinetic contours in the brain. Cereb Cortex 13:189–202.

Zihl J, von Cramon D, Mai N. 1983. Selective disturbance of movement vision after bilateral brain damage. Brain 106:313–40.

Specialized and independent processing of orientation and shape in visual field maps LO1 and LO2

Edward H Silson[1], Declan J McKeefry[2], Jessica Rodgers[1], Andre D Gouws[1], Mark Hymers[1] & Antony B Morland[1,3]

We identified human visual field maps, LO1 and LO2, in object-selective lateral occipital cortex. Using transcranial magnetic stimulation (TMS), we assessed the functions of these maps in the perception of orientation and shape. TMS of LO1 disrupted orientation, but not shape, discrimination, whereas TMS of LO2 disrupted shape, but not orientation, discrimination. This double dissociation suggests that specialized and independent processing of different visual attributes occurs in LO1 and LO2.

The human brain contains areas that exhibit selective responses to a variety of visual stimuli[1] and categories[2–4]. These areas often comprise multiple visual field maps, each of which may perform a unique set of analyses[1,5,6]. However, it remains unclear what computations are performed in maps that subdivide larger, functionally selective visual areas and how they contribute to visual perception.

The lateral occipital complex (LOC) is a large area of extra-striate cortex that is selectively responsive to a variety of objects[2]. Anatomically, LOC has been divided into a more dorsal and posterior region, referred to as the lateral occipital cortex, and a more ventral and anterior region, which is located in the posterior aspect of the fusiform gyrus[2,7]. Notably, recent neuroimaging studies have shown that lateral occipital cortex itself contains at least two (and probably more; A.A. Brewer & B. Barton, *Perception* 40 S48, 2011) visual field maps, LO1 and LO2 (refs. 8,9). LO1 exhibits greater orientation selectivity[9], whereas LO2 is more responsive to complex objects[8]. These findings have led to the idea that LO2 undertakes more sophisticated spatial analyses than LO1 and, as a result, LO2 is considered to be more involved in the processing of shape[8]. However, there is little direct evidence to support this segregation of function between LO1 and LO2. To address this, we employed TMS in conjunction with functional magnetic resonance imaging (fMRI) visual field mapping techniques[10] to ascertain whether neural activity in LO1 and LO2 causally underpins perception of orientation and shape, respectively.

LO1 and LO2 were identified in each participant using fMRI (**Fig. 1a**). The locations (**Table 1**) and retinotopic features (**Supplementary Fig. 1**) of the two visual field maps were consistent with previous findings[8]. We then applied TMS to the centroids of LO1 and LO2 while subjects performed orientation discrimination of sinusoidal gratings and shape discrimination of radial frequency patterns (**Fig. 1b**). Visual stimuli were presented at threshold (75% correct, see Online Methods). In each task, performance was assessed for a no-TMS condition (to establish a performance baseline) and for TMS conditions in which repetitive pulse trains were delivered concurrently with the test stimulus at the targeted cortical sites. The LO1 and LO2 target sites were separated by ~11 mm (**Supplementary Table 1**) and we therefore needed to ensure that TMS had sufficient spatial specificity to independently disrupt processing in LO1 and LO2. To this end, we selected a control TMS site that was medial of LO1 by the same distance that separated LO1 and LO2 (**Fig. 2a**). Selecting a control site medial of LO1, and therefore nearer primary visual cortex (V1), also allowed us to determine whether the spread of TMS into V1 could account for any discrimination deficits observed

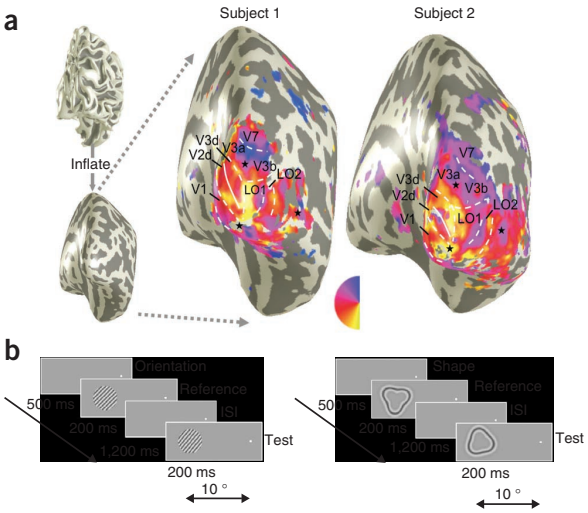

Figure 1 Visual field maps and visual task schematics. (**a**) Surface reconstructions of the gray matter–white matter interface of two subjects. Right hemispheres are viewed from behind; gyri are light gray, sulci dark gray. Superimposed on these inflated surfaces, in false color, are the response phases of the BOLD signal generated by fMRI retinotopic mapping procedures. Asterisks indicate the locations of representations of the fovea. In both subjects, boundaries defining LO1 and LO2 occur at the upper (blue) and lower (yellow) vertical meridians, as indicated on the half color wheel. White dashed and solid lines indicate the representations of the vertical and horizontal meridians, respectively. The meridians define the boundaries between neighboring visual field maps. (**b**) Trial structure for the orientation (left) and shape (right) discrimination tasks. In the TMS trials, pulse trains were delivered coincident and coextensive with the test stimuli.

[1]York Neuroimaging Centre, Department of Psychology, University of York, York, UK. [2]Bradford School of Optometry and Vision Science, University of Bradford, Bradford, UK. [3]Centre for Neuroscience, Hull-York Medical School, York, UK. Correspondence should be addressed to A.B.M. (antony.morland@york.ac.uk).

Received 6 December 2012; accepted 8 January 2013; published online 3 February 2013; doi:10.1038/nn.3327

Table 1 Talairach coordinates (mm) of the LO1 and LO2 centroids (mean and range) for all 12 subjects, including the LO1 and LO2 centroids (mean and range) from ref. 9

		Talairach coordinates					
		LO1			LO2		
		x	*y*	*z*	*x*	*y*	*z*
Current study	Right	31	−87	9	40	−81	9
	Range	24, 40	−91, −82	3, 18	35, 48	−88, −72	0, 19
	Left	−29	−92	7	−37	−83	7
	Range	−38, −22	96, −87	4, 13	−46, −31	−87, −76	3, 11
Ref. 9	Right	32	−89	2.6	38	−82	0.6
	Range	24, 38	−98, −81	−8, 13	32, 46	−89, −72	−13, 12
	Left	−31	−90	1.4	−38	−83	−0.1
	Range	−37, −26	−101, −82	−12, 11	−43, −31	−92, −67	−13, −11

following TMS of LO1 and LO2. This is particularly important for orientation discrimination because neurons in V1, which lies closer to LO1 than LO2, exhibit orientation selectivity.

We hypothesized that LO1 and LO2 have causal roles in orientation and shape discrimination, respectively. Thus, an interaction between site (LO1 versus LO2) and task (orientation versus shape) should be evident. We found that this was indeed the case; a two-way ANOVA confirmed a significant site by task interaction ($F = 15.154$, degrees of freedom (df) = 3 and 33, $P = 2.556 \times 10^{-6}$; **Fig. 2b**). The effect of task was not significant ($F = 1.391$, df = 1 and 11, $P = 0.268$). The effect of site was significant ($F = 5.572$, df = 3 and 33, $P = 0.003$), presumably reflecting the overall drop in performance resulting from TMS of LO1 and LO2. No pair-wise site comparisons were significant ($P > 0.077$). Although it is essential to identify an initial site by task interaction, additional analyses are required to determine whether task-dependant effects of TMS are specific to LO1 and LO2. For orientation discrimination, a one-way ANOVA revealed a significant effect of site ($F = 12.514$, df = 3 and 33, $P = 1.260 \times 10^{-5}$). Pair-wise comparisons (Bonferroni corrected) revealed that this was solely a result of a decrease in performance when stimulating LO1 compared with all other conditions (LO1 versus no TMS, $P = 0.010$; LO1 versus control, $P = 0.010$; LO1 versus LO2, $P = 0.008$). No other pair-wise comparisons were significant ($P = 1.00$ in all cases). For shape discrimination, a one-way ANOVA revealed a significant effect of site ($F = 6.302$, df = 3 and 33, $P = 0.002$). This effect was caused entirely by a decrease in performance when LO2 was stimulated compared with all other conditions (LO2 versus no TMS, $P = 0.023$; LO2 versus control, $P = 0.019$; LO2 versus LO1, $P = 0.018$; Bonferroni corrected). Comparisons between all remaining conditions were not significant ($P = 1.00$ in all cases). The absence of any effect at the control site (**Fig. 2b**) allows us to be confident that TMS acts sufficiently locally to examine our hypotheses about LO1 and LO2. Moreover, the deficits induced by TMS of LO1 and LO2 cannot be attributed to nonfocal spread of TMS into the representation of the stimulus in V1 or other antecedent visual field maps, V2 and V3 (**Supplementary Figs. 1** and **2**). It is also clear that the effects of TMS on discrimination performance cannot be explained by either a speed accuracy trade-off or by spatial relationships between the TMS coil and the cortical targets (**Supplementary Fig. 3** and **Supplementary Table 2**). The nature of deficits induced by TMS suggests that computations of orientation and shape are specific to LO1 and LO2, respectively. The results also reveal a double dissociation between these map-specific computations, indicating that they are performed independently.

Our results reveal two important features of extra-striate cortical function. First, we found that LO1 and LO2 have specialized roles in the processing of two different, relatively low-level visual attributes. Our results extend recent findings[9] to indicate that LO1 is an area of extra-striate cortex that is causally involved in orientation processing. This finding is consistent with neuropsychological studies that found deficient processing of orientation following damage to lateral occipital cortex[11,12]. We also observed that neural activity in LO2 causally underpins the processing of shape, defined by differences in curvature. It remains to be seen whether the processing of shape on the basis of other visual attributes is also dependent on computations in LO2 (ref. 13). Second, the double dissociation of function in LO1 and LO2 indicates that orientation and shape can be processed independently of one another. In this respect, the existence of separable functional processing pathways mirrors those which have been a persistent feature of many models of the primate visual system. For example, human neuropsychological evidence has highlighted the processing of visual information in dorsal[14] and ventral[11] streams. In these streams, at a smaller spatial scale, neuroimaging[1] and neurostimulation[15] studies have shown the existence of functionally selective extra-striate brain areas that process different types of visual information independently of one another. Notably, in monkey the functional independence exhibited by neighboring visual field maps is underpinned by parallel anatomical connections from lower tier visual areas[16]. It is therefore likely that the independent functional roles that we identified for the visual field maps LO1 and LO2 result from similar patterns of parallel connectivity with antecedent visual areas. Although our results depend on there being parallel cortical connections, they do not rule out the presence of serial connections that are often highlighted as an important feature of cortical organization[17].

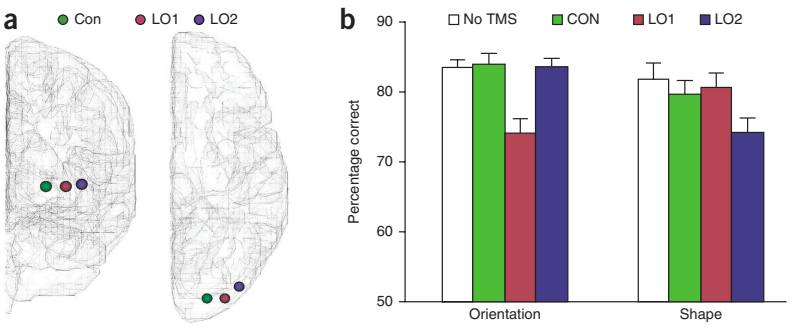

Figure 2 Target locations for TMS and behavioral results. (**a**) TMS targets of a representative subject, overlaid on wire representations of the right hemisphere of the MNI brain. The centroids for LO1 (red; center), LO2 (purple) and the control (CON, green; most medial) are shown. (**b**) Mean percentage correct discrimination for orientation and shape tasks averaged across subjects. These data demonstrate that deficits in orientation processing only occurred after stimulation of LO1, whereas deficits in shape processing only occurred following stimulation of LO2—a double dissociation. Error bars represent s.e.m.

We found that different, relatively low-level visual attributes are analyzed in visual field maps that lie in object-selective lateral occipital cortex[6,8]. These computations are performed independently in LO1 and LO2, creating an organizational framework that offers an efficient way of encoding complex visual forms across multiple visual field maps. Category selectivity, in regions of visual cortex larger than the visual field maps that they encompass, may therefore emerge from specialized, map-specific computations of differing visual attributes that make up stimuli in different categories. Our framework is consistent with previous proposals explaining category selectivity on the basis of neural encoding of simple features[18]. However, instead of these features being computed in large overlapping maps[18], our work indicates that the features are computed independently in discrete regions[19] that map the visual field.

METHODS

Methods and any associated references are available in the online version of the paper.

Note: Supplementary information is available in the online version of the paper.

ACKNOWLEDGMENTS

We are grateful to T. Andrews, H. Baseler and A. Wade for their useful discussion of the study and earlier drafts of the manuscript. We also thank R. Baker, J. Blake, C. Breare, E. Cooper, E. Reeves, E. Shah and S. Strong for their assistance in performing the experiments. We thank the Department of Psychology, University of York, which funds the PhD studentship award to E.H.S. and summer bursary award to J.R.

AUTHOR CONTRIBUTIONS

E.H.S. jointly designed the study, acquired and analyzed the neuroimaging and TMS data, jointly programmed the stimuli, and wrote the manuscript. D.J.M. jointly designed the study, analyzed the TMS data and wrote the manuscript. J.R. analyzed the neuroimaging data. A.D.G. acquired and analyzed the neuroimaging data and jointly programmed the stimuli. M.H. analyzed the neuroimaging data and jointly programmed the stimuli. A.B.M. jointly designed the study, acquired and analyzed the neuroimaging and TMS data, jointly programmed the stimuli, and wrote the manuscript. All authors contributed to the earlier drafts of the manuscript.

COMPETING FINANCIAL INTERESTS

The authors declare no competing financial interests.

Published online at http://www.nature.com/doifinder/10.1038/nn.3327.
Reprints and permissions information is available online at http://www.nature.com/reprints/index.html.

1. Zeki, S. *Cold Spring Harb. Symp. Quant. Biol.* **55**, 651–661 (1990).
2. Malach, R. *et al. Proc. Natl. Acad. Sci. USA* **92**, 8135–8139 (1995).
3. Kanwisher, N., McDermott, J. & Chun, M.M. *J. Neurosci.* **17**, 4302–4311 (1997).
4. Epstein, R. & Kanwisher, N. *Nature* **392**, 598–601 (1998).
5. Brewer, A.A., Liu, J.J., Wade, A.R. & Wandell, B.A. *Nat. Neurosci.* **8**, 1102–1109 (2005).
6. Wandell, B.A., Dumoulin, S.O. & Brewer, A.A. *Neuron* **56**, 366–383 (2007).
7. Grill-Spector, K. *et al. Neuron* **24**, 187–203 (1999).
8. Larsson, J. & Heeger, D.J. *J. Neurosci.* **26**, 13128–13142 (2006).
9. Larsson, J., Landy, M.S. & Heeger, D.J. *J. Neurophysiol.* **95**, 862–881 (2006).
10. McKeefry, D.J., Burton, M.P., Vakrou, C., Barrett, B.T. & Morland, A.B. *J. Neurosci.* **28**, 6848–6857 (2008).
11. Goodale, M.A., Milner, A.D., Jakobson, L.S. & Carey, D.P. *Nature* **349**, 154–156 (1991).
12. James, T.W., Culham, J., Humphrey, G.K., Milner, A.D. & Goodale, M.A. *Brain* **126**, 2463–2475 (2003).
13. Ellison, A. & Cowey, A. *Neuropsychologia* **47**, 1609–1614 (2009).
14. Perenin, M.T. & Vighetto, A. *Brain* **111**, 643–674 (1988).
15. Pitcher, D., Charles, L., Devlin, J.T., Walsh, V. & Duchaine, B. *Curr. Biol.* **19**, 319–324 (2009).
16. Shipp, S. & Zeki, S. *Nature* **315**, 322–325 (1985).
17. Felleman, D.J. & Van Essen, D.C. *Cereb. Cortex* **1**, 1–47 (1991).
18. Op de Beeck, H.P., Haushofer, J. & Kanwisher, N.G. *Nat. Rev. Neurosci.* **9**, 123–135 (2008).
19. Weiner, K.S. & Grill-Spector, K. *Trends Cogn. Sci.* **16**, 251–254 (2012).

ONLINE METHODS

Subjects. The study included 12 subjects (age 21–45, 5 male). All subjects had normal or corrected-to-normal vision and gave informed consent in accordance with the Declaration of Helsinki. The York Neuroimaging Centre Ethics Committee approved the study.

MRI protocol. fMRI and structural MRI data were acquired using an eight-channel, phase-array head coil on a GE 3-Tesla Sigma HD Excite scanner. For structural data, multi-average, whole-head T1-weighted anatomical volumes were acquired for each subject (repetition time = 7.8 ms, echo time = 3 ms, TI = 450 ms, field of view = 290 × 290 × 176, 256 × 256 × 176 matrix, flip angle = 20°, 1.13 × 1.13 × 1.0 mm^3). Anatomical data were segmented into gray and white matter for subsequent visualization in volume and inflated cortical views[20,21]. For functional data, gradient recalled echo pulse sequences were used to measure T2* blood oxygen level–dependent data (repetition time = 2,000 ms, echo time = 30 ms, field of view = 192 cm, 64 × 64 matrix, 26 contiguous slices with 3-mm thickness). Images were read-out using an EPI echo planar imaging (EPI) sequence. Magnetization was allowed to reach a steady state by discarding the first five volumes. Eight fMRI runs were acquired (4 × rings, 4 × wedges) and data were averaged across runs. The stimuli used for visual field mapping were identical to those published previously[22].

fMRI data analysis. Data were analyzed following previously described methods[23–25]. In addition, individual hemispheres of acquired anatomical volumes were segmented into white and gray matter volumes using the Freesurfer4 autorecon script (http://surfer.nmr.mgh.harvard.edu/) followed by manual topology checking using mrGray, part of the Stanford VISTA toolbox.

Identification of visual field maps LO1 and LO2. We identified retinotopically organized cortical maps in 24 hemispheres. LO1 extended anteriorly and laterally from the boundary of V3d, the dorsal division of V3 (V3d) progressing gradually from the lower vertical meridian toward the upper vertical meridian. LO2 neighbored and was the mirror-reverse of LO1. That is, LO1 and LO2 were two hemifield maps in the lateral occipital cortex[8] (**Supplementary Material**). The (**Supplementary Fig. S1**) LO1 and LO2 maps are therefore separate from the maps found in caudal extra-striate cortex that include hV4, VO1 and VO2 (ref. 8) that include; human V4 (hV4) and the ventral occipital maps, VO1 and VO2.

Targets for TMS were selected in the hemisphere in which LO1 and LO2 were most readily identifiable. In each individual, centroids for LO1 and LO2 were calculated and used for TMS targeting. The cortical targets of interest are separated by a relatively small distance (**Supplementary Table 1**) and we assumed that TMS would act sufficiently locally to elicit differential behavioral effects following stimulation of LO1 and LO2. To test this assumption we selected a control site by first calculating the distance between the centroids of LO1 and LO2 and then moving that distance toward the midline from LO1. The control site was chosen to be closer to V1 than the other TMS targets and could therefore be used to rule out the possibility that differential effects of TMS may arise from its action spreading into V1, when LO1 or LO2 were stimulated. In all subjects, the location of the control site fell in V3d. The TMS Brainsight system (Rogue Research) was used to position the coil such that each target site could be stimulated.

Psychophysical Stimuli and Procedures. Stimuli for the behavioral and TMS experiments were generated using MATLAB (Mathworks) and displayed on a Mitsubishi Diamond Pro 2070^{SB} display with a refresh rate of 60 Hz, controlled by a VISAGE graphics card (Cambridge Research Systems). Grating stimuli were luminance modulated sinusoidal gratings (50% contrast) presented in a circular aperture (diameter = 4°) and had a spatial frequency of 2 cpd. Shape stimuli were radial frequency patterns[26] (50% contrast) with a fixed radial frequency of 3. All stimuli had a mean luminance of 31 cd m^{-2} and were presented on a uniform gray background of the same luminance.

The visual tasks that we employed were orientation discrimination of sinusoidal gratings and shape discrimination of radial frequency patterns. The parameters for psychophysical and TMS experiments differed only in the stimuli presented. All measurements employed a 2AFC procedure two-alternative-forced-choice (2AFC).

Visual stimuli were centered at 10° eccentricity along the horizontal meridian into the visual field contralateral to TMS. Stimuli were viewed monocularly with the dominant eye from a distance of 57 cm. Subjects fixated a central black dot (diameter = 0.3°) throughout the experiment. A fixed reference stimulus was presented first (200 ms), followed by an interstimulus interval (1,200 ms) and finally by a test stimulus (200 ms). Subjects judged whether the test stimulus was more vertical or horizontal (orientation discrimination), or spikier or smoother (shape discrimination), than the reference. To capture individual psychometric functions for orientation and shape discrimination respectively, we presented seven test stimuli (including one that matched the reference): three linearly spaced orientations and amplitudes above and below the reference. The phases of the reference and test gratings were randomized to prevent the orientation task from being performed via local luminance cues. Likewise, the orientations of the reference and test frequency patterns were randomized to prevent the shape discrimination task from being performed via local orientation cues. The spacing of the test stimuli were chosen for each individual on the basis of performance on a single, 70 trial, pilot run. Each of the five subsequent experimental run consisted of 70 trials. A cumulative Gaussian was fitted to the data from each subject to model the psychometric functions. We established thresholds (75% correct) for orientations more vertical and more horizontal than the reference and shapes spikier and smoother than the reference, resulting in two threshold orientations and two threshold shapes for each subject. During the application of TMS to cortical targets (control site, LO1, LO2) and baseline (no TMS), only the two threshold stimuli were presented as test stimuli in an identical trial structure to that used to establish thresholds.

TMS Protocol. A train of four biphasic (equal relative amplitude) TMS pulses, separated by 50 ms (20 Hz) at 70% of the maximum stimulator output (2.6 T) were applied to the subject's scalp using a figure-of-eight coil (50-mm external diameter of each ring) connected to a Magstim Rapid2 stimulator (Magstim). Subjects were seated in a purpose built chair with chin rest and forehead support. The coil was secured mechanically and placed directly above each cortical target (control site, LO1, LO2) with the handle orientatated parallel with the floor. The position of the coil was monitored and tracked in real time allowing the displacement between the intended and actual site of TMS delivery to be measured.

Each subject underwent eight counterbalanced sessions (2 tasks × (3 TMS sites + 1 no TMS)). Each TMS session (orientation and shape) contained 100 trials (50 per threshold stimulus). TMS pulses were delivered concurrently with the presentation of the test stimulus. This temporal configuration was identical to that used in previous studies from our laboratory[10,27] where induced functional deficits were found to be maximized when TMS was delivered coincident with the stimulus onset.

Data and statistical analysis. Before data analysis some trials (~4%) were removed on the basis of two criteria: trials for which coil displacement was large (>2.5 mm) and trials for which reaction time was greater than 2,000 ms after the cessation of the presentation of the test stimulus.

Statistics were calculated using the SPSS software package (IBM). We employed two-way repeated-measures ANOVAs to examine the effects of discrimination (% correct), and three potentially confounding variables (reaction time, coil-target distance and coil-target orientation). Subsequent one-way repeated-measures ANOVAs were calculated for each task considered separately. In the case of a significant main effect, two-tailed pair-wise comparisons were calculated and corrected for multiple comparisons (Bonferroni corrected). For each ANOVA, we initially established whether the ANOVA adhered to the assumption of sphericity, using Mauchly's test. When the assumption of sphericity was violated, two approaches to correcting the degrees of freedom were taken to allow appropriate interpretation of the *F* value that resulted from the ANOVA. The Greenhouse-Geisser correction to the degrees of freedom was routinely used when the estimate of sphericity was less than 0.75, but when the estimate of sphericity exceeded this value, the more liberal Huynh-Feldt correction was applied. Departures from sphericity were only observed in the reaction time data presented in **Supplementary Figure 3**. Even though, in these cases, sphericity never exceeded 0.75, we reported both corrections to ensure that we did not mask any significant results by using a conservative correction.

20. Gouws, A., Woods, W., Millman, R., Morland, A. & Green, G. *Front. Neuroinform.* **3**, 9 (2009).
21. Wandell, B.A., Chial, S. & Backus, B.T. *J. Cogn. Neurosci.* **12**, 739–752 (2000).
22. Baseler, H.A. *et al. Nat. Neurosci.* **14**, 649–655 (2011).
23. DeYoe, E.A. *et al. Proc. Natl. Acad. Sci. USA* **93**, 2382–2386 (1996).
24. Engel, S.A., Glover, G.H. & Wandell, B.A. *Cereb. Cortex* **7**, 181–192 (1997).
25. Sereno, M.I. *et al. Science* **268**, 889–893 (1995).
26. Wilkinson, F., Wilson, H.R. & Habak, C. *Vision Res.* **38**, 3555–3568 (1998).
27. McKeefry, D.J., Gouws, A., Burton, M.P. & Morland, A.B. *Neuroscientist* **15**, 489–506 (2009).

Behavioral/Cognitive

On the Role of Suppression in Spatial Attention: Evidence from Negative BOLD in Human Subcortical and Cortical Structures

André D. Gouws,[1] Ivan Alvarez,[1] David M. Watson,[1] Maiko Uesaki,[1] Jessica Rogers,[1] and Antony B. Morland[1,2]

[1]York Neuroimaging Centre, Department of Psychology, University of York, York YO10 5DD, United Kingdom, and [2]Centre for Neuroscience, Hull-York Medical School, York YO10 5DD, United Kingdom

There is clear evidence that spatial attention increases neural responses to attended stimuli in extrastriate visual areas and, to a lesser degree, in earlier visual areas. Other evidence shows that neurons representing unattended locations can also be suppressed. However, the extent to which enhancement and suppression is observed, their stimulus dependence, and the stages of the visual system at which they are expressed remains poorly understood. Using fMRI we set out to characterize both the task and stimulus dependence of neural responses in the lateral geniculate nucleus (LGN), primary visual cortex (V1), and visual motion area (V5) in humans to determine where suppressive and facilitatory effects of spatial attention are expressed. Subjects viewed a lateralized drifting grating stimulus, presented at multiple stimulus contrasts, and performed one of three tasks designed to alter the spatial location of their attention. In retinotopic representations of the stimulus location, we observed increasing attention-dependent facilitation and decreasing dependence on stimulus contrast moving up the visual hierarchy from the LGN to V5. However, in the representations of unattended locations of the LGN and V1, we observed suppression, which was not significantly dependent on the attended stimulus contrast. These suppressive effects were also found in the pulvinar, which has been frequently associated with attention. We provide evidence, therefore, for a spatially selective suppressive mechanism that acts at a subcortical level.

Key words: **contrast response; lateral geniculate nucleus; negative BOLD; spatial attention; suppression; visual cortex**

Introduction

Spatial attention ensures that sensory processing is biased toward behaviorally relevant locations, allowing for enhanced perception of visual stimuli at attended locations. However, this benefit comes at the cost of impoverished perception of stimuli located elsewhere (Posner, 1980; Duncan, 2006). Potentially, attention-dependent enhanced perception could be underpinned by neural facilitation of signals at representations of attended stimuli while impoverished perception may result from suppression of neural activity at representations of unattended locations. However, the extent to which each of these effects is observed and the stages of the visual system at which these effects can be measured is not well understood.

While attentional enhancement is small or absent when the firing rates of single neurons are assessed in early visual structures (Motter, 1993; Luck et al., 1997), fMRI and ERP measurements in human appear to show larger attentional modulation of signals in primary visual cortex (V1; Gandhi et al., 1999; Martínez et al., 1999; Somers et al., 1999) and the LGN (O'Connor et al., 2002). However, there is greater agreement across different methodologies that attention enhances signals in extrastriate visual areas, with a consensus that attention-dependent enhancement of neural signals increases further up the visual hierarchy (Treue and Martinez-Trujillo, 2007; Boynton, 2011).

Attention-related suppression has been reported in V1 and even the LGN in an autoradiographic study of macaque monkeys (Vanduffel et al., 2000). It is also clear that baseline firing of single neurons in V4 and V2, but not V1, is lower when attention is switched from inside to outside the nonstimulated cell's receptive field (Luck et al., 1997). Similarly, fMRI studies have revealed attention-dependent inhibition (Slotnick et al., 2003) and negative BOLD signals in V1 (and nearby extrastriate areas; Tootell et al., 1998a, 1998b; Smith et al., 2000; 2004; Shmuel et al., 2002). It appears, therefore, that there is an important attentional role for suppression in early visual structures.

Studies evaluating suppression through negative BOLD responses in the human visual system have focused on visual cortex, characterizing either the task or the stimulus dependence of suppression. This leaves three important gaps in our knowledge. First, because there is evidence that facilitatory effects of attention are expressed at some, but not all, stimulus contrasts, there is a need to evaluate how suppression relates to task as a function of the characteristics of the stimulus. Second, the role of suppression, as measured in macaque, has not yet been characterized in

Received Jan. 13, 2014; revised June 4, 2014; accepted June 20, 2014.

Author contributions: A.D.G. and A.B.M. designed research; A.D.G., I.A., D.M.W., M.U., J.R., and A.B.M. performed research; A.D.G., I.A., D.M.W., M.U., J.R., and A.B.M. analyzed data; A.D.G. and A.B.M. wrote the paper.

The authors declare no competing financial interests.

Correspondence should be addressed to André D. Gouws, York Neuroimaging Centre, Department of Psychology, University of York, York YO10 5DD, UK. E-mail: andre.gouws@ynic.york.ac.uk.

DOI:10.1523/JNEUROSCI.0164-14.2014

 0270-6474/14/3410347-14$15.00/0

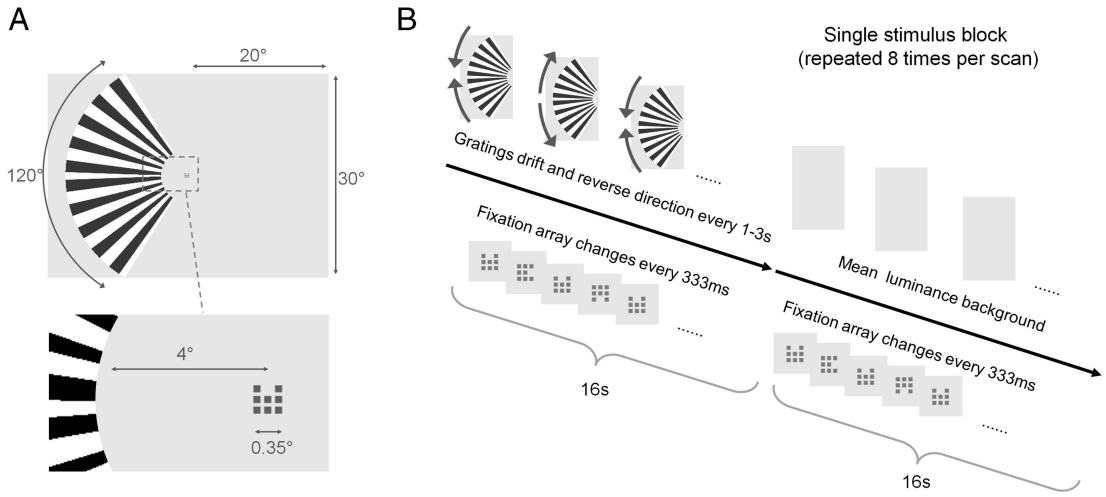

Figure 1. Stimulus configuration and timings. ***A***, The stimulus comprised two components in all experiments: a large, lateralized drifting grating and a dynamic fixation array of nine subsquares. ***B***, The central fixation array was presented throughout each scan, always changing every 333 ms. The fixation elements were all red. The grating was presented for 16 s, reversing direction randomly every 1–3 s, and then removed to reveal the equiluminant background for 16 s. Eight repeats of this 32 s cycle were included in each scan. Subjects either counted reversals of the grating, counted target changes at fixation, or viewed passively in separate sessions of four scans of the same task type.

human subcortical structures. Third, previous approaches to characterizing the LGN′s contribution to attentional modulation have not been optimized to allow the contributions of suppression and enhancement to be disambiguated. This study aimed to characterize the dependence of negative BOLD signals on attention and stimulus contrast, asking the following questions: Is the attention-dependent neural suppression observed in macaque LGN also found in the LGN of humans? How does suppression in the thalamus and cortex depend on the stimulus characteristics of the attended stimulus and the task undertaken? Is the suppression expressed in the LGN and visual cortex also expressed elsewhere?

Materials and Methods

Two separate experiments were devised to characterize the task and stimulus dependence of visual responses in cortical and subcortical structures. The initial experiment was designed to assess solely the effect of task with high-contrast stimuli. A follow-up experiment was designed to examine the effects of task over a range of stimulus contrasts.

Subjects

Fifteen healthy subjects (nine female; mean age, 24.3 years) with normal or corrected-to-normal vision participated in the study after giving informed consent in accordance with the Declaration of Helsinki. The study was approved by the York Neuroimaging Centre Research Governance Committee (Department of Psychology, University of York). Ten subjects took part in the investigation of task dependence. Three of the initial 10 subjects and a further five new subjects took part in the subsequent investigation of contrast and task dependence of BOLD signals.

Visual stimuli

For the initial experiment (designed to assess solely the effect of task), high-contrast visual stimuli were rear-projected (Dukane Image Pro 8942 LCD projector) onto an acrylic screen in the bore of the MRI scanner. Lying supine, subjects viewed the stimuli via a front-silvered mirror placed above the head coil. The presentation of a lateralized visual stimulus can give rise to negative BOLD responses in the visual cortex ipsilateral to the stimulus. Given the size of the LGN, negative responses ipsilateral to a lateralized stimulus are more likely to be detected than those that might flank the positive responses in the LGN contralateral to the stimulus. With this in mind, we presented a large, high-contrast, lateralized, moving pattern to subjects to measure in the hemisphere contralateral to the stimulus positive BOLD responses that we could disambiguate from negative BOLD responses in the hemisphere ipsilateral to the stimulus. The stimuli were presented in the configuration summarized in Figure 1. Subjects maintained central fixation on a fixation array comprising 9×9 pixels (0.35° visual angle). The fixation array was divided into nine subsquares of 3×3 pixels each. The subsquare at the center of the fixation array was always on. Every 333 ms, one of the eight surrounding subsquares would randomly disappear. The same surround subsquare could not disappear in consecutive intervals. The periodic change at fixation was used throughout the entire scan period of all fMRI datasets acquired. While fixating the central stimulus, the subjects were also presented with a peripheral stimulus comprising a 120° sector of an annulus (inner radius, 4°; outer radius, 18°), equally divided by the horizontal meridian. Upper and lower halves of the peripheral stimulus were filled with drifting square-wave gratings (spatial frequency, 0.08 cycles per degree of polar angle; contrast, 100%; frequency, 6 Hz) that always had opposite motion directions (clockwise or counter-clockwise) and reversed unpredictably during a 16 s interval (block). Each 16 s block of peripheral stimulation was followed by a 16 s block where the fixation array alone was presented on the background (spatially uniform gray with luminance equal to the mean luminance of the gratings, 42 cdm^{-2}). Each of the 10 subjects underwent three experimental data-acquisition sessions; subjects were instructed to (1) fixate the central red stimulus throughout the scan (passive viewing task), (2) count the cumulative total of motion reversals of the peripheral stimulus (stimulus-related task), and (3) count the number of disappearances of the "12 o'clock" element in the fixation array (central task). For stimulus-related and central task conditions, subjects reported the count verbally after each scan. In each of the three scan sessions, four fMRI runs were acquired.

In the follow-up experiments to characterize the effect of stimulus contrast and task on BOLD responses, all software and hardware remained unchanged. Only two methodological changes were made from the initial experiment. First, the stimulus was respecified: the peripheral grating stimulus was modulated sinusoidally using only the red and green guns. The blue gun was set to zero because the blue value of some pixels in the projector array did not reproduce the selected stimulus level, giving rise to blue or yellow high- or low-lights, which could interfere with our measurements. The second methodological change from the initial experiment was a reduction in the number of tasks undertaken by each subject to just two: in each of eight sessions, eight subjects were required to complete either the previously described stimulus-related or central task, while the peripheral stimuli were presented at one of four contrast levels (6, 12, 25, or 100%). The passive task condition was thus omitted. Four repeat scans for each stimulus/task combination were ac-

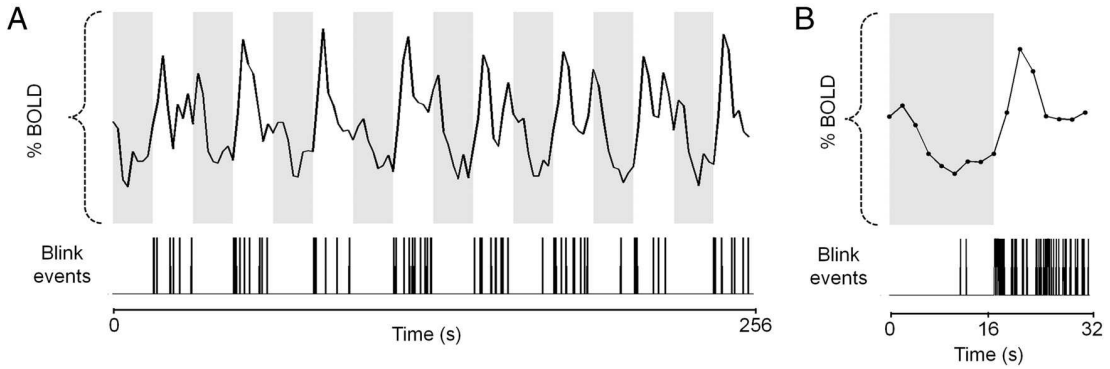

Figure 2. Negative BOLD responses may be correlated with systematic variations in blink activity. Mean data of four scans acquired from one participant under stimulus-related task conditions at 100% stimulus contrast. ***A***, The mean 256 s BOLD time series from V1 ipsilateral to the stimulus. Gray and white backgrounds represent the periods of stimulus presentation and absence, respectively. Below the BOLD time series, we plot the blink events gathered from the corresponding eye video data. The majority of blink events appears to fall in the "grating-off" (white) period. ***B***, The data presented in ***A*** were averaged over the eight stimulus cycles to produce a mean BOLD response over a single-stimulus cycle with the corresponding blink distribution. Also apparent is a high density of blink events immediately following the offset of the grating stimulus (gray/white border), which is in turn followed by the pronounced overshoot of the BOLD response plotted above it.

quired in a single session. Condition order was counterbalanced across subjects. Across all measurements made, a single subject was always presented with stimuli in a single visual field. The visual field tested was counterbalanced across subjects.

MRI acquisition

Functional data. Data were acquired using a 3 tesla MRI scanner (Signa Excite, GE Healthcare) using an eight-channel phased-array head coil at the York Neuroimaging Centre. For fMRI acquisitions, gradient recalled echo pulse EPI sequences were used to measure T2* BOLD data (TR, 2000 ms; TE, 30 ms; FOV, 192 mm; flip angle, 90°; 128 × 128 matrix; 22 contiguous slices with 2.4 mm slice thickness; voxel size, 1.5 × 1.5 × 2.4 mm^3). Para-axial slices were oriented to lie approximately parallel to the anterior–posterior commissure line, ensuring coverage of the occipital lobe. Magnetization was allowed to reach a steady state by discarding the first five volumes.

Structural data. We acquired proton density images (TR, 2520 ms; TE, 35 ms; flip angle, 90°; matrix size, 512 × 512; FOV, 192 mm; 22 contiguous slices; slice thickness, 2.4 mm; voxel size, 0.375 × 0.375 × 2.4 mm^3; two averages) to allow the LGN to be identified (Devlin et al., 2006). Proton-density-weighted scans were acquired at the start of each session for each subject at the same slice orientation and prescription used to acquire the functional data. T1-weighted sagittal images (TR, 7.80 ms; TE, 3 ms; flip angle, 20°; matrix size, 256 × 256; FOV, 290 mm; 176 slices; slice thickness, 1 mm; voxel size, 1.13 × 1.13 × 1 mm^3) were acquired to provide a high-resolution, whole-brain anatomical images and a canonical frame of reference to which all other functional and anatomical volumes were aligned.

Defining regions of interest

Proton-density-weighted anatomical images were assessed to provide volume definitions for the LGN regions of interest (ROIs) in all subjects using previously described criteria (Fujita et al., 2001; Devlin et al., 2006). Reassuringly, the resultant LGN tissue volumes estimated using this approach are highly comparable to the volumes reported in a histological assessment of human LGN volume (Andrews et al., 1997): the volume of our group mean left and right LGN ROIs were 128.2 ± 12.64 mm^3 and 138.0 ± 13.59 mm^3, respectively. V5/MT+ can be reliably localized 1 cm superior to the junction of the inferior temporal sulcus (ITS) and the ascending limb of the ITS (AL-ITS; Dumoulin et al., 2000). Interpolated slices through a near-isotropic T1-weighted MRI volume (1 × 1.13 × 1.13 mm^3) were generated using custom software (Gouws et al., 2009), allowing bilateral identification of the junction between the ITS and the AL-ITS in all control subjects. The voxel 1 cm superior to this junction (along the AL-ITS) in the reformatted slice was used as the center of a spherical ROI of 1 cm radius. All subjects undertook fMRI retinotopic mapping procedures that allowed V1 to be identified. Specific stimulus and MRI acquisitions are specified here (Baseler et al., 2011). The T1-weighted structural scans for each subject were segmented into white and gray matter using mrGray (VistaSoft toolbox; http://white.stanford.edu/software/). The ROIs defined for V1 and V5 were transformed into this anatomical space within the VistaSoft toolbox. Only ROI voxels spatially corresponding to gray matter were retained for the final V1 and V5 ROI analysis.

fMRI data analysis

Under normal circumstances, fMRI analysis is largely restricted to using the stimulus as the explanatory variable, with the addition of other variables that seek to explain variance related to individual variations in hemodynamic responses. In the experiments we report here, the period during which the grating is off could elicit a greater number of blinks from subjects, particularly if this period follows a stimulus period in which the subject is performing a task. Blink-related signals have previously been discussed as potential sources of noise in fMRI measurements (Hupé et al., 2012), although the effects of systematic variation in blink pattern were not considered. Given these findings and our prediction that blinking may occur at systematically different rates during stimulus and control blocks, we sought to assess blinking in each subject. During all fMRI data acquisition, therefore, video data (30 Hz) were gathered for each subject's right eye via a long-range infrared camera (Eyetrack 6000 LR006, Applied Science Laboratories). Video files were post-processed offline. Initially, blinks were identified when the correlation of each video frame with its predecessor dropped below 0.8. For quality control and verification of the algorithm's success, we subsequently manually assessed each video and found that the automated detection had an error rate of 2%. Manually detected events were used to generate a timing file of each scan's blink events, which was later incorporated as an explanatory variable event file in general linear modeling (GLM) techniques to account for blinking patterns as a potential confound in our BOLD response estimates.

In Figure 2, we show an exemplar dataset supporting our concern that the timing of blink events is temporally correlated with the offset of an attended stimulus. It is clear in this example that the blink events are largely restricted to the period during which the grating stimulus is absent. It is also clear that the highest density of blink events is seen in the period immediately following the offset of the grating stimulus. Thus systematic variation in blink patterns, which have the ability to generate retinal and thus cortical signals, needs to be addressed as a potential confound in our estimates of BOLD responses, particularly in the context of negative BOLD. We therefore account for blinks in our fMRI analysis described below.

Functional data were corrected for within and across scan motion by aligning all volumes in the dataset to the first volume of the first scan of

the session using MCFLIRT (a linear registration tool for motion correction of fMRI data; Jenkinson et al., 2002). We used the VistaSoft toolbox for Matlab (v7.8.1, MathWorks) to view unsmoothed data in a canonical anatomical framework. The time series had the linear trend removed (no other temporal filtering was applied) and was converted to percentage signal change. Mean time series for each scan were generated by first averaging the signal from all voxels within each of the ROIs and then averaging across the four scans that were acquired for each task/stimulus condition. We applied GLM to the time series data using the Matlab regression statistics function (regstats). Predictor time series were generated by convolving the SPM (http://www.fil.ion.ucl.ac.uk/spm/software/spm8/) double-gamma hemodynamic response function (spm_hrf) with the stimulus and blink event timings and durations. Temporal derivatives of the predictors and a constant term were also entered into the GLM. The outcome measures used here are percentage signal change values for the stimulus and blink predictors. We ran independent GLMs for each contrast in the follow-up experiment when investigating responses at the stimulus representation. This allows for the effects of blinks to vary depending on the contrast presented, an appropriate precaution given the potential nonlinear interaction between stimulus and blink-driven activity. However, for ROIs without a representation of the peripheral stimulus, the time series at each contrast level were concatenated. We modeled, with a single GLM, the concatenated data with four stimulus predictors (one for each stimulus contrast) but only a single blink predictor (generated by temporally concatenating the blink predictors at each contrast level). This approach allows the stimulus predictor's contribution to vary across contrast levels as it should, but holds the blinks' contribution constant across all stimulus contrast levels. This approach is required because the effect of blinks should not be permitted to vary across conditions in regions that do not represent the stimulus.

Bootstrapping was used to estimate the mean contrast response function for each ROI and task condition. Each subject contributed a mean response value at each contrast level (6, 12, 25, and 100%). Eight subjects were selected at random from the possible eight samples, with replacement. An estimate of the mean response at each contrast level was generated by averaging across these eight samples. A power function $R_c = bC^{\gamma}$ was used to fit the four estimated means. R is the measured response at a given input luminance contrast C, b is a multiplicative constant, and γ is an exponent. The fitting process was applied to multiple resampled datasets to generate 5×10^5 power functions, which allowed the modeled response maximum R_{100} and semisaturation contrast C_{50} to be derived. The frequency distributions of differences in these outcome measures resulting from different tasks were also computed and allowed the probability of a genuine difference to be estimated, as reported by the p values in the manuscript.

Whole-brain GLM analyses were also conducted using FEAT (http://www.fmrib.ox.ac.uk/fsl). Motion correction was followed by spatial smoothing (Gaussian, FWHM 3 mm) and temporal high-pass filtering (0.01 Hz). First-level analyses estimated the effects of stimulus and blink regressors (generated as before) for each scan. Additional steps included linear alignment of individual scan data into a canonical structural space, the MNI brain, using FLIRT (Jenkinson et al., 2002). Second-level, fixed-effects analyses generated estimates of within-individual mean responses. Third-level, mixed-effects analyses estimated the group mean responses. Statistical images were thresholded using clusters determined by $Z > 1.63$ and a corrected cluster significance threshold of $p = 0.05$. To examine the thalamus, we masked the whole-brain group mean statistical images with a probabilistic thalamic atlas volume included with FSL4.1 (Behrens et al., 2003). This atlas divides the thalamus into seven distinct volumes defined by the probability of connectivity with various cortical regions. We were also keen to capture any activity in the superior colliculus so extended the thalamic ROI slightly to capture the top of the brainstem: a spherical volume of radius 8 mm was centered on the MNI coordinate (1.0, −29.0, −2.0) and appended to the existing probabilistic thalamic mask. Only significant clusters falling within this volume are described in analyses.

Behavioral data analysis

We calculated the mean percentage error score for each participant as a function of the stimulus-contrast/task combination, for the stimulus-related and central task conditions (no counting task was performed under passive viewing conditions). For each individual scan, we first calculated the absolute difference between the reported number of target events and the presented target count, and converted this to percentage error value. This value was averaged across the four scans acquired for each individual subject for a given stimulus contrast/task combination. The resultant individual subject mean percentage errors were analyzed with a repeated-measures ANOVA to explore an effect of task alone in the initial experiment ($n = 10$, two task conditions at a single stimulus contrast). For the follow-up experiment, a repeated-measures ANOVA was applied to the individual subject mean percentage error values to explore main effects of task and stimulus contrast ($n = 8$, two tasks, four stimulus contrast levels).

Results

The first aim of our study was to determine whether negative BOLD responses could be detected in the LGN. While subjects attended to a large, lateralized drifting grating, i.e., under stimulus-related task conditions, there is clear evidence of negative BOLD responses in the time series derived from LGN ipsilateral to the stimulus (Fig. 3*B*, top). Moreover, and as expected, V1 ipsilateral to the stimulus also exhibited robust negative signals (Fig. 3*C*, top).

The stimulus-related task we used draws attention to the stimulus and attention has been shown to influence both positive and negative BOLD responses. To investigate the role of attention in modulating BOLD signals, we compared the results from the stimulus-related task data with our two additional conditions. Under passive viewing conditions, negative BOLD responses in the LGN and V1 ipsilateral to the stimulus appear reduced in amplitude relative to the stimulus-related task condition (Fig. 3*B*,*C*, middle), while having subjects perform a central task throughout the scan largely abolished the negative responses in those structures (Fig. 3*B*,*C*, bottom).

Positive BOLD responses were observed in the LGN, V1, and V5 contralateral to the stimulus (Fig. 3*D*,*E*), while V5 ipsilateral to the stimulus also exhibited positive BOLD responses (Fig. 3*E*), presumably because of the large receptive fields found in this cortical region (Zeki, 1969; Allman and Kaas, 1971; Amano et al., 2009). In the LGN and V1 contralateral to the stimulus, differences in task condition appeared to have little effect on positive BOLD responses. However, the magnitude of the positive BOLD responses found in V5 contralateral and ipsilateral to the stimulus was reduced for the passive viewing task and still further reduced for the central task compared with the stimulus-related task. It would appear therefore that early visual structures (the LGN and V1) contralateral to the stimulus exhibit positive BOLD responses that are modulated very little by attention, while their counterparts ipsilateral to the stimulus exhibit negative responses that are strongly affected by attention. The extrastriate motion area V5 exhibits positive BOLD responses that are strongly modulated by attention in both hemispheres.

The repeated-measures ANOVA revealed that subjects performed significantly ($F_{(1,9)} = 58.32$, $p = 3.20 \times 10^{-5}$) worse on the central task (error rate, 7.78 ± 1.01%) than the stimulus-related task (error rate, 0.99 ± 0.37%).

An interesting feature of the negative BOLD responses is a positive overshoot after stimulus cessation (Fig. 3*B*), especially noticeable under stimulus-related task conditions. Having seen the positive overshoot in pilot data, we hypothesized that it could be driven by an increase in blinking after stimulus cessation. We

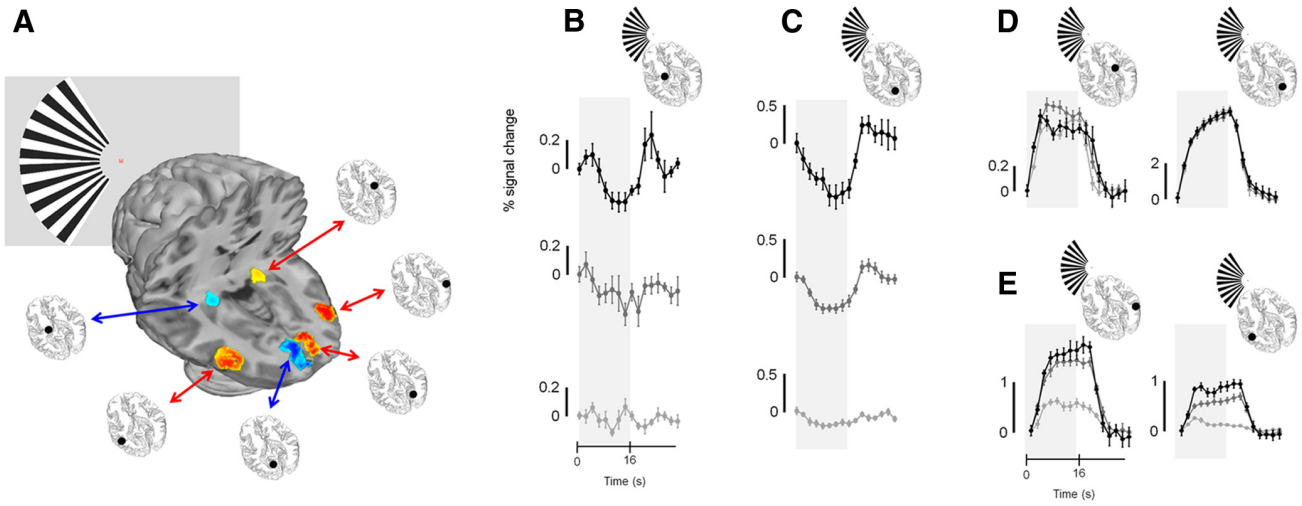

Figure 3. Group mean ($n = 10$) fMRI responses for the LGN, V1, and V5. ***A***, Schematic of the stimulus configuration along with the locations of the LGN, V1, and V5 ROIs used to extract the time series data illustrated in ***B–E***. ***B–E***, Note that time series data are separated by condition in ***B*** and ***C***, but overlaid in ***D*** and ***E***. Time series data are given for the LGN (***B***) and V1 (***C***) ipsilateral to the stimulus for the stimulus-related (top, black), passive-fixation (middle, mid-gray), and central (bottom, light gray) tasks. ***D***, the responses obtained from the LGN (left) and V1 (right) contralateral to the stimulus. ***E***, the responses obtained from V5 contralateral (left) and ipsilateral (right) to the stimulus. The same shading of the lines and symbols in ***B*** and ***C*** are used in ***D*** and ***E*** to reflect the different task conditions. In all cases a single time series per subject was computed from four runs. The time series was then collapsed over a single stimulus cycle of 32 s for each subject. The single cycles were then averaged across all subjects to generate the responses plotted in the figure. Error bars indicate SEMs across subjects. The shaded gray region in all time series plots indicates the period during which the grating stimulus was presented.

took the precaution therefore of video recording the subjects' eyes during our experiments to allow blinks to be detected (see Materials and Methods). An examination of how blink rate varies during the stimulus cycle reveals that, after stimulus cessation, the group mean blink rate increases markedly for the stimulus-related and passive viewing tasks, but not for the central task (Fig. 4*A*). It is vital therefore to account for any contribution that blink-related activity makes to the BOLD signals we measure. This can be done by performing GLM in which we use the stimulus as an explanatory variable (Fig. 4*B*) or both the stimulus and the blink rate as explanatory variables (Fig. 4*C*). For the group data, these two models were compared with hierarchical modeling. This analysis revealed that introducing blink rate as an explanatory variable accounts for additional variance, particularly in the LGN (R^2 change, 0.23; F change, 28.762; $p < 10^{-10}$) and V1 (R^2 change, 0.044; F change, 12.835; $p < 10^{-5}$) ipsilateral to the stimulus. We also applied the same modeling approach to evaluate blink-related signals at the individual subject level because blink rates vary between subjects and tasks (Fig. 4*A*). This analysis revealed that in those subjects who increased their blink rate after stimulus cessation responses were partially, but significantly, driven by blinks. The quantitative analysis that we take forward for the rest of this study therefore accounts for the blink-related activity in all ROIs in each individual.

To examine the effect of task on cortical and subcortical visual signals, we derived the percentage BOLD response, specific to the stimulus, for each subject for all ROIs and task conditions (Fig. 5) using GLM techniques as described in the Materials and Methods section. We used one-way repeated-measures ANOVA to determine whether there were task-related changes in the BOLD responses we derived. We found significant main effects of task on the negative BOLD responses in the LGN ($F_{(2,18)} = 6.196$, $p = 0.009$) and V1 ($F_{(2,18)} = 15.32$, $p = 0.00013$) ipsilateral to the stimulus. The effect of task also followed a significant linear trend as a function of task (stimulus-related through passive viewing to central task) in the LGN ($F_{(1,9)} = 17.68$, $p = 0.002$) and V1 ($F_{(1,9)} = 18.91$, $p = 0.002$). Pairwise tests revealed significant differences between the stimulus-related and central tasks in the LGN ($p = 0.007$), and between the central task and both the stimulus-related ($p = 0.006$) and passive viewing ($p = 0.008$) tasks in V1. Task-dependent positive BOLD responses were also observed in V5 contralateral ($F_{(2,18)} = 26.75$, $p = 4 \times 10^{-6}$) and ipsilateral ($F_{(2,18)} = 18.68$, $p = 4.1 \times 10^{-5}$) to the stimulus. The responses decreased systematically with a linear trend as a function of task (stimulus-related through passive viewing to central task) in contralateral V5 ($F_{(1,9)} = 68.21$, $p = 1.7 \times 10^{-5}$) and ipsilateral V5 ($F_{(1,9)} = 22.67$, $p = 0.001$). Pairwise tests also revealed that the responses obtained from V5, contralateral and ipsilateral to the stimulus, under the central task differed significantly from the responses obtained under the other task conditions (contralateral V5: stimulus-related vs central, $p = 5.1 \times 10^{-5}$; passive viewing vs central, $p = 0.002$; ipsilateral V5: stimulus-related vs central, $p = 0.003$; passive viewing vs central, $p = 0.001$). In contrast, the positive BOLD responses in LGN and V1 exhibited no significant changes under the different task conditions (LGN: $F_{(2,18)} = 2.169$, $p = 0.143$; V1: $F_{(2,18)} = 0.247$, $p = 0.784$).

The statistical analysis of the BOLD responses confirms the observations we made on the time series. In short, the LGN and V1 ipsilateral to the stimulus exhibit task-related negative BOLD responses, while we were unable to detect task-dependent changes in positive BOLD responses in the LGN and V1 contralateral to the stimulus. However, a strong task-dependent change in positive BOLD responses in V5 bilaterally was observed. Negative BOLD signals have been shown to be scaled inversions of positive BOLD responses (Shmuel et al., 2002). For this reason we decided to examine whether stimulus contrast, which strongly affects positive BOLD responses, would also affect negative BOLD responses in early visual structures. Also, task-related effects on positive responses in early visual structures have been reported to occur only at intermediate contrast levels rather than at the high contrast we presented (but see Gandhi et al., 1999; Li et al., 2008).

To determine the effect of contrast on the negative BOLD responses found in structures ipsilateral to the stimulus, we per-

formed a follow-up experiment: we used a stimulus configuration identical to the one used in the initial experiment, but this time we presented sinusoidal grating components at different contrasts under only two of our previous task conditions, the stimulus-related and central tasks. Group mean time series for the LGN, V1, and V5 contralateral and ipsilateral to the stimulus, at the four contrast levels tested (6, 12, 25, and 100%), are shown in Figure 6. Responses from V1 and the LGN ipsilateral to the stimulus exhibit markedly different responses compared with their counterparts contralateral to the stimulus (Fig. 6*A*,*B*). First, upward deflections are evident in the negative responses following stimulus cessation. As previously discussed, these reflect blink-related activity that is accounted for in our analyses. Second, the negative responses appear strongly dependent on task; only the stimulus-related task results in consistent negative responses, whereas the positive responses are observed under both task conditions. Third, negative responses appear largely independent of the stimulus contrast, showing that they are not simply scaled inversions of the positive, highly contrast-dependent responses found in their contralateral counterparts (Fig. 6*A*,*B*, compare top left, top right). In V5, both contralateral and ipsilateral to the stimulus, positive responses are observed. As before, the stimulus-related task results in markedly larger responses than those obtained during the central task (Fig. 6*C*). The responses also appear to have only a weak relationship with stimulus contrast.

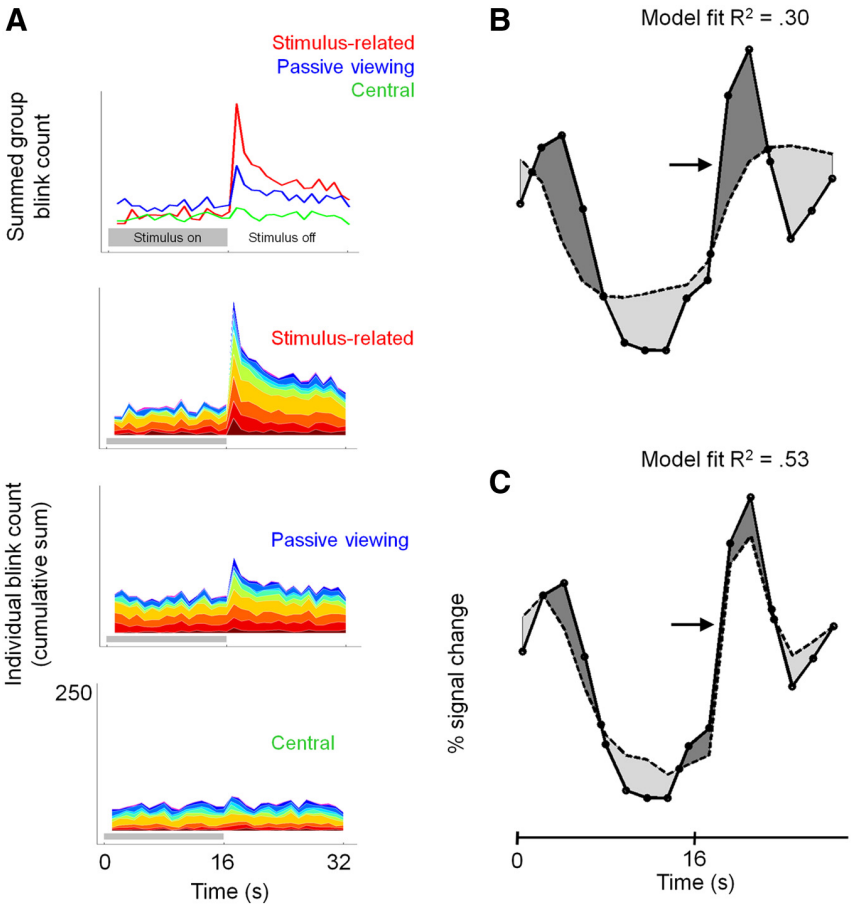

Figure 4. Blink rates and their effect on modeling BOLD responses. ***A***, Top, How the number of blinks per TR (2 s) varies over the time course of a single stimulus/control block of 32 s. Data are summed across the subject group ($n = 10$) for three task conditions as indicated in the panel. The panels below (from top to bottom) show the contribution of each subject (different colors) to the mean response for stimulus-related tasks, passive viewing, and central tasks. ***B***, The group mean BOLD response for the LGN ipsilateral to the grating stimulus (filled circles) with the modeled response (dashed black line) based on stimulus explanatory variables only. Differences between the modeled and measured response (the residual error after modeling) are highlighted in gray. ***C***, The same data as shown in ***B***, but in this case the fit includes the blink rate as an explanatory variable. R^2 values are given for model fits (see text for details).

As before, we measured performance on both the stimulus-related and central tasks. The group mean error (1.04 ± 0.21%) under stimulus-related task conditions was significantly ($F_{(1,7)} = 23.89$, $p = 0.002$) lower than during the central task (5.78 ± 0.90%). However, no significant effect of contrast ($F_{(3,21)} = 1.405$, $p = 0.269$) or interaction between task and contrast ($F_{(3,21)} = 2.002$, $p = 0.145$) was detected. Thus, for the follow-up experiment, participants again performed significantly worse on the central task than on the stimulus-related task, but performance did not change within task as a function of contrast.

To quantify the effects observed in the time series (Fig. 6) we estimated BOLD responses from each individual, for each condition, by applying GLM. As before, our model included each individual's blink pattern as an explanatory variable. The mean stimulus-related BOLD responses, for the group of eight subjects, are plotted as a function of contrast in Figure 7. We use repeated-measures ANOVA approaches with task and stimulus contrast as main effects to assess the data. In the LGN ipsilateral to the stimulus (Fig. 7*A*), the effect of task ($F_{(1,7)} = 6.170$, $p = 0.042$), but not contrast ($F_{(3,21)} = 0.405$, $p = 0.751$), was significant. The interaction between task and contrast was not significant ($F_{(3,21)} = 2.422$, $p = 0.094$). A similar picture emerged for V1 ipsilateral to the stimulus (Fig. 7*B*); the negative responses were not significantly dependent on contrast ($F_{(3,21)} = 0.990$, $p = 0.417$), but were dependent on task ($F_{(1,7)} = 7.202$, $p = 0.031$) and there was no significant interaction ($F_{(3,21)} = 1.679$, $p = 0.202$). Our finding that negative BOLD signals in the LGN and V1 ipsilateral to the stimulus exhibit little or no contrast dependence requires careful comparison with previous results (Shmuel et al., 2002), which showed contrast-dependent negative BOLD signals in V1. Shmuel et al. evaluated the BOLD signals at the stimulus representation and in a region flanking it in V1. When we consider a similar region of V1 flanking the stimulus representation (Fig. 7*D*), we too find negative BOLD signals that vary with contrast [$F_{(3,21)} = 2.466$, $p = 0.045$ (one-tailed)], but only when under the central task conditions, which match well with the task used by Shmuel et al. Interestingly, when a stimulus-related task is performed, we observed responses from this "flanking" region that are not significantly dependent on contrast ($F_{(3,21)} = 0.284$, $p = 0.837$), mirroring the negative responses we found in V1 of the hemisphere ipsilateral to the stimulus (Fig. 7*B*).

In the LGN contralateral to the stimulus (Fig. 7*A*), the effect of contrast ($F_{(3,21)} = 36.07$, $p = 1.812 \times 10^{-8}$), but not task ($F_{(1,7)} = 0.014$, $p = 0.909$), was significant. The interaction was not significant ($F_{(3,21)} = 0.054$, $p = 0.983$). In V1 contralateral to the stim-

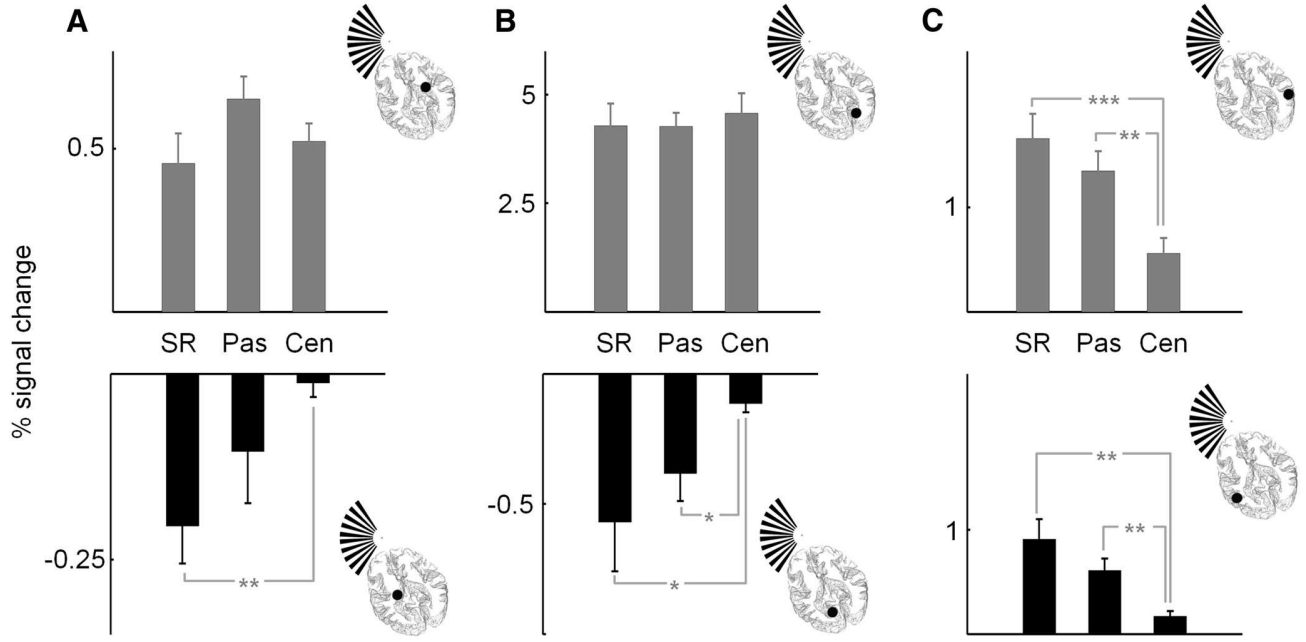

Figure 5. The effect of task on BOLD responses in the LGN, V1, and V5. ***A–C***, The group mean stimulus-related activity is given for the LGN (***A***), V1 (***B***), and V5 (***C***). In each panel, the data presented in the upper and lower plots illustrate the responses obtained from the brain regions contralateral and ipsilateral to the stimulus, respectively. Error bars are the SEM. Significant linear trends of response as a function of task were detected in all structures ipsilateral to the stimulus and in V5 contralateral to the stimulus (see text for details). Significant pairwise differences in responses are highlighted: ***$p < 0.001$, **$p < 0.01$, and *$p < 0.05$ (two-tailed). SR, Stimulus-related task; Pas, passive viewing; Cen, central task.

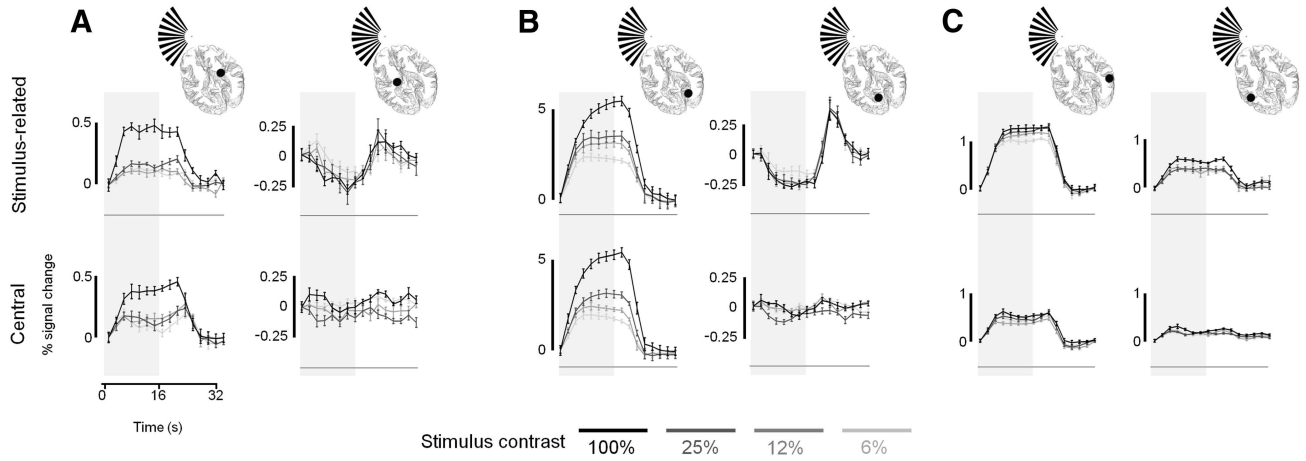

Figure 6. Group mean BOLD time series obtained from the LGN, V1, and V5 at different stimulus contrasts. ***A–C***, Data are given for the LGN (***A***), V1 (***B***), and V5 (***C***). In each panel the data for the hemisphere contralateral and ipsilateral to the stimulus are given in the left and right plots, respectively. Data are given for four contrast levels (as indicated by the key) and for stimulus-related task (top row) and central task (bottom row). Error bars indicate SEMs across subjects. Time series data are generated and presented as described in Figure 3.

ulus (Fig. 7*B*), the highly contrast-dependent positive signals ($F_{(3,21)} = 73.558$, $p = 2.627 \times 10^{-11}$) were dependent on task if, as justified on the basis of previous research showing only attention-dependent increases in response, a one-tailed hypothesis is considered ($F_{(1,7)} = 3.921$, $p = 0.044$). However, no significant interaction was detected ($F_{(3,21)} = 1.557$, $p = 0.229$). In V5, both ipsilateral and contralateral to the stimulus (Fig. 7*C*), highly significant effects of task were observed (ipsilateral: $F_{(1,7)} = 92.03$, $p = 2.811 \times 10^{-5}$; contralateral: $F_{(1,7)} = 224.8$, $p = 1.409 \times 10^{-6}$) along with a subtle, but significant trend with contrast in the hemisphere contralateral to the stimulus (contralateral: $F_{(1,7)} = 9.316$, $p = 0.019$; ipsilateral: $F_{(1,7)} = 1.506$, $p = 0.259$). For V5, no significant interaction of task and stimulus contrast was detected in either hemisphere (contralateral: $F_{(3,21)} = 0.192$, $p = 0.901$; ipsilateral: $F_{(3,21)} = 1.510$, $p = 0.241$).

There is the strong *a priori* evidence from fMRI for contrast-dependent and task-dependent responses in the stimulus representations of the LGN (Kastner et al., 1999) and V1 (Buracas and Boynton, 2007). The use of repeated-measures ANOVAs is appropriate for evaluating unknown response relationships with contrast and task, like those we have assessed in the LGN and V1 ipsilateral to the stimulus. However, ANOVAs are not as sensitive as modeling techniques used previously to characterize the effects of task on the largely predictable contrast–response relationships obtained from early visual structures (Buracas and Boynton, 2007; Li et al., 2008; Murray, 2008). To increase our sensitivity to

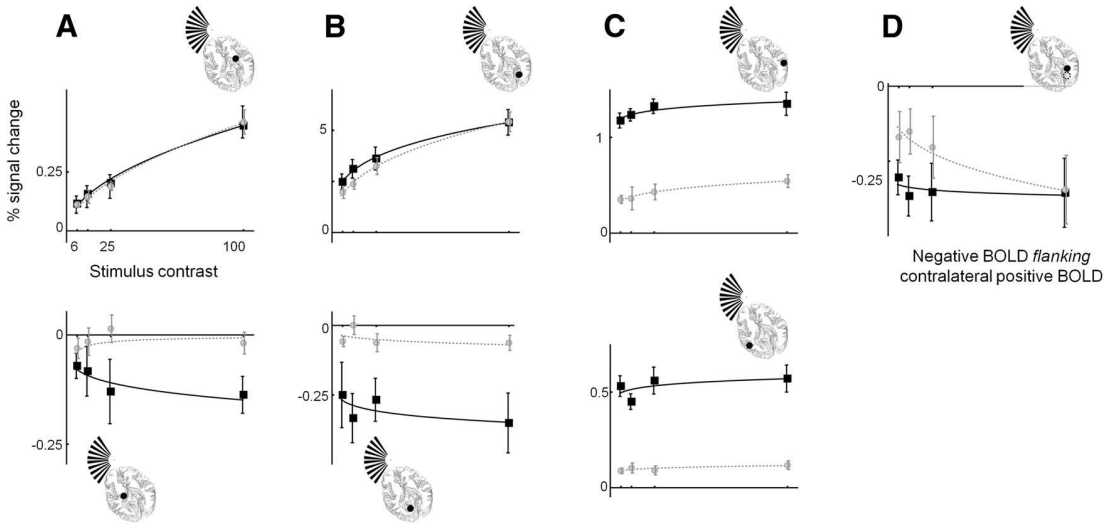

Figure 7. Contrast responses for different visual structures obtained under stimulus-related (black squares, solid black lines) and central (gray circles, dashed gray lines) task conditions. ***A–C***, Data are given for the LGN (***A***), V1 (***B***), and V5 (***C***) contralateral (top row) and ipsilateral (bottom row) to the stimulus. ***D***, Data for the region of V1 in the hemisphere contralateral to the stimulus that flanks the stimulus representation. The lines through the data were generated by fitting a power function to the data as described in the text. Error bars indicate SEMs of the mean across subjects.

Table 1. R_{100} and C_{50} values for positive BOLD regions of interest: the LGN, V1, and V5[a]

	Contralateral			Ipsilateral
Outcome measure	LGN	V1	V5	V5
C_{50}				
Stimulus-related	29.1% (12.0–39.3%)	7.99% (6.00–10.6%)[b]	0.01% (0.00–0.02%)	0.01% (0.00–0.02%)
Central	24.8% (17.4–33.1%)	16.10%(11.7–21.7%)[b]	1.20% (0.01–4.65%)	0.19% (0.00–1.96%)
R_{100}				
Stimulus-related	0.37% (0.26–0.47%)	4.58% (3.7–5.6%)	1.31% (1.17–1.49%)[b]	0.64% (0.55–0.73%)[b]
Central	0.39% (0.31–0.47%)	4.76% (4.0–5.5%)	0.56% (0.45–0.67%)[b]	0.11% (0.08–0.14%)[b]

[a]Data are given for the stimulus-related and central tasks for structures contralateral to the stimulus for the LGN and V1, and bilaterally for V5. Mean modeled values are given with 95% confidence range in parentheses.
[b]Significant effects of task between conditions.

subtle task-dependent changes, particularly in the contrast responses obtained from the LGN and V1 contralateral to the stimulus, we extended our analysis to include the same modeling approach as others (Buracas and Boynton, 2007; Li et al., 2008; Murray, 2008). Specifically, we used a power function (Buracas and Boynton, 2007) to fit the contrast response functions from the LGN and V1 contralateral to the stimulus (see Materials and Methods). This approach also allows for a more direct comparison of our results with those from earlier studies. From the resultant model fits, we derived two outcome measures: the modeled response at 100% contrast, R_{100}, and the contrast, C_{50}, at which the modeled response reaches half R_{100}. We used resampling techniques to establish whether these outcome measures were significantly affected by task (see Materials and Methods).

We summarize the results of power function fitting to all positive BOLD regions of interest in Table 1. C_{50} and R_{100} values are given for the LGN and V1 contralateral to the stimulus, and for V5 bilaterally. In the LGN contralateral to the stimulus, we detect no effect of task on either outcome measure. An effect of task on C_{50} ($p = 0.008$), but not R_{100}, was observed in V1 contralateral to the stimulus. In contrast, V5 exhibited a significant attention-related increase in R_{100} ($p < 5 \times 10^{-4}$), but not C_{50}. This pattern was also a feature of the attention-related effect in V5 ipsilateral to the stimulus (R_{100}: $p < 5 \times 10^{-4}$). The quantitative comparisons reveal that the response change in V1 caused by attention shows increased responses at intermediate, but not maximum, stimulus contrast, a pattern commonly referred to as contrast gain. Attention-dependent changes of V5 responses on the other hand can be attributed to either increased baseline or response gain-type mechanisms.

Up to now we have shown that BOLD signals in the LGN and V1 are reduced compared with baseline in representations of unattended locations in the stimulus-related task. We believe the decrease in BOLD signal relates to a suppression of neural responses at representations of unattended locations in the LGN and V1. If this is the case, such suppression should also be present in representations of unattended locations when our central task is performed. But, because the central task is performed throughout stimulus and nonstimulus blocks, the neural firing will be constant across all blocks and will therefore not be detected with conventional fMRI analysis. However, we are able to take an alternative approach to examine whether suppression is present during the central task: immediately before acquiring our fMRI time series, we acquired dummy volumes that allow magnetization to reach a steady state. These volumes are automatically discarded by the scanner. During the dummy acquisitions, subjects fixated passively and only started to perform the central task following the dummy acquisitions. If neural suppression drives the decreases in BOLD signals we record, a negative deflection in the early part of the time series should be evident for the ROIs that represent unattended locations where no stimulus is presented. We found evidence for this initial negative deflection in the time series obtained from the LGN and V1 across all contrast conditions (Fig. 8*A*,*C*). To add context, we show how the initial nega-

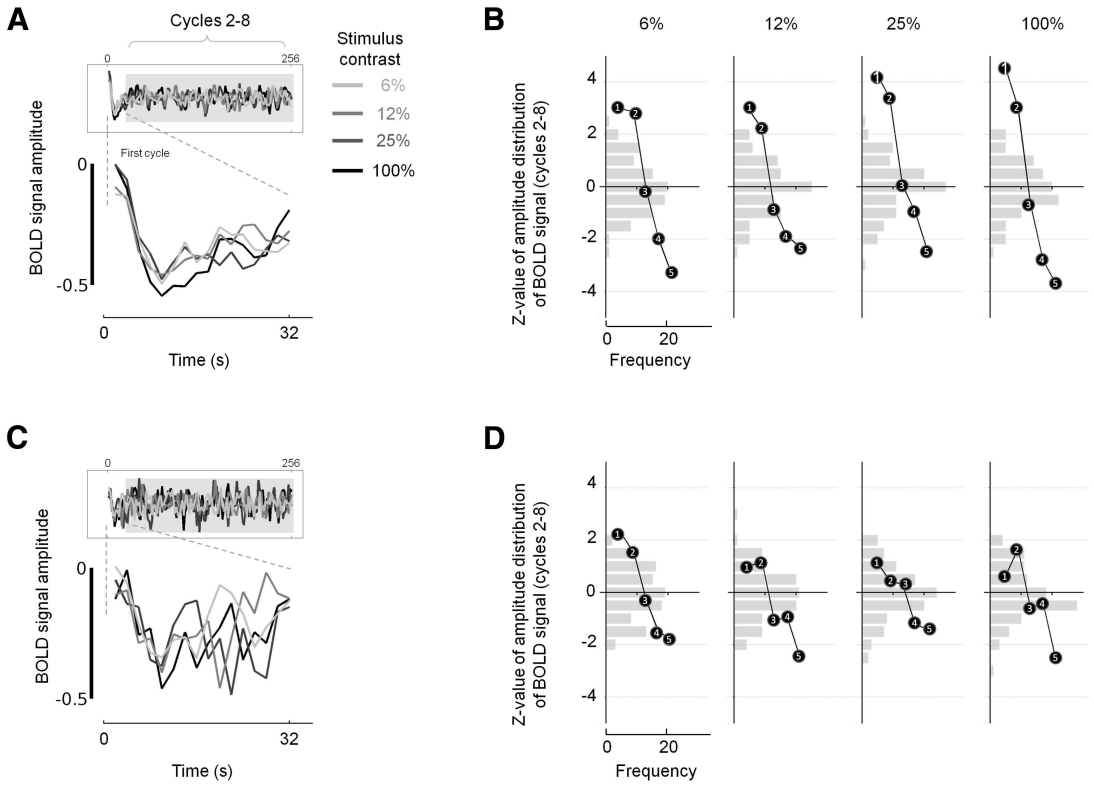

Figure 8. ***A–D***, Initial negative deflections in BOLD signals at representations of unattended locations in V1 (***A***, ***B***) and the LGN (***C***, ***D***). ***A***, Group mean BOLD signals are plotted as a function of time for the initial stimulus cycle of 32 s with the full scan duration time series inset for reference. Data are plotted for the central task, which was performed throughout the scans, and for stimulus contrasts of 6, 12, 25, and 100%. There is a negative deflection in all time series for V1 (***A***) over the first 8–10 s (data samples 1–5 at an acquisition repetition time of 2 s). The signal then exhibits a modest increase, but does not recover to its initial value. The initial negative deflection is not observed in data acquired on a phantom, meaning that magnetization changes cannot explain the effects illustrated. ***B***, To assess the significance of the initial negative deflection, we compared the amplitude values of the first 10 s (5 samples) of each mean time series with the distribution of the amplitude values of the same time series after the end of the first stimulus cycle (gray shaded regions of the insets of ***A*** and ***C***, representing 33–256 s, samples 17–128). *Z*-transformed frequency distributions of V1 amplitudes for samples 17–128 are given for each stimulus contrast in light gray bars on the vertical axes. The Z-transformed amplitudes of the first five data points are overlaid on this distribution for comparison. ***C***, ***D***, Data for the LGN were subjected to the same analysis described for V1 and are shown in the same format as ***A*** and ***B***.

Table 2. Initial negative deflection under central task conditions in LGN and V1 ipsilateral to the stimulus[a]

Percentage stimulus contrast	LGN				V1			
Z	6	12	25	100	6	12	25	100
Time point 1	2.24	1.01	1.13	0.65	2.98***	2.92**	4.26***	4.53***
Time point 2	1.50	1.20	0.42	1.66*	2.86**	2.21**	3.37***	3.01***
Time point 3	−0.31	−1.12	0.33	−0.61	−0.13	−0.86	0.07	−0.67
Time point 4	−1.54	−0.91	−1.22	−0.38	−2.00*	−1.88*	−0.94	−2.80**
Time point 5	−1.74*	−2.40**	−1.40	−2.49**	−3.28***	−2.27**	−2.43**	−3.68***
Gradient	−3.15***	−2.9**	−1.97*	−2.1*	−4.68***	−3.89***	−4.11***	−5.8***

[a]This table summarizes the *Z* statistic obtained by comparing BOLD amplitude at each of the five initial BOLD signal time points (samples) with the remainder of the time series (samples 17–128). The bottom row of the table shows the *Z* statistic resulting from a comparison between the gradient computed across those initial five samples with the gradient across comparable consecutive five-sample sets (taken from samples 17–128). Values with asterisks highlight significant effects between the samples (*$p < 0.05$, **$p < 0.01$, ***$p < 0.001$).

tive deflection compared with the distribution of BOLD amplitudes recorded after the first stimulus cycle (Fig. 8*B*,*D*). A clear pattern emerges across contrast conditions. Specifically, the first and fifth temporal samples of the time series frequently represent the maximum and minimum recorded amplitude, respectively. The amplitudes obtained at temporal samples 2–4 frequently decrease sequentially between the values recorded at samples 1 and 5. The first and fifth samples are therefore always significantly different in V1 and frequently in the LGN from samples obtained after the initial stimulus cycle (Table 2).

To characterize further the initial negative deflection in the time series, we computed the gradient over the first five samples using least-squares regression. For statistical comparison, we generated a null distribution of slopes for the rest of the dataset by iteratively sampling 108 sets of five consecutive data points from the start of the second stimulus cycle to the end of the time series. The Z-scores of the computed slopes and associated significance are given in Table 2. It is clear that in all cases the initial slope is significantly different for those computed for the remainder of the time series.

We now ask how the suppression in the representations of unattended locations in the LGN might arise. One potential source of suppression in the LGN is feedback from V1. However, the LGN also has connections to other subcortical structures that could play a role. Specifically, the pulvinar and superior colliculus, which have been implicated in attention and connect directly

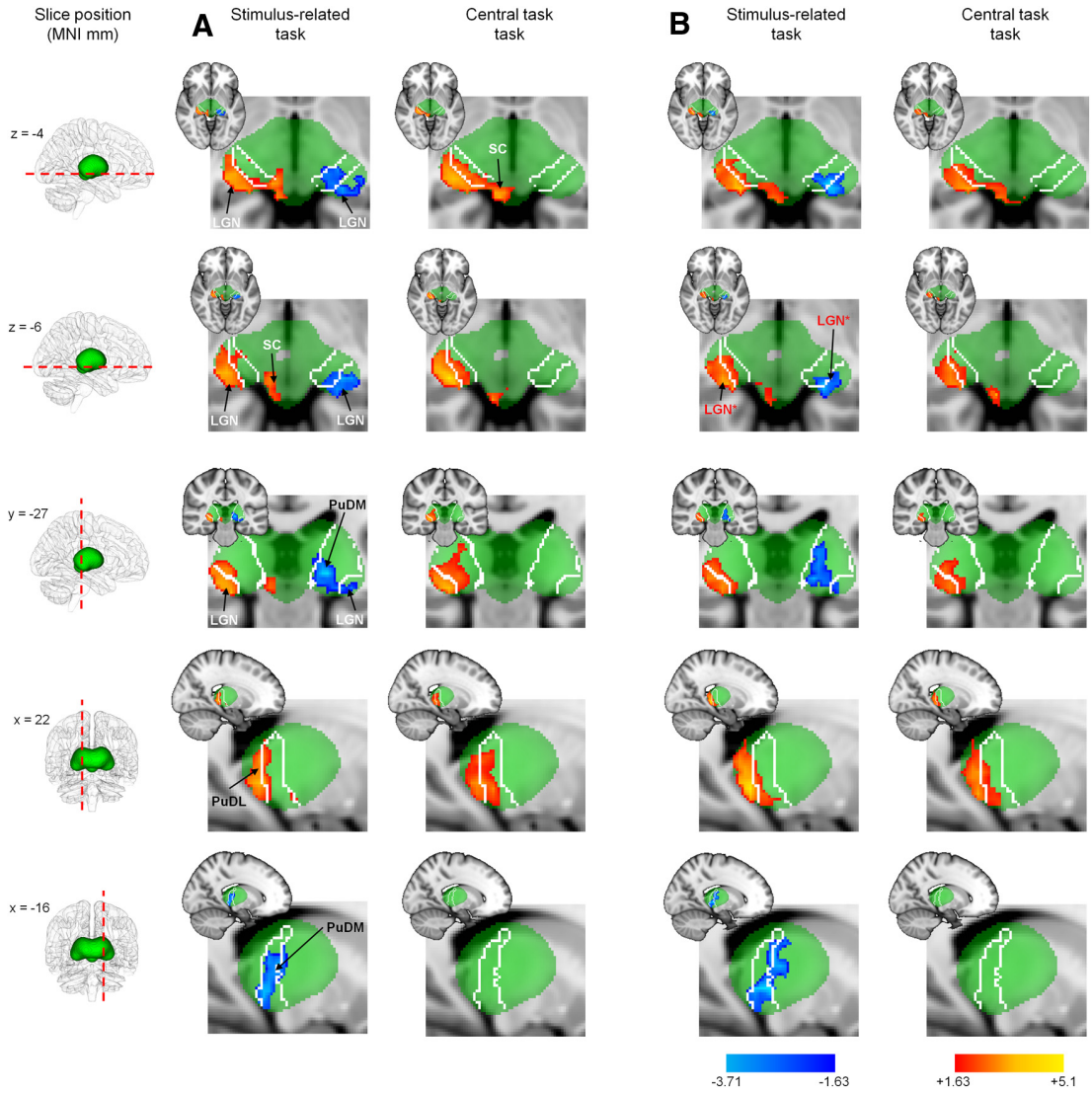

Figure 9. Patterns of thalamic activation and suppression under different task conditions. ***A***, ***B***, *Z*-score maps for stimulus > no stimulus (hot colors) and stimulus < no stimulus (cool colors) for our initial experiments (***A***) and for the 100% contrast condition in our follow-up experiment (***B***). Data are shown for axial (top 2 rows), coronal (middle row), and sagittal (bottom 2 rows) sections. These results were thresholded using clusters determined by $Z > 1.63$ and a cluster-corrected significance threshold of $p < 0.05$; note also that no small-volume correction has been applied. The green region depicts the extent of a standard thalamic probability atlas described in MNI space; the white outline drawn within the thalamus depicts the extent of the region with the greatest connectivity probability to parietal regions (see Materials and Methods). The data in ***A*** and ***B*** exhibit remarkably similar features: activation is restricted to the LGN, SC, and dorsolateral pulvinar (PuDL) contralateral to the stimulus under both task conditions, while suppression is observed in the both LGN and dorsomedial pulvinar (PuDM) ipsilateral to the stimulus but only under stimulus-related task conditions. In ***B***, the region labeled LGN* (in red) highlights the position of the centers of the LGN ROIs identified in a previous study (Kastner et al., 2004).

or indirectly with the LGN (Saalmann and Kastner, 2009), may also contribute to suppression in the LGN. To investigate the role of these structures, we performed a prospective whole-brain analysis on data acquired in our initial experiments and in the 100% contrast condition of the follow-up experiments. The positive and negative signals in subcortical structures for the stimulus-related and central tasks are shown in Figure 9. The first striking feature of the analysis is that the results obtained in the follow-up experiment (Fig. 9*B*) almost perfectly replicate those of the initial experiments (Fig. 9*A*). The details of the results are discussed with respect to the initial experiment only. First, consistent with our ROI analysis, the positive and negative signals in the LGN are evident contralateral and ipsilateral to the stimulus, respectively. As expected the negative signals are only detected during the stimulus-related task. Importantly, the LGN regions highlighted by the analysis coincide with our anatomically defined LGN ROIs and previously published coordinates (Fig. 9*B*) for the LGN (Kastner et al., 2004). Second, the superior colliculus and the dorsolateral aspects of the pulvinar contralateral to the stimulus exhibit significant positive responses under both task conditions. Third, the dorsomedial aspects of the pulvinar ipsilateral to the stimulus exhibit negative responses during the stimulus-related task. It is important to note that the pulvinar responses found contralateral and ipsilateral to the stimulus occupy distinct and separate aspects of the pulvinar, which have connections to different cortical locations. The dorsolateral pulvinar has a greater proportion of occipital projections than the dorsomedial pulvinar, which connects preferentially to parietal cortex (Gutierrez et al., 2000; Behrens et al., 2003).

Given the consistency between the patterns of responses obtained for the two separate experiments (Fig. 9, compare *A*, *B*), we

used the significant clusters of positive and negative responses obtained from the group analysis of the initial experiment (Fig. 9*A*) as independent ROIs for extracting contrast responses for the superior colliculus, dorsolateral pulvinar contralateral to the stimulus, and the dorsomedial pulvinar ipsilateral to the stimulus. The ROIs were back-projected into the individual subject anatomies using the inverse affine transformations calculated in the alignment of the functional data to the individual subject anatomy, and subsequently to the MNI template brain. Following back-projection of the ROIs into the individual subject coordinate space, the contiguous clusters reaching statistical significance for both the dorsolateral and dorsomedial pulvinar ROIs fell within the anatomical bounds of the thalamus, and thus were not subjected to further restriction. Back-projection of the superior colliculus ROIs sometimes resulted in individual subject ROIs capturing voxels representing CSF rather than brain tissue. Functional MRI measurements from the superior colliculus are known to be particularly susceptible to physiological noise sources (Wall et al., 2009) partly due to the fact that the structure lies immediately adjacent to the CSF. Taking direction from previous studies (Limbrick-Oldfield et al., 2012), we took the precaution of restricting the back-projected superior colliculus ROIs to brain matter, manually excluding any voxels corresponding to CSF. This resulted in superior colliculus ROIs of a mean volume of 41.2 ± 7.1 mm^3, which is consistent with that previously reported by Schneider and Kastner (2009). The mean center of mass of the revised superior colliculus ROIs was at MNI coordinates $x = 6$, $y = -32$, $z = -4$, which lies in the center of a superior colliculus ROI previously reported (Limbrick-Oldfield et al., 2012).

The time series and contrast response functions for the dorsomedial and dorsolateral pulvinar ROIs, where responses were most significant, are shown in Figure 10. There appears to be an effect of task, but not contrast, in the dorsomedial pulvinar, and contrast, but not task, in the dorsolateral pulvinar. As for the LGN, V1, and V5 data previously described, we use repeated-measures ANOVA approaches with task and stimulus contrast as main effects to assess these data from the pulvinar along with those derived from the superior colliculus ROIs. In the dorsomedial pulvinar ipsilateral to the stimulus, a main effect of task ($F_{(1,7)} = 8.009$, $p = 0.025$), but not contrast ($F_{(3,21)} = 0.624$, $p = 0.607$), was evident (Fig. 10*A*). There was no interaction between contrast and task ($F_{(3,21)} = 0.085$, $p = 0.967$). This is the pattern of response we found in the LGN and V1 ipsilateral to the stimulus. The dorsolateral pulvinar contralateral to the stimulus (Fig. 10*B*) exhibited responses that were dependent on contrast ($F_{(3,21)} = 25.08$, $p = 3.872 \times 10^{-7}$) but not task ($F_{(1,7)} = 2.800$, $p = 0.138$) and there was no interaction ($F_{(3,21)} = 0.633$, $p = 0.602$). The results are therefore consistent with those we measured in the LGN contralateral to the stimulus. In the superior colliculus contralateral to the stimulus, the responses were influenced by task ($F_{(1,7)} = 6.318$, $p = 0.040$) but not contrast ($F_{(3,21)} = 1.575$, $p = 0.23$). No interaction was evident ($F_{(3,21)} = 0.521$, $p = 0.673$).

A clear feature of the positive BOLD responses we obtained from the stimulus representations in the LGN, V1, and V5 is an increasing task dependence, but reducing contrast dependence as we move up the visual hierarchy, a pattern of results consistently reported in single-unit, evoked-potential, and fMRI studies of attention (for review, see Carrasco, 2011). A recent Normalization Model of Attention (Reynolds and Heeger, 2009; Boynton, 2011) successfully predicts qualitatively different effects of attention on cortical responses that have been reported in the literature. The key feature of this model is an early "attention field" that acts before cortical responses are normalized. The model also

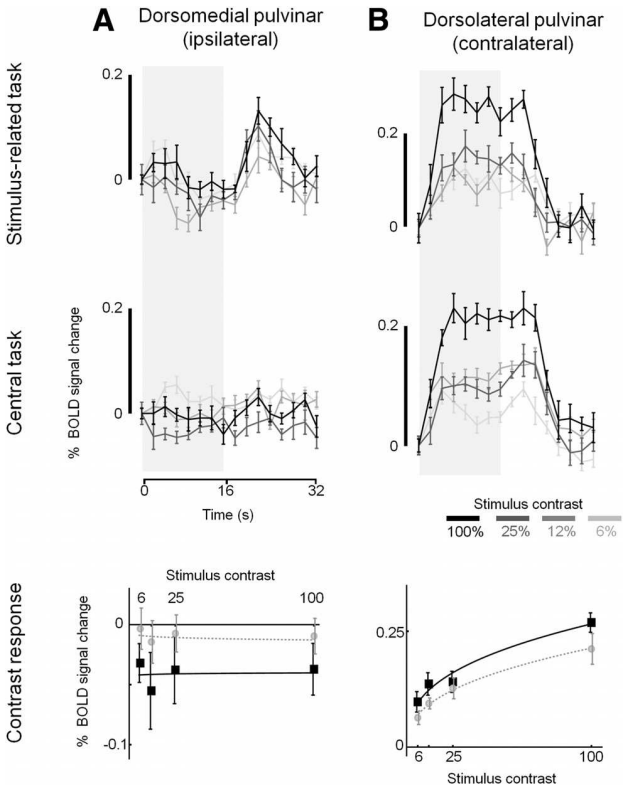

Figure 10. Group mean BOLD time series (top 2 rows) and contrast response functions (bottom row). ***A***, ***B***, Data are given for (***A***) the dorsomedial pulvinar ipsilateral to the stimulus and (***B***) the dorsolateral pulvinar contralateral to the stimulus. Time series data are given for four contrast levels for stimulus-related task (top row) and central task (middle row), and were generated and displayed as described in Figure 3. Scale bar to the left of each plot indicates 0.2% BOLD signal change. Contrast response functions (bottom row) are shown for the stimulus-related task (black squares) and central tasks (gray circles).

has the following advantages: (1) the effect of multiple stimuli of different sizes and locations can be accounted for; (2) the model allows manipulation of the spatial parameters of an attention field as well as receptive fields, allowing the modeling of effects in different visual areas; (3) the receptive fields are modeled by taking the extent of both the excitatory center and suppressive surround into account.

Reynolds and Heeger (2009) showed that when the attention field is large compared with the visual stimulus, a contrast gain effect of attention is observed, but when the attention field is comparable in size to the stimulus, the result is a response gain attentional effect (see Table 3). Importantly, the authors kept the receptive field properties constant because they were modeling the effect of attention in a single visual area. Here, we determined whether the model can account for the response characteristics we observed in two different visual areas—V1 and V5. To account for attentional effects in V1 and V5, we varied the receptive field parameters of the model, while necessarily holding the attention field and stimulus parameters fixed (Table 3). For V1, therefore, we used relatively small receptive fields compared with V5. We also modified the attention field, which in our case now suppresses unattended locations rather than facilitating attended locations as used by default in the model. As can be seen in Figure 11, this approach yields contrast responses that adequately capture the type of responses we measured. For V1, where receptive fields are small relative to the attention field, attention to the large lateralized stimulus produces a leftward shift in the contrast re-

Table 3. Model parameters[a]

Model description	Stimulus 1 size	Stimulus 2 size	Attention field size	Excitatory center size	Inhibitory surround size
Reynolds and Heeger, Fig. 2*A*	3	3	30	5	20
Reynolds and Heeger, Fig 2*B*	5	5	3	5	20
V1	50.4[b]	1.3[b]	30	1	4
V5	50.4[b]	1.3[b]	30	15	60

[a]Summary of the input parameters (arbitrary units, only relative sizes are meaningful) to "The Normalization Model of Attention" (Reynolds and Heeger, 2009). For context, the top two rows summarize the values used by Reynolds and Heeger to introduce the model and its effects (Reynolds and Heeger, 2009; their Fig. 2*A*, *B*). The bottom two rows show the model input parameters representing our stimuli and the receptive field sizes of V1 and V5. We used sigma values (see Reynolds and Heeger, 2009, for description) of 7.5×10^{-5} for V1 and 10^{-5} for V5 to account for differences in the well documented compressiveness between the contrast response functions of V1 and V5.

[b]Scaled by 3.6 units per degree of visual angle; see text for explanation.

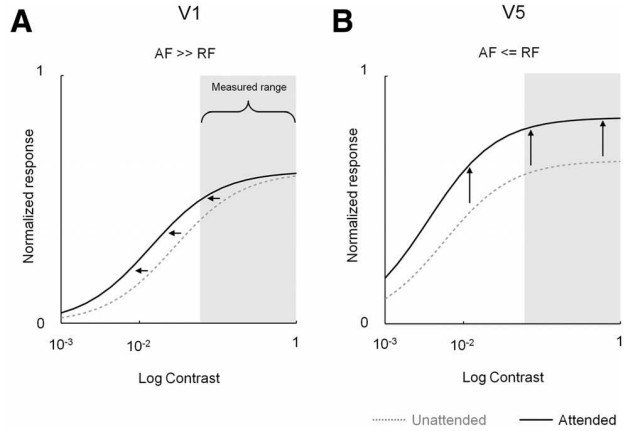

Figure 11. The Normalization Model of Attention: predicted effects in V1 and V5. ***A***, ***B***, Normalized model-predicted contrast responses (based on the input parameters defined in Table 3) are plotted for V1 (***A***) and V5 (***B***). The relatively large attention field (AF) to receptive field (RF) size ratio in V1 (***A***) results in contrast gain at the attended locations. For V5 (***B***), the lower AF to RF size ratio results in an effect of attention that is carried by a response gain-type mechanism. Note that these effects result from modeling the AF as suppressive at unattended locations rather than enhancing responses at attended locations. Note also that the portion of the model-predicted contrast response overlapping our sampled empirical data range (contrast, 6–100%) is qualitatively very similar to our measured data for V1 (compare Fig. 11*A* with Fig. 7*B*) and V5 (compare Fig. 11*B* with Fig. 7*C*).

sponse function, analogous to a contrast gain-type mechanism. For V5, where receptive fields are comparable in size to the attention field, attention produces a response modulation that is carried largely by a response gain-type mechanism. Accordingly, a single, early attention field that acts by suppressing unattended locations can account for the types of response we observe in conjunction with known differences in receptive field properties of neurons in V1 and V5. The data presented in Figures 9 and 10 suggest that a suppressive, early attention field may reside in the pulvinar.

Discussion

Our new, inter-related findings shed light on how the human brain represents visual information under different task and stimulus conditions. The key finding we make is that in the representations of unattended locations, negative BOLD signals are present and show little evidence of stimulus-contrast dependence. These negative signals are found in a network of brain areas, including both cortical (V1) and subcortical (LGN and pulvinar) structures. Moreover, we were able to disambiguate negative BOLD signals from signals arising from blinks, which are seldom considered as a potential confound (but see Hupé et al., 2012). Given the evidence that links negative BOLD responses to other physiological markers of neural suppression (Goense et al., 2012; Mullinger et al., 2014), we discuss our results in terms of the suppressive effects of attention. An autoradiography study in macaque (Vanduffel et al., 2000) showed suppression of the both the LGN and V1 at representations of unattended locations, features we reproduced in human and characterized further. Previous human fMRI studies showed suppression in V1 (Tootell et al., 1998a; Smith et al., 2000; Shmuel et al., 2002; Wade and Rowland, 2010) and some, most relevant to our study, explored suppression specifically in the hemisphere ipsilateral to a lateralized visual stimulus (Tootell et al., 1998a; Smith et al., 2000). However, even these most-relevant fMRI studies examined responses under a single stimulus and task condition. Moreover, the study on macaque first showing suppression in the LGN and V1 effectively used one stimulus condition with two tasks. We set out therefore to characterize suppression as a function of task and stimulus contrast in the LGN and V1 and found that suppression is highly task-dependent, but depends very little on stimulus contrast. The suppression we observed is also consistent with reported attention-related changes of baseline firing of neurons that are not stimulated: the firing rates of V4 and V2, but not V1, neurons with receptive fields that do not represent the stimulus decrease when attention is directed outside compared with inside the receptive field (Luck et al., 1997). Overall, therefore, our results highlight a task-dependent suppression of neural activity in very early visual structures as an important component of attention.

Our study also characterized how task affects positive signals as a function of contrast at stimulus representations in the LGN and V1. A key finding is that the stimulus-driven activity within the stimulus representation in the LGN does not increase when stimuli are attended. This is consistent with single-unit (Mehta et al., 2000a,b) and autoradiography measurements on macaque (Vanduffel et al., 2000). An early fMRI study demonstrated large attention-related increases in the activity of the human LGN (O'Connor et al., 2002), but more recent studies have found more modest attention-related changes (Schneider and Kastner, 2009; Schneider, 2011). Our results seem more consistent with the recent work and can be largely reconciled with the earlier study on the basis of methodological differences. By alternating stimulation from one hemifield to the other, without a baseline condition, the approach used by O'Connor et al. (2002) could capture both modest attention-dependent increases (Schneider and Kastner, 2009), along with perhaps larger effects reflecting a release from suppression that we measure here. We did, however, detect an attention-dependent increase in the superior colliculus contralateral to the stimulus, consistent with literature highlighting an attentional role of this structure (Schneider and Kastner, 2009; Katyal et al., 2010; Lovejoy and Krauzlis, 2010; Schneider, 2011; Krauzlis et al., 2013; Katyal and Ress, 2014).

The stimulus-driven positive signals in V1 that we measured were larger when the stimulus is attended, consistent with the fMRI literature. This effect is most obvious at intermediate and low contrasts, a finding replicated across multiple studies (Martínez et al., 1999; Somers et al., 1999; Buracas and Boynton, 2007;

Li et al., 2008). At high contrast, we find no attention-related increase in responses at the stimulus representation, consistent with one study (Li et al., 2008), but not another (Gandhi et al., 1999). It is possible that if we increased our task difficulty (our tasks were easier than those used in other studies), an effect of attention on V1 signals and indeed the LGN might emerge across all contrasts. In any case, it is clear that both baseline shifts (Ress et al., 2000; Murray, 2008) and contrast gain appear to interact in early visual areas under different task conditions to give rise to differing overall effects of attention on fMRI contrast response functions (Li et al., 2008).

The attention-dependent suppression we reveal in the LGN is unlikely to originate there. We found two other structures, V1 and the dorsomedial pulvinar, that also exhibit suppression. V1 has extensive feedback connections to LGN and the pulvinar, so it could be the source of suppression in both thalamic structures. However, it is also plausible that the pulvinar is the source of suppression in V1 and the LGN and there is direct evidence for the former (Purushothaman et al., 2012). The pulvinar has long been associated with attention (Chalupa et al., 1976). Also, human lesion (Rafal and Posner, 1987; Snow et al., 2009) and neuroimaging studies (Kastner et al., 2004; Cotton and Smith, 2007) have documented the involvement of the pulvinar in attention. Particularly relevant to our study, attentional deficits have also been reported in the hemifield contralateral to the hemisphere in which the pulvinar was inhibited (Desimone et al., 1990). The pulvinar also has feedforward and feedback connections with occipital, parietal, and frontal cortex (Shipp, 2003). The reductions in signals we observe during the stimulus-related task are largely restricted to the aspects of the pulvinar that connect strongly, but not exclusively, to the parietal cortex (Gutierrez et al., 2000; Behrens et al., 2003). It is possible therefore that the attention-related suppression arises in parietal cortex and is fed back to the pulvinar, which in turn influences signaling in the LGN and V1. The conduit for influencing signals in the LGN may be via V1 or perhaps the thalamic reticular nucleus, which could act as the intermediary that links the suppression we observe in the pulvinar to the LGN (McAlonan et al., 2008; Saalmann and Kastner, 2009). Our responses within the stimulus representations in the pulvinar do not appear to be modulated by attention. It is also clear that these stimulus representations do not occupy the same regions of the pulvinar as those that are suppressed by attention in the opposite hemisphere. It is important therefore to consider the subdivisions of the pulvinar because they appear to play different roles with respect to stimulus and task conditions (Robinson and Petersen, 1992; Shipp, 2003).

Given the suppression we find in subcortical areas, we asked whether a leading model of attention that invokes an early attention field can account for our results. The Normalization Model of Attention (Reynolds and Heeger, 2009), with the modification of a suppressive rather than facilitatory attention field, was able to account for the types of response we observed in V1 and V5. While we have shown that early suppression in an attention field can adequately account for our responses in V1 and V5, it may also play a role in other attentional effects. For example, others have put forward the idea that shifts in V5 receptive field location can be explained on the basis of the attentional suppression of some but not all of V1's inputs to V5 neurons (Anton-Erxleben et al., 2009), for which we provide evidence here.

We have shown that suppression is found in the representations of unattended locations of the LGN and V1. Similar effects were also found in the pulvinar. Importantly, these attention-related decreases in neural response carried little or no information about the attended stimulus. It is clear therefore that suppression, most notably in subcortical structures, plays an important role in spatial attention in human. Our findings have a number of important implications. First, suppression is an expression of negative feedback, a system that is both more stable and energetically efficient than excitatory, positive feedback systems (Niven and Laughlin, 2008). Second, a leading model of attention (Reynolds and Heeger, 2009) proposes the concept of a low-level attention field, which our results indicate could be suppressive and could reside in the pulvinar. Related to both points is the fact that large increases in neural responses in extrastriate visual cortex can result from relatively small, but widespread suppressive effects in antecedent visual structures.

References

Allman JM, Kaas JH (1971) A representation of the visual field in the caudal third of the middle tempral gyrus of the owl monkey (*Aotus trivirgatus*). Brain Res 31:85–105. CrossRef Medline

Amano K, Wandell BA, Dumoulin SO (2009) Visual field maps, population receptive field sizes, and visual field coverage in the human MT+ complex. J Neurophysiol 102:2704–2718. CrossRef Medline

Andrews TJ, Halpern SD, Purves D (1997) Correlated size variations in human visual cortex, lateral geniculate nucleus, and optic tract. J Neurosci 17:2859–2868. Medline

Anton-Erxleben K, Stephan VM, Treue S (2009) Attention reshapes center-surround receptive field structure in macaque cortical area MT. Cereb Cortex 19:2466–2478. CrossRef Medline

Baseler HA, Gouws A, Haak KV, Racey C, Crossland MD, Tufail A, Rubin GS, Cornelissen FW, Morland AB (2011) Large-scale remapping of visual cortex is absent in adult humans with macular degeneration. Nat Neurosci 14:649–655. CrossRef Medline

Behrens TE, Johansen-Berg H, Woolrich MW, Smith SM, Wheeler-Kingshott CA, Boulby PA, Barker GJ, Sillery EL, Sheehan K, Ciccarelli O, Thompson AJ, Brady JM, Matthews PM (2003) Non-invasive mapping of connections between human thalamus and cortex using diffusion imaging. Nat Neurosci 6:750–757. CrossRef Medline

Boynton GM (2011) Spikes, BOLD, attention, and awareness: a comparison of electrophysiological and fMRI signals in V1. J Vis 11(5):12. CrossRef Medline

Buracas GT, Boynton GM (2007) The effect of spatial attention on contrast response functions in human visual cortex. J Neurosci 27:93–97. CrossRef Medline

Carrasco M (2011) Visual attention: the past 25 years. Vision Res 51:1484–1525. CrossRef Medline

Chalupa LM, Coyle RS, Lindsley DB (1976) Effect of pulvinar lesions on visual pattern discrimination in monkeys. J Neurophysiol 39:354–369. Medline

Cotton PL, Smith AT (2007) Contralateral visual hemifield representations in the human pulvinar nucleus. J Neurophysiol 98:1600–1609. CrossRef Medline

Desimone R, Wessinger M, Thomas L, Schneider W (1990) Attentional control of visual perception: cortical and subcortical mechanisms. Cold Spring Harb Symp Quant Biol 55:963–971. CrossRef Medline

Devlin JT, Sillery EL, Hall DA, Hobden P, Behrens TE, Nunes RG, Clare S, Matthews PM, Moore DR, Johansen-Berg H (2006) Reliable identification of the auditory thalamus using multi-modal structural analyses. Neuroimage 30:1112–1120. CrossRef Medline

Dumoulin SO, Bittar RG, Kabani NJ, Baker CL Jr, Le Goualher G, Bruce Pike G, Evans AC (2000) A new anatomical landmark for reliable identification of human area V5/MT: a quantitative analysis of sulcal patterning. Cereb Cortex 10:454–463. CrossRef Medline

Duncan J (2006) EPS Mid-Career Award 2004: brain mechanisms of attention. Q J Exp Psychol (Hove) 59:2–27. CrossRef Medline

Fujita N, Tanaka H, Takanashi M, Hirabuki N, Abe K, Yoshimura H, Nakamura H (2001) Lateral geniculate nucleus: anatomic and functional identification by use of MR imaging. AJNR Am J Neuroradiol 22:1719–1726. Medline

Gandhi SP, Heeger DJ, Boynton GM (1999) Spatial attention affects brain activity in human primary visual cortex. Proc Natl Acad Sci U S A 96:3314–3319. CrossRef Medline

Goense J, Merkle H, Logothetis NK (2012) High-resolution fMRI reveals laminar differences in neurovascular coupling between positive and negative BOLD responses. Neuron 76:629–639. CrossRef Medline

Gouws A, Woods W, Millman R, Morland A, Green G (2009) DataViewer3D: an open-source, cross-platform multi-modal neuroimaging data visualization tool. Front Neuroinform 3:9. CrossRef Medline

Gutierrez C, Cola MG, Seltzer B, Cusick C (2000) Neurochemical and connectional organization of the dorsal pulvinar complex in monkeys. J Comp Neurol 419:61–86. CrossRef Medline

Hupé JM, Bordier C, Dojat M (2012) A BOLD signature of eyeblinks in the visual cortex. Neuroimage 61:149–161. CrossRef Medline

Jenkinson M, Bannister P, Brady M, Smith S (2002) Improved optimization for the robust and accurate linear registration and motion correction of brain images. Neuroimage 17:825–841. CrossRef Medline

Kastner S, Pinsk MA, De Weerd P, Desimone R, Ungerleider LG (1999) Increased activity in human visual cortex during directed attention in the absence of visual stimulation. Neuron 22:751–761. CrossRef Medline

Kastner S, O'Connor DH, Fukui MM, Fehd HM, Herwig U, Pinsk MA (2004) Functional imaging of the human lateral geniculate nucleus and pulvinar. J Neurophysiol 91:438–448. Medline

Katyal S, Ress D (2014) Endogenous attention signals evoked by threshold contrast detection in human superior colliculus. J Neurosci 34:892–900. CrossRef Medline

Katyal S, Zughni S, Greene C, Ress D (2010) Topography of covert visual attention in human superior colliculus. J Neurophysiol 104:3074–3083. CrossRef Medline

Krauzlis RJ, Lovejoy LP, Zénon A (2013) Superior colliculus and visual spatial attention. Annu Rev Neurosci 36:165–182. CrossRef Medline

Li X, Lu ZL, Tjan BS, Dosher BA, Chu W (2008) Blood oxygenation level-dependent contrast response functions identify mechanisms of covert attention in early visual areas. Proc Natl Acad Sci U S A 105:6202–6207. CrossRef Medline

Limbrick-Oldfield EH, Brooks JC, Wise RJ, Padormo F, Hajnal JV, Beckmann CF, Ungless MA (2012) Identification and characterisation of midbrain nuclei using optimised functional magnetic resonance imaging. Neuroimage 59:1230–1238. CrossRef Medline

Lovejoy LP, Krauzlis RJ (2010) Inactivation of primate superior colliculus impairs covert selection of signals for perceptual judgments. Nat Neurosci 13:261–266. CrossRef Medline

Luck SJ, Chelazzi L, Hillyard SA, Desimone R (1997) Neural mechanisms of spatial selective attention in areas V1, V2, and V4 of macaque visual cortex. J Neurophysiol 77:24–42. Medline

Martínez A, Anllo-Vento L, Sereno MI, Frank LR, Buxton RB, Dubowitz DJ, Wong EC, Hinrichs H, Heinze HJ, Hillyard SA (1999) Involvement of striate and extrastriate visual cortical areas in spatial attention. Nat Neurosci 2:364–369. CrossRef Medline

McAlonan K, Cavanaugh J, Wurtz RH (2008) Guarding the gateway to cortex with attention in visual thalamus. Nature 456:391–394. CrossRef Medline

Mehta AD, Ulbert I, Schroeder CE (2000a) Intermodal selective attention in monkeys. II: physiological mechanisms of modulation. Cereb Cortex 10:359–370. CrossRef Medline

Mehta AD, Ulbert I, Schroeder CE (2000b) Intermodal selective attention in monkeys. I: distribution and timing of effects across visual areas. Cereb Cortex 10:343–358. CrossRef Medline

Motter BC (1993) Focal attention produces spatially selective processing in visual cortical areas V1, V2, and V4 in the presence of competing stimuli. J Neurophysiol 70:909–919. Medline

Mullinger KJ, Mayhew SD, Bagshaw AP, Bowtell R, Francis ST (2014) Evidence that the negative BOLD response is neuronal in origin: a simultaneous EEG-BOLD-CBF study in humans. Neuroimage 94:263–274. CrossRef Medline

Murray SO (2008) The effects of spatial attention in early human visual cortex are stimulus independent. J Vis 8(10):2.1–11. CrossRef Medline

Niven JE, Laughlin SB (2008) Energy limitation as a selective pressure on the evolution of sensory systems. J Exp Biol 211:1792–1804. CrossRef Medline

O'Connor DH, Fukui MM, Pinsk MA, Kastner S (2002) Attention modulates responses in the human lateral geniculate nucleus. Nat Neurosci 5:1203–1209. CrossRef Medline

Posner MI (1980) Orienting of attention. Q J Exp Psychol 32:3–25. CrossRef Medline

Purushothaman G, Marion R, Li K, Casagrande VA (2012) Gating and control of primary visual cortex by pulvinar. Nat Neurosci 15:905–912. CrossRef Medline

Rafal RD, Posner MI (1987) Deficits in human visual spatial attention following thalamic lesions. Proc Natl Acad Sci U S A 84:7349–7353. CrossRef Medline

Ress D, Backus BT, Heeger DJ (2000) Activity in primary visual cortex predicts performance in a visual detection task. Nat Neurosci 3:940–945. CrossRef Medline

Reynolds JH, Heeger DJ (2009) The normalization model of attention. Neuron 61:168–185. CrossRef Medline

Robinson DL, Petersen SE (1992) The pulvinar and visual salience. Trends Neurosci 15:127–132. CrossRef Medline

Saalmann YB, Kastner S (2009) Gain control in the visual thalamus during perception and cognition. Curr Opin Neurobiol 19:408–414. CrossRef Medline

Schneider KA (2011) Subcortical mechanisms of feature-based attention. J Neurosci 31:8643–8653. CrossRef Medline

Schneider KA, Kastner S (2009) Effects of sustained spatial attention in the human lateral geniculate nucleus and superior colliculus. J Neurosci 29:1784–1795. CrossRef Medline

Shipp S (2003) The functional logic of cortico-pulvinar connections. Philos Trans R Soc Lond B Biol Sci 358:1605–1624. CrossRef Medline

Shmuel A, Yacoub E, Pfeuffer J, Van de Moortele PF, Adriany G, Hu X, Ugurbil K (2002) Sustained negative BOLD, blood flow and oxygen consumption response and its coupling to the positive response in the human brain. Neuron 36:1195–1210. CrossRef Medline

Slotnick SD, Schwarzbach J, Yantis S (2003) Attentional inhibition of visual processing in human striate and extrastriate cortex. Neuroimage 19:1602–1611. CrossRef Medline

Smith AT, Singh KD, Greenlee MW (2000) Attentional suppression of activity in the human visual cortex. Neuroreport 11:271–277. CrossRef Medline

Smith AT, Williams AL, Singh KD (2004) Negative BOLD in the visual cortex: evidence against blood stealing. Hum Brain Mapp 21:213–220. CrossRef Medline

Snow JC, Allen HA, Rafal RD, Humphreys GW (2009) Impaired attentional selection following lesions to human pulvinar: evidence for homology between human and monkey. Proc Natl Acad Sci U S A 106:4054–4059. CrossRef Medline

Somers DC, Dale AM, Seiffert AE, Tootell RB (1999) Functional MRI reveals spatially specific attentional modulation in human primary visual cortex. Proc Natl Acad Sci U S A 96:1663–1668. CrossRef Medline

Tootell RB, Mendola JD, Hadjikhani NK, Liu AK, Dale AM (1998a) The representation of the ipsilateral visual field in human cerebral cortex. Proc Natl Acad Sci U S A 95:818–824. CrossRef Medline

Tootell RB, Hadjikhani N, Hall EK, Marrett S, Vanduffel W, Vaughan JT, Dale AM (1998b) The retinotopy of visual spatial attention. Neuron 21:1409–1422. CrossRef Medline

Treue S, Martinez-Trujillo JC (2007) Attending to features inside and outside the spotlight of attention. Neuron 55:174–176. CrossRef Medline

Vanduffel W, Tootell RB, Orban GA (2000) Attention-dependent suppression of metabolic activity in the early stages of the macaque visual system. Cereb Cortex 10:109–126. CrossRef Medline

Wade AR, Rowland J (2010) Early suppressive mechanisms and the negative blood oxygenation level-dependent response in human visual cortex. J Neurosci 30:5008–5019. CrossRef Medline

Wall MB, Walker R, Smith AT (2009) Functional imaging of the human superior colliculus: an optimised approach. Neuroimage 47:1620–1627. CrossRef Medline

Zeki SM (1969) The secondary visual areas of the monkey. Brain Res 13:197–226. CrossRef Medline

Neuro-Ophthalmology, 33, 149–157, 2009

ISSN: 0165-8107 print / 1744-506X online
DOI: 10.1080/01658100903050053

informa
healthcare

The Organization of the Visual Cortex in Patients with Scotomata Resulting from Lesions of the Central Retina

Heidi A. Baseler and Andre Gouws
Department of Psychology, University of York, York

Antony B. Morland
Department of Psychology and Hull-York Medical School, University of York, York

ABSTRACT

Primary visual cortex can undergo forms of reorganization following bilateral lesions to the retinas of animals. Brain cells that originally received input from retinal tissue that was lesioned become responsive to retina that remains intact. In humans, reorganization of the primary visual cortex has been found in adult patients with congenital foveal lesions. More recent investigations of patients with macular degeneration, who acquired retinal lesions later, have yielded mixed results. In this paper we review the evidence for and characteristics of cortical reorganization in humans and animals and suggest how it might be evaluated in the context of strategies for treating retinal disease.

Keywords: Macular degeneration; retinotopy; visual cortex; reorganization; plasticity

INTRODUCTION

Over recent years, much research has been devoted to understanding how the brain reacts to the loss of sensory input. Within the visual domain, there has been great interest in determining whether visual processing in the brain changes or "reorganizes" in response to retinal lesions. Many studies have used animal models to examine the recovery of brain function following artificially induced retinal lesions. In humans, in whom retinal lesions can result from eye disease, significant changes have been found when retinal lesions are present from birth. Research has been undertaken to investigate what happens to cortical responses following central retinal lesions acquired later in life, with some authors reporting reorganization. Such reorganization could prove to be an effective adaptive strategy, conferring advantages on the patient in terms of visual outcome and consequent quality of life. Moreover, understanding how any changes emerge over time is important so that visual rehabilitation might be administered at appropriate times to encourage and harness cortical reorganization. At the same time, however, reorganization could work against treatments that aim to restore retinal input from the lesioned region; reorganized cortex may not be best suited to process these newly restored signals. Deciding whether to administer various treatments hinges on knowing whether or not the patient's brain is able to cope effectively with restored visual input. Therefore, it may be valuable to assess the extent to which a patient's cortex has reorganized before undertaking treatment in order to predict how well the treatment might work. Determining the time period during which no reorganization occurs may also be important in governing when patients should receive restorative treatment.

In this review, we outline the current state of knowledge regarding reorganization of the visual cortex, first and briefly in animal models and then more extensively

Received 13 May 2009; accepted 17 May 2009.

Address correspondence to Antony B. Morland, Department of Psychology, University of York, York, YO10 5DD. E-mail: arm501@york.ac.uk

in humans. We report on the limits of reorganization and the conditions under which it is observed. We also review preliminary evidence that indicates that the cortex may undergo detrimental changes as a result of being deprived of its visual input.

BASIC CONCEPTS

Before embarking on a review of the evidence for and against reorganization, it is worth describing the basic concepts, terms and nomenclature that has been used in studies of cortical reorganization following lesions of the retina.

The mammalian brain contains several maps of the visual field. The cortical neurons within each map respond to stimuli within a specific region of visual space (the *receptive field* of the cell). Neighboring regions in space project to neighboring cells in the retina, which in turn send their input to neighboring cells in primary visual cortex. This preservation of orderly mapping from eye to brain is referred to as being *retinotopic*.

In humans, the retinotopic map in primary visual cortex (*V*1) occupies a total cortical surface area roughly the size of a credit card* in each hemisphere, with each hemisphere representing the contralateral visual field. However, the representation in the cortex is somewhat distorted, being disproportionately large for the central retina (*macula*) relative to the peripheral retina, a feature known as *cortical magnification*. When the retina is damaged, the prediction is that, at least initially, the cortical representations of the lesioned area will no longer be visually driven because all of their functional input has effectively been removed. Therefore, a macular lesion would eliminate input to a relatively large proportion of visual cortex. The region of cortex that no longer receives input is often referred to as the *Lesion Projection Zone* or*LPZ*.[1] If activity is recorded in the LPZ, it is usually taken as a signature of reorganization of the visual cortex. A schematic of the visual cortical representation and concepts and terms relating to reorganization are shown in Figure 1.

REORGANIZATION OF VISUAL CORTEX IN ANIMAL MODELS

Kaas and colleagues[2] recorded from neurons in primary visual cortex of cats and mapped their receptive field locations. The authors then induced a lesion to the area centralis (analogous to the human macula) of one eye of the cats and enucleated the fellow eye, removing input to central representations in cortex. Single neuron responses were again recorded from primary visual cortex following these induced retinal lesions. The compelling result was that neurons that had originally received input from the now lesioned regions of the retina became responsive to stimuli presented to intact, but more peripheral, retinal locations. Similar findings were reported in adult monkeys by Heinen and Skavenski,[3] who showed that the receptive fields of visual cortical neurons shifted peripherally following bilateral foveal retinal lesions. The scale of this remapping was highly significant but modest in spatial extent, restricted to a few millimetres in the cortex. In a series of papers, Gilbert and colleagues characterised the remapping of visual cortex in animal models (see Gilbert,[4] and Calford,[5] for reviews).

There is some controversy over the role of retinal recovery in reported measures of cortical reorganization.[6] The reported changes in the neural responses in primary visual cortex could be predicted if the retina were to recover at the fringe of the lesion, and therefore would not provide evidence of reorganization. One counter to this proposal is that there was little evidence of a widespread recovery of responses in the LPZ of the lateral geniculate nucleus (LGN), the structure which receives input from the retina before relaying it to the visual cortex.[7,8] The authors concluded, therefore, that reorganization is a feature of the cortex and not one seen throughout the visual system as a result of retinal recovery.

The presence of reorganization is further questioned by a recent report using functional magnetic resonance imaging (fMRI) of the visual cortex in adult monkeys after inducing retinal lesions.[9] Their failure to find cortical activity in the LPZ in V1 generated a heated debate with much criticism being levelled at the fMRI technique. Nevertheless, fMRI is a well-established method for mapping visual cortex (see Wandell, Brewer & Dougherty[10] for a review) and directly related to physiological signals.[11,12] Moreover, it has been used effectively to measure signals that are consistent with visual cortical reorganization.[13,14]

It appears, therefore, that the original consensus that the visual cortex undergoes a remapping following retinal lesions has been questioned by some more recent animal studies (for further debate on this topic the reader is directed to a review by Smirnamkis and Wandell, 2009). At the same time, however, recent reports of evidence of widespread reorganization continue to be published in high-profile journals.[15]

*This rather useful measure was first encountered by the authors when discussing visual cortical areas with Christopher Tyler, PhD, Smith-Kettlewell Eye Research Institute, San Francisco.

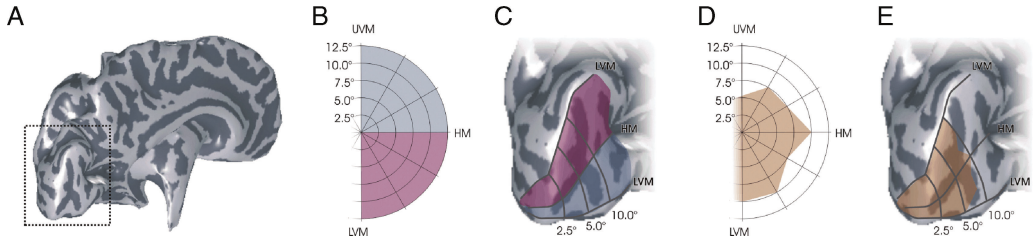

Figure 1. Schematics showing the visual field representation in primary visual cortex and the Lesion Projection Zone (LPZ). In A the left hemisphere of a partially inflated brain is illustrated as if viewed from a posterior-medial position. Sulcal and gyral features are shaded with dark and light grey respectively. The square depicted with a broken line indicates the region of the brain that is shown magnified in panels C and E. B: A visual field coordinate map of the central 12.5 degrees of visual angle, with upper and lower quadrants colored blue and pink, respectively. C: The mapping of the visual field map onto the cortex in and surrounding the calcrine sulcus. The upper and lower visual quadrants are represented in the lower and upper regions of the cortex. A disproportionate area of cortex is devoted to central visual field coordinates, a feature referred to as cortical magnification. D: The visual field with a shaded area indicating a central scotoma. E: The transformation into cortical coordinates of the scotoma shown in panel D. This shaded region is the Lesion Projection Zone.

CHANGES IN VISUAL CORTICAL FUNCTION AND STRUCTURE IN HUMAN PATIENTS WITH RETINAL SCOTOMATA

While a considerable amount of research has provided support for cortical reorganization in animals with retinal lesions, it has only been by means of recent technological advances that researchers have been able to ask similar questions in humans. Functional MRI was introduced in the 1990s as a groundbreaking new tool to map the human brain noninvasively and with high spatial precision. To map retinotopic early visual areas, a subject is presented with visual stimuli that move progressively through the visual field.[16–20] This elicits a "travelling wave" of activation in the occipital lobes that can be observed by measuring the blood oxygenation level dependent (BOLD) signal changes in MR images acquired throughout the stimulation period. The lower resolution functional images are aligned and transformed to high resolution structural MR images acquired from the same subject. The anatomical images provide detailed information so that functional activity can be localized and associated with specific

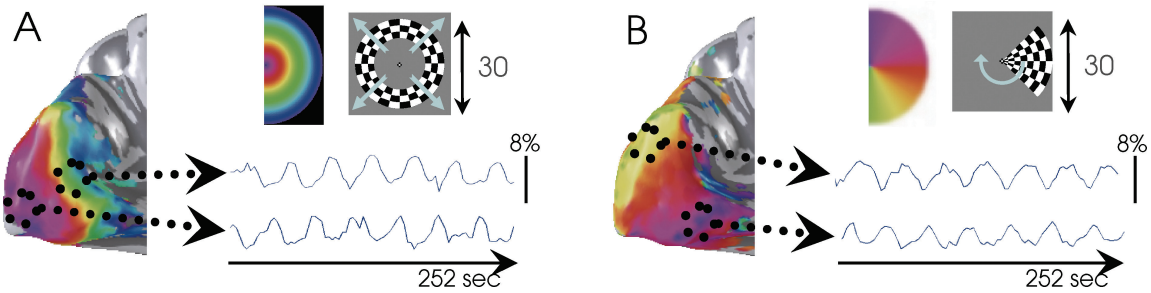

Figure 2. Retinotopic mapping: Stimuli, Visual Field Maps and Time Series. A: In the upper right of the figure a ring checkerboard is shown with arrows to indicate that it cycles through the visual field from center to periphery, to resume its original, central position after 36s. To the left of the stimulus is a false color map of the location of the visual stimulus that is used to color code the brain responses superimposed on the surface reconstruction shown to the left of panel A. This surface reconstruction shows the mapping of the visual field with central location represented at the occipital pole and a smooth progressive representation of increasing eccentricity moving from the pole anteriorly. Circles highlight regions of the brain for which time series have bee calculated and presented to the right of the panel. The signal approximates to a sinusoid, the phase of which encoded the position in the visual field to which the brain responds. It is clear from the two time series that the phase (latency) differs reflecting the sensitivity to different field locations. In panel B the stimulus, visual field mapping and time series are shown for the complementary stimulus, which is a wedge shaped checkerboard that rotates around its apex and resumes its original position in 36s. At the same time as allowing eccentricity's complementary, polar angle coordinate to be mapped on the surface of the brain (left), this mapping experiment also yields the cortical representations of the vertical and horizontal meridians, which mark boundaries between visual areas.

brain structures, including the cerebral cortex (grey matter).[21] The cortical sheet can then be computationally inflated or flattened so that the topography of the visual maps can be assessed without the folds found in the original surface.[10,22] The steps associated with this retinotopic mapping technique are shown in Figure 2.

Retinotopic mapping techniques have been applied successfully to investigate cortical remapping in individuals with congenital retinal lesions.[13,14] Complete rod monochromacy is a genetic disorder resulting in a lack of functioning cone photoreceptors in the retina. As the central 1 deg of the retina (the *foveola*) normally contains only cones, rod monochromats have permanent, bilateral scotomata in the central retina. Because of cortical magnification of central vision, the small foveolar blind spots project to a relatively large area in the brain, which is now deprived of its normal, feedforward visual input. Patients of this type therefore offer a rare opportunity to examine the potential of the cortex to reorganize retinal input in the face of established, long-term retinal lesions. The patients who were studied had reasonably stable fixation, which allowed the retinotopic data to be examined in considerable detail. The authors found that the regions of the cortex that would normally represent the lesioned retina responded instead to neighboring intact retina. This remapping of visual information was of a similar nature to that observed in previous animal studies, but appeared to extend over a larger cortical distance and could not be replicated in normal individuals: when the visual conditions of rod monochromats were reproduced in control individuals by presenting stimuli scotopically (i.e., at very low luminances visible only to the rods and not cones), no activation was found in the region of cortex receiving input from the central, rod-free zone of the retina. No changes were observed in the activation patterns in control subjects, even after maintaining scotopic viewing conditions for as long as six days.[13]

After cortical reorganization was demonstrated in humans with long-standing congenital retinal lesions, the next question was whether lesions acquired later in life would yield similar cortical changes. Retinotopic mapping methods were used to map visual cortex in an individual with extensive bilateral retinal lesions caused by geographic atrophy.[23] The distribution of cortical activity in this patient was consistent with a normal retinotopic representation of the intact retina, with a lack of activation in the region representing the lesioned part of the retina (LPZ). It is of note, however, that a small part of the central retina remained intact in this patient. Although this feature served as an advantage in the study by allowing the subject to maintain stable fixation, a subsequent study suggested that so-called "foveal sparing" is associated with an absence of remapping.[24] Indeed, the location of a retinal lesion has been shown to have an effect on whether or not reorganization is observed in animal models (e.g., Rosa, Schmid & Calford.[25]).

Following the study by Sunness et al. Baker et al.[26] pursued the issue of cortical organization in two patients with acquired bilateral retinal lesions resulting from juvenile macular degeneration (*JMD*). The patients had large scotomata which may have been present many years before testing; the patients were diagnosed at ages <40 and 11 and tested at 56 and 50 years, respectively. In a departure from the retinotopic mapping methodology used in previous studies, the authors presented blocks of stimuli comprising faces, objects or scenes, and required their participants to perform a *one-back* task. Participants were presented with a series of different faces (or objects or scenes, depending on the block) and were asked to indicate whether or not the current stimulus was the same as the one presented immediately before ("one-back" in the series). The activity elicited by viewing such complex images under these task conditions included areas of the early visual cortex which would ordinarily be innervated by damaged regions of the retina in these patients. The evidence of this widespread activity led the authors to conclude that there had been a "large-scale reorganization of visual processing." Note that this wording does not necessarily imply that the primary visual cortex had undergone an intrinsic remapping of the retinal input that remained in these patients. Indeed, the authors raise the possibility that the activity recorded in the early visual areas of these patients may be caused by feedback from higher extrastriate visual areas.

To explore whether the different outcomes of the Sunness et al. and Baker et al. studies depended on stimulus or task differences, Masuda et al.[27] performed an experiment, again testing patients with JMD. The investigators used both simple stimuli (reversing checkerboards and drifting contrast patterns) and more complex stimuli (faces and scrambled faces) under three different conditions: passive viewing, performing a stimulus-related task and performing a task unrelated to the stimulus. The results were varied across subjects; one of the four patients showed no activity in the LPZ, while the other three showed activity that only arose when performing a stimulus-related task. The authors concluded that when activity is observed in the LPZ it is a consequence of the task, not the stimulus; for example, activity was observed in the LPZ for a one-back task when viewing faces, but not when the faces were viewed passively.

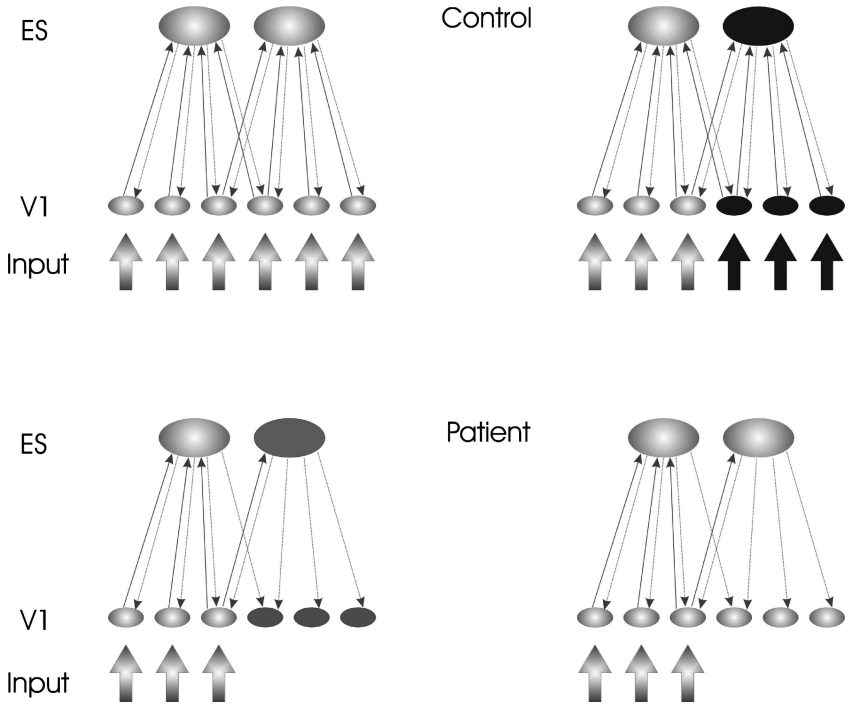

Figure 3. Feedback explanation of activity in the LPZ (after Masuda et al.[27]). In the top pair of panels, we consider the intact visual system. On the left we depict retinal afferents converging on V1 and then V1 units projecting to a smaller number of extrastiate (ES) units. The light shading of the units and arrows indicates that the units are signalling a high contrast stimulus. To the right we show the same intact visual system, but in this case the input corresponds to a stimulus that has a high contrast region (light shaded arrows) neighbored by a zero contrast region (black arrows). The V1 and ES units are shaded to reflect the appropriate encoding of the stimulus, an encoding that would result whether a task was performed or not. In the lower pair of panels schematics of a visual system compromised by retinal lesion are given. Now the retinal input is capable of encoding only a restricted region (light shaded arrows) of the high contrast stimulus. This input is then encoded by a similarly restricted number of VI and ES units. At the same time however, the absence of input leaves the remaining V1 and ES units firing spontaneously (the dark grey shading). This spontaneous firing would not result in recordable BOLD responses because they would not be modulated by the stimulus cycle. To the right the same stimulus is considered, but in this case a task is being performed. The result of the task is to increase activity in ES units each time the stimulus is presented and the task performed resulting in activity in V1 units because of the feedback connections.

It is also noteworthy that the patient in whom no activity in the LPZ was observed in the Masuda et al.[27] study was the oldest at the time of testing (57) and was diagnosed latest (at the age of 41). The other patients were diagnosed at the ages of 9, 18 and 28, and tested at the ages of 31, 22 and 38, respectively. It is possible, therefore, that absolute age or age of lesion onset may be important factors in determining whether activation can be detected in the LPZ.

Finally, the authors reasoned that the term "large-scale reorganization" should not be used in reference to the activity they and Baker et al.[26] observed in the LPZ, because this term implies the underlying presence of anatomical changes. Instead, they suggest that the activity can be explained on the basis of an absence of the normal input signal in conjunction with normal feedback from extrastriate regions. Thus, while the activations are abnormal, they do not necessarily rely on reorganization of neural processing. A schematic showing how feedback can explain activity in the LPZ is given in Figure 3.

Revisiting their original study, Baker et al.[24] tested five additional patients, again using complex stimuli (objects) and a one-back task, and found results broadly similar in nature to the ones originally reported in three of the patients (activation of the LPZ when stimulating peripheral visual field), but not in the other two (no activation of the LPZ). The latter two were different from the other three in that they retained some portion of central visual function ("foveal sparing"), a characteristic they shared with the patient reported by Sunness et al.[23] who also showed little or no LPZ activation. The

authors surmised that the presence of visual sensitivity in the fovea might preclude cortical reorganization. Of the patients in whom the authors claimed to replicate their original findings, the activity in the LPZ did not show one of the main features of the original study, that being a contiguous swathe of activity from the representation of the intact retina through to cortex at the occipital pole where the damaged retina would originally have been represented. These differences appear to need some explanation.

In addition, the authors in this study[24] presented supplementary data from two subjects showing activation in the LPZ with passive stimulation (checkerboards, no task). This is contrary to the results reported by Masuda et al.[27] showing LPZ activity only when subjects performed a stimulus-related task. The existence of LPZ activation under passive stimulation would lend support to the theory that these signals reflect a permanent remapping of early visual areas rather than simply feedback from extrastriate cortex. However, studies from the same lab show activation in unstimulated, foveal cortex in control subjects when performing a task related to peripherally presented stimuli.[28] In fact, numerous studies have reported stimulus-related activation in regions of occipital cortex not directly represented by the stimulated visual field, although the activation is often inhibitory in nature.[12,29–32]

A more recent study looked at whether remapping of the LPZ was experience-dependent.[33] They found activity in the LPZ in patients when they were viewing stimuli with their preferred retinal locus (*PRL*). The study was successful in showing this feature in the imaging data, but unfortunately was not successful in showing other predicted responses in control or patient data. For example, the study showed no positive stimulus related activity in the calcarine cortex of normal participants. It is hard therefore to assess the positive result obtained for patients in the context of a failure to obtain other predicted positive results. The question the authors raise is, however, an interesting one: Does the original cortical representation of the fovea (and hence fixation), remap when fixation is centred on a different, eccentric region of the retina? Dilks et al.[34] have gone some way to addressing this issue and have in fact refuted the proposal made by Schumacher et al.[33] They find that activity in the LPZ, again in response to complex stimuli viewed while performing a task, is not dependent on presenting stimuli to the LPZ [34].

Overall, therefore, the fMRI studies of patients with central scotomata show two rather different patterns of reorganization. In those patients who have scotomata at birth, the reorganization appears to involve remapping of the retinal input and is reasonably consistent with the type of reorganization observed in animal models. It should be noted, however, that the reorganization observed in humans was greater in its extent (in cortical distance) than that frequently observed in animal models. This increase could arise from either the congenital nature of the scotomata or from the length of time the subjects had the scotomata. The second pattern of reorganization appears to be more general and more widespread. The cortical representation of the scotoma is activated,[26] but that activation is not always contiguous with that elicited by stimulation of intact retina.[24] In animal models reorganization appears to be contiguous, so it would not predict a widespread region of activation in the LPZ detached from the activation resulting from signals arising in intact retina. It appears, therefore, that the results in patients with scotomata acquired late in life represent a reorganization that may differ considerably from the type found in animal models or humans with congenital lesions.

To date, most reports of reorganization in humans have been based on very few patients of varying aetiology. Of the patients studied, those who exhibited widespread activity in the LPZ also had the largest, most longstanding scotomata, typically from juvenile macular degeneration (*JMD*). While observing reorganization in such patients is of great interest to neuroscientists, the relative rarity of JMD and the long-term age and stability of their lesions make these observations less relevant in the context of what might happen in age-related macular degeneration (*AMD*), the leading cause of blindness. Indeed, an abstract reporting a study on four patients with AMD indicates that three of the four patients tested showed no evidence of activity in the LPZ.[35] It is clear that a study evaluating a greater number of patients is needed, comparing LPZ activation in patients with JMD and AMD, so that reasonable inferences about group differences can be made. Given the variety of results and patients tested previously, it would also be germane to examine the period of time that is required to reconfigure the LPZ such that it begins to respond. This issue might best be approached with a longitudinal study.

Our group is currently undertaking a group study of patients with AMD and JMD. Our preliminary results indicate that there is no evidence of activity in the LPZ when patients view checkerboards passively. An example of one patient's data is shown in Figure 4. Responses are observed in regions of the brain that map the retina that remains intact in the patient, but the occipital pole displays no evidence of similar activity. In a group analysis including 12 patients thus far, we have found no significant large-scale remapping in human primary

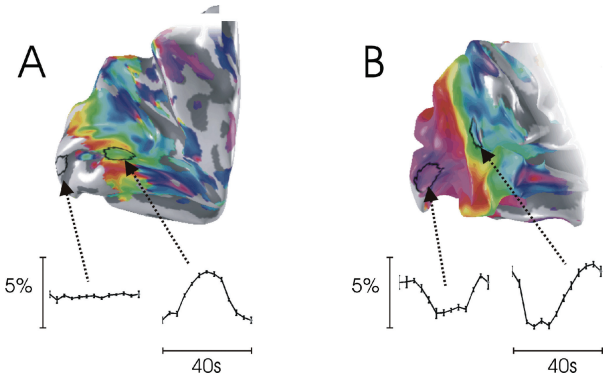

Figure 4. Surface reconstructions of the left occipital lobes of a patient with MD (A) and control (B). In A the progression of the visual field representation in the patient ceases some distance short of the occipital pole and there is no activity (above threshold) related to central stimulus locations, which would be shown in purple. Also rendered on the surface of the visual cortex are two circular regions of interest highlighted by the arrows. The time series (collapsed across the seven stimulus cycles presented) are plotted below the surface reconstruction with only the anterior region of interest in the fundus of the calcarine sulcus displaying detectable activity. Note the time series were generated from all voxels in the region of interest and not just those for which a threshold has been applied. In B the data for a normal control are shown with the chief difference from the patient being robust activity at the occipital pole. Time series for the regions of interest indicated by the broken lines are plotted below the surface reconstruction and in this case strong modulatory activity is observed at both sites.

visual cortex in either AMD or JMD. Our results appear to be consistent with those of Sunness et al.[23] and Masuda et al.[27] but are contrary to those found by Baker et al.[24] Therefore, we conclude that widespread remapping is not a feature that can be generalized to the MD population at large.

In some respects, the absence of activity in the LPZ may be a blessing in disguise for patients; it appears to indicate that the early visual cortex does not undergo an extensive remapping, which would leave the cortex inappropriately configured to process retinal signals that are restored by treatment. At the same time, however, the absence of evidence of remapping does not rule out the possibility that cortical tissue degenerates, rendering it less sensitive to restored retinal signals. Indeed, there is evidence that when transcranial magnetic stimulation (*TMS*) is applied to the visual cortex of blind individuals, higher stimulation levels are required to elicit phosphenes the more profoundly blind patients are.[36] This finding indicates that the longer the visual cortex remains without a visual input, the less responsive the cortex becomes, at least in the context of eliciting visual sensations. A recent study also sheds light on the issue of cortical changes resulting from the removal of sensory input.[37] The study used anatomical imaging to compare cortical volume within the occipital lobe between various patient groups and control individuals. They found that cortical volume was reduced in patients in portions of the occipital lobe representing the lesioned area of the retina: Central scotomata as a result of AMD were associated with cortical thinning at the occipital pole, while more peripheral scotomata resulting from glaucoma were associated with volume reductions in the more anterior regions of the medial aspects of the occipital lobe. The results indicate that the cortex is likely to undergo some form of degeneration as a result of removed input. How such degeneration is related to the presence or absence of activity in the LPZ is clearly of interest.

DISCUSSION

Visual areas of the brain in blind patients have been shown to respond differently from normal, particularly when performing a task. One remarkable example of this is the cross-modal activation of visual cortex in blind patients when reading Braille.[38,39] (for a review, see Sadato[40]). Within the visual domain alone, some patients with blindness originating in the central retina exhibit visually driven activation in regions of cortex normally representing the damaged retina. Although the source of activation in the LPZ of these patients is unknown, several theories have been proposed. These fall into two broad categories: (1) an intrinsic remapping of cortical neurons subserved by the post-lesional development of new connections; or (2) an unmasking of existing connections when the primary input is removed. Overall, the evidence seems to point towards the latter of these two interpretations. That is, the effects of normal cortico-cortical connections on activity in early visual areas are unmasked when the feed-forward input to those early visual areas is removed. In control subjects, these long-range connections may not be unmasked when normal feed-forward inputs exist to relay the absence of a visual stimulus (e.g., a uniform, grey "artificial scotoma").

Nevertheless, in some patients with MD there is no evidence of activity in the LPZ even when task conditions favor feedback signals. Masuda et al.[27] indicate that the variation between patients' responses might be accounted for by variations in the balance between feed-forward and feed-back signals converging on V1. For example, incomplete scotomata or unilateral scotomata would allow a sufficient feed-forward signal to null the feedback

signal. Another way of viewing heterogeneity of responses in LPZ might be to consider the results of Boucard et al.[37] alongside the feedback model. It may be that feedback signals can no longer be nulled by the intrinsic functioning of deafferented V1 only after V1 undergoes degeneration. This hypothesis could be tested directly by testing patients longitudinally after they lose macular vision bilaterally.

How does the activity in the LPZ found in humans with MD compare to that reported in animal models? The reorganization found in animal models is highly significant, but is frequently modest (e.g., Darian-Smith & Gilbert[8] but also see Keck et al.[15]). This type of topographical remapping has also been reported in those with congenital deficits that render patients blind in the fovea.[13] The widespread activity in the LPZ observed in some patients with MD.[26] appears to differ qualitatively from that found in many studies of animal models and that found in humans with congenital deficits. First, the activity found in the LPZ can be spatially distant from the activity associated with intact retinal input. Second, the activity in the LPZ is not always contiguous with the activity driven by intact retina. These differences mean that it is less likely for the activity in the LPZ to be governed by the reorganizing processes that have been observed in animal models. Overall therefore it seems sensible to seek an alternative explanation for the results in human patients. As described above the explanation that appears most apt is one that posits an unmasking of cortico-cortical feedback. Moreover, it is well established that early visual areas are widely interconnected, not only with downstream visual areas,[41] but also with other sensory areas[42,43] throughout the brain. That these connections would be revealed in the absence of the primary feedforward input seems highly plausible.

While the case for a feedback mediated response in the LPZ of humans appears quite compelling, it still needs to be demonstrated unequivocally. This issue along with some others that we pose below are important in the context of understanding cortical organization and signalling following retinal lesions in humans. First, is there an actual, intrinsic remapping of the visual cortex? Second, does the visual cortex maintain normal levels of responsivity following deafferentation and if so, for how long? Third, does the activity in the LPZ play a functional role in vision of patients with retinal lesions?

We plan to address these questions using transcranial magnetic stimulation. When TMS is applied to the scalp over occipital cortex, individuals report the perception of phosphenes, and this method can be used to map the topographical representation in visual cortex.[44–46] If direct stimulation of the LPZ in patients results in the perception of phosphenes that are displaced peripherally relative to control subjects, this would indicate that remapping of the LPZ. Indeed, abnormal mapping of phosphenes has been observed in one individual with severed optic nerves,[47] demonstrating that TMS can be applied to map phosphenes in blind individuals, and that there may be genuine topographic reorganization in some cases.

ACKNOWLEDGEMENTS

The authors acknowledge with thanks the funding of their work provided by the Medical Research Council (Grant reference: G0401339). We are also indebted to our colleagues, Gary Rubin, Adnan Tufail, Michael Crossland and Mary Feely, at the Institute of Ophthalmology, London. We are also very grateful for the feedback on drafts of this article provided by Professor Brian Wandell, Stanford University.

REFERENCES

1. Schmid LM, et al. Visuotopic reorganization in the primary visual cortex of adult cats following monocular and binocular retinal lesions. *Cereb Cortex* 1996;6(3):388–405.
2. Kaas JH, et al. Reorganization of retinotopic cortical maps in adult mammals after lesions of the retina. *Science* 1990;248(4952):229–231.
3. Heinen SJ, Skavenski AA. Recovery of visual responses in foveal V1 neurons following bilateral foveal lesions in adult monkey. *Exp Brain Res.* 1991;83(3):670–674.
4. Gilbert CD. Horizontal integration and cortical dynamics. *Neuron.* 1992;9(1):1–13.
5. Calford MB. Dynamic representational plasticity in sensory cortex. *Neuroscience* 2002;111(4):709–738.
6. Horton JC, Hocking DR. Effect of early monocular enucleation upon ocular dominance columns and cytochrome oxidase activity in monkey and human visual cortex. *Vis Neurosci.* 1998;15(2):289–303.
7. Gilbert CD, Wiesel TN. Receptive field dynamics in adult primary visual cortex. *Nature* 1992;356(6365):150–152.
8. Darian-Smith C, Gilbert CD. Topographic reorganization in the striate cortex of the adult cat and monkey is cortically mediated. *J Neurosci.* 1995;15(3 Pt 1):1631–1647.
9. Smirnakis SM, et al. Lack of long-term cortical reorganization after macaque retinal lesions. *Nature* 2005;435(7040):300–307.
10. Wandell BA, Brewer AA, Dougherty RF. Visual field map clusters in human cortex. *Philos Trans R Soc Lond B Biol Sci.* 2005;360(1456):693–707.
11. Logothetis NK, et al. Neurophysiological investigation of the basis of the fMRI signal. *Nature* 2001;412(6843):150–157.
12. Pasley BN, Inglis BA, Freeman RD. Analysis of oxygen metabolism implies a neural origin for the negative BOLD response in human visual cortex. *Neuroimage* 2007;36(2):269–276.
13. Baseler HA, et al. Reorganization of human cortical maps caused by inherited photoreceptor abnormalities. *Nat Neurosci.* 2002;5(4):364–370.
14. Morland AB, et al. Abnormal retinotopic representations in human visual cortex revealed by fMRI. *Acta Psychol (Amst)* 2001;107(1–3):229–247.

15. Keck T, et al. Massive restructering of neuronal circuits during functional reorganization of adult visual cortex. *Nat Neurosci.* 2008;11(10):1162–1167.
16. DeYoe EA, et al. Functional magnetic resonance imaging (FMRI) of the human brain. *J Neurosci Methods* 1994;54(2):171–187.
17. DeYoe EA, et al. Mapping striate and extrastriate visual areas in human cerebral cortex. *Proc Natl Acad Sci USA* 1996;93(6):2382–2386.
18. Engel SA, Glover GH, Wandell BA. Retinotopic organization in human visual cortex and the spatial precision of functional MRI. *Cereb Cortex* 1997;7(2):181–192.
19. Engel SA, et al. fMri of human visual cortex [letter] [published erratum appears in *Nature* 1994 Jul 14;370(6485):106]. *Nature*, 1994;369(6481):525.
20. Sereno MI, et al. Borders of multiple visual areas in humans revealed by functional magnetic resonance imaging [see comments]. *Science* 1995;268(5212):889–893.
21. Teo PC, Sapiro G, Wandell BA. Creating connected representations of cortical gray matter for functional MRI visualization. *IEEE Trans Med Imaging* 1997;16(6):852–863.
22. Wandell BA, Chial S, Backus BT. Visualization and measurement of the cortical surface. *J Cogn Neurosci* 2000;12(5):739–752.
23. Sunness JS, Liu T, Yantis S. Retinotopic mapping of the visual cortex using functional magnetic resonance imaging in a patient with central scotomas from atrophic macular degeneration. *Ophthalmology* 2004;111(8):1595–1598.
24. Baker CI, et al. Reorganization of visual processing in macular degeneration: replication and clues about the role of foveal loss. *Vision Res*. 2008;48(18):1910–1919.
25. Rosa MG, Schmid LM, Calford, MB. Responsiveness of cat area 17 after monocular inactivation: limitation of topographic plasticity in adult cortex. *J Physiol.* 1995;482(Pt 3):589–608.
26. Baker CI, et al. Reorganization of visual processing in macular degeneration. *J Neurosci*. 2005;25(3):614–618.
27. Masuda Y, et al. V1 projection zone signals in human macular degeneration depend on task, not stimulus. *Cereb Cortex* 2008;18(11):2483–2493.
28. Williams MA, et al. Feedback of visual object information to foveal retinotopic cortex. *Nat Neurosci*. 2008;11(12):1439–1445.
29. Bressler D, Spotswood N, Whitney D. Negative BOLD fMRI response in the visual cortex carries precise stimulus-specific information. *PLoS ONE* 2007;2(5):e410.
30. Serences JT, Boynton GM, Feature-based attentional modulations in the absence of direct visual stimulation. *Neuron* 2007;55(2):301–312.
31. Shmuel A, et al. Negative functional MRI response correlates with decreases in neuronal activity in monkey visual area V1. *Nat Neurosci*. 2006;9(4):569–577.
32. Shmuel A, et al. Sustained negative BOLD, blood flow and oxygen consumption response and its coupling to the positive response in the human brain. *Neuron.* 2002;36(6):1195–1210.
33. Schumacher EH, et al. Reorganization of visual processing is related to eccentric viewing in patients with macular degeneration. *Restor Neurol Neurosci.* 2008;26(4–5):391–402.
34. Dilks DD, et al. Reorganization of visual processing in macular degeneration is not specific to the "preferred retinal locus." *J Neurosci.* 2009;29(9):2768–2773.
35. Cheung S-H, et al. Limited retinotopic reorganization in age-related macular degeneration. *Journal of Vision* 2005;5(8): 299.
36. Gothe J, et al. Changes in visual cortex excitability in blind subjects as demonstrated by transcranial magnetic stimulation. *Brain* 2002;125(Pt 3):479–490.
37. Boucard CC, et al. Changes in cortical grey matter density associated with long-standing retinal visual field defects. *Brain* In Press.
38. Cheung SH, et al. Retinotopically specific reorganization of visual cortex for tactile pattern recognition. *Curr Biol.* 2009;19(7):596–601.
39. Sadato N, et al. Activation of the primary visual cortex by Braille reading in blind subjects. *Nature* 1996;380(6574):526–528.
40. Sadato N. How the blind "see" Braille: lessons from functional magnetic resonance imaging. *Neuroscientist* 2005;11(6):577–582.
41. Gattass R, et al. Cortical visual areas in monkeys: location, topography, connections, columns, plasticity and cortical dynamics. *Philos Trans R Soc Lond B Biol Sci*. 2005;360(1456):709–731.
42. Driver J, Noesselt T. Multisensory interplay reveals crossmodal influences on 'sensory-specific' brain regions, neural responses, and judgments. *Neuron* 2008;57(1):11–23.
43. Rockland KS, Ojima H. Multisensory convergence in calcarine visual areas in macaque monkey. *Int J Psychophysiol*. 2003;50(1–2):19–26.
44. Fernandez E, et al. Mapping of the human visual cortex using image-guided transcranial magnetic stimulation. *Brain Res Brain Res Protoc.* 2002;10(2):115–124.
45. Kammer T, et al. Transcranial magnetic stimulation in the visual system. II. Characterization of induced phosphenes and scotomas. *Exp Brain Res*. 2005;160(1):129–140.
46. Kammer T, et al. Transcranial magnetic stimulation in the visual system. I. The psychophysics of visual suppression. *Exp Brain Res*. 2005;160(1):118–128.
47. Cowey A, Walsh V. Magnetically induced phosphenes in sighted, blind and blindsighted observers. *Neuroreport* 2000;11(14):3269–3273.

nature neuroscience

Large-scale remapping of visual cortex is absent in adult humans with macular degeneration

Heidi A Baseler[1], André Gouws[1,6], Koen V Haak[2,6], Christopher Racey[1], Michael D Crossland[3,4], Adnan Tufail[3,4], Gary S Rubin[3], Frans W Cornelissen[2] & Antony B Morland[1,5]

The occipital lobe contains retinotopic representations of the visual field. The representation of the central retina in early visual areas (V1–3) is found at the occipital pole. When the central retina is lesioned in both eyes by macular degeneration, this region of visual cortex at the occipital pole is accordingly deprived of input. However, even when such lesions occur in adulthood, some visually driven activity in and around the occipital pole can be observed. It has been suggested that this activity is a result of remapping of this area so that it now responds to inputs from intact, peripheral retina. We evaluated whether or not remapping of visual cortex underlies this activity. Our functional magnetic resonance imaging results provide no evidence of remapping, questioning the contemporary view that early visual areas of the adult human brain have the capacity to reorganize extensively.

The human brain contains maps of the retina on the surface of the occipital lobes[1]. Abnormal visual development can modify these retinotopic maps[2–5]. Under circumstances in which individuals acquire early visual experience in the presence of a lesion to the center of the retina, reorganization of the visual representation occurs[6]. The visual brain in these individuals remaps by allocating a larger than normal area of cortex to intact, peripheral vision. Although brain plasticity is clearly possible when neural changes occur early in life, the adult brain also appears to be capable of plasticity. Experimentally induced retinal lesions in adult animals can lead to a remapping of primary visual cortex to respond to inputs from nearby intact retina[7–13]. We sought to determine whether cortical remapping generalizes to humans who acquire retinal lesions in adulthood.

Several groups have investigated reorganization in human adult cortex when retinal lesions were acquired as a result of disease (macular degeneration). These studies have produced variable results, generating some controversy. One group[14] found no evidence of activity in parts of visual cortex that normally receive input from lesioned retina (the lesion projection zone) in a single, elderly individual. Another study[15], on the other hand, reported widespread activation of the lesion projection zone in two adults with juvenile macular degeneration and suggested that this might reflect a cortical remapping via horizontal connections similar to, but larger than, those found in earlier animal studies. The remapping hypothesis is supported by another functional magnetic resonance imaging (fMRI) study claiming that activation of deprived cortex can be generated by eccentric fixation[16]. Stimulating the occipital cortex of an individual blinded in adulthood by trauma to the optic nerves resulted in abnormal phosphene maps, also suggesting cortical remapping[17]. Despite these reports, the implication that remapping is responsible for the large-scale spread of activation in the lesion projection zone of individuals with retinal lesions acquired in adulthood has been seriously questioned[18–20].

Using methods that explicitly evaluate visual cortical maps, we sought to determine whether humans with lesions acquired in adulthood exhibit reorganization in the form of cortical remapping of visual input over the large-scale seen in individuals with congenital foveal loss of vision[6]. In contrast with prior studies largely restricted to a few individuals with juvenile forms of macular degeneration (JMD), we compared responses in a large number of individuals in two different age groups: those with JMD and those with the more common age-related form (AMD), and their age-matched controls. We found no evidence of large-scale remapping in early visual areas in adults with acquired retinal lesions. Indeed, the area of activity in primary visual cortex measured in these individuals was no different from that predicted on the basis of normal retinotopic maps. Furthermore, the absence of cortical remapping was not dependent on the age at which the individuals acquired retinal lesions in adulthood.

RESULTS

Cortical responses were measured in 16 individuals with macular degeneration (see **Table 1**) and 12 age-matched controls with normal vision using fMRI. Individuals with macular degeneration had bilateral lesions for at least 1 year and had developed a stable preferred retinal locus that allows good fixation performance. We tested two age groups: young (mean age = 30) and elderly (mean age = 76). Participants passively viewed flickering checkerboard stimuli configured in a ring that expanded through increasing eccentricity or a wedge that rotated around a central point. Such stimuli reliably modulate blood oxygenation level–dependent signals and are used to map visual areas in occipital cortex[1,21–24]. Response magnitude was

[1]York Neuroimaging Centre, Department of Psychology, University of York, York, UK. [2]Laboratory for Experimental Ophthalmology and BCN Neuroimaging Centre, University Medical Centre Groningen, University of Groningen, Groningen, The Netherlands. [3]Institute of Ophthalmology, University College London, London, UK. [4]Moorfields Eye Hospital NHS Foundation Trust, London, UK. [5]Hull-York Medical School, York, UK. [6]These authors contributed equally to this work. Correspondence should be addressed to A.B.M. (a.morland@psychology.york.ac.uk).

Received 22 September 2010; accepted 28 February 2011; published online 27 March 2011; doi:10.1038/nn.2793

Table 1 Summary of affected individuals in the study

Diagnosis	Sex	Age (years)	Eye tested	Lesion diameter (°)	Acuity (logMAR)	BCEA (°)
AMD	F	90.9	Right	9	0.92	17.7
AMD	F	83.5	Right	8	0.98	12.43
AMD	F	81.8	Left	7	0.54	17.7
AMD	M	76.3	Left	6	0.36	8.26
AMD	M	80.2	Left	10	1.06	15.16
AMD	F	70.8	Left	4	0.9	12.37
AMD	M	83.8	Left	15	0.86	20.37
AMD	M	80.6	Right	13	0.76	5.33
Stargardt's	M	19.8	Left	5	0.74	11.71
Stargardt's	F	19.7	Left	3	1.02	2.24
Stargardt's	M	49.5	Right	6	0.56	14.47
Stargardt's	F	41.2	Right	10	0.9	1.69
Stargardt's	F	34.7	Right	8	1.08	13.54
Stargardt's	F	39.4	Right	9	0.98	18.11
Stargardt's	F	24.3	Left	3.5	0.66	9.33
Stargardt's	M	35.8	Left	17	1.12	13.26

BCEA, bivariate contour ellipse area (a measure of fixation ability using microperimetry); logMAR, log(minimum angle of resolution).

first evaluated using coherence as an outcome measure, as in previous similar fMRI studies[18,25] (Online Methods).

We made coherence maps for each of the individuals in the two groups, those with macular degeneration (the patient group) and the age-matched controls (the control group). Although control subjects showed substantial visually driven responses throughout visual cortex, both the young and elderly patient groups only displayed substantial responses in the anterior occipital lobe. Strong responses in these individuals are therefore limited to regions of the cortex that normally map peripheral (that is, intact) retina (**Fig. 1**).

Responses in the lesion projection zone were compared quantitatively with those in regions that are normally driven by intact retina using regions of interest (ROIs) defined anatomically to avoid any bias toward activation patterns. In both hemispheres, one region was selected at the occipital pole, normally representing the central visual field, and another region in the fundus of the calcarine sulcus, normally representing more peripheral locations. The BOLD signal plotted as a function of time showed robust modulations in response to stimulus onset at both the occipital pole and calcarine sulcus in controls (**Fig. 1**). Clear differences in the response latency of the signals measured at the occipital pole and calcarine sulcus reflect the normal retinotopic mapping of early visual areas. Fourier analysis was also applied to the average time series (**Fig. 1**). The resultant spectra (and associated z scores) are consistent with the time series, showing robust signals at the stimulation frequency at both cortical locations in the control group, but only at the calcarine sulcus in the patient group.

Group effects

Our data analysis (**Fig. 1**) captured responses in individuals and conformed to the approach used in previous work on a limited number of cases[15,18,26]. Extending our analysis to the group level, we categorized participants according to age and visual status (young and elderly, patient and control). Responses were assessed at three cortical locations: the two mentioned above (calcarine sulcus and occipital pole; **Fig. 1**), and a third control region located further anterior in the brain in non-visual cortex, chosen to serve as a baseline measure.

The results for the elderly group are shown in **Figure 2a**. We performed a two-way analysis of variance (ANOVA) with visual status (patient versus control group) and ROI (calcarine sulcus versus occipital pole versus control region) as main factors. A significant main effect was found for both visual status ($F = 8.62$, $P < 0.01$) and brain region ($F = 24.20$, $P < 10^{-6}$), with a significant interaction ($F = 3.30$, $P < 0.05$). *Post hoc* tests (corrected for multiple comparisons) revealed a significant difference between the patient and control groups at the occipital pole ($P < 0.01$), but none at the calcarine sulcus or at the control region. In the patient group, signals at the occipital pole were not significantly different from the baseline measure at the control region ($P > 0.05$), but were significantly different from signals from the intact retina at the calcarine sulcus ($P < 0.001$). Patient group responses at the calcarine sulcus were robust and well above baseline ($P < 0.001$). In the control group, signals at the occipital pole and calcarine sulcus were not significantly different from one another ($P > 0.05$), but both differed significantly from the baseline response (calcarine sulcus versus control region, $P < 0.001$; occipital pole versus control region, $P < 0.05$).

Previous work that revealed activity in the lesion projection zone primarily tested individuals who acquired lesions earlier in adulthood than the individuals with AMD that we examined. Comparing the young patient group with the young control group, however, yielded the same results as in the elderly patient group (**Fig. 2b**), with significant main effects of visual status ($F = 52.32$, $P < 10^{-7}$) and ROI ($F = 95.72$, $P < 10^{-15}$) and a significant interaction between them ($F = 18.36$, $P < 10^{-5}$). *Post hoc* tests (corrected) also revealed the same pattern of results as in the elderly groups, but with all differences achieving significance at $P < 0.001$. Large-scale remapping appears to be absent independent of the age in adulthood at which the retinal lesions are acquired.

To test the reproducibility of our results, we acquired additional data on a separate day in most participants ($n = 20/28$) and found

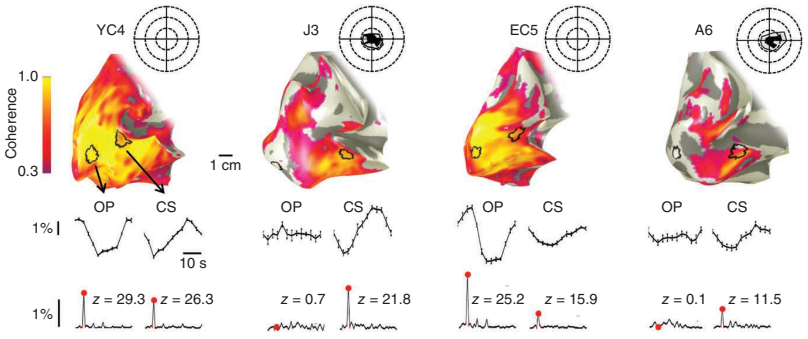

Figure 1 Cortical responses to visual stimulation. BOLD responses for four individuals (from left to right): a young control subject (YC4, age 30), a young patient (J3, age 49), an elderly control subject (EC5, age 66) and an elderly patient (A6, age 70). Visual field results from microperimetry for each subject are inset to the right of each brain image and indicate absolute (black) and partial (gray) scotoma. Dotted concentric circles represent 5, 10 and 15 deg eccentricity. BOLD response coherence is encoded in color and superimposed on smoothed, left occipital lobes. Single cycle time series averages are shown for the two occipital ROIs representing central (occipital pole, OP) and more peripheral retina (calcarine sulcus, CS). Fast Fourier transforms were performed on each full time series and amplitude spectra are also shown for each ROI; stimulus frequency (seven cycles per scan) is indicated by the red dot. z scores indicate the number of s.d. the FFT amplitude at the stimulus frequency differs from the distribution of all of the other frequency amplitudes.

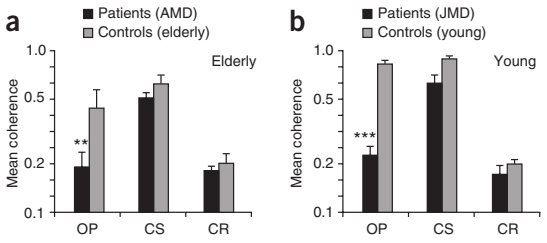

Figure 2 Mean coherences for each ROI, averaged across individuals for each group. CR, control region in nonvisual cortex. Error bars indicate standard error. $***P < 0.001$, $**P < 0.01$. (**a**) Elderly patients (AMD) versus elderly controls. (**b**) Young patients (JMD) versus young controls.

that the data conformed to the same pattern. Repeated-measures ANOVA revealed no main effect of session in all groups ($P > 0.05$). Combining data across sessions, we also tested explicitly for statistical differences associated with age across groups. A three-way ANOVA was performed on the elderly and young groups, with ROI, visual status and age as factors. As in the individual age groups, significant main effects of visual status ($F = 23.40$, $P < 10^{-5}$) and ROI ($F = 60.00$, $P < 10^{-15}$) were found, as well as a significant interaction between them ($F = 7.18$, $P < 0.01$). There was also a main effect of age ($F = 8.82$, $P < 0.01$), a feature that we have noted previously[27]. However, there were no significant interactions between age and visual status ($F = 2.09$, $P = 0.15$) or age and ROI ($F = 2.31$, $P = 0.11$). Thus, although age affects the overall magnitude of fMRI responses, it does so similarly in both the patient and control groups and does not alter the pattern of differences found between them.

Simulating retinal lesions in controls

Using a control region in a nonvisual brain area as a baseline measure comes with the danger that small, but genuine, occipital signals may escape detection, for example, if signal-to-noise ratios vary across the brain[28] or if the control region is in fact responsive to visual stimuli. To improve the specificity of our measurements, we compared signals in the same region of visual cortex (the occipital pole) in control subjects in the presence or absence of visual stimulation. We scanned 12 new control subjects (mean age = 27) while they passively viewed the expanding ring checkerboard stimulus either in full or with a central mask (gray disk radius = 7.5 degrees) simulating a macular lesion (**Fig. 3**). The presence of the central mask in the stimulus largely removes significant responses from the occipital pole.

Using the new baseline measure, we compared responses from the young control group with those from the young patient group and the control group from the first experiment, averaged across sessions (**Fig. 4**). A two-way ANOVA revealed main effects of group (patient versus control versus new control groups, $F = 38.57$, $P < 10^{-9}$) and ROI (occipital pole versus calcarine sulcus, $F = 56.08$, $P < 10^{-8}$), as well as a significant interaction between them ($F = 8.50$, $P < 0.001$). *Post hoc* tests (corrected) showed that these effects were carried by important features at the occipital pole and calcarine sulcus. First, responses at the occipital pole did not differ significantly between the patient group and the new control group shown the simulated scotoma ($P > 0.05$), but both were significantly below those of the original control group shown the full stimulus ($P < 10^{-5}$ for both comparisons). Second, responses at the calcarine sulcus in all three groups were significantly above baseline, as expected ($P < 0.001$). The patient group responses at the calcarine sulcus fell significantly below those of the original age-matched controls ($P < 0.05$). In summary, our results using an improved baseline measure again support the absence of large-scale remapping in individuals with macular degeneration.

Partial volume effects

Even though stimulation of peripheral retina is expected to produce fMRI responses of equal magnitude in both patient and control groups, we noted that signals at the calcarine sulcus were relatively reduced in both the elderly and young patient groups (calcarine sulcus; **Fig. 2**) and significantly so when data were combined across sessions ($P < 0.05$; **Fig. 4**). Because lesion size was variable across the patient group, the anatomically defined ROI at the calcarine sulcus could include tissue in the lesion projection zone, effectively reducing the signal there. Such 'partial volume' effects are therefore predicted to be more likely when retinal lesions are large.

A multiple regression was performed with lesion size (mean lesion diameter; **Table 1**) and age as regressors, as age was shown previously to have a negative effect on fMRI responses (see above). The analysis revealed an overall significant relationship between lesion size, age and response (coherence) at the calcarine sulcus ($R^2 = 0.308$, $P < 0.05$). Consistent with the partial volume prediction, the effect was carried entirely by lesion size (t(one-tailed) = −1.95, $P = 0.036$) rather than age (t(one-tailed) = −0.74, $P = 0.238$). In contrast, no such

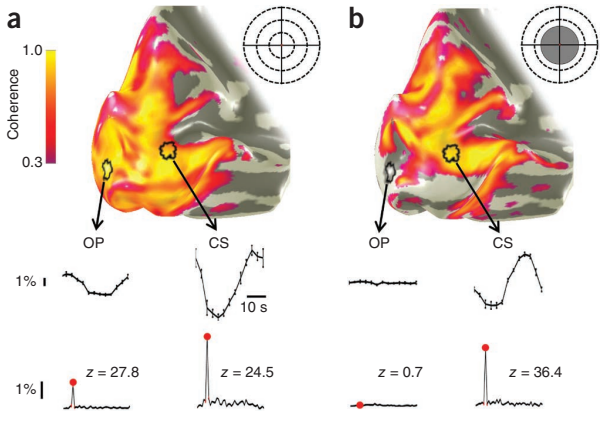

Figure 3 Simulating retinal lesions in a control subject. In both panels, the left occipital lobe of a control subject is shown with BOLD signal coherence superimposed on the surface. Below each panel time series (averaged to a single stimulus cycle) and amplitude spectra of the time series are given for circular regions of cortex at the occipital pole and calcarine sulcus. (**a**) Response to expanding checkerboard ring stimulus spanning full field. (**b**) Response to same stimulus as in **a**, but with central ±7.5 deg masked with a uniform, mean luminance gray disc. Data are presented as in **Figure 1**.

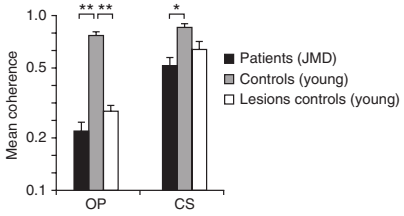

Figure 4 Occipital lobe responses compared across groups and ROIs. Mean coherences averaged across sessions and across individuals from three groups: young patient data from experiment 1, young control data from experiment 1 and lesion control group data from experiment 2 using new baseline measure at the occipital pole in response to stimulus with central ±7.5 deg masked with uniform gray. $**P < 0.01$, $*P < 0.05$. Error bars indicate s.e.m.

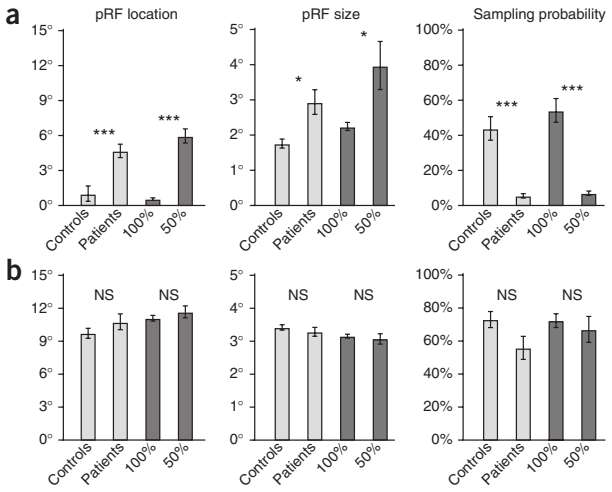

Figure 5 Receptive field characteristics. (**a**,**b**) Population receptive field (pRF) characteristics in the lesion projection zone (**a**) and the calcarine sulcus (**b**). Mean pRF locations and sizes and the sampling probability (percent voxels exceeding 15% variance explained) are shown. Light gray bars show data for individuals with macular degeneration and age-matched controls. Data are given for combined age groups, as none of the outcome measures showed group contrasts (patient group versus control group) that were specific to age (location, $F = 0.27$, $P = 0.603$; size, $F = 3.36$, $P = 0.074$; sampling probability, $F = 0.27$, $P = 0.603$). In two patients, we were unable to derive population receptive field estimates in the lesion projection zone. Dark gray bars show data for controls that were presented the unmasked (100%) stimulus or the stimulus simulating a central scotoma (50% masked). $^*P < 0.05$, $^{***}P < 0.001$. Error bars refer to s.e.m.

relationship was found in regions where no response was predicted and partial volume effects were less likely, either well inside the lesion projection zone at the occipital pole ($R^2 = 0.059$, $P = 0.336$) or at the control region in nonvisual cortex ($R^2 = 0.055$, $P = 0.346$).

Receptive field characteristics

Although there were no significant group differences in occipital pole signals between the patient group and the control group with simulated retinal lesions, there was a hint that occipital pole signals in both groups may exceed those found in the control region (**Fig. 2**). It is possible that these signals are visually driven by a small proportion of neurons with large and/or eccentric receptive fields[19,29] that extend into areas of stimulated retina.

To investigate the properties of potential visually driven signals, we modeled population receptive fields[30] of responses in an enlarged region centered on the occipital pole region described above (Online Methods; **Supplementary Results** and **Supplementary Fig. 1**). The mean population receptive field location and size around the occipital pole were abnormally large in both the patient group (location, $t = 3.81$, $P < 0.001$; size, $t = 2.90$, $P = 0.01$) and the control group when central retinal lesions are simulated (location, $t = 7.90$, $P < 0.001$; size, $t = 2.44$, $P = 0.032$) (**Fig. 5**). The significant shift in population receptive field location (**Fig. 5a**) implies an apparent shift in the representation of these voxels, that is, rendering them 'ectopic'. In contrast, population receptive fields in the calcarine sulcus region (**Fig. 5**) did not differ significantly either between the patient and control groups (location, $t = 1.09$, $P = 0.285$; size, $t = 0.72$, $P = 0.481$) or between masked and unmasked conditions for the controls (location, $t = 0.84$, $P = 0.414$; size, $t = 0.44$, $P = 0.669$). Fixation instability in the patient group cannot account for the effects observed, as the patient and control groups with simulated lesions showed similar results and both the occipital pole and calcarine sulcus regions would be affected[5], which they clearly were not.

Cortical representation

Using phase encoded stimuli also allows the cortical mapping of retinal coordinates to be assessed at an individual level. **Figure 6** shows fMRI response maps in the occipital lobes of several individuals in the elderly and young groups. Although subjects with normal vision showed complete retinal representations throughout the occipital lobes (**Fig. 6a**), individuals with macular degeneration showed response maps that were consistent with the projection from intact parts of retina only (**Fig. 6b**).

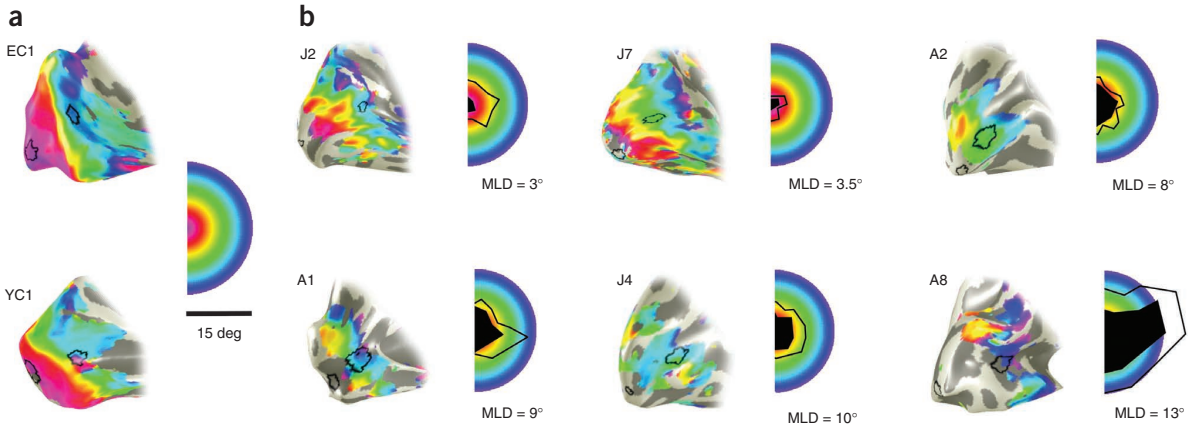

Figure 6 Individual eccentricity maps. (**a**,**b**) FMRI response maps of visual eccentricity superimposed on individual left, partially inflated, occipital lobes for control subjects (**a**) and six affected individuals (**b**). False color is used to indicate the position on the retina (see semi-circular key) to which the cortex is responsive. In **b**, filled black regions of the semicircular key indicate the absolute retinal lesion (scotoma), whereas outlined region exhibits significant, but not absolute, loss of vision. Patient group cortical maps are presented in ascending order (from left to right starting on the top row) of mean lesion diameter (MLD). The cortical representations closely corresponded to the spared retina. Indeed, even retinal locations with reduced sensitivity elicited activity. In all cases, however, the cortical activity did not spread to encompass the occipital pole. Note that this is a different subset of participants than those shown in **Figure 1**.

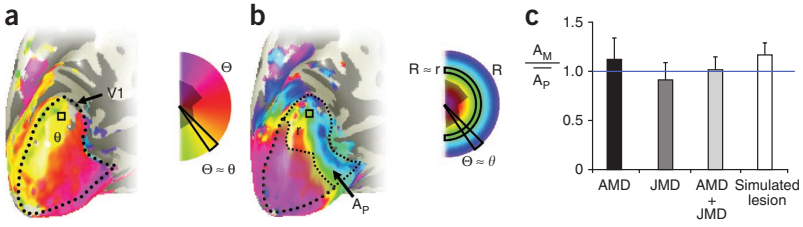

Figure 7 The cortical area representing intact visual field. (**a**,**b**) Schematic of the method by which the area of primary visual cortex representing a subject's intact visual field (measured by microperimetry) is predicted on the basis of normal retinotopic mapping. First, the primary visual cortex boundary was determined in each control participant by identifying the representations of the upper (purple) and lower (green) vertical meridians in calcarine cortex, as indicated by the dotted line on the surface reconstruction of the occipital lobe for one control participant (**a**). Second, we determined whether a voxel (as indicated by the small square in **a** and **b**) has a polar angle phase, θ, that is among the values of polar angle in the intact visual field, Θ (see inset false color map showing the location of the scotoma (shaded) and intact (unshaded) regions). If this is the case, as it is in the illustrated example, we then determined whether the eccentricity represented by the voxel, r, is among the eccentricities in the intact field, R, at the polar angle θ. If the voxel's polar coordinate (r,θ) is among the set of coordinates (R,Θ) of intact visual field locations, the voxel is retained. The predicted cortical area representing the patient's intact visual field, A_P, is then computed from all the retained voxels. For each patient, multiple values of A_P (one for each of the age-matched control retinotopic maps) were obtained and then averaged to compute the mean predicted area of activated V1, $\bar{A}_P$. In each patient, the area of active primary visual cortex, A_M, was also measured. (**c**) The ratio of A_M to $\bar{A}_P$ for the participant groups. No significant differences between groups or between group values and unity were found ($P > 0.05$). Nonsignificant differences from unity present in the AMD and simulated lesion groups are likely the results of the minority of ectopically responding voxels found in **Figure 5**, which could not be predicted from normal retinotopic maps. Error bars indicate s.e.m.

Furthermore, the extent of activation and its phase reflect the size of the spared retina. A large retinal lesion results in a smaller activation area on the brain (for example, A8) and vice versa (for example, J2).

To compare cortical maps quantitatively, we measured the area of activity in the primary visual cortex, A_M, for each patient and control participant with simulated lesions and compared it with a mean predicted area, $\bar{A}_P$, which was determined from the individual's scotoma and normal mappings of age-matched controls (Online Methods and **Fig. 7**). The ratio $A_M/\bar{A}_P$ was compared across participant groups and we found no significant effect of group ($F = 0.81$, $P = 0.46$; **Fig. 7**). Moreover, all groups exhibited ratios that were no different from unity (AMD, $t = 0.59$, $P = 0.57$; JMD, $t = -0.55$, $P = 0.60$; controls, $t = 1.93$, $P = 0.08$), an indication that the area of primary visual cortex activated in all participant groups can be predicted on the basis of normal retinotopic maps. Because each ratio was computed with age-matched control data, patient groups were combined to increase statistical power, but we still found no significant difference between the patient and control groups ($t = -0.81$, $P = 0.41$) or difference from unity in the ratio ($t = 0.14$, $P = 0.89$). Given the variance for patient and control groups in our ratio measure, a significant (at $P < 0.05$) difference in the ratio (of 0.23) would occur if the mean increase in cortical area compared with controls exceeded 160 mm^2 in each hemisphere. This is relatively small compared with the total area of primary visual cortex (~2,500 mm^2, see ref. 31). Our analysis provides strong, quantitative evidence that the extent of early visual cortical activity in the patient and control groups can be predicted on the basis of normal retinotopic maps.

DISCUSSION

Seminal work on early visual deprivation in animals has shown that visual cortex can develop to devote more of its territory to intact visual input at the expense of its representation of impoverished input[32–35]. Such reallocation of cortical processing has also been demonstrated when early visual areas remap following congenital retinal lesions in human[6]. In adulthood, the cortex is less plastic, but even so, remapping of the visual cortical representation has been inferred on the basis of ectopic receptive fields in the lesion projection zone in animal models[7–13]. This effect is, however, rather modest and has been called into question recently[19]. Even so, recent studies of human adults[15,26] suggest a large-scale extension of remapping of the type reported in animal models. We aimed to test explicitly whether or not visual cortical mapping changes following retinal lesions in adult humans. Our results indicate that it does not in three different ways.

First, we found that at the occipital pole, a cortical location that we are certain lies in the lesion projection zone, the signals observed in the patient group are no different than those found in the control group in whom we simulated a central scotoma. The spatially specific ROI analysis has been used extensively previously[15,26] and has been shown to be highly sensitive to remapping[6]. Our result runs contrary to the view that the occipital pole in V1 takes on a new mapping to respond strongly to peripheral stimuli in a way that differs from normal. Previous work in this area has been limited to small numbers of affected individuals and control participants[15,26]. Moreover, previous work has used task-stimulus combinations[15,26] that produced widespread signals in the lesion projection zone in affected individuals, but less in controls, most likely as a result of feedback from extrastriate cortex rather than remapping[18].

Second, our results indicate that throughout the lesion projection zone there are voxels with 'ectopic' receptive fields, but they are equally common and represent the same regions of visual field in both the patient and control group. This finding speaks more generally to the way in which ectopic receptive fields should be interpreted. Frequently, the existence of ectopic receptive fields has been taken as evidence for remapping[7–13]. That ectopic characteristics can be recorded from normally sighted controls challenges this notion, particularly in the context of fMRI research[15,26]. Furthermore, we found that voxels with ectopic receptive fields were not restricted to the fringe of the lesion projection zone, where most electrophysiological measurements have been taken[7–13]. We propose, as have others[19,30], that each cortical location (voxel) contains many neurons, the responses of which can be influenced by stimuli at a range of locations, but that the overall population response is heavily weighted to a modal location. If stimuli are presented only to locations that are a considerable distance from this modal location, the responses of the voxel will be weak, but could be driven by neurons with receptive fields that are large, displaced or large and displaced (see **Supplementary Fig. 1**). We found that only 5–7% of voxels in the lesion projection zone could be classified as responsive, meaning that such signals could escape detection with conventional analyses that average signals over the whole ROI. Notably, the probability of detecting a voxel with ectopic receptive fields is similar to the probability of detecting a neuron with ectopic receptive fields[13]. The ectopic signals in the lesion projection zone may originate from

various sources, including feedback[36–38] and lateral connections[39,40]. Task-specific feedback could elicit more activity in the lesion projections zone in the patient group than in the control group because of the absence of feedforward signals in the patient group[18]. Nevertheless, our results indicate that there is no need to invoke remapping as an explanation of responses in V1 of individuals with macular degeneration.

Third, our study performed for the first time, to the best of our knowledge, a quantitative assessment of the area of cortex driven by intact retina in individuals with retinal disease. The limited size of the patient and control groups coupled with the well-known large variance in visual cortical area across participants[31,41] has prevented such an analysis in previous studies. Our results indicate that the representation of the visual field in V1 in affected individuals can be predicted accurately on the basis of normal retinotopic mapping and that no significant remapping or reorganization was evident. The measures that we derived are sensitive to relatively small changes in cortical maps (<6.5% of V1). This allows us to conclude that there is no remapping of visual cortex over the scale seen in those with congenital central retinal lesions[6]. If neural responses change over time in a very small strip of cortex on the edge of the lesion projection zone, as some have proposed for animal models[7–13], this could escape detection with our analysis. However, we are principally concerned with a large-scale extension of this type of remapping, which we conclude does not exist in humans with central retinal lesions acquired in adulthood.

Consistent with our results, some previous studies on individuals have also found no evidence of remapping of primary visual cortex following retinal damage. A study using cytochrome oxidase to measure activity in an individual with macular degeneration and in macaque models of visual deafferentation found no long-term changes in primary visual cortical organization[42]. Using fMRI and retinotopic mapping methods similar to our own, no activation was found in the lesion projection zone in another individual with macular degeneration[14]. It has been proposed that this negative finding could be a result of the spared foveal vision that this individual exhibited[26]. With this in mind, we only included individuals with central lesions without foveal sparing. A combined fMRI and multiunit neurophysiological study in a carefully controlled animal model (homonymous retinal, but not macular, lesions induced in adult macaques) also showed no long-term changes that would indicate remapping of visual cortex[25]. A recent report of a case series of four individuals with age-related macular degeneration and four with the juvenile form also indicates limited reorganization, but explicit mapping experiments to assess group differences in cortical mapping quantitatively were not undertaken[43]. Having assessed retinotopic maps quantitatively in 16 affected individuals, we are confident that the absence of cortical remapping following retinal lesions in adulthood is a general finding.

The stability of visual organization that we observed may prove to be beneficial. Many of the most promising treatments aimed at restoring vision at the retinal level, such as anti-angiogenic injections, retinal prosthetics and stem-cell therapy, rely on the assumption that cortical circuitry remains largely unchanged. That we can detect no functional abnormality in the visual cortex of affected individuals is reassuring. However, the long-term removal of the principal input to visual cortex can give rise to a reduction in cortical volume[44]. It therefore remains to be seen if neurons in the lesion projection zone can process input normally once it is restored.

METHODS

Methods and any associated references are available in the online version of the paper at http://www.nature.com/natureneuroscience/.

Note: Supplementary information is available on the Nature Neuroscience website.

ACKNOWLEDGMENTS

We would like to thank all of our participants. We thank Edward Silson for constructive discussion of the manuscript. We are also grateful to the Medical Research Council for funding this study (G0401339). K.V.H. and F.W.C. were supported by a grant from Stichting Nederlands Oogheelkundig Onderzoek and by European Union grants #043157 (Syntex) and #043261 (Percept). A.T., G.S.R. and M.D.C. also received financial support from the Department of Health through an award made by the National Institute for Health Research to Moorfields Eye Hospital National Health Service (NHS) Foundation Trust and University College London Institute of Ophthalmology for a Specialist Biomedical Research Centre for Ophthalmology. The views expressed in this publication are those of the authors and not necessarily those of the NHS, the National Institute for Health Research, the Department of Health or the EU commission.

AUTHOR CONTRIBUTIONS

H.A.B. and A.G. acquired and analyzed the neuroimaging data and prepared the manuscript. K.V.H. designed and implemented an analysis to determine the population receptive field characteristics and prepared the manuscript. C.R. acquired neuroimaging data. M.D.C. recruited patients, acquired and analyzed clinical data. A.T. recruited and assessed patients. G.S.R. jointly designed the study, recruited patients and acquired and analyzed clinical data. F.W.C. designed an analysis to determine the population receptive field characteristics and prepared the manuscript. A.B.M. jointly designed the study, acquired and analyzed the neuroimaging data and prepared the manuscript. All authors contributed to drafts of the manuscript.

COMPETING FINANCIAL INTERESTS

The authors declare no competing financial interests.

Published online at http://www.nature.com/natureneuroscience/.
Reprints and permissions information is available online at http://npg.nature.com/reprintsandpermissions/.

1. Wandell, B.A., Dumoulin, S.O. & Brewer, A.A. Visual field maps in human cortex. *Neuron* **56**, 366–383 (2007).
2. Morland, A.B., Baseler, H.A., Hoffmann, M.B., Sharpe, L.T. & Wandell, B.A. Abnormal retinotopic representations in human visual cortex revealed by fMRI. *Acta Psychol. (Amst.)* **107**, 229–247 (2001).
3. Hoffmann, M.B., Tolhurst, D.J., Moore, A.T. & Morland, A.B. Organization of the visual cortex in human albinism. *J. Neurosci.* **23**, 8921–8930 (2003).
4. Muckli, L., Naumer, M.J. & Singer, W. Bilateral visual field maps in a patient with only one hemisphere. *Proc. Natl. Acad. Sci. USA* **106**, 13034–13039 (2009).
5. Levin, N., Dumoulin, S.O., Winawer, J., Dougherty, R.F. & Wandell, B.A. Cortical maps and white matter tracts following long period of visual deprivation and retinal image restoration. *Neuron* **65**, 21–31 (2010).
6. Baseler, H.A. *et al.* Reorganization of human cortical maps caused by inherited photoreceptor abnormalities. *Nat. Neurosci.* **5**, 364–370 (2002).
7. Kaas, J.H. *et al.* Reorganization of retinotopic cortical maps in adult mammals after lesions of the retina. *Science* **248**, 229–231 (1990).
8. Heinen, S.J. & Skavenski, A.A. Recovery of visual responses in foveal V1 neurons following bilateral foveal lesions in adult monkey. *Exp. Brain Res.* **83**, 670–674 (1991).
9. Chino, Y.M., Kaas, J.H., Smith, E.L. III, Langston, A.L. & Cheng, H. Rapid reorganization of cortical maps in adult cats following restricted deafferentation in retina. *Vision Res.* **32**, 789–796 (1992).
10. Gilbert, C.D. & Wiesel, T.N. Receptive field dynamics in adult primary visual cortex. *Nature* **356**, 150–152 (1992).
11. Darian-Smith, C. & Gilbert, C.D. Topographic reorganization in the striate cortex of the adult cat and monkey is cortically mediated. *J. Neurosci.* **15**, 1631–1647 (1995).
12. Kaas, J.H. Sensory loss and cortical reorganization in mature primates. *Prog. Brain Res.* **138**, 167–176 (2002).
13. Giannikopoulos, D.V. & Eysel, U.T. Dynamics and specificity of cortical map reorganization after retinal lesions. *Proc. Natl. Acad. Sci. USA* **103**, 10805–10810 (2006).
14. Sunness, J.S., Liu, T. & Yantis, S. Retinotopic mapping of the visual cortex using functional magnetic resonance imaging in a patient with central scotomas from atrophic macular degeneration. *Ophthalmology* **111**, 1595–1598 (2004).
15. Baker, C.I., Peli, E., Knouf, N. & Kanwisher, N.G. Reorganization of visual processing in macular degeneration. *J. Neurosci.* **25**, 614–618 (2005).
16. Schumacher, E.H. *et al.* Reorganization of visual processing is related to eccentric viewing in patients with macular degeneration. *Restor. Neurol. Neurosci.* **26**, 391–402 (2008).
17. Cowey, A. & Walsh, V. Magnetically induced phosphenes in sighted, blind and blindsighted observers. *Neuroreport* **11**, 3269–3273 (2000).

18. Masuda, Y., Dumoulin, S.O., Nakadomari, S. & Wandell, B.A. V1 projection zone signals in human macular degeneration depend on task, not stimulus. *Cereb. Cortex* **18**, 2483–2493 (2008).
19. Wandell, B.A. & Smirnakis, S.M. Plasticity and stability of visual field maps in adult primary visual cortex. *Nat. Rev. Neurosci.* **10**, 873–884 (2009).
20. Masuda, Y. *et al.* Task-dependent V1 responses in human retinitis pigmentosa. *Invest. Ophthalmol. Vis. Sci.* **51**, 5356–5364 (2010).
21. DeYoe, E.A. *et al.* Mapping striate and extrastriate visual areas in human cerebral cortex. *Proc. Natl. Acad. Sci. USA* **93**, 2382–2386 (1996).
22. Engel, S.A., Glover, G.H. & Wandell, B.A. Retinotopic organization in human visual cortex and the spatial precision of functional MRI. *Cereb. Cortex* **7**, 181–192 (1997).
23. Engel, S.A. *et al.* fMri of human visual cortex. *Nature* **369**, 525 (1994).
24. Sereno, M.I. *et al.* Borders of multiple visual areas in humans revealed by functional magnetic resonance imaging. *Science* **268**, 889–893 (1995).
25. Smirnakis, S.M. *et al.* Lack of long-term cortical reorganization after macaque retinal lesions. *Nature* **435**, 300–307 (2005).
26. Baker, C.I., Dilks, D.D., Peli, E. & Kanwisher, N. Reorganization of visual processing in macular degeneration: replication and clues about the role of foveal loss. *Vision Res.* **48**, 1910–1919 (2008).
27. Crossland, M.D., Morland, A.B., Feely, M.P., von dem Hagen, E. & Rubin, G.S. The effect of age and fixation instability on retinotopic mapping of primary visual cortex. *Invest. Ophthalmol. Vis. Sci.* **49**, 3734–3739 (2008).
28. Parrish, T.B., Gitelman, D.R., LaBar, K.S. & Mesulam, M.M. Impact of signal-to-noise on functional MRI. *Magn. Reson. Med.* **44**, 925–932 (2000).
29. Cavanaugh, J.R., Bair, W. & Movshon, J.A. Nature and interaction of signals from the receptive field center and surround in macaque V1 neurons. *J. Neurophysiol.* **88**, 2530–2546 (2002).
30. Dumoulin, S.O. & Wandell, B.A. Population receptive field estimates in human visual cortex. *Neuroimage* **39**, 647–660 (2008).
31. Andrews, T.J., Halpern, S.D. & Purves, D. Correlated size variations in human visual cortex, lateral geniculate nucleus, and optic tract. *J. Neurosci.* **17**, 2859–2868 (1997).
32. Hubel, D.H. & Wiesel, T.N. The period of susceptibility to the physiological effects of unilateral eye closure in kittens. *J. Physiol. (Lond.)* **206**, 419–436 (1970).
33. Hubel, D.H., Wiesel, T.N. & LeVay, S. Plasticity of ocular dominance columns in monkey striate cortex. *Phil. Trans. R. Soc. Lond. B* **278**, 377–409 (1977).
34. Le Vay, S., Wiesel, T.N. & Hubel, D.H. The development of ocular dominance columns in normal and visually deprived monkeys. *J. Comp. Neurol.* **191**, 1–51 (1980).
35. Horton, J.C. & Hocking, D.R. Timing of the critical period for plasticity of ocular dominance columns in macaque striate cortex. *J. Neurosci.* **17**, 3684–3709 (1997).
36. Williams, M.A. *et al.* Feedback of visual object information to foveal retinotopic cortex. *Nat. Neurosci.* **11**, 1439–1445 (2008).
37. Angelucci, A. & Bullier, J. Reaching beyond the classical receptive field of V1 neurons: horizontal or feedback axons? *J. Physiol. (Paris)* **97**, 141–154 (2003).
38. Angelucci, A. & Sainsbury, K. Contribution of feedforward thalamic afferents and corticogeniculate feedback to the spatial summation area of macaque V1 and LGN. *J. Comp. Neurol.* **498**, 330–351 (2006).
39. Lund, J.S. Anatomical organization of macaque monkey striate visual cortex. *Annu. Rev. Neurosci.* **11**, 253–288 (1988).
40. Gilbert, C.D. & Wiesel, T.N. Morphology and intracortical projections of functionally characterised neurones in the cat visual cortex. *Nature* **280**, 120–125 (1979).
41. Dougherty, R.F. *et al.* Visual field representations and locations of visual areas V1/2/3 in human visual cortex. *J. Vis.* **3**, 586–598 (2003).
42. Horton, J.C. & Hocking, D.R. Monocular core zones and binocular border strips in primate striate cortex revealed by the contrasting effects of enucleation, eyelid suture, and retinal laser lesions on cytochrome oxidase activity. *J. Neurosci.* **18**, 5433–5455 (1998).
43. Liu, T. *et al.* Incomplete cortical reorganization in macular degeneration. *Invest. Ophthalmol. Vis. Sci.* **51**, 6826–6834 (2010).
44. Boucard, C.C. *et al.* Changes in cortical grey matter density associated with long-standing retinal visual field defects. *Brain* **132**, 1898–1906 (2009).

ONLINE METHODS

Participants. Eight individuals with stabilized AMD (ages 70–90) and a further eight with the JMD (Stargardt's Disease) (ages 19–49) were recruited at the Moorfields Eye Hospital, London. All of the participants had established bilateral lesions for at least 1 year, with a central scotoma of less than 10-deg radius spanning the fovea and a stable preferred retinal locus. Visual field sensitivity and fixation ability for all participants were evaluated directly on the retina using an MP1 microperimeter (NIDEK). Location of the foveal center, preferred retinal locus coordinates and fixation stability (bivariate contour ellipse area of fixation measurements) were determined using methods outlined in Timberlake *et al.* (2005). The mean diameter of the absolute retinal lesion was also computed from the microperimetry maps.

Five age-matched participants (ages 61–77) were recruited as controls for the AMD group and seven age-matched participants (ages 18–37) as controls for the JMD group. A further 12 control participants (ages 18–41) were recruited for a follow up experiment simulating retinal lesions. All control participants had normal or corrected-to-normal vision. Experimental protocols were approved by the London Multicenter Research Ethics Committee, Royal Holloway University of London Ethics Committee and the York Neuroimaging Center Science and Ethics Committee.

Scanning. fMRI and structural MRI data were acquired using 8-channel, phase-array head coils on either a Siemens Trio 3 Tesla at the Combined Universities Brain Imaging Center (Royal Holloway University of London), or on a GE 3-Tesla Signa HD Excite scanner at the York Neuroimaging Center (University of York).

For structural data, multi-average, whole-head T1-weighted anatomical volumes were acquired for each participant (1.0–1.13 mm^3 isotropic). Sequences used were 3D-MDEFT on the Siemens Trio or 3D-FSPGR on the GE Signa; imaging parameters in both sequences provide good gray-white contrast allowing the segmentation of anatomical data into gray and white matter, and subsequent visualization in volume and inflated cortical views. For functional data, gradient recalled echo pulse sequences were used to measure T2* BOLD data (repetition time = 3,000 ms, echo time = 30 ms, field of view = 28.8 cm, 128 × 128 matrix, 25 contiguous slices with 3-mm slice thickness). Images were read out using an EPI sequence. Magnetization was allowed to reach a steady state by discarding the first five volumes, an automated feature on both the scanners used.

Stimuli. Computer-generated visual stimuli were presented using a LCD projector (Sanyo PLC-XP40L at Royal Holloway University of London, Dukane ImagePro 8942 at the University of York); stimuli were rear projected onto an acrylic screen situated in the bore of the MRI scanner, behind the participant's head. Participants viewed the stimuli via a mirror mounted on the head coil. Standard retinotopic mapping stimuli were used: a rotating wedge to map polar angle and an expanding annulus to map eccentricity[21–24]. Stimuli were generated with MATLAB (Mathworks) and controlled by MatVis (Neurometrics Institute). All stimuli were unmasked portions of a 100% contrast radial checkerboard with 8 rings and 24 radial segments on a mean gray background. Contrast reversal rate was 6 Hz. Each scan contained either the expanding annulus or rotating wedge. Projector throw was adjusted to stimulate the central 30 × 30 deg of visual angle (15-deg radius). The wedge stimulus was a 90-deg wedge of the flickering checkerboard, rotating about the center of the screen. The ring stimulus comprised three rings of the checkerboard that increased in angular extent (to a maximum of 15 deg). As it moved out from the center of the visual field; each ring was replaced by a new ring at the center as the existing ring approached the edge of the visual field. Both the wedge and ring stimuli had a period of 36 s and were repeated for seven full cycles.

Experiment 1. The standard expanding ring and rotating wedge stimuli described above were used. In addition, the position of a red fixation cross was manipulated to ensure that stimuli were centered on each individual participant's retina. For control participants, a red fixation cross was placed at the center of the stimulus. For the patient group, the cross was placed at each individual's stable preferred retinal locus, as measured by microperimetry. Four ring and four wedge datasets were typically collected for each participant during a single visit, except where participant discomfort or excessive movement required fewer scans. Only three scans were collected during the first session in two individuals with AMD and two individuals with JMD and only two scans were performed on one of the elderly controls. Scans were repeated in a second visit in most participants (20 out of 28). Four scans were again performed during the second session, except in two individuals with AMD (three scans) and four individuals with JMD (three had three scans, one had two scans).

Experiment 2. As in Experiment 1, standard retinotopic mapping stimuli were used. A red fixation cross was placed in the center of the stimulus. In separate scans, the 12 control participants were either shown the full stimulus (ring and wedge) or a masked version (of the rings) to simulate a central lesion. The mask consisted of a centrally placed static disk (7.5-deg radius) at mean luminance gray such that the central portion of the visual field was constant throughout the scan (**Fig. 3**). At least two scans were acquired for each condition. 10 of the 12 participants returned for a second scanning session on a separate date.

Data analysis. Data were analyzed using publicly available tools (http://white.stanford.edu/software/). Most data analysis was performed in Matlab using the mrVISTA toolbox. For anatomical data, the occipital cortices of acquired anatomical volumes were manually segmented into white and gray volumes (mrGray)[45]. The cortical surface (gray matter) of each subject was constructed and rendered in three dimensions from this segmentation using mrMesh/mrVista[46].

For function data, functional images were corrected for spatial inhomogeneity (mrInitRet). Motion correction was achieved using FSL's MCFLIRT[47]. Functional time series were high-pass filtered to remove baseline drifts. Percent signal change was computed for each voxel by dividing by and subtracting its mean amplitude value over time. The strength of stimulus-synchronized activity at each voxel was assessed using coherence. Coherence (C) is defined as the Fourier amplitude of the BOLD signal at the stimulus fundamental frequency ($f_0 = 7$) divided by the sum of amplitudes of frequency bins around the fundamental ($C = A(f_0) / \sum \sqrt{A(f)^2}$) (refs. 18–25). The visual field representation of each voxel in cortex was derived by using the Fourier phase at the stimulus frequency, corresponding to the relative delay of the cyclical response[22,48]. Functional data were averaged across scans for repeated scans (usually four) within a session for each individual. Functional data were manually aligned to the high-resolution anatomical volume and visualized in three dimensions.

ROIs were defined by an algorithm that gathered all contiguous gray matter in a circular patch 8 mm in diameter centered on a selected point in the high-resolution structural data. Three ROIs were chosen in each hemisphere of each participant based strictly on anatomical criteria: one at the occipital pole to represent activity from the fovea (the lesion projection zone in patients), one more anterior in the calcarine sulcus to represent activity from more peripheral retina (which is intact in patients) and one further anterior in the brain on the lateral aspect of the frontal lobes, serving as a control region in the first experiment. The mean coherence was calculated across voxels in an ROI for each individual and averaged across scans in each session. The fMRI noise distribution is not normal and may differ from one individual to the next or from one day to the next. To normalize the responses, the logarithm of the resulting coherence data was taken before averaging data across scanning sessions and across participants[49].

We assessed the degree to which the time series of any voxel in predefined regions of interest in the gray matter fitted a series of receptive field models as described previously[30]. Best fitting models were retained if they accounted for more than 15% of the variance of the time series of each voxel as in previous research[50]. The retained models were then averaged across voxels to give an overall measure of the population receptive field properties for each ROI. The data used for modeling were for the expanding ring stimuli only because it was for this presentation that we had a comparable number of runs across the participant groups, and it was the only stimulus that was masked to simulate retinal lesions. It is important to note that the candidate models were identical for all stimulus conditions and we did not restrict the receptive field models to any locations or sizes. The ROIs considered were calcarine sulcus, as specified above, and occipital pole, but in this case the diameter of occipital pole was 20 mm to gain increased sensitivity. Although the 20-mm diameter ROI might capture some signals from tissue receiving input from intact retina in patients with small retinal lesions, we ensured that for the control participants receiving full-field and simulated lesion stimulation, the occipital pole ROI only included voxels responding to eccentricities less than 7.5 deg when the full stimulus was presented.

We computed the area of primary visual cortex, A_M, that exhibited activity above a coherence threshold of 0.30 for all participants in the patient and control groups in whom we simulated retinal lesions. Using responses to rotating wedge stimuli, we first identified the cortical representations of the upper and lower vertical meridians marking the boundaries of V1 in each participant (see **Fig. 7**). We then defined a V1 ROI that was bounded by the extrapolation of the vertical meridians to the occipital pole and an anterior boundary that was just beyond the limit of activity in response to rotating wedges. This region was not restricted to those voxels that exceeded a specific threshold, but rather was a generously defined estimate of the extent of V1. Voxels in this V1 region that responded to rings at a coherence of greater than 0.30 were retained for the calculation of the area of significant activity in V1. The cortical area of activity was calculated using methods described previously[41]. We then computed a series of estimates of the predicted area of activation, A_P, based on the intact regions of visual field in patients (see **Fig. 7** for a schematic of the method). For each patient, we computed estimates from the corresponding group of age-matched controls (for example, for each individual with JMD we obtained seven estimates, one from each of the young control subjects). The mean predicted area, $\bar{A}_P$, was then computed. We repeated these computations to obtain $\bar{A}_P$ for controls with simulated central visual loss. Note that these computations were also based on the original data from the young control subjects. If remapping were to occur, A_M will exceed $\bar{A}_P$ and thus a ratio of the A_M to $\bar{A}_P$ will exceed unity. Using the ratio as our outcome measure is essential because it accounts for individual differences in retinal lesion size.

Statistical analyses. Statistics were calculated using functions in the MATLAB Statistical Toolbox. A two-way analysis of variance was performed on the averaged expanding ring data (for each session) for the elderly group and for the young group. Visual status (patient versus control) and ROI (occipital pole versus calcarine sulcus versus control region) were the independent variables and log coherence (fMRI response magnitude) was the dependent variable. A repeated-measures ANOVA was performed on the data to test for significant differences within subjects across two sessions. To test for age effects, a three-way analysis of variance was performed on the combined data, with age, visual status and ROI as factors. All ANOVAs employed a Type III sum of squares calculation, and all subsequent multiple comparisons were corrected using the Tukey-Kramer criterion, as appropriate for an unbalanced design with unequal number of subjects across groups. A multiple regression analysis was performed on the patient data to determine the effects of lesion size and age on log coherence responses for each ROI. For the receptive field analysis, we used Student *t* tests to evaluate group differences in eccentricity and size of the receptive fields and sampling probability at each cortical location. Linear regression was used to assess the relationship between eccentricity and size of population receptive fields in the occipital pole ROI; 95% confidence intervals in the linear correlation parameters was estimated using jackknife resampling, taking into consideration the unequal number of points contributed by each participant. For the cortical area measures in **Figure 7**, group effects and deviations of the area ratio from unity were evaluated using *t* tests and ANOVAs, respectively.

45. Teo, P.C., Sapiro, G. & Wandell, B.A. Creating connected representations of cortical gray matter for functional MRI visualization. *IEEE Trans. Med. Imaging* **16**, 852–863 (1997).
46. Wandell, B.A., Chial, S. & Backus, B.T. Visualization and measurement of the cortical surface. *J. Cogn. Neurosci.* **12**, 739–752 (2000).
47. Jenkinson, M., Bannister, P., Brady, M. & Smith, S. Improved optimization for the robust and accurate linear registration and motion correction of brain images. *Neuroimage* **17**, 825–841 (2002).
48. Wandell, B.A., Brewer, A.A. & Dougherty, R.F. Visual field map clusters in human cortex. *Phil. Trans. R. Soc. Lond. B* **360**, 693–707 (2005).
49. Lewis, S.M. *et al.* Logarithmic transformation for high-field BOLD fMRI data. *Exp. Brain Res.* **165**, 447–453 (2005).
50. Winawer, J., Horiguchi, H., Sayres, R.A., Amano, K. & Wandell, B.A. Mapping hV4 and ventral occipital cortex: the venous eclipse. *J. Vis.* **10**, 1–22 (2010).

1040-5488/11/8810-1255/0 VOL. 88, NO. 10, PP. 1255–1261
OPTOMETRY AND VISION SCIENCE

CASE REPORT

Objective Visual Assessment of Antiangiogenic Treatment for Wet Age-Related Macular Degeneration

Heidi A. Baseler*, André Gouws†, Michael D. Crossland‡, Carmen Leung, Adnan Tufail§, Gary S. Rubin*, and Antony B. Morland*

Purpose. To assess cortical responses in patients undergoing antiangiogenic treatment for wet age-related macular degeneration (AMD) using functional magnetic resonance imaging (fMRI) as an objective, fixation-independent measure of topographic visual function.
Methods. A patient with bilateral neovascular AMD was scanned using fMRI before and at regular intervals while undergoing treatment with intravitreal antiangiogenic injections (ranibizumab). Blood oxygenation level-dependent signals were measured in the brain while the patient viewed a stimulus consisting of a full-field flickering (6 Hz) white light alternating with a uniform gray background (18 s on and 18 s off). Topographic distribution and magnitude of activation in visual cortex were compared longitudinally throughout the treatment period (<1 year) and with control patients not currently undergoing treatment. Clinical behavioral tests were also administered, including visual acuity, microperimetry, and reading skills.
Results. The area of visual cortex activated increased significantly after the first treatment to include more posterior cortex that normally receives inputs from lesioned parts of the retina. Subsequent treatments yielded no significant further increase in activation area. Behavioral measures all generally showed an improvement with treatment but did not always parallel one another. The untreated control patient showed a consistent lack of significant response in the cortex representing retinal lesions.
Conclusions. Retinal treatments may not only improve vision but also result in a concomitant improvement in fixation stability. Current clinical behavioral measures (e.g., acuity and perimetry) are largely dependent on fixation stability and therefore cannot separate improvements of visual function from fixation improvements. fMRI, which provides an objective and sensitive measure of visual function independent of fixation, reveals a significant increase in visual cortical responses in patients with wet AMD after treatment with antiangiogenic injections. Despite recent evidence that visual cortex degenerates subsequent to retinal lesions, our results indicate that it can remain responsive as its inputs are restored.
(Optom Vis Sci 2011;88:1255–1261)

Key Words: wet age-related macular degeneration (AMD), ranibizumab, functional MRI (fMRI), microperimetry

In recent years, new treatments have been advanced to treat age-related macular degeneration (AMD), such as antiangiogenic ocular injections, and a number of novel approaches to restore vision are under development, including retinal prosthetics and stem cell therapy.[1] Each of these treatments is aimed at restoring retinal function and relies on the assumption that the visual cortex remains both responsive and topographically configured to process reestablished inputs. Nevertheless, recent studies have questioned this assumption. Some studies indicate that cortex receiving inputs from a lesioned part of retina can degenerate and lose function.[2] Still other studies suggest that visual cortex can undergo plastic changes when its inputs are removed by retinal lesions, reallocating cortical resources once used for processing central vision to processing peripheral vision.[3–6] As visual information is processed retinotopically within visual cortex, any plastic changes that result in a remapping of inputs could cause a disrup-

*PhD
†BSc
‡PhD, MCOptom, FAAO
§MD, FRCOphth
York Neuroimaging Centre, Department of Psychology, University of York, York, United Kingdom (HAB, AG, ABM), Institute of Ophthalmology, University College London, London, United Kingdom (MDC, AT, GSR), Moorfields Eye Hospital NHS Foundation Trust, London, United Kingdom (MDC, AT, GSR), and Hull-York Medical School, York, United Kingdom (CL, ABM)

tion or distortion of visual processing if retinal function is later restored. Certain studies, however, provide evidence against visual cortical remapping in adults with retinal lesions.[7–10] The disagreement among studies may be attributable to different interpretations of signals found in cortex deprived of retinal input and individual differences, particularly because most research has been done on a few select case studies. On the basis of our more recent work on a relatively large number of patients, however, we feel that we have resolved the debate by finding an absence of remapping in adults with established bilateral macular degeneration.[11] It is important, therefore, to determine whether visual cortex that has been deprived of input in adulthood can generally recover function after treatment sufficiently to support vision across the visual field.

Not all patients who have a good retinal anatomical response to treatment for macular degeneration have improved visual function. Therefore, while undergoing treatment for diseases such as macular degeneration, a reliable and accurate method for assessing visual progress is essential. Many clinical behavioral measures of visual function are indirect and rely on patient self-reporting, depend on fixation ability, and may test the visual field only partially or sparsely. Functional magnetic resonance imaging (fMRI) is an imaging technique that has been developed over the past 20 years, gaining popularity within the neuroscience community as a tool to explore cortical function non-invasively in human participants (see ref. 12 for a review). As a result, fMRI has become widely available and can be adapted to run on most clinical MRI scanners. fMRI can provide a sensitive and objective measure of visual function throughout the entire visual field, independent of fixation or cognitive status, while putting very little demand on the patient.

The goals of the current study were (1) to determine whether visual cortex can resume normal function when its damaged retinal inputs are restored and (2) to assess the suitability of fMRI as an objective measure of visual function to complement standard clinical behavioral tests. We evaluated visual cortical responses in a patient during the course of antiangiogenic treatment for wet age-related MD. The patient's cortical responses were also compared with results of standard clinical behavioral tests (visual acuity, microperimetry, reading ability, and fixation stability), performed on the same day.

CASE REPORT

Participants

Participants were recruited from Moorfields Eye Hospital, London. Informed consent was obtained from all participants after explanation of the nature and possible consequences of the study, as specified by the Declaration of Helsinki. Experimental protocols were approved by the London Multicenter Research Ethics Committee and the Royal Holloway University of London Ethics Committee.

The patient undergoing treatment was an 80-year-old woman with bilateral AMD. Her right eye had exudative AMD with a visual acuity of 0.38 logMAR (20/50) and was being treated with regular injections of ranibizumab (Lucentis). Injections were administered at day 0, day 33, day 68, and day 165. Her left eye had longstanding macular scarring with no recent progression and visual acuity of 1.10 logMAR (20/250). The patient was phakic but had no visually significant cataract. She did not read for pleasure, and she rated her general health as "moderately good."

The control participant (i.e., not currently undergoing treatment) was an 80-year-old man with established AMD. He had bilateral disciform scarring from AMD. Corrected visual acuity was 0.76 logMAR (~20/125) in the right eye and 1.08 logMAR (20/250) in the left eye. He had mild nuclear sclerosis in both eyes, did not read for pleasure, and rated his general health as "good."

Clinical Measures

Visual field sensitivity and fixation ability were evaluated directly on the retina of both the treated and untreated fellow eye using an MP1 microperimeter (NIDEK Co. Ltd., Italy). Participants were instructed to fixate on a red cross, 2° in diameter. Location of the foveal center, preferred retinal locus coordinates, and fixation stability (bivariate contour ellipse area of fixation measurements) were determined using methods outlined in Crossland et al.[13] Visual field sensitivity was evaluated across a 40° diameter circular region centered approximately on the fovea. Stimuli consisted of single points of light (78 to 134) presented randomly across a circular grid at 100% (0 dB attenuation, maximum luminance reported as 127 cd/m^2) for 200 ms (Goldmann III). Participants were instructed to respond with a button press when a stimulus was detected. Results were reported as the percentage of lights detected within the central 10° macular region, where damage is likely to be greatest. This was defined as a circular region of $\pm$5° around the foveal center estimated using criteria outlined in Timberlake et al.[14] Visual acuity was assessed at each clinical visit using a standard Early Treatment Diabetic Retinopathy Study (ETDRS) logMAR chart (Precision Vision, La Salle, IL). Contrast sensitivity was measured monocularly in the better eye using a Pelli-Robson chart (Clement Clarke International, Essex, UK) at 1 m with appropriate refractive correction and was scored in the manner recommended by Elliott et al.[15] Reading performance was assessed binocularly using the MNRead test.[16]

MRI Scanning

Structural and functional MRI data were acquired using eight-channel, phase-array head coils on a Siemens Trio 3 Tesla at the Combined Universities Brain Imaging Centre (CUBIC) at Royal Holloway, University of London.

Structural Data

Multiaverage, whole-head T1-weighted anatomical volumes were acquired for each participant (1.0 mm^3 isotropic). Imaging sequences were 3D-MDEFT, using parameters that provided good contrast allowing the segmentation of anatomical data into gray and white matter. Segmented gray matter was then rendered for visualization in volume and inflated cortical views.

Functional Data

Gradient recalled echo pulse sequences were used to measure T2*-weighted blood oxygenation level-dependent (BOLD) data. Images were read out using an echo-planar imaging sequence (rep-

etition time = 3000 ms, echo time = 30 ms, field of view = 28.8 cm, 128 × 128 matrix, and 25 contiguous slices with 3 mm slice thickness).

Visual Stimuli for fMRI

The visual stimulus consisted of full-field luminance modulation at 6 Hz, maximum contrast. An LCD projector (SanyoPLC-XP40Ls) presented stimuli from behind the participant's head through the bore of the MRI scanner onto a mirror mounted on the head coil. Luminance was first reduced by mounting crossed (45°) polarizing filters directly in front of the projector lens. Participants wore MRI-compatible goggles fitted with three layers of a translucent white film to produce uniform full-field illumination, resulting in a final minimum luminance of 1 cd/m^2, a maximum luminance of 43 cd/m^2, and a contrast of 95%. Participants were instructed simply to keep both eyes open and reasonably still during the scan; no fixation was required. Stimuli were controlled by MatVis (Neurometrics Institute, Oakland, CA, http://neurometrics.com) and were presented for 18 s, followed by 18 s of a static, mean luminance field, repeated for seven cycles in each scan.

fMRI Data Analysis

Data analysis was performed primarily in MATLAB (The Mathworks, Natick, MA) using the publicly available mrVista toolbox (http://white.stanford.edu/software/).

Structural Data

The occipital cortices of acquired anatomical volumes were manually segmented into white and gray volumes (mrGray).[17] The cortical surface (gray matter) of each subject was constructed and rendered in 3D from this segmentation using mrMesh/mrVista.

Functional Data

Functional images were corrected for spatial inhomogeneity. Motion correction was achieved using FSL's MCFLIRT.[18] Functional time series were high-pass filtered to remove baseline drifts. The percent signal change was computed for each voxel by subtracting mean of the signal from the time series and then dividing by the mean of the signal. The strength of stimulus-synchronized activity at each voxel was assessed using coherence. Coherence (C) is defined as the Fourier amplitude of the BOLD signal at the stimulus fundamental frequency ($f_0 = 7$) divided by the sum of amplitudes of frequency bins around the fundamental ($C = A(f_0)/\Sigma\ (A(f)^2)^{1/2}$).[8,9] Functional data were averaged across scans for repeated scans (usually four) within a session for each subject. Functional data were manually aligned to the high-resolution anatomical volume and visualized in 3D.

Region of Interest Selection

Regions of interest (ROIs) were defined anatomically by an algorithm that gathered all contiguous gray matter within a circular patch of a specified diameter centered on a selected point within the high-resolution structural data. This allowed ROIs of equal cortical area to be compared across hemispheres and participants.

fMRI Response Area

Responses were first assessed within a relatively large region (80 mm in diameter) that extended from the occipital pole (OP) anterior, centered in the calcarine sulcus (CS). Based on our experience, this region typically includes V1 (primary visual cortex) and part of V2.[12,19] fMRI response area was defined as the percentage of significantly active voxels within this region, calculated by dividing the number of voxels exceeding a coherence of 0.23 by the total number of voxels in the ROI, multiplied by 100. Voxels above this threshold were deemed significant, because for the number of time samples acquired in each scan (84), the estimated probability that a voxel will exhibit a coherence >0.23 is 0.035 ($p < 0.05$, uncorrected).[20] Next, we tested for significant differences in fMRI response across scanning sessions. Because of our small sample size (four repeat scans per session), it was not possible to test that the assumptions required for applying an analysis of variance are met. Therefore, a resampling technique was used to assess the statistical significance of variability between sessions relative to variability across runs within sessions. First, the 16 scans (four scans in each of four sessions) were shuffled, and two groups of four different scans were selected from the 16 scans. Next, the mean proportion of active voxels was determined for each group of four shuffled scans, and the difference was taken between the mean of each group. This shuffling, mean and difference procedure was repeated 10,000 times. The probability that two fMRI sessions activated the same number of voxels was calculated by adding up the proportion of voxel differences in the shuffled data that exceeded the difference between the means of two actual sessions. fMRI response area was compared over the course of four sessions for the treated patient with two separate sessions acquired in the untreated age-matched control with established AMD.

fMRI Response Magnitude

To compare responses in cortical regions representing lesioned and intact retina, two smaller ROIs, 10 mm in diameter, were also chosen in each hemisphere of each participant based strictly on anatomical criteria. One was centered at the OP to represent activity from the fovea (the "lesion projection zone" in patients), and the other was centered further anterior within the CS to represent activity from more peripheral retina (which has remained intact in patients with MD). The mean coherence was calculated across voxels within each ROI and averaged across hemispheres and scans within each session. The resampling procedure outlined above was then applied to each of the smaller ROIs to test for statistical differences in fMRI response magnitude across sessions.

RESULTS

Clinical Measures

Table 1 summarizes results of clinical measures evaluated during each of four visits by the patient undergoing treatment. fMRI scans were performed on the same day, after clinical evaluation.

Microperimetry

Fig. 1a to d shows the visual field sensitivity measurements acquired using microperimetry from each visit. The size of the

TABLE 1.
Clinical evaluation of treated patient

Visit[a]	VA treated eye (logMAR)	VA untreated eye (logMAR)	Contrast sensitivity (log units)	Reading acuity (logMAR)	Critical print size (logMAR)	Peak reading speed (wpm)	Bivariate contour ellipse area (arcmin^2)
1	0.38	1.10	1.1	0.61	1	161	1848
2	0.2	1.18	—	0.56	0.9	182	1253
3	0.28	1.22	—	0.50	0.7	123	1301
4	0.22	0.84	1.3	0.42	0.7	140	1895

[a] Visits: 1, 16 d before first treatment; 2, 20 d after first treatment; 3, 35 d after second treatment; 4, 8 d after final treatment.

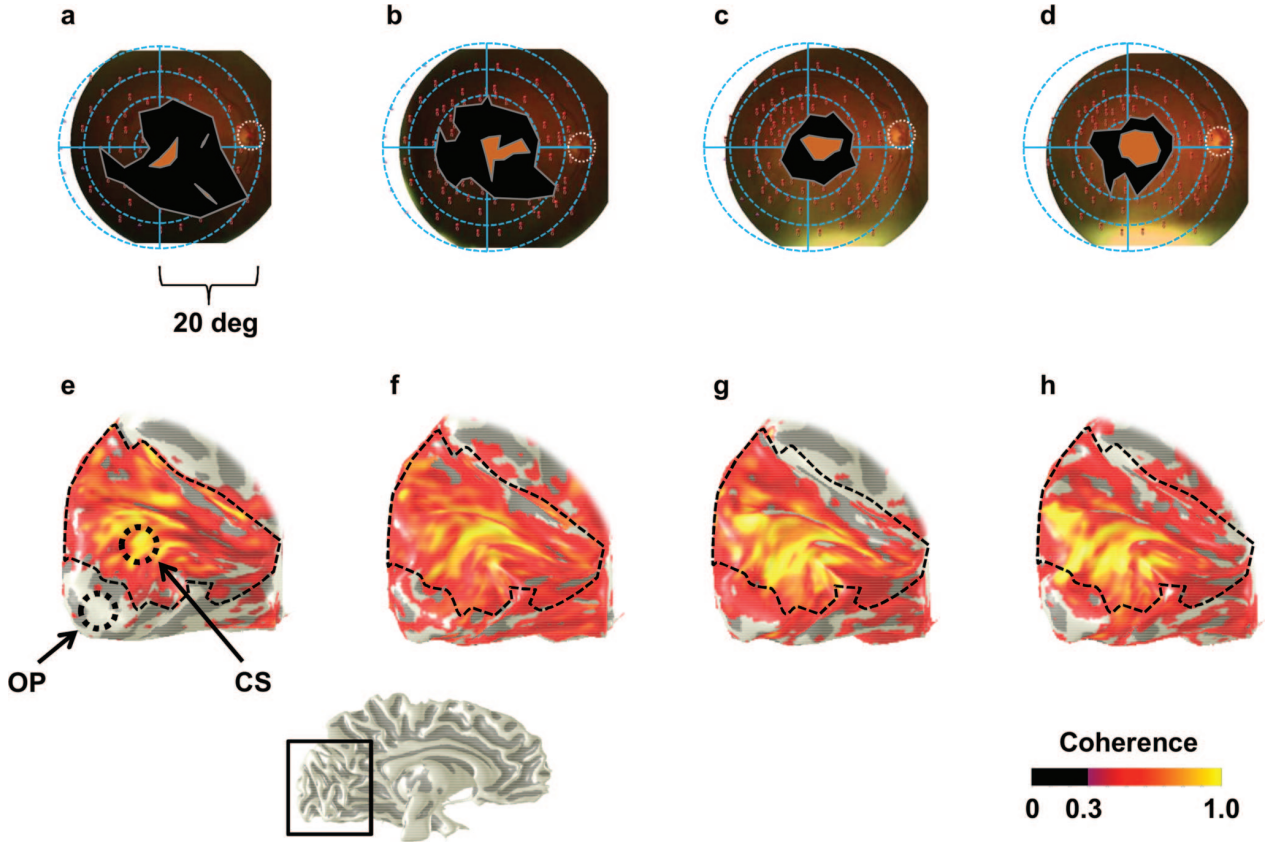

FIGURE 1.
Microperimetry data (a-d) and fMRI data (e-h) from each of four visits during patient treatment with ranibizumab. (a, e) 16 d before first treatment; (b, f) 20 d after first treatment; (c, g) 35 d after second treatment, 1 d after third treatment; (d, h) 8 d after fourth treatment. (a-d) Microperimetry: The scotoma (where no lights were detected) is indicated by the black filled region. The brown central region indicates a central area where lights were detected. The optic nerve head is indicated by the white dotted ellipse. The circular grid indicates the 40° diameter area tested by microperimetry; each gradation represents 5° visual angle. (e-h) fMRI: Each panel shows the medial surface of the left occipital lobe, rendered in 3D from structural MRI of whole brain (inset shows enlarged area represented in black rectangle). Coherence values, representing the strength of the BOLD response to visual stimulation, are superimposed in color, where a coherence of 1.0 represents the maximum possible response; coherence threshold was set to 0.30. OP: occipital pole region of interest, which receives inputs from the central retina, lesion site in this patient. CS: calcarine sulcus region of interest, which receives inputs from more peripheral retina, intact in this patient.

absolute scotoma (black region) decreased over time in conjunction with ranibizumab treatments. In addition, a central area where lights were detected (brown region) appeared to increase in size, indicating that some light sensitivity was regained centrally.

fMRI: Whole Brain Analysis

Fig. 1e to h shows the results from four separate fMRI scanning sessions done in conjunction with each clinical visit. Each panel contains an image of the medial surface of the left occipital lobe rendered in 3D. The superimposed color represents coherence, a measure of the magnitude of the BOLD signal in response to the visual stimulus. Before treatment (Fig. 2e), responses are restricted to anterior/superior portions of the occipital lobe (CS); the posterior portion, which normally responds to stimulation in the central visual field (OP), remains largely unresponsive. Sixteen days after the first treatment, however, signals have begun to fill in the posterior OP region (Fig. 2f). Signals continue to strengthen over time,

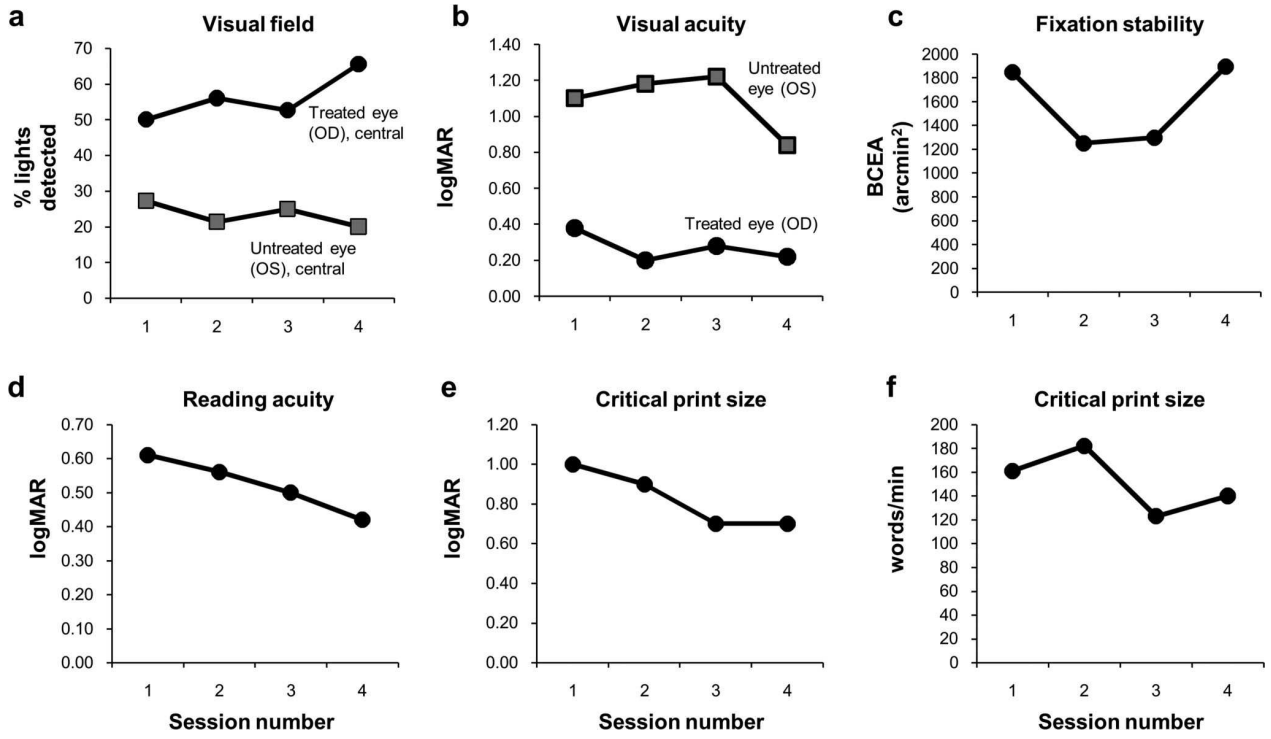

FIGURE 2.

Clinical measures of vision in patient before and during ongoing treatment with ranibizumab. Session 1: 16 d before first treatment; 2: 20 d after first treatment; 3: 35 d after second treatment and 1 d after third treatment; 4: 8 d after fourth treatment. (a) Visual field results in the treated eye (OD) and untreated eye (OS) with microperimetry, measured over a 10° circular field centered on the macula; (b) Visual acuity (logMAR) of the treated eye (OD) and untreated eye (OS); (c) Fixation stability measured using microperimetry. BCEA: bivariate contour ellipse area, defined as the best fitting ellipse containing 68% of individual fixations, in arcmin^2; (d-f) Three different measures of reading ability, assessed with MNREAD.

extending toward the OP, but fail to fill in completely. Subjects with normal vision show a more uniform spread of responses throughout the occipital cortex to full-field stimulation (not shown).

Clinical Behavioral Measures

Fig. 2 shows the results from several clinical measures of visual function made during each session. Microperimetry revealed an increase in the proportion of lights detected in the central visual field of the treated eye, from 50% before treatment to 65% after the fourth treatment, with the largest improvement observed between the third and fourth visits (Fig. 2a). The untreated eye, however, showed little change in sensitivity across the four visits. Visual acuity showed the greatest improvement in the treated eye after the first treatment, from 0.38 to 0.20 logMAR (Fig. 2b). Subsequent visits revealed no further improvement, with acuity remaining stable at around 0.2 logMAR after the final treatment. Acuity in the untreated eye, however, remained poor at <1.0 logMAR, improving slightly to 0.84 logMAR at the final visit. Fixation stability improved dramatically after the first treatment, remaining stable at the third visit, but then was worse at the fourth visit (Fig. 2c). Reading measures using MNREAD showed a general improvement over the course of treatment (Fig. 2d to f). Reading acuity improved continuously over the course of the four measurement sessions from 0.61 to 0.42 logMAR, and critical print size improved from 1.0 to 0.7 logMAR. Reading speed was more variable; although there was some improvement after the first treatment (from 161 to 182 words/min), reading was slower during subsequent visits (123 to 140 words/min).

fMRI: ROI Analysis

Fig. 3 shows the results from quantitative analyses performed on regions of interest in the occipital lobes. fMRI response area was assessed as the percentage of significantly active voxels within a large region of interest (80 mm diameter) including posterior and medial parts of the occipital lobe. In the treated patient, the area activated by the visual stimulus increased significantly, nearly doubling after the first treatment ($p_{12} < 0.0001$). There was no significant difference in response area between subsequent sessions ($p_{23} = 0.983$; $p_{34} = 0.373$; and $p_{24} = 0.957$), and the fourth session remained higher than the pretreatment level ($p_{14} = 0.045$). In contrast, the untreated patient's response area showed no significant difference between sessions ($p_{12} = 0.741$; Fig. 3a).

fMRI response magnitude was then assessed in the treated patient within two smaller regions of interest (10 mm diameter): one at the OP reflecting processing of inputs from central retina, and another more anterior within the CS reflecting processing from more peripheral retina (Fig. 3b). Response magnitude at OP increased significantly after the first treatment ($p_{12} = 0.022$) and did not change significantly in subsequent treatments ($p_{23} = 0.223$; $p_{34} = 0.884$; and $p_{24} = 0.664$), although the overall change between the pretreatment and final session was not quite significant ($p_{14} = 0.064$). In contrast,

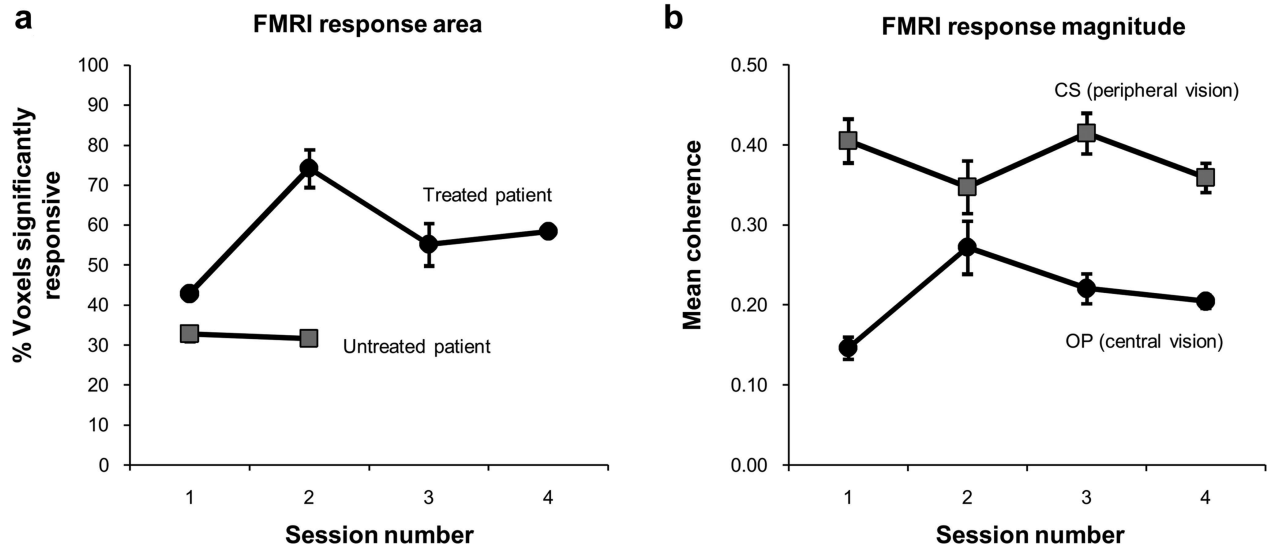

FIGURE 3.

fMRI responses measuring cortical activity before and during ongoing treatment with ranibizumab. Sessions 1 to 4, as in Fig. 2. (a) fMRI response area, measured as the percentage of significantly active voxels within a large cortical region (80 mm in diameter) including the posterior and medial occipital lobes. Data are shown for the patient undergoing treatment compared with an age-matched control patient with established bilateral AMD, who was not undergoing treatment but scanned during two separate sessions. Error bars, representing variability within a scanning session, are smaller than the data points when not visible. (b) fMRI response magnitude, measured as the average coherence across scans within each session, for two regions of interest, each 10mm in diameter—one at the occipital pole (OP) representing central vision and one more anterior in the calcarine sulcus (CS)—representing more peripheral (intact) vision. Error bars represent variability across scans within each session.

response magnitudes in cortex representing intact retina (CS) did not change significantly after the first treatment ($p_{12} = 0.983$). Although there was a significant difference between response magnitudes in the second and third sessions in this region ($p_{23} = 0.013$), no other difference between sessions was significant ($p_{34} = 0.858$; $p_{24} = 0.150$; and $p_{14} = 0.819$). Although the significance values reported here reflect the outcome of our more rigorous resampling method, it is worth noting that a similar pattern of results emerged from the application of a general linear model, i.e., repeated measures analysis of variance with post hoc t-tests.

DISCUSSION

In this case study, we have shown that regions of visual cortex that have been deprived of input by macular lesions can resume activity when retinal input is restored. Visual cortical activity was monitored using fMRI in a patient before and between treatments with ranibizumab. Cortical responses were absent from regions receiving input from the macular lesion before treatment but were present and began to fill in the silent region over the course of treatment.

Recent studies have provided evidence that visual cortex can degenerate in long-term blindness[21] and even following retinal lesions acquired later in life.[2] Other studies have suggested that visual cortical resources can be reallocated to other functions, either processing other sensory modalities in complete blindness[22] or other parts of the visual field.[3–5] Despite these claims, we have evidence that in our single case study at least visual cortex seems to have remained viable, resuming its role in visual processing when its inputs are restored.

The increase in cortical activity also paralleled the return of visual function as measured by clinical behavioral measures, such as visual acuity, visual field, fixation stability, and reading ability. Visual ability assessed by these measures, however, can be confounded with other factors. Visual acuity and reading tests are limited in their ability to give a holistic picture of visual function. Both require proper optical correction and may not reveal partial or patchy lesions, as the patient may be able to complete the tests using some remaining "islands" of vision. Furthermore, acuity and reading tests by their very nature focus on reading ability but may fail to reveal general visual abilities more relevant or important to the patient than reading, such as that necessary for effective social interaction and communication, facial recognition, or viewing visual media (e.g., television, film, and visual art.).[23–26] Although visual perimetry gives a better assessment of function across the visual field, it relies on good fixation to provide accurate measurements. In addition, it requires a subjective response by the patient (either verbal or a finger press), which could be a challenge for patients with mobility or cognitive impairment issues. As with some other measures of visual function, perimetry may be subject to learning effects. Although the patients in this study had little or no prior experience with microperimetry, however, an improvement in these data is unlikely to reflect a learning effect because (1) the untreated eye showed no marked improvement across sessions and (2) the treated eye improved most between the third and fourth sessions. Finally, most visual perimetry methods fail to assess vision in the far periphery, which is important for visual navigation and driving. Using fMRI as an objective measure and a simple visual paradigm, we were able to assess visual function in patients throughout the visual field without the need for optical correction, fixation stability, motor responses, or subjective outcome measures.

Although both the area and magnitude of the fMRI response in the patient increased over the course of treatment, it is important to note that cortical function did not return to the extent that can

be observed in subjects with normal vision. A silent region at the OP persisted even after several treatments, also reflected by the central scotoma present in the microperimetry data. From our data, we cannot ascertain the source of the remaining central scotoma. Additional measures designed to assess retinal health (e.g., optical coherence tomography or electroretinography) and cortical function (e.g., transcranial magnetic stimulation) might provide answers to this question in future studies.

In this case study, we have demonstrated that fMRI can provide a useful "readout" of retinal damage, assessing visual function across the entire visual field. As a clinical technique, fMRI can provide an objective, non-invasive measure of visual function without relying on a patient's fixation ability, mobility, response capabilities, or cognitive status. fMRI shows promise as a valuable method of assessing and monitoring changes in vision, particularly as advanced treatments to restore retinal function become more common.

ACKNOWLEDGMENTS

We would like to thank our participants. The views expressed in this publication are those of the authors and not necessarily those of the NHS, the National Institute for Health Research or the Department of Health.

This work was supported by the Medical Research Council (G0401339). AT, GSR, and MDC also received financial support from the Department of Health through an award made by the National Institute for Health Research to Moorfields Eye Hospital NHS Foundation Trust and UCL Institute of Ophthalmology for a Specialist Biomedical Research Centre for Ophthalmology.

This study was also presented in part at the ARVO Annual Meeting in May 2010, Ft. Lauderdale, Florida.

Received October 4, 2010; revision received June 6, 2011.

REFERENCES

1. Vugler AA. Progress toward the maintenance and repair of degenerating retinal circuitry. Retina 2010;30:983–1001.
2. Boucard CC, Hernowo AT, Maguire RP, Jansonius NM, Roerdink JB, Hooymans JM, Cornelissen FW. Changes in cortical grey matter density associated with long-standing retinal visual field defects. Brain 2009;132:1898–906.
3. Baker CI, Peli E, Knouf N, Kanwisher NG. Reorganization of visual processing in macular degeneration. J Neurosci 2005;25:614–8.
4. Baker CI, Dilks DD, Peli E, Kanwisher N. Reorganization of visual processing in macular degeneration: replication and clues about the role of foveal loss. Vision Res 2008;48:1910–9.
5. Schumacher EH, Jacko JA, Primo SA, Main KL, Moloney KP, Kinzel EN, Ginn J. Reorganization of visual processing is related to eccentric viewing in patients with macular degeneration. Restor Neurol Neurosci 2008;26:391–402.
6. Liu T, Cheung SH, Schuchard RA, Glielmi CB, Hu X, He S, Legge GE. Incomplete cortical reorganization in macular degeneration. Invest Ophthalmol Vis Sci 2010;51:6826–34.
7. Sunness JS, Liu T, Yantis S. Retinotopic mapping of the visual cortex using functional magnetic resonance imaging in a patient with central scotomas from atrophic macular degeneration. Ophthalmology 2004;111:1595–8.
8. Smirnakis SM, Brewer AA, Schmid MC, Tolias AS, Schuz A, Augath M, Inhoffen W, Wandell BA, Logothetis NK. Lack of long-term cortical reorganization after macaque retinal lesions. Nature 2005;435:300–7.
9. Masuda Y, Dumoulin SO, Nakadomari S, Wandell BA. V1 projection zone signals in human macular degeneration depend on task, not stimulus. Cereb Cortex 2008;18:2483–93.
10. Baseler HA, Gouws A, Morland AB. The organization of the visual cortex in patients with scotomata resulting from lesions of the central retina. Neuro-Ophthalmology 2009;33:149–57.
11. Baseler HA, Gouws A, Haak KV, Racey C, Crossland MD, Tufail A, Rubin GS, Cornelissen FW, Morland AB. Large-scale remapping of visual cortex is absent in adult humans with macular degeneration. Nat Neurosci 2011;14:649–55.
12. McKeefry DJ, Gouws A, Burton MP, Morland AB. The noninvasive dissection of the human visual cortex: using FMRI and TMS to study the organization of the visual brain. Neuroscientist 2009;15:489–506.
13. Crossland MD, Dunbar HM, Rubin GS. Fixation stability measurement using the MP1 microperimeter. Retina 2009;29:651–6.
14. Timberlake GT, Sharma MK, Grose SA, Gobert DV, Gauch JM, Maino JH. Retinal location of the preferred retinal locus relative to the fovea in scanning laser ophthalmoscope images. Optom Vis Sci 2005;82:177–85.
15. Elliott DE, Bullimore MA, Bailey IL. Improving the reliability of the Pelli-Robson contrast sensitivity test. Clin Vis Sci 1991;6:471–5.
16. Legge GE, Ross JA, Luebker A, LaMay JM. Psychophysics of reading. VIII. The Minnesota Low-Vision Reading Test. Optom Vis Sci 1989;66:843–53.
17. Teo PC, Sapiro G, Wandell BA. Creating connected representations of cortical gray matter for functional MRI visualization. IEEE Trans Med Imaging 1997;16:852–63.
18. Jenkinson M, Bannister P, Brady M, Smith S. Improved optimization for the robust and accurate linear registration and motion correction of brain images. Neuroimage 2002;17:825–41.
19. Andrews TJ, Halpern SD, Purves D. Correlated size variations in human visual cortex, lateral geniculate nucleus, and optic tract. J Neurosci 1997;17:2859–68.
20. Bandettini PA, Jesmanowicz A, Wong EC, Hyde JS. Processing strategies for time-course data sets in functional MRI of the human brain. Magn Reson Med 1993;30:161–73.
21. Noppeney U, Friston KJ, Ashburner J, Frackowiak R, Price CJ. Early visual deprivation induces structural plasticity in gray and white matter. Curr Biol 2005;15:R488–90.
22. Sadato N, Pascual-Leone A, Grafman J, Ibanez V, Deiber MP, Dold G, Hallett M. Activation of the primary visual cortex by Braille reading in blind subjects. Nature 1996;380:526–8.
23. Bullimore MA, Bailey IL, Wacker RT. Face recognition in age-related maculopathy. Invest Ophthalmol Vis Sci 1991;32:2020–9.
24. Mangione CM, Gutierrez PR, Lowe G, Orav EJ, Seddon JM. Influence of age-related maculopathy on visual functioning and health-related quality of life. Am J Ophthalmol 1999;128:45–53.
25. Tejeria L, Harper RA, Artes PH, Dickinson CM. Face recognition in age related macular degeneration: perceived disability, measured disability, and performance with a bioptic device. Br J Ophthalmol 2002;86:1019–26.
26. Boucart M, Dinon JF, Despretz P, Desmettre T, Hladiuk K, Oliva A. Recognition of facial emotion in low vision: a flexible usage of facial features. Vis Neurosci 2008;25:603–9.

Antony B. Morland
Department of Psychology
University of York
York YO10 5DD
United Kingdom
e-mail: a.morland@psychology.york.ac.uk